Multi-Passband Filters and Tunable Filters Design Based on Coupled Resonator Circuits

Mofei Guo

A thesis submitted to the University of Birmingham for the degree of Doctor of Philosophy

School of Electronic, Electrical and Systems Engineering

The University of Birmingham

January, 2016

Abstract

This thesis investigates multi-passband and tunable microwave filters, it includes a new generalised design technique for multi-passband filters and a new coupling tuning structure for tunable waveguide filters.

The synthesis technique is an analytical approach and offers very fast solutions to the design once the desired filter specifications are given. The technique calculates the coupling matrix and external Q-factors for a wide range of filter specifications. The centre frequency and bandwidth of each passband, and the number of passbands can all be arbitrarily chosen. To verify the calculations, multi-passband filters are realised by using multi-passband resonator sections. Two X-band waveguide multi-passband filter examples are given to validate the theory. Besides the innovation in synthesis technique, new designs of fully tunable waveguide filters are also presented. These filters are based on the new coupling tuning structure and a separate frequency tuning structure offering tuning in both centre frequency and bandwidth of the filter. One tunable bandpass filter and one tunable notch filter is implemented in X-band waveguide circuit.

Acknowledgments

Firstly, I am extremely grateful for the patient guidance of my supervisor Prof Michael Lancaster through my time in the University of Birmingham. I have benefited much from his constant support and instructive ideas. Without his help, the work presented here may never be accomplished. I would also like to express my gratitude to Dr. Paul Smith for the valuable discussions and comments on my work.

My thanks also go to the colleagues in EDT group at University of Birmingham for the kind support and friendship during my research. In particular, I would like to thank Dr. Xiaobang Shang and Dr. Wenlin Xia for many inspired discussions on my work. I would also like to thank Donna Johnson and Warren Hay for their strong support during filter fabrication and measurement.

I also appreciate the financial support from the Engineering School Scholarship of the University of Birmingham.

Finally, my sincere gratitude goes to my parents who always give, but never ask.

Table of Contents

CHAPTER 1 INTRODUCTION

The work presented in this thesis can be generally categorised into two parts, which are: (1) the design of multi-passband filters using analytical synthesis technique; (2) the designs of tunable rectangular waveguide filters, which include a tunable bandpass filter and a tunable notch filter.

1.1 Thesis Motivation

There have been extensive studies on multi-passband frequency selective circuits [1]. They are widely used in wireless communication and satellite applications, where multi-channel signals are transmitted or received through one beam [2]. As shown in Figure 1.1, there are broadly three configurations of them. Figure 1.1(a) shows a conventional configuration which has channelized banks of bandpass filters and power dividers / combiners. The shortcoming of this configuration is size of the circuit and power loss in the signal splitting and combining process [1]. Figure 1.1(b) shows another configuration which uses multiplexer and power combiner, but it still has disadvantages such as, inter-module matching issues. Besides, the design of wide-band power combiner becomes a critical issue in both configurations [1]. Compared with these two, the third one shown in Figure 1.1(c) solves all these issues by only using a single circuit that performs the multi-passband filtering function.

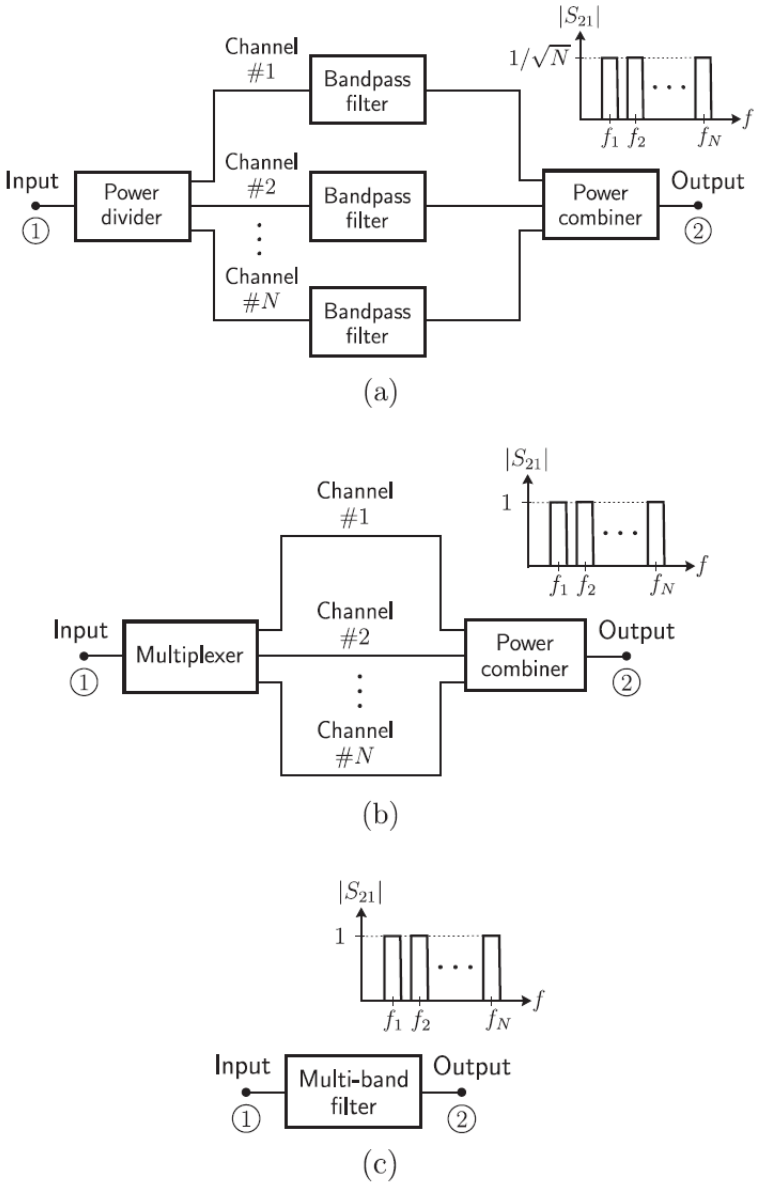

Figure 1.1 The configurations of the three kinds of frequency-selective circuits, (a) Channelized bank of bandpass filters with input/output power divider/combiner, (b) Input multiplexer with output power combiner, (c) Multi-passband filter (reproduced from [1])

One of the critical parts in multi-passband filter design is the synthesis of coupling matrix and external *Q*-factors with the desired filter specifications. The concepts of coupling matrix and external *Q*-factors, together with classic synthesis techniques for filters are introduced in Chapter 2. All the coupling matrices presented in this thesis are $N \times N$ matrices, each defines the inter-resonator couplings of the filter [3]. Generally, there are two ways to obtain a matrix; one is optimisation, and the other one is analytical synthesis. In this thesis, an analytical

synthesis technique for multi-passband filter is investigated. Compared with optimisation methods, this analytical synthesis technique provides a very fast and efficient solution.

This technique is based on lowpass to multi-passband frequency transformation which maps a lowpass prototype response onto multiple frequency bands. From the topology point of view, the frequency transformation is realised by the so called multi-passband resonator section, which is also the basic building block for the proposed multi-passband filter. As long as the filter specifications are given clearly, this technique can guarantee there exists a solution that satisfies the desired specifications. This means that a multi-passband filter with arbitrary specifications can be generated; the relevant coupling matrix and external Q-factors can be calculated. Two selected multi-passband filters are implemented in the form of rectangular waveguide. The measured results are given in the thesis.

Nowadays, tunable filters become more important in wireless communications and satellite applications. For example, most of the commercial communication satellites use fixed filter banks to fulfil flexibilities in centre frequency and bandwidth, but people are still putting efforts in making more flexible tunable payloads for satellite applications. The critical driver behind is to have more channels, longer lifetime and less weight at the same time [4]. It is quite obvious that mass and size are the key factors in satellite applications. Tunable devices permit multi-functional operations to be carried out with less volume of hardware which promisingly makes the payload smaller and lighter. Therefore, with a smaller size, more payloads may be added onto a satellite to enhance the performance, or more fuels can be carried to prolong its operation.

The tunable filters implemented by cavity resonators enjoy good insertion loss level, good selectivity and transmission responses with little distortion [5, 6]. This is because it maintains a high unloaded Q-factor Q_u over the tuning range. So far, the published tunable cavity filters

are mainly based on dielectric resonators with elaborate MEMS tuning elements integrated inside the cavity. These filters possess good frequency tuning ability, but do not have flexibility in bandwidth [5, 7-14]. On the other hand, most tunable filters implemented in planar circuits can achieve flexibilities in both frequency and bandwidth [4, 7, 15-39], but in general, their performances are not as good as that of the tunable cavity filters.

The tunable rectangular waveguide filters proposed in the thesis provide a good compromise between tuning flexibilities and performance. This attributes to the design of a new coupling tuning structure based on rectangular waveguide. It changes the coupling between adjacent resonators; while maintains an acceptable insertion loss with the integration of chokes. A tunable bandpass filter and a tunable notch filter are designed and implemented in the form of rectangular waveguide. The passband centre frequency, the bandwidth and the notch position, can all be tuned. Both filters are fabricated and measured; the results are presented in the thesis.

1.2 Thesis Overview

The thesis is formed of seven chapters. Chapter 3 and 4 consists of the first part of work which comprises the design of the multi-passband filter. The second part of work about the tunable waveguide filter design is included in Chapter 5 and 6. The thesis is organised as follows.

Chapter 1 states the motivations and objectives of the work in this thesis. The overview of the thesis is included in this chapter as well.

Chapter 2 introduces the fundamental theories that are used in the design of multi-passband filters and tunable filters. It includes the general filter theory, coupling matrix theory and the classic synthesis techniques for bandpass filters. The characteristic polynomials are also

discussed, as they are used in the analytical multi-passband filter synthesis technique for plotting the *S*-parameters.

Chapter 3 investigates an analytical synthesis technique for multi-passband filter. In order to show the freedom of this design technique, seven design examples are given; they have different centre frequencies, different bandwidths, different passband numbers and different passband shapes. For each example, its topology, *S*-parameters, coupling matrix and external *Q*-factors are calculated and presented. The generalised multi-passband filter topologies are also proposed in this chapter.

Chapter 4 shows the waveguide implementation of the multi-passband filter. In the first part, the classic design technique of rectangular waveguide filters is introduced. It discusses the relationship between the coupling matrix and the dimensions of a real rectangular waveguide filter. In the second part, a 10^{th} order five-passband filter with Chebyshev response which is implemented in rectangular waveguide is presented. The measured results are given and analysed. In the third part, another design example of a 20^{th} order five-passband filter with quasi-elliptic response is presented, together with the measured results and analysis.

Chapter 5 discusses the design of tunable waveguide circuits. A new coupling tuning structure with choke is presented in this chapter. It enables coupling tuning, while maintain the unloaded *Q*-factors of the resonator. This coupling tuning structure, together with a separate frequency tuning element are the two basic building components for the proposed tunable filter. As an example, a 3^{rd} order tunable bandpass filter is designed and fabricated; the measured results are given in the end of the chapter.

Chapter 6 is about the design of tunable notch filter, which uses the knowledges in Chapter 3 and Chapter 5. A design example of 4^{th} order tunable notch filter is given. It is based on the

dual-passband filter topology. The filter is implemented in the form of rectangular waveguide. The measured results are given.

Chapter 7 concludes the whole thesis. It also gives the possible future plans based on the current achievements.

Reference:

1. Gomez, G., et al. "Microwave transversal six-band bandpass planar filter for multi-standard wireless applications," in *IEEE Radio and Wireless Symposium (RWS),* 2011.
2. Juseop, L. and K. Sarabandi, "A Synthesis Method for Dual-Passband Microwave Filters," *IEEE Transaction on Microwave Theory and Techniques* , 2007. **55**(6): p. 1163-1170.
3. Hong, J.-S. and M.J. Lancaster, "Microstrip Filters for RF/Microwave Applications" 2001: John Wiley and Sons Ltd, United Kingdom.
4. Ming, Y., et al., "The Sound the Air Makes: High-Performance Tunable Filters Based on Air-Cavity Resonators," *IEEE Microwave Magazine*, 2014. **15**(5): p. 83-93.
5. Mansour, R.R., et al., "High-Q Tunable Filters: Challenges and Potential," *IEEE Microwave Magazine*, 2014. **15**(5): p. 70-82.
6. Manuel Sanchez-Renedo, R.G.-G., Jose I. Alonso, Cesar Briso-Rodriguez, "Tunable Combline Filter With Continuous Control of Center Frequency and Bandwidth," *IEEE TRANSACTION ON MICROWAVE THEORY AND TECHNIQUES* , 2005. **53**(1): p. 9.
7. Winter Dong, Y. and R.R. Mansour, "Tunable Dielectric Resonator Bandpass Filter With Embedded MEMS Tuning Elements," *IEEE Transaction on Microwave Theory and Techniques*, 2007. **55**(1): p. 154-160.
8. Huang, F., S. Fouladi, and R.R. Mansour, "High-Q Tunable Dielectric Resonator Filters Using MEMS Technology," *IEEE Transaction on Microwave Theory and Techniques*, 2011. **59**(12): p. 3401-3409.
9. Fengxi, H. and R. Mansour. "A novel varactor tuned dielectric resonator filter," in *IEEE MTT-S International Microwave Symposium Digest (IMS),* 2013.
10. Fouladi, S., et al., "High-Q Narrowband Tunable Combline Bandpass Filters Using MEMS Capacitor Banks and Piezomotors," *IEEE Transaction on Microwave Theory and Techniques*, 2013. **61**(1): p. 393-402.
11. Yassini, B., Y. Ming, and B. Keats, "A Ka-Band Fully Tunable Cavity Filter," *IEEE Transaction on Microwave Theory and Techniques*, 2012. **60**(12): p. 4002-4012.
12. Snyder, R.V. "A wide-band tunable filter technique based on double-diplexing and low-Q tuning elements," in *IEEE MTT-S International Microwave Symposium Digest.* 2000.
13. Yassini, B., et al., "A Ku-Band High-Q Tunable Filter With Stable Tuning Response," *IEEE Transaction on Microwave Theory and Techniques,* 2009. **57**(12): p. 2948-2957.

14. Kurudere, S. and V.B. Erturk, "Novel Microstrip Fed Mechanically Tunable Combline Cavity Filter," *IEEE Microwave and Wireless Components Letters*, 2013. **23**(11): p. 578-580.
15. Peng, W. and I. Hunter, "Electronically Tunable Filters,". *IEEE Microwave Magazine*, 2009. **10**(6): p. 46-54.
16. Peng, W. and I.C. Hunter, "A New Class of Low-Loss High-Linearity Electronically Reconfigurable Microwave Filter,". *IEEE Transaction on Microwave Theory and Techniques*, 2008. **56**(8): p. 1945-1953.
17. Alaa I. Abunjaileh, I.C.H., "Tunable Bandpass and Bandstop Filters Based on Dual-Band Combline Structures," *IEEE TRANSACTION ON MICROWAVE THEORY AND TECHNIQUES* , 2010. **58**(12): p. 10.
18. Rebeiz, G.M., et al., "Tuning in to RF MEMS,". *IEEE Microwave Magazine*, 2009. **10**(6): p. 55-72.
19. Jia-Sheng, H., "Reconfigurable planar filters,". *IEEE Microwave Magazine*, 2009. **10**(6): p. 73-83.
20. Naglich, E.J., D. Peroulis, and W.J. Chappell. "Wide spurious free range positive-to-negative inter-resonator coupling structure for reconfigurable filters," *IEEE MTT-S International Microwave Symposium Digest (IMS),* 2013.
21. Sirci, S., et al. "Analog tuning of compact varactor-loaded combline filters in substrate integrated waveguide," *42nd European Microwave Conference (EuMC),* 2012.
22. Mira, F., J. Mateu, and C. Collado, "Mechanical Tuning of Substrate Integrated Waveguide Resonators," *IEEE Microwave and Wireless Components Letters*, 2012. **22**(9): p. 447-449.
23. Armendariz, M., V. Sekar, and K. Entesari. "Tunable SIW bandpass filters with PIN diodes," *2010 European Microwave Conference (EuMC),* 2010.
24. Joshi, H., et al., "High-Q Fully Reconfigurable Tunable Bandpass Filters," *IEEE Transaction on Microwave Theory and Techniques*, 2009. **57**(12): p. 3525-3533.
25. Torregrosa-Penalva, G., et al., "A simple method to design wide-band electronically tunable combline filters," *IEEE Transaction on Microwave Theory and Techniques,* 2002. **50**(1): p. 172-177.
26. Wen-Teng, L. and C.K.C. Tzuang, "K-band quasi-planar tapped combline filter and diplexer," *IEEE Transaction on Microwave Theory and Techniques*, 1993. **41**(2): p. 215-223.
27. Xu-Guang, W., C. Young-Ho, and Y. Sang-Won, "A Tunable Combline Bandpass Filter Loaded With Series Resonator," *IEEE Transaction on Microwave Theory and Techniques*, 2012. **60**(6): p. 1569-1576.
28. Matthaei, G.L., "Narrow-band, fixed-tuned, and tunable bandpass filters with zig-zag hairpin-comb resonators," *IEEE Transaction on Microwave Theory and Techniques*, 2003. **51**(4): p. 1214-1219.
29. Han-Ul, M., et al. "Size-reduced tunable hairpin bandpass filter using aperture coupling with enhanced selectivity and constant bandwidth," *IEEE MTT-S International Microwave Symposium Digest* 2008.
30. Xiu Yin, Z., et al., "RF Tunable Bandstop Filters With Constant Bandwidth Based on a Doublet Configuration," *IEEE Transaction on Industrial Electronics,* 2012. **59**(2): p. 1257-1265.
31. Tsuzuki, G., et al. "Ultra-Selective Constant-Bandwidth Electromechanically Tunable HTS Filters," *IEEE MTT-S International Microwave Symposium Digest,* 2006.
32. Psychogiou, D. and D. Peroulis, "Tunable VHF Miniaturized Helical Filters," *IEEE Transaction on Microwave Theory and Techniques*, 2014. **62**(2): p. 282-289.

33. Xiu Yin, Z., et al., "Low-Loss Frequency-Agile Bandpass Filters With Controllable Bandwidth and Suppressed Second Harmonic," *IEEE Transaction on Microwave Theory and Techniques*, 2010. **58**(6): p. 1557-1564.
34. Manh-Tai, N., W.D. Yan, and E.P.W. Horne. "Broadband tunable filters using high Q passive tunable ICs," *IEEE MTT-S International Microwave Symposium Digest,* 2008.
35. Sirci, S., et al. "Varactor-loaded continuously tunable SIW resonator for reconfigurable filter design,". *41st European Microwave Conference (EuMC),* 2011.
36. Sekar, V., M. Armendariz, and K. Entesari, "A 1.2&1.6-GHz Substrate-Integrated-Waveguide RF MEMS Tunable Filter," *IEEE Transaction on Microwave Theory and Techniques*, 2011. **59**(4): p. 866-876.
37. Arif, M.S. and D. Peroulis, "All-Silicon Technology for High-Q Evanescent Mode Cavity Tunable Resonators and Filters," *Journal of Microelectromechanical Systems,* 2014. **23**(3): p. 727-739.
38. Da-Peng, W., C. Wen-quan, and P. Russer. "Tunable Substrate-Integrated Waveguide (SIW) Dual-Mode Square Cavity Filter with Metal Cylinders," *IEEE MTT-S International Microwave Workshop Series on Art of Miniaturizing RF and Microwave Passive Components,* 2008.
39. Hyunseong, K., et al. "Silicon-based substrate-integrated waveguide-based tunable band-pass filter using interdigital MEMS capacitor," *2013 Asia-Pacific Microwave Conference Proceedings (APMC),* 2013.

CHAPTER 2 FUNDAMENTAL THEORY

2.1 Overview of Microwave Filters

A filter is a frequency selective device; it usually has two ports. From the input port to the output port, it permits a good transmission for the desired frequency band(s) while stops the undesired one(s). In General, the filter can be categorised into four types: lowpass, high-pass, bandpass and band-stop [1]. Based on different transfer functions, there are various kinds of responses, what will be discussed here is Chebyshev response, Butterworth response and Quasi-elliptic response [2].

Figure 2.1 presents the layout of a typical two-port network connected with a source and a load, which is used in a classical methodology for filter analysis. In Figure 2.1, V_1, V_2 and I_1, I_2 are the voltage and current variables for the ports; Z_{01} and Z_{02} are the impedances of the terminals. E_s is the source voltage [3].

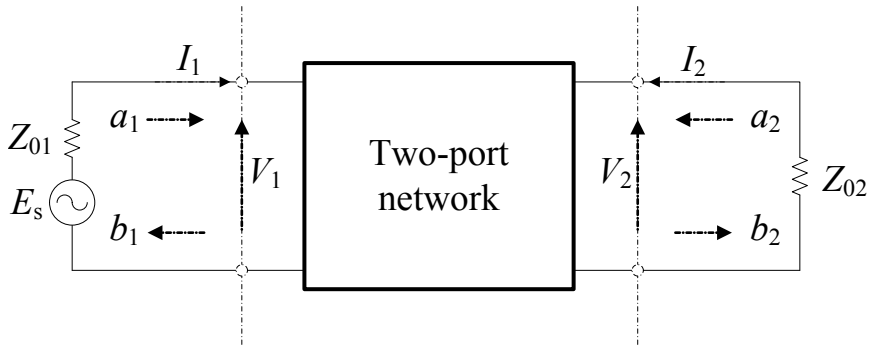

Figure 2.1 A two-port network representation with network variables [3]

a_1, b_1 and a_2, b_2 are wave variables. They are introduced because of the difficulty in measuring the voltage and current at radio frequency. a and b indicate incident waves and reflected waves, respectively. They are expressed in terms of voltage and current and are given by [3],

$$a_n = \frac{1}{2}\left(\frac{V_n}{\sqrt{Z_{0n}}} + \sqrt{Z_{0n}} \cdot I_n \right)$$
$$b_n = \frac{1}{2}\left(\frac{V_n}{\sqrt{Z_{0n}}} - \sqrt{Z_{0n}} \cdot I_n \right) \quad n=1 \text{ and } 2 \tag{2-1}$$

For the same reason as above, the scattering parameters (*S*-parameters) are introduced to indicate the transmitted and reflected energy [4]. The *S*-parameters for the two-port network shown in Figure 2.1 are given as [3],

$$S11 = \left.\frac{b_1}{a_1}\right|_{a_2=0} \qquad S12 = \left.\frac{b_1}{a_2}\right|_{a_1=0}$$
$$S21 = \left.\frac{b_2}{a_1}\right|_{a_2=0} \qquad S22 = \left.\frac{b_2}{a_2}\right|_{a_1=0} \tag{2-2}$$

The *S*-parameters in (2-2) are obtained when the impedances are perfectly matched at both ports. *S*11 and *S*22 are the reflection coefficients, whereas *S*12 and *S*21 are the transmission coefficients. In this thesis, the filters are reciprocal and symmetric two-port networks, hence $S12 = S21^*$ and $S11 = S22$. Because the *S*-parameters are complex, they are usually expressed in terms of amplitude and phases. The amplitudes of the *S*-parameters are defined as [3],

$$L_A = -20\log|S21| \quad \text{dB}$$
$$L_R = -20\log|S11| \quad \text{dB} \tag{2-3}$$

where L_A and L_R denote the insertion loss and return loss, respectively. The logarithm operation is base 10. Normally, rather than using the phase of *S*21 (ϕ_{21}), the group delay (τ_d) is introduced to characterize the phase response of the filter, which is defined as [3],

$$\tau_d = \frac{d\phi_{21}}{d\omega} \tag{2-4}$$

where ϕ_{21} is an angle in radians, ω is the angular frequency in rad/s. The group delay is the real-time delay between the input port and the output port of a filter which a signal travels through.

2.2 The Lowpass Prototype Filters and Filter Transfer Functions

2.2.1 Lowpass Prototype Filters

The lowpass prototype filter plays an important role in realising the filter transfer function into real circuits, which is a critical part of the filter synthesis [5-7]. In Figure 2.2, a ladder network structure and its duality of a normalised lowpass prototype filter are shown. They are based on lumped-elements which include capacitors, inductors and resistors.

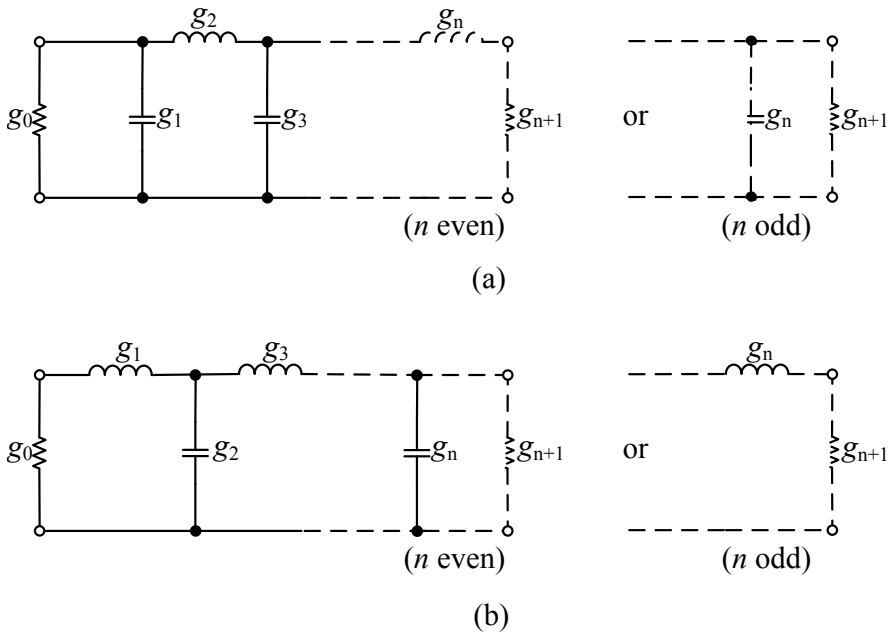

Figure 2.2 The lowpass prototype filters with (a) a ladder network structure and (b) its dual

Both ladder networks produce the same n^{th} order all-pole filter responses. g_0 and g_{n+1} denote the terminal element immittances (they are usually pure resistances or conductances) which are unity; whereas g_1 to g_n denote the inductances or capacitances of the filter elements. Generally, the microwave filter design begins with a normalised lowpass prototype filter

whose source element value ($g_0 = 1$) and cut-off angular frequency ($\Omega_C = 1$) are unity [4]. This simplifies the filter design procedure, since the prototype filter has a normalised impedance and bandwidth. Then, by applying the lowpass to bandpass frequency transformation, the bandpass response can be obtained. Depending on the value of each element (inductors or capacitors), the lowpass prototype circuit may generate different responses. But since most of the designs in this thesis are based on Chebyshev response, the discussion on Chebyshev response will be given in detail first. It is then followed by brief discussions about Butterworth (maximally-flat) filter and quasi-elliptic filter. The synthesis procedures of *g*-values for Chebyshev filter and Butterworth filter are given in the following sections.

2.2.2 Chebyshev Lowpass Prototype Response and Transfer Function

A typical lowpass prototype Chebyshev response has an equal-ripple passband and maximally flat stopband. This is illustrated in an example response shown in Figure 2.3. The Chebyshev response can be defined by an amplitude-squared transfer function [3],

$$\left|S21\left(j\Omega\right)\right|^2 = \frac{1}{1+\varepsilon^2 \cdot T_n^{\,2}\left(\Omega\right)} \tag{2-5}$$

here Ω is the angular frequency (rad/s) in normalised frequency domain, ε is the ripple constant which can be obtained from the level of passband ripple L_{Ar} (the maximum attenuation in passband, Figure 2.3(b)),

$$\varepsilon = \sqrt{10^{\frac{L_{Ar}}{10}} - 1} \tag{2-6}$$

$T_n\left(\Omega\right)$ is a Chebyshev function which can be defined as [3],

$$T_n(\Omega) = \begin{cases} \cos\left(n \cdot \cos^{-1}\Omega\right) & |\Omega| \le 1 \\ \cosh\left(n \cdot \cosh^{-1}\Omega\right) & |\Omega| \ge 1 \end{cases} \tag{2-7}$$

where n is the order of the Chebyshev filter, which implies there are n elements in the lowpass prototype circuit (Figure 2.2).

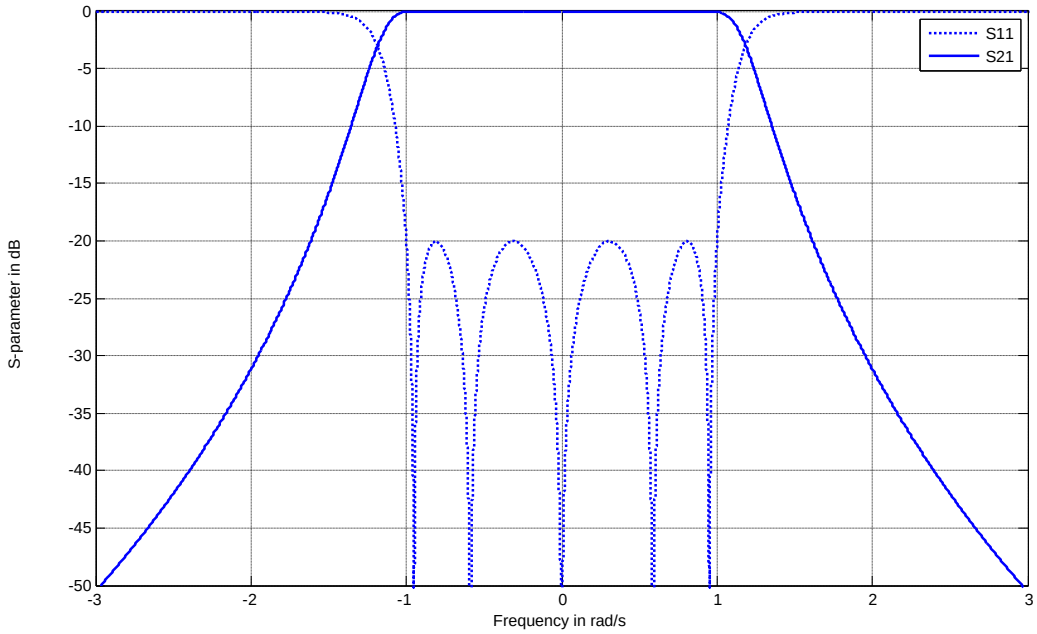

(a)

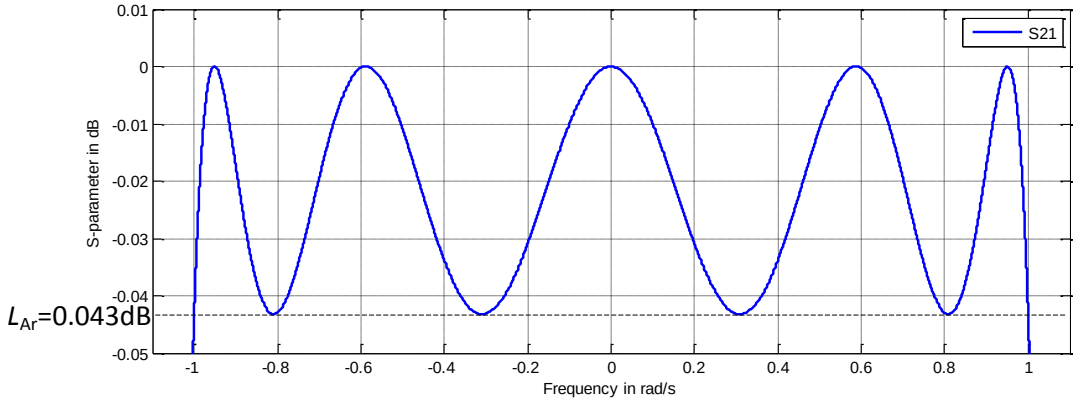

(b)

Figure 2.3 A 5th order lowpass prototype Chebyshev response with maximum passband return loss at 20dB, (a) the amplitude response of *S*-parameter, (b) the extended view of *S*21 showing passband ripple

Figure 2.3(a) shows a 5th order Chebyshev response; in order to illustrate the passband ripple, an extended view of $S21$ is given in Figure 2.3(b). Since it is a prototype filter, the cut-off angular frequency is normalised to one ($\Omega_C = \pm 1$). The passband ripple level (L_{Ar}) is 0.043dB, which corresponds to a 20dB maximum return loss for a lossless filter ($|S11|^2 + |S21|^2 = 1$). Because all the transmission zeros of $S21$ are located at infinity, it is also called an all-pole Chebyshev filter. For an all-pole chebyshev lowpass prototype filter, its g-values in the equivalent circuit (Figure 2.2) can be synthesised from the equation-set below [3],

$$
\begin{aligned}
\beta &= \ln\left(\frac{\sqrt{1+\varepsilon}+1}{\sqrt{1+\varepsilon}-1}\right) \\
\gamma &= \sinh\left(\frac{\beta}{2n}\right) \\
g_0 &= 1.0 \\
g_1 &= \frac{2}{\gamma}\sin\left(\frac{\pi}{2}\right) \\
g_i &= \frac{1}{g_{i-1}} \cdot \frac{4\sin\left[\frac{(2i-1)\pi}{2n}\right]\cdot\sin\left[\frac{(2i-3)\pi}{2n}\right]}{\gamma^2 + \sin^2\left[\frac{(i-1)\pi}{n}\right]} \qquad (i = 2,3,\ldots,n) \\
g_{n+1} &= \begin{cases} 1.0 & n \quad odd \\ \coth^2\left(\frac{\beta}{4}\right) & n \quad even \end{cases}
\end{aligned}
\tag{2-8}
$$

where β and γ are the variables introduced for the synthesis of g-values. For the 5th order lowpass prototype Chebyshev filter shown in Figure 2.3, its g-values have been calculated and given in Table 2.1.

g_0	g_1	g_2	g_3	g_4	g_5	g_6
1	0.9714	1.3721	1.8014	1.3721	0.9714	1

Table 2.1 The g values for the example of 5th order Chebyshev filter

2.2.3 Butterworth (Maximally-Flat) Lowpass Prototype Response and Transfer Function

A generalized amplitude-squared transfer function of Butterworth filters is defined as [7],

$$\left|S21(j\Omega)\right|^2 = \frac{1}{1+\varepsilon^2\left(\frac{\Omega}{\Omega_C}\right)^{2n}} \tag{2-9}$$

where ε is the ripple constant given in (2-6). However, unlike Chebyshev filter, the cut-off frequency (Ω_C) is usually specified as a frequency point which corresponds to a 3dB insertion loss ($\varepsilon = 1$). So for the lowpass prototype Butterworth filters ($\Omega_C = 1$), (2-9) can be re-written as [3],

$$\left|S21(j\Omega)\right|^2 = \frac{1}{1+\Omega^{2n}} \tag{2-10}$$

The corresponding *g*-values (also refer to Figure 2.2) of a Butterworth lowpass prototype filter can be synthesised by following equation-set [3],

$$\begin{aligned} g_0 &= g_{n+1} = 1.0 \\ g_i &= 2\sin\left(\frac{(2i-1)\pi}{2n}\right) \quad (i = 1, 2, \ldots, n) \end{aligned} \tag{2-11}$$

An example of a 5th order Butterworth filter is given, the *g*-values is presented in Table 2.2, whereas the response is shown in Figure 2.4.

g_0	g_1	g_2	g_3	g_4	g_5	g_6
1	0.6180	1.6180	2	1.6180	0.6180	1

Table 2.2 The *g*-values for the example of the 5th order Butterworth filter

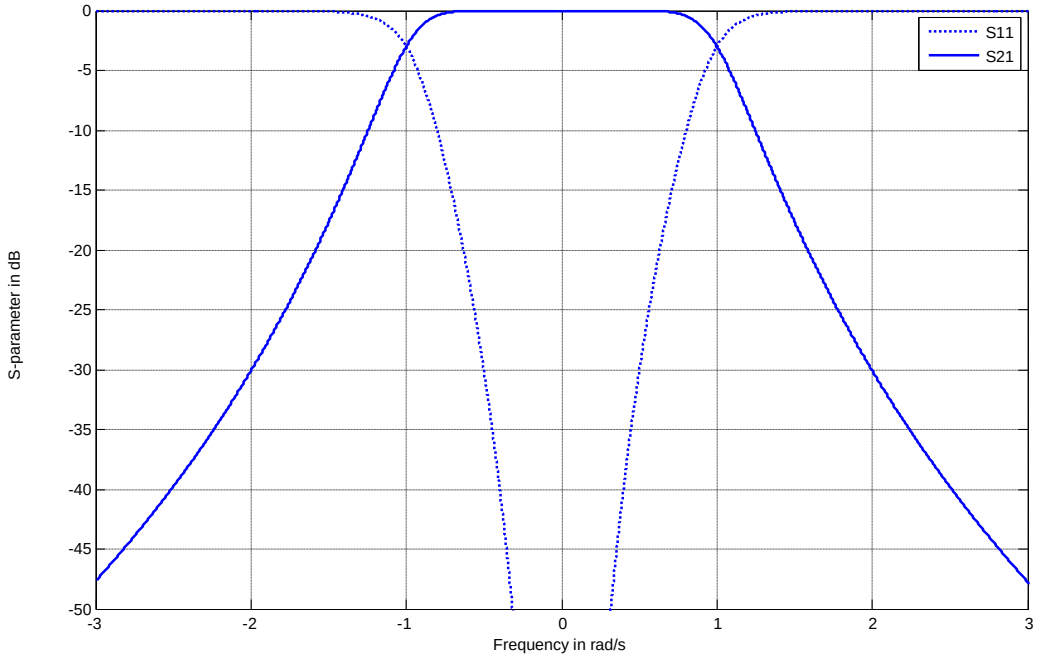

Figure 2.4 A 5th order lowpass prototype Butterworth response

2.2.4 Quasi-Elliptic Lowpass Prototype Response and Transfer Function

Elliptic filters were introduced due to higher demands in selectivity; thanks to having all transmission zeros at finite frequencies, the elliptic filters have a much sharper cut-off rate compared with all-pole Chebyshev and Butterworth filters [8]. This feature improves the selectivity of a filter. However, because of the sophisticated synthesis procedure and difficulties in circuit implementation, a more practical alternative namely the quasi-elliptic filter has been developed. There are both finite and infinite transmission zeros for the response of a quasi-elliptic filter [9].

The amplitude-squared transfer function for quasi-elliptic filter is defined as [10],

$$\left|S21\left(j\Omega\right)\right|^2 = \frac{1}{1+\varepsilon^2 \cdot F_N^2\left(\Omega\right)} \tag{2-12}$$

where $F_N\left(\Omega\right)$ is expressed as [10],

$$F_n\left(\Omega\right) = \cosh\left[\left(n-2\right)\cosh^{-1}\left(\Omega\right) + \cosh^{-1}\left(\frac{\Omega_a\Omega-1}{\Omega_a-\Omega}\right) + \cosh^{-1}\left(\frac{\Omega_a\Omega+1}{\Omega_a+\Omega}\right)\right] \tag{2-13}$$

in which n is the order of the filter; $\Omega = \pm\Omega_a$ ($\Omega_a > 1$) are the frequencies of the transmission zeros outside the passband. The detailed process of quasi-elliptic filter synthesis is presented in [9, 11]. However, it is a rather sophisticated procedure and there are no closed-form equations for the synthesis of g-values [2]. So a table that contains design data of quasi-elliptic filters which can be found in [10] and is always useful during the design.

Optimisation is another way to obtain a quasi-elliptic filter. Some details about it are given in Appendix I. Here, an example response of a 4th order lowpass prototype quasi-elliptic filter is given in Figure 2.5. The maximum passband return loss is 20dB, while the two out-of-passband transmission zeros fall on $\Omega = \pm 1.6$. For comparison, a 4th order lowpass prototype Chebyshev filter with same maximum passband return loss is given in the figure as well. It can be observed that the quasi-elliptic filter obtains a better selectivity compared with the same order Chebyshev response in the area between the two transmission zeros.

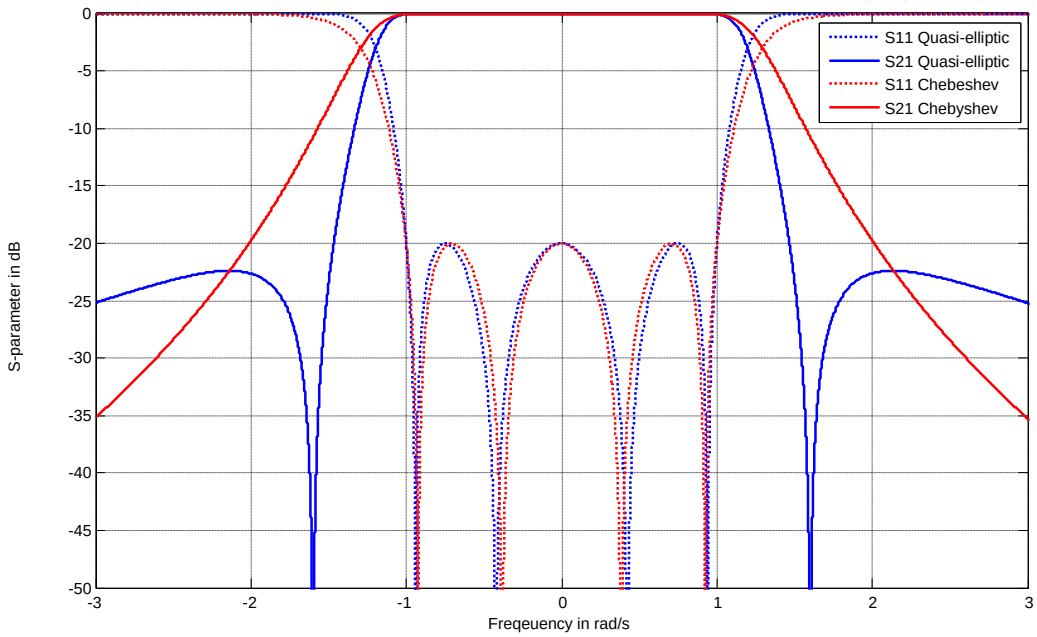

Figure 2.5 In blue: a 4th order lowpass prototype quasi-elliptic response with two finite frequency transmission zeros on ±1.6. In red: a 4th order lowpass prototype Chebyshev response

2.3 Immittance Inverters

Both impedance (*K*-) inverters and admittance (*J*-) inverters are immittance inverters [3]. An ideal *K*-inverter or *J*-inverter works as a 1/4 wavelength transmission line with a characteristic impedance of *K* or characteristic admittance of *J* at all frequencies [2].

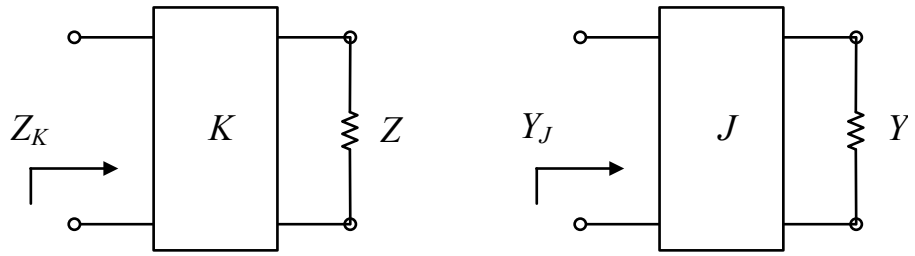

Figure 2.6 A definition schematic of impedance (*K*-) inverter and admittance (*J*-) inverter

As shown in Figure 2.6, for a two-port network with an immittance inverter in between the load immittance at one port and the immittance which is seen from the other port, will have the following relationships [7].

$$Z_K = \frac{K^2}{Z}, \qquad Y_J = \frac{J^2}{Y} \tag{2-14}$$

It shows that if one port is loaded with an impedance *Z* or admittance *Y*, the *K*-inverter or *J*-inverter will convert it into an arbitrary impedance Z_K or admittance Y_J by manipulating the value of *K* or *J*. Both *K* and *J* are real. It can also be found that if the load is inductive or capacitive, it will be capacitive or inductive seen from the other port; this implies that there is a ±90° phase shift for the immittance inverter. *K*-inverter and *J*-inverter are interconvertible under certain conditions which for example $K = 1/J$; when this condition is reached, they will share same inverting properties [2].

There are also many other forms of circuits that perform as immittance inverters besides the 1/4 wavelength transmission line; lumped-element equivalents which are shown in Figure 2.7 and Figure 2.8 are popular ones.

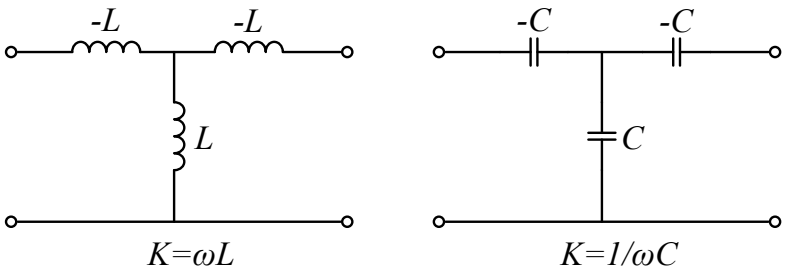

(a) (b)

Figure 2.7 Lumped-element equivalent of *K*-inverters

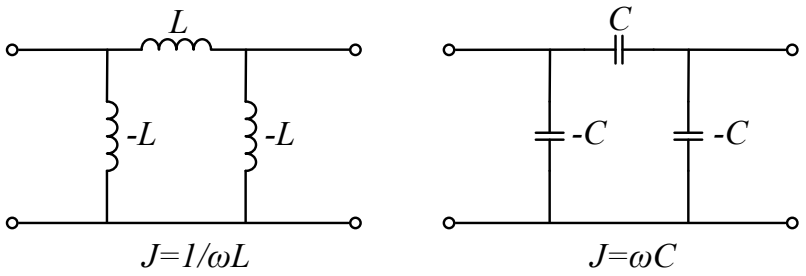

(a) (b)

Figure 2.8 Lumped-element equivalent of *J*-inverters

It is interesting to find that some element values in the above lumped-element equivalents are negative, which means it is impossible to achieve them in the form of real components. However, in practice, since the inverters are essential building blocks of a filter and are supposed to be connected with resonators, the negative elements will always be absorbed by the adjacent resonators [2]. As these are not ideal inverters, they are sensitive to frequency change; but for narrowband applications, they are still effective. According to [7], when using the above lumped-element inverters, filters that have up to 20% fractional bandwidth can be achieved if implemented with half-wavelength resonators.

As shown in Figure 2.9, if it is in a two-port network, a series inductor which connected to the external ports through inverters may be seen as a shunt capacitance from both ports and vice versa [3]. This makes it more convenient to implement a filter, because the element

immittance can be manipulated through the values of *J* or *K*. For instance, the lowpass prototype filter with a ladder network shown in Figure 2.2 can be converted into the forms shown in Figure 2.10 [3]. This structure is useful in lowpass to bandpass frequency transformation which is going to be discussed in next section.

Figure 2.9 A shunt capacitor and a series inductor are interconvertible through immittance inverters [3]

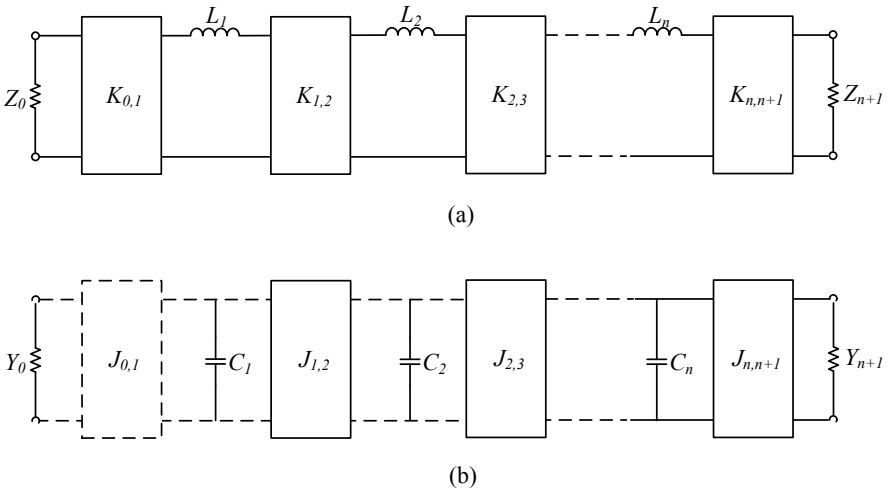

Figure 2.10 A modified lowpass prototype filter with immittance inverters

Likewise, a series tuned resonator and a shunt tuned resonator are also interconvertible through immittance inverter. Details are omitted here; the full information is given in [3].

2.4 Lowpass to Bandpass Frequency Transformation

The frequency transformation usually begins with a normalised lowpass prototype filter shown in Figure 2.2. A lowpass prototype filter can be transformed into many types of filters; conventionally, these include a practical lowpass filter, a highpass filter, a bandstop filter and a bandpass filter. In this section, the lowpass to bandpass frequency transformation is presented.

A lowpass prototype filter response can be mapped to a bandpass response with an arbitrary centre frequency (ω_0) and passband-edges (ω_1 , ω_2) by applying the lowpass to bandpass frequency transformation [3, 7, 12],

$$\Omega = \frac{\Omega_C}{FBW}\left(\frac{\omega}{\omega_0} - \frac{\omega_0}{\omega}\right) \tag{2-15}$$

where FBW is the fractional bandwidth; FBW and ω_0 can be defined as,

$$FBW = \frac{\omega_2 - \omega_1}{\omega_0}, \quad \omega_0 = \sqrt{\omega_1 \cdot \omega_2} \tag{2-16}$$

By applying (2-15) to the series inductors and shunt capacitors shown in Figure 2.10, it is interesting to find that a series inductor or a shunt capacitor in lowpass prototype frequency domain will be transformed into a series or a parallel LC resonator in the de-normalised frequency domain. This transformation is illustrated in Figure 2.11.

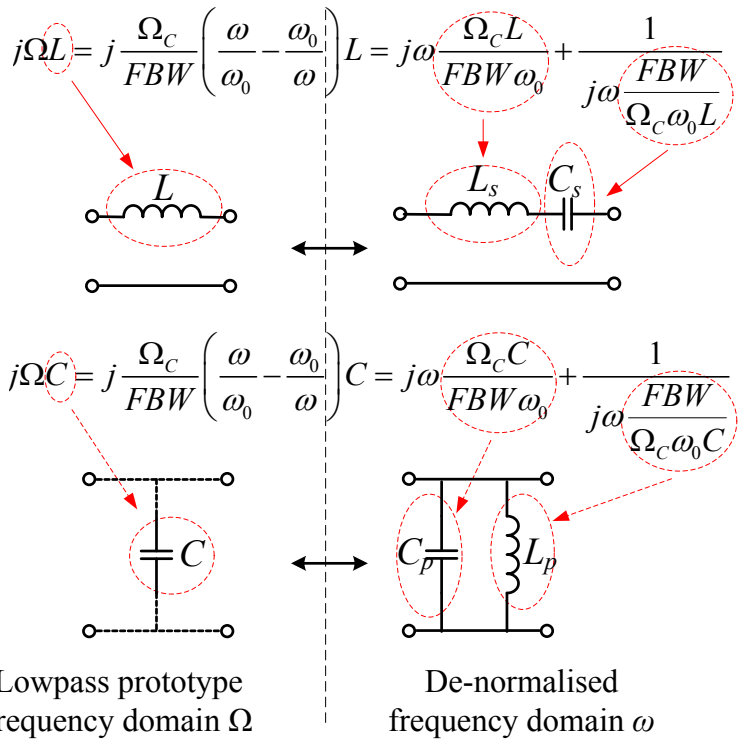

Figure 2.11 A schematic of lowpass to bandpass frequency transformation

L_s and C_s are the elements in series LC resonator, L_p and C_p are the elements in parallel LC resonator. Similarly, applying the lowpass to bandpass frequency transformation to the lowpass prototype filter (Figure 2.10), a bandpass circuit can be obtained as shown in Figure 2.12 [7].

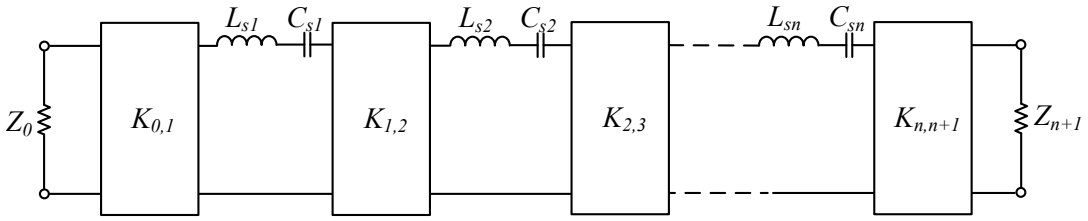

(a)

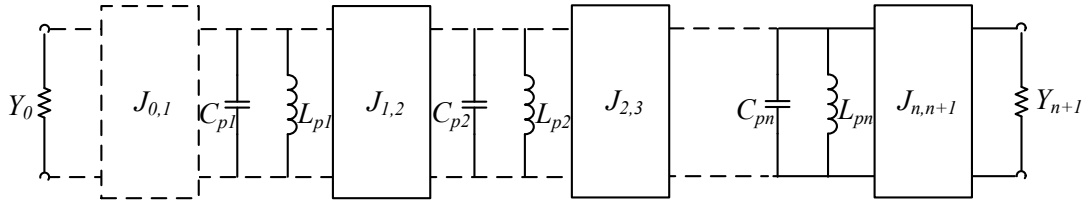

(b)

Figure 2.12 A bandpass filter with LC resonators and inverters

The elements in the bandpass filter can be obtained by [3],

$$\begin{cases} L_{si} = \dfrac{\gamma_0 \Omega_C g_i}{FBW\,\omega_0} \\ C_{si} = \dfrac{FBW}{\gamma_0 \Omega_C \omega_0 g_i} \end{cases} \qquad \begin{cases} L_{pi} = \dfrac{\gamma_0 FBW}{\Omega_C \omega_0 g_i} \\ C_{pi} = \dfrac{\Omega_C g_i}{\gamma_0 FBW\,\omega_0} \end{cases} \tag{2-17}$$

where γ_0 is the impedance scaling factor defined by [3],

$$\gamma_0 = \begin{cases} Z_0 / g_0 \\ g_0 / Y_0 \end{cases} \tag{2-18}$$

Since it is quite difficult to realise lumped-element circuits at radio and microwave frequencies, distributed-element circuits become good alternatives in microwave filter design. Couple-resonator circuit which is introduced to help the design of the distributed-element

circuits will be discussed in next section. The bandpass equivalent circuit which only contains inverters and resonators (Figure 2.12) provides more flexibility in design of coupled-resonator circuits, such as microstrip filters and waveguide filters. It is worth mentioning that rectangular waveguide is the form in which the filters discussed in this thesis are realised.

2.5 Coupling Matrix Representation of Coupled-Resonator Filter

The history of coupling matrix dates back to 1970s when the required performance of spaceborne device was boosted by the rapid expanding of satellite communication industry. The innovation of the coupling matrix method in filter design was firstly proposed in a set of papers by Atia and Williams [13-16]. Instead of extracting the electrical elements one by one which is necessary in classical element extraction method, the coupling matrix method gives a full map of the network with its matrix elements having one to one correspondences with every physical component in the filter equivalent circuit [17]. This allows techniques such as matrix rotation (or similarity transformation) and matrix inversion to be used and to reconfigure the matrix which physically alters the coupling arrangement of the filter so as to meet the specified design requirements.

Section 2.5.1 introduces the well-known theory of general coupling matrix which starts from a set of loop or node equations. Section 2.5.2 discusses synthesis techniques which are used to extract coupling coefficients and external Q-factors.

2.5.1 The Theory of General Coupling Matrix

There are two types of equivalent circuits for a two-port coupled-resonator filter; Figure 2.13(a) shows the magnetic coupled model; Figure 2.13(b) shows the electric coupled model.

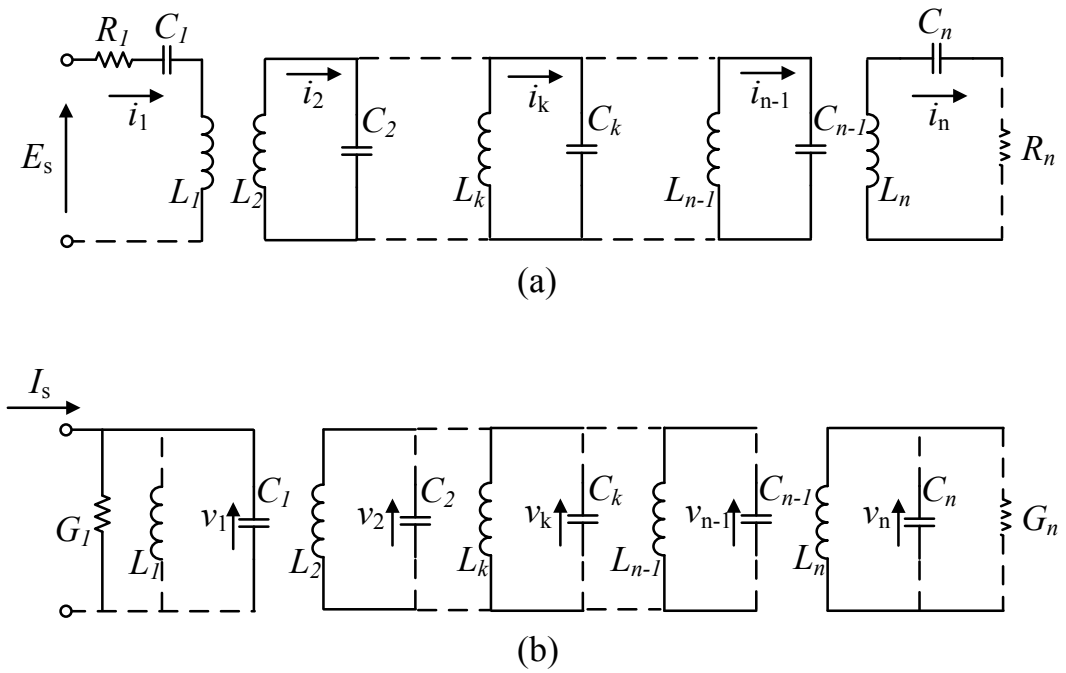

Figure 2.13 Equivalent of *n*-coupled resonator circuit for (a) loop-equation formulation (magnetic coupled), (b) node-equation formulation (electric coupled)[3]

As shown in Figure 2.13, resistance, conductance, inductance and capacitance are represented by R, G, L and C, respectively. R_1, G_1, L_1 and C_1 are source elements; R_n, G_n, L_n and C_n are load elements. R_k, G_k, L_k and C_k are elements for resonator k. E_s and I_s are the source voltage and current, respectively. For *k*th resonator, v_k is the node voltage (magnetic coupled model), i_k is the loop current (electric coupled model); they are supposed to have the same direction for all the nodes and loops.

The analyses for both models can be done in a similar way, so only the analysis of magnetic coupled one is given here. The discussion follows that in reference [3]. By applying the Kirchhoff's voltage law (the sum of voltage drops around a closed loop is zero) to the equivalent circuit shown in Figure 2.13(a) , where there are *n* loop equations can be obtained [3],

$$\begin{aligned}
\left(R_1 + j\omega L_1 + \frac{1}{j\omega C_1}\right)\cdot i_1 - j\omega L_{1,2}\cdot i_2 \quad \cdots \quad - j\omega L_{1,n}\cdot i_n &= E_s \\
-j\omega L_{2,1}\cdot i_1 - \left(j\omega L_2 + \frac{1}{j\omega C_2}\right)\cdot i_2 \quad \cdots \quad - j\omega L_{2,n}\cdot i_n &= 0 \\
&\vdots \\
-j\omega L_{n,1}\cdot i_1 - j\omega L_{n,2}\cdot i_2 \quad \cdots \quad + \left(R_n + j\omega L_n + \frac{1}{j\omega C_n}\right)\cdot i_n &= 0
\end{aligned} \tag{2-19}$$

where $L_{i,j} = L_{j,i}$ is the mutual inductance between i^{th} and j^{th} resonator; the above set of equations can also be presented in the form of matrix [3],

$$\begin{bmatrix}
R_1 + j\omega L_1 + \frac{1}{j\omega C_1} & -j\omega L_{1,2} & \cdots & -j\omega L_{1,n} \\
-j\omega L_{2,1} & j\omega L_2 + \frac{1}{j\omega C_2} & \cdots & -j\omega L_{2,n} \\
\vdots & \vdots & \ddots & \vdots \\
-j\omega L_{n,1} & -j\omega L_{n,2} & \cdots & R_n + j\omega L_n + \frac{1}{j\omega C_n}
\end{bmatrix} \cdot \begin{bmatrix} i_1 \\ i_2 \\ \vdots \\ i_n \end{bmatrix} = \begin{bmatrix} E_s \\ 0 \\ 0 \\ 0 \end{bmatrix} \tag{2-20}$$

or in a more generalised expression,

$$[Z]\cdot[i] = [E_s]$$

where $[Z]$ is the $n \times n$ impedance matrix. A filter is synchronously tuned when all of its resonators are resonating at the same frequency $\omega_0 = 1/\sqrt{LC}$, where $L = L_1 = L_2 = \cdots L_n$, $C = C_1 = C_2 = \cdots C_n$. In this case, the impedance matrix in (2-20) can be expressed as [3],

$$[Z] = \omega_0 L \cdot FBW \cdot \overline{[Z]} \tag{2-21}$$

in which $\overline{[Z]}$ is the normalized impedance matrix but only for synchronously tuned filter [3].

$$\overline{[Z]}=\begin{bmatrix} \dfrac{R_1}{\omega_0 L\cdot FBW}+p & -j\dfrac{\omega L_{1,2}}{\omega_0 L\cdot FBW} & \cdots & -j\dfrac{\omega L_{1,n}}{\omega_0 L\cdot FBW} \\ -j\dfrac{\omega L_{2,1}}{\omega_0 L\cdot FBW} & p & \cdots & -j\dfrac{\omega L_{2,n}}{\omega_0 L\cdot FBW} \\ \vdots & \vdots & \ddots & \vdots \\ -j\dfrac{\omega L_{n,1}}{\omega_0 L\cdot FBW} & -j\dfrac{\omega L_{n,2}}{\omega_0 L\cdot FBW} & \cdots & \dfrac{R_n}{\omega_0 L\cdot FBW}+p \end{bmatrix} \tag{2-22}$$

where $p=j\dfrac{1}{FBW}\left(\dfrac{\omega}{\omega_0}-\dfrac{\omega_0}{\omega}\right)$ is the complex lowpass frequency variable. As a narrow-band filter, it can be assumed that $\omega/\omega_0\approx 1$, then the matrix (2-22) can be simplified as [3],

$$\overline{[Z]}=\begin{bmatrix} \dfrac{1}{q_{e1}}+p & -jm_{1,2} & \cdots & -jm_{1,n} \\ -jm_{2,1} & p & \cdots & -jm_{2,n} \\ \vdots & \vdots & \ddots & \vdots \\ -jm_{n,1} & -jm_{n,2} & \cdots & \dfrac{1}{q_{en}}+p \end{bmatrix} \tag{2-23}$$

where $m_{i,j}=m_{j,i}$ is the normalised coupling coefficient between resonator ith and jth; q_{ei} (i=1,n) are the normalised external Q-factors. They can be defined and related to the practical (de-normalised) coupling coefficient $M_{i,j}$ and external Q-factor Q_{ei} by [3],

$$\begin{aligned} m_{i,j}&=\frac{M_{i,j}}{FBW}=\frac{L_{i,j}}{L}\cdot\frac{1}{FBW} && i\neq j \\ q_{ei}&=Q_{ei}\cdot FBW=\frac{\omega_0 L}{R_i}\cdot FBW && i=1,n \end{aligned} \tag{2-24}$$

For the case of asynchronously tuned filter (each resonator has an individual resonant frequency of $\omega_{0i}=1/\sqrt{L_iC_i}$), the normalised coupling coefficient is defined by [3],

$$m_{i,j}=\frac{M_{i,j}}{FBW}=\frac{L_{i,j}}{\sqrt{L_iL_j}}\cdot\frac{1}{FBW} \qquad i\neq j \tag{2-25}$$

while the normalised impedance matrix is obtained by adding self-couplings $m_{i,i}$ into the main diagonal elements in matrix (2-23), which is shown as [3],

$$\overline{[Z]}=\begin{bmatrix} \frac{1}{q_{e1}}+p-jm_{1,1} & -jm_{1,2} & \cdots & -jm_{1,n} \\ -jm_{2,1} & p-jm_{2,2} & \cdots & -jm_{2,n} \\ \vdots & \vdots & \ddots & \vdots \\ -jm_{n,1} & -jm_{n,2} & \cdots & \frac{1}{q_{en}}+p-jm_{n,n} \end{bmatrix} \tag{2-26}$$

Similarly, for the electric coupled model, by applying the Kirchhoff's current law to the equivalent circuit shown in Figure 2.13(b), the normalised admittance matrix $\overline{[Y]}$ can be obtained as well. It is interesting to find that $\overline{[Y]}$ shares the same form of $\overline{[Z]}$, which means a general matrix $[A]$ may describe all types of couplings in a filter (regardless of whether it is an electric coupling or a magnetic coupling). $[A]$ is formed by three matrices [3],

$$[A]=\begin{bmatrix} \frac{1}{q_{e1}} & 0 & \cdots & 0 \\ 0 & 0 & \cdots & 0 \\ \vdots & \vdots & \ddots & \vdots \\ 0 & 0 & \cdots & \frac{1}{q_{en}} \end{bmatrix}+p\begin{bmatrix} 1 & 0 & \cdots & 0 \\ 0 & 1 & \cdots & 0 \\ \vdots & \vdots & \ddots & \vdots \\ 0 & 0 & \cdots & 1 \end{bmatrix}-j\begin{bmatrix} m_{1,1} & m_{1,2} & \cdots & m_{1,n} \\ m_{2,1} & m_{2,2} & \cdots & m_{2,n} \\ \vdots & \vdots & \ddots & \vdots \\ m_{n,1} & m_{n,2} & \cdots & m_{n,n} \end{bmatrix} \tag{2-27}$$

or in a more generalised expression,

$$[A]=[q]+p[U]-j[m]$$

where $[q]$ is an $n\times n$ matrix with q_{e1} and q_{en} representing for the normalised external Q-factors, $[U]$ is an $n\times n$ unit matrix, $[m]$ is an $n\times n$ reciprocal matrix which is the so-called general coupling matrix. All the diagonal elements will be zeros when the filter is synchronously tuned.

Because the coupled-resonator equivalent circuit (Figure 2.13) is a two-port network (Figure 2.1), the *S*-parameters can be obtained by [3],

$$\begin{aligned} S11 &= \pm\left(1-\frac{2}{q_{e1}}\left[A\right]_{11}^{-1}\right) \\ S21 &= 2\frac{1}{\sqrt{q_{e1}\cdot q_{en}}}\left[A\right]_{n1}^{-1} \end{aligned} \tag{2-28}$$

With the help of coupling matrix theory, the design of coupled-resonator filter can be simplified and extracted as the synthesis of the general coupling matrix and external *Q*-factors.

2.5.2 Synthesis of Coupling Matrix and External *Q*-factors

The bandpass filters that can be described by standard transfer functions have *g*-values for their lowpass prototype equivalent circuits. These *g*-values are used in the synthesis of the external *Q*-factors and coupling coefficients for these filters. The corresponding equations are given as [3],

$$\begin{aligned} m_{i,i+1} &= \frac{M_{i,i+1}}{FBW} = \frac{1}{\sqrt{g_i\cdot g_{i+1}}} \qquad i = 1,2,\ldots,n-1 \\ q_{e1} &= Q_{e1}\cdot FBW = g_0\cdot g_1 \\ q_{en} &= Q_{en}\cdot FBW = g_n\cdot g_{n+1} \end{aligned} \tag{2-29}$$

However, the classical synthesis method may not work on more complicated cases. For the designs of more complex filters, other methods such as optimisation becomes a more practical solution, but the classical synthesis method may still make contributions as it provides good starting values for the optimisation [18-20].

2.6 Polynomial Representations of Transfer Functions

This section discusses the polynomial representation of transfer functions, as it is involved in the multi-passband filter synthesis technique which is presented in Chapter 3.

Generally, for any lossless two-port filter network with n inter-coupled resonators, the transfer function can be defined by a ratio of two polynomials [17]. To begin with, here is the well-known amplitude squared transfer function that defines any two-port lossless filter network [3],

$$\left|S21(s)\right|^2 = \frac{1}{1+\varepsilon^2 \cdot \left|D_n(s)\right|^2} \tag{2-30}$$

where $s = \sigma + j\Omega$ is the complex frequency variable, $D_n(s)$ is the characteristic function which determines an n^{th} order filter response. $D_n(s)$ can be expressed by a ratio of two polynomials,

$$D_n(s) = \frac{F_n(s)}{P_n(s)} \tag{2-31}$$

The $F_n(s)$ and $P_n(s)$ together with another polynomial $E_n(s)$ are the so-called characteristic polynomials, which can be used to define the *S*-parameters as shown in (2-32) [19],

$$\begin{aligned} S11(s) &= \frac{F_n(s)}{E_n(s)} \\ S21(s) &= \frac{P_n(s)/\varepsilon}{E_n(s)} \end{aligned} \tag{2-32}$$

where the ripple constant ε for Chebyshev response is defined as below in order to normalise the equal ripple level of $S21$ at $\Omega = \pm 1$ [19],

$$\varepsilon = \frac{1}{\sqrt{10^{\frac{RL}{10}} - 1}} \cdot \left.\frac{P_n(s)}{F_n(s)}\right|_{s=j} \tag{2-33}$$

here *RL* is the passband return loss level in dB.

It can be observed from (2-32) that $S11(s)$ and $S21(s)$ share the same denominator which is $E_n(s)$. Since $P_n(s)/\varepsilon$ is the numerator of $S21(s)$, it determines the transmission zeros of the

filter's response. For the same logic, $F_n(s)$ determines the reflection zeros. What should be noticed is that all of the three characteristic polynomials are assumed to be normalised (the coefficient of highest order term is unity) [4].

Thanks to their natural relationships with transmission zeros and reflection zeros, the characteristic polynomials can always be defined in terms of their roots,

$$\begin{aligned} P_n(s) &= \prod_{i=1}^{n_z}(s - TZ_i) \\ F_n(s) &= \prod_{i=1}^{n}(s - RZ_i) \end{aligned} \tag{2-34}$$

where TZ_i and RZ_i represent the frequency points of the transmission zeros and reflection zeros on the normalised frequency domain, respectively; n_z represent the number of the finite frequency transmission zeros; the number of the reflection zeros is always the same as the order of the filter, which is *n* in this case.

With $P_n(s)$ and $F_n(s)$ known, as long as $E_n(s)$ is obtained, the *S*-parameters can be determined. By using alternating pole method, $E_n(s)$ can be obtained. Since these three characteristic polynomials are not independent from each other, they can be expressed in one equation by applying the conservation of energy law [4],

$$\begin{aligned} S11(s)S11(s)^* + S21(s)S21(s)^* &= 1 \\ F_n(s)F_n(s)^* + \frac{1}{\varepsilon^2}P_n(s)P_n(s)^* &= E_n(s)E_n(s)^* \end{aligned} \tag{2-35}$$

where $*$ denotes the complex conjugate. Since $P_n(s)$ and $F_n(s)$ are known, by applying polynomial multiplications to the left hand side of (2-35), $E_n(s)E_n(s)^*$ can be obtained. There will be 2*n* roots of $E_n(s)E_n(s)^*$ on the complex plane; they are symmetrical to the

imaginary axis. The roots of $E_n(s)$ is strictly Hurwitz polynomial, which satisfies two conditions:

- The polynomial is real when *s* is real;
- The roots have non-positive real parts.

Therefore, the roots of $E_n(s)E_n(s)^*$ on the left half plane have to belong to $E_n(s)$, while the roots on the right half plane belong to $E_n(s)^*$. Hence, $E_n(s)$ is obtained [4].

References:

1. Pozar, D.M., *Microwave Engineering (Third Edition)*2005: John Wiley & Sons, Inc.
2. Zhou, J., *Microwave and Millimeter Wave Technologies from Photonic Bandgap Devices to Antenna and Applications*, ed. I. 2010, Online: Intech.
3. Hong, J.-S. and M.J. Lancaster, *Microstrip Filters for RF/Microwave Applications* 2001: John Wiley and Sons Ltd, United Kingdom.
4. Cameron, R.J., R. Mansour, and C.M. Kudsia, *Microwave Filters for Communication Systems: Fundamentals, Design and Applications,* 2007, Wiley.
5. Darlington, S., *Synthesis of Reactance 4-poles which Produce Prescribed Insertion Loss Characteristics: Including Special Applications to Filter Design* 1939: Columbia university.
6. Saal, R. and E. Ulbrich, "On the Design of Filters by Synthesis," *IRE Transactions on Circuit Theory*, 1958. **5**(4): p. 284-327.
7. Matthaei, G.L., L. Young, and E.M.T. Jones, *Microwave filters, impedance-matching networks, and coupling structures* 1964: McGraw-Hill.
8. Rhodes, J.D., *Theory of Electrical Filters* 1976: Wiley.
9. Rhodes, J.D. and S.A. Alseyab, "The generalized chebyshev low-pass prototype filter," *International Journal of Circuit Theory and Applications*, 1980. **8**(2): p. 113-125.
10. Hong, J.-S. and M.J. Lancaster, "Design of highly selective microstrip bandpass filters with a single pair of attenuation poles at finite frequencies,". *IEEE Transaction on Microwave Theory and Techniques*, 2000. **48**(7): p. 1098-1107.
11. Levy, R., "Filters with Single Transmission Zeros at Real or Imaginary Frequencies," *IEEE Transaction on Microwave Theory and Techniques*, 1976. **24**(4): p. 172-181.
12. Collin, R.E., *Foundations for Microwave Engineering* 2001: Wiley.
13. Atia, A.E., A.E. Williams, and R.W. Newcomb, "Narrow-band multiple-coupled cavity synthesis," *IEEE Transaction on Circuits and Systems*, 1974. **21**(5): p. 649-655.
14. Atia, A.E. and A.E. Williams, "Narrow-Bandpass Waveguide Filters," *IEEE Transaction on Microwave Theory and Techniques*, 1972. **20**(4): p. 258-265.
15. Atia, A.E.W., A. E. , "New types of bandpass filters for satellite transponders," *COMSAT Tech*, 1971. **1**: p. 23.

16. Atia, A.E. and A.E. Williams. "Non-Minimum Phase, Optimum Amplitude, Bandpass Waveguide Filters. in Microwave Symposium," *IEEE G-MTT International*. 1973.
17. Cameron, R.J., "Advanced Filter Synthesis," *IEEE Microwave Magazine*, 2011. **12**(6): p. 42-61.
18. Cameron, R.J., "Advanced coupling matrix synthesis techniques for microwave filters," *IEEE Transaction on Microwave Theory and Techniques*, 2003. **51**(1): p. 1-10.
19. Cameron, R.J., "General coupling matrix synthesis methods for Chebyshev filtering functions," *IEEE Transaction on Microwave Theory and Techniques*, 1999. **47**(4): p. 433-442.
20. Lenoir, P., et al., "Synthesis and design of asymmetrical dual-band bandpass filters based on equivalent network simplification," *IEEE Transaction on Microwave Theory and Techniques*, 2006. **54**(7): p. 3090-3097.
21. Nicholson, G.L., "Development of Mathematical Design and Computer Program for a Gross Coupled Microwave Filter," School of Electronic, Electrcal and Computer Engineering 2009, University of Birmingham:. p. 233.

CHAPTER 3 A GENERALISED ANALYTICAL SYNTHESIS TECHNIQUE FOR MULTI-PASSBAND FILTERS

3.1 Introduction

Conventionally, the well-known lowpass to bandpass frequency transformation maps the lowpass prototype response into a higher frequency band. (3-1) is another form of frequency transformation given in (2-15), which is used in the lowpass to bandpass frequency scaling procedure [1],

$$\Omega = B(\omega) = \frac{\omega_o}{BW}\left(\frac{\omega}{\omega_o} - \frac{\omega_o}{\omega}\right) \tag{3-1}$$

where ω is the frequency variable in de-normalised frequency domain; Ω is the frequency variable for lowpass prototype in normalised frequency domain; ω_o is the centre frequency of the de-normalised passband; BW is the equal ripple bandwidth of the de-normalised passband. Figure 3.1 gives a more illustrative view of the de-normalised procedure based on (3-1), where ω_L and ω_H are the lower and higher passband limits, respectively.

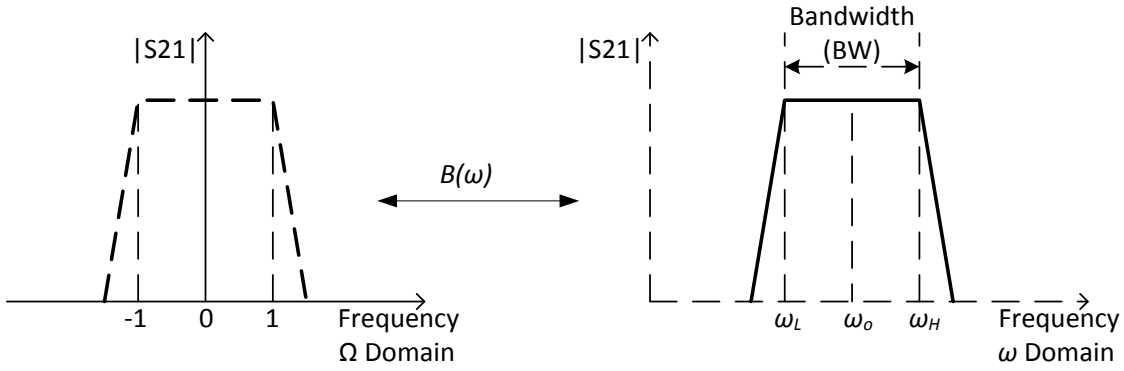

Figure 3.1 The conventional de-normalised procedure for bandpass filter

Now, let us consider another situation, by applying a new frequency transformation $M(\omega)$, the lowpass prototype response is mapped into multiple higher frequency bands in one de-normalising procedure. Figure 3.2 gives an illustrative view of this procedure, where ω_{Li} and ω_{Hi} are the passband limits for i^{th} passband.

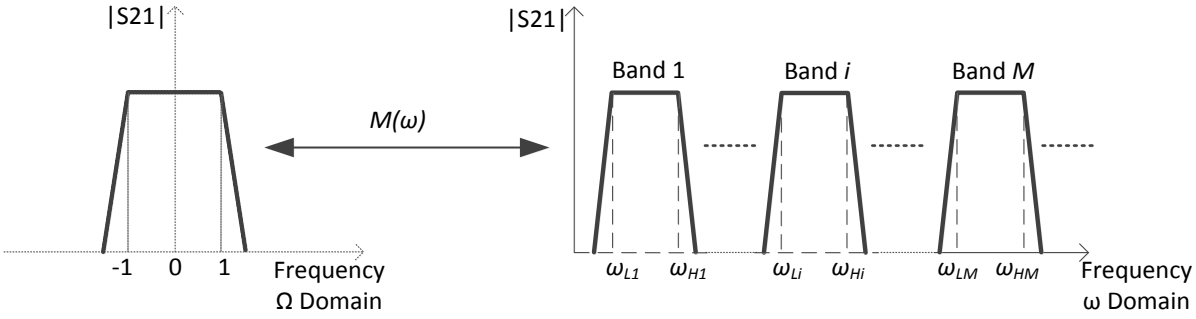

Figure 3.2 The de-normalised procedure for multi-passband filter

Starting with the dual-passband synthesis technique which was investigated by Macchiarella [2], followed by two triple-passband synthesis techniques which were investigated by Chen and Hao [3, 4], this chapter will go through the synthesis technique step by step. At the end, a new generalised approach of multi-passband filter design is given; it gives an analytical solution including coupling matrix, external *Q*-factors and *S*-parameters. At the end of the chapter, three design examples of five-passband filter is presented for verification of the novel generalised approach.

3.2 Dual-Passband Filter Synthesis Technique

The technique described here provides a method that can design a dual-passband filter through an analytical synthesis procedure. What makes this technique distinct from the others is that it produces arbitrary asymmetrical bandwidths and controls the positions of the stopband without involvement of numerical optimisation [2]. This synthesis technique derives the so-called interim parameters (the resonant frequency and the susceptance slope parameter of each resonator) directly from the desired passband limits; the interim parameters together with the *J*-values from the lowpass prototype are sufficient for calculating the full filter design parameters (coupling matrix and external *Q*-factors). This analytical method is more effective than optimisation methods. However, since the synthesis procedure is sophisticated, an example will be given first, and then followed by a discussion about more generalised dual-passband filter structure.

3.2.1 A 4th Order Dual-Passband Filter with Chebyshev Response

For the sake of simplicity, a 4th order dual-passband filter is used as an example here to illustrate the synthesis procedure.

The synthesis procedure has two steps. The first step is the synthesis of a 2nd order all-pole Chebyshev lowpass prototype which is described in Chapter 2; the second step is applying the lowpass to dual-passband frequency transformation $D(\omega)$ which maps the lowpass prototype response into a dual-passband de-normalised response. Figure 3.3 below illustrates the transformation procedure,

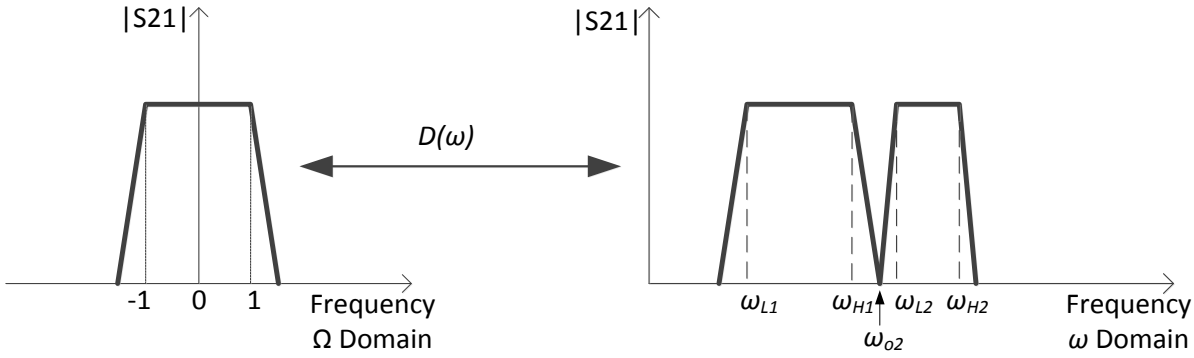

Figure 3.3 Lowpass to dual-passband frequency transformation procedure

where ω_{L1}, ω_{H1} are the passband limits for first band; ω_{L2}, ω_{H2} are the passband limits for second band; they are the passband specifications of the filter. ω_{o2} is the frequency of the transmission zero between the passbands. The two passbands don't need to be symmetrical or share equal bandwidth. However, each passband will have the same shape of in-band and out-of-band response [2], and this is determined by the lowpass prototype response.

The corresponding dual-passband frequency transformation which is used for the above de-normalising procedure is given in [2],

$$\Omega = D(\omega) = b_1\left(\frac{\omega}{\omega_{o1}} - \frac{\omega_{o1}}{\omega}\right) - \frac{1}{b_2\left(\frac{\omega}{\omega_{o2}} - \frac{\omega_{o2}}{\omega}\right)} \tag{3-2}$$

where b_1, ω_{o1}, b_2 and ω_{o2} together fully define the above frequency transformation (3-2). It is worth mentioning that, other than defining the frequency transformation, these four interim parameters also physically define all resonators in the proposed dual-passband filter. Among them, b_1 and b_2 are the susceptance slope parameters, ω_{o1} and ω_{o2} are the resonant frequencies of resonators. More details are given in the following paragraphs.

The topology of a 4th order dual-passband filter is shown in Figure 3.4(a), with all the relevant design parameters labelled. Meanwhile, the equivalent circuits correspond to the

topology are given in Figure 3.4(b) and Figure 3.4(c), labelled with the interim parameters and the *J*-inverters that are connected to the bandpass resonators. Among the interim parameters, b_1 and ω_{o1} describe the bandpass resonator 1 and 2, b_2 and ω_{o2} describe the bandstop resonator 3 and 4;

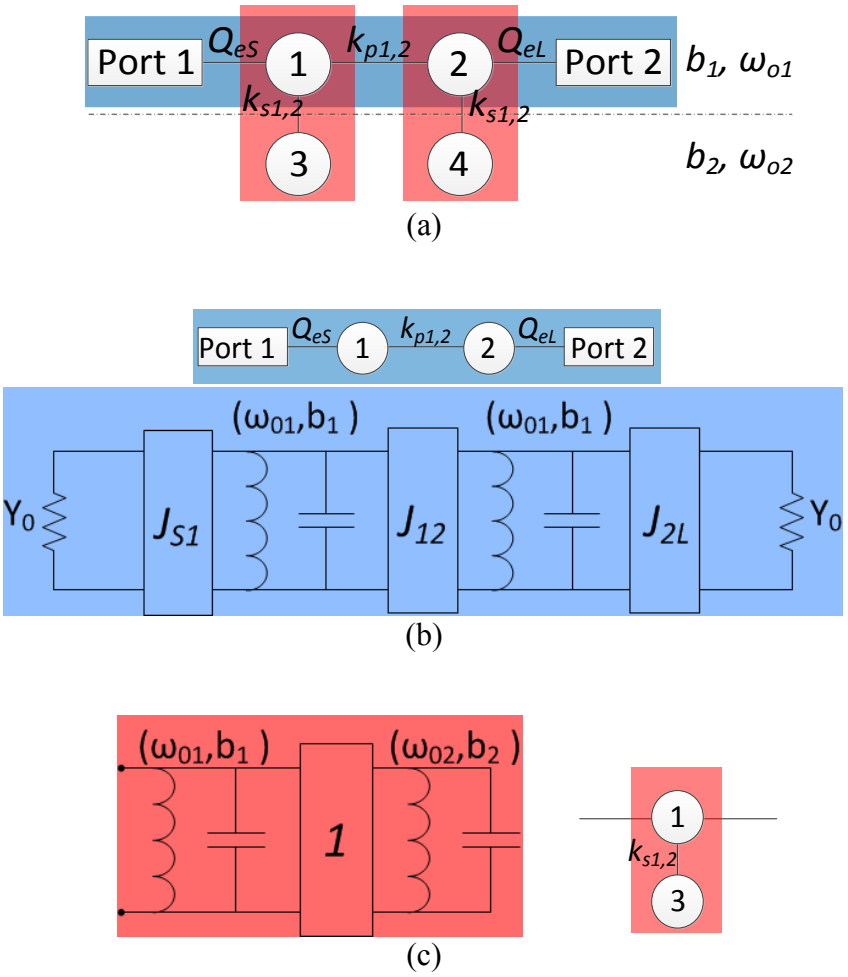

Figure 3.4 (a) The topology of a 4th order dual-passband filter, (b) The equivalent circuit for bandpass resonators and ports, (c) The equivalent circuit for multi-passband resonator section

Figure 3.4(a) shows the 4th order dual-passband topology, where the circles represent the resonators; the solid lines represent the direct couplings.

The two bandpass resonators together with the two ports are labelled in blue. Q_{eS} and Q_{eL} are the external Q-factors to source and load, respectively. $k_{p1,2}$ is the coupling between two bandpass resonators [2].

A bandpass resonator and the bandstop resonator coupled to it forms a so-called multi-passband resonator section (in this example, resonator 1 and 3 forms one section, resonator 2 and 4 forms the other one). Such sections are labelled in red. Both sections share the same topology, and $k_{s1,2}$ is the coupling between the bandpass and the bandstop resonator.

Figure 3.4(b) shows the equivalent circuit for the blue part of the topology. Y_0 is the normalised admittance, J_{12} is the value of J-inverter between resonator 1 and 2, J_{S1} and J_{2L} are the values of J-inverters that connected to the two ports. ω_{o1} and b_1 are the frequency and the susceptance slope parameter, respectively, for both bandpass resonators. This blue part alone produces a 2nd order all-pole Chebyshev response.

Figure 3.4(c) shows the equivalent circuit of the red parts of the topology. Because both sections in the filter share the same topology, this equivalent circuit applies to both sections. The value of J-inverter between the bandpass resonator and the bandstop resonator is 1. ω_{o2} and b_2 are the frequency and the susceptance slope parameter, respectively, for both bandstop resonators.

The susceptance slope parameter b_i and the resonant frequency ω_{oi} are physically defined by (3-3) and (3-4), respectively, where L_i and C_i are the equivalent inductance and capacitance of the corresponding resonator [5].

$$b_i = \omega_{oi} \cdot C_i \tag{3-3}$$

$$\omega_{oi} = \frac{1}{\sqrt{L_i \cdot C_i}} \tag{3-4}$$

The corresponding coupling matrix of the 4th order dual-passband filter shown in Figure 3.4(a) is given below in (3-5),

$$[M]=\begin{pmatrix} k_1 & k_{p1,2} & k_{s1,2} & 0 \\ k_{p1,2} & k_1 & 0 & k_{s1,2} \\ k_{s1,2} & 0 & k_2 & 0 \\ 0 & k_{s1,2} & 0 & k_2 \end{pmatrix} \tag{3-5}$$

The elements in coupling matrix and the external Q-factors can be synthesized through the (3-6) to (3-11) shown below,

k_p is the coupling between bandpass resonators [1, 5],

$$k_{p1,2}=\frac{J_{12}}{b_1}=\frac{1}{b_1\sqrt{g_1\cdot g_2}} \tag{3-6}$$

k_s is the coupling between bandpass and bandstop resonators [5],

$$k_{s1,2}=\frac{1}{\sqrt{b_1\cdot b_2}} \tag{3-7}$$

k_i is the self-coupling [6],

$$k_i=\frac{\omega_{oi}}{\omega_o}-\frac{\omega_o}{\omega_{oi}}\ (i=1,2) \tag{3-8}$$

It is worth mentioning that the above centre frequency ω_o here is obtained from,

$$\omega_o=\sqrt{\omega_{L1}\cdot\omega_{H2}} \tag{3-9}$$

Q_{eS} is the external Q-factor to source [1, 5],

$$Q_{eS}=\frac{b_1}{J_{S1}^{\ 2}}=b_1\cdot g_0\cdot g_1 \tag{3-10}$$

Q_{eL} is the external Q-factor to load [1, 5],

$$Q_{eL} = \frac{b_1}{J_{2L}^{\ 2}} = b_1 \cdot g_2 \cdot g_3 \tag{3-11}$$

The values of J-inverters can be obtained from the standard all-pole Chebyshev filter synthesis procedure that is discussed in Chapter 2.

A relationship between the interim parameters (ω_{o1} , ω_{o2} , b_1 , b_2) and the passband specifications ($\omega_{L1}, \omega_{L2}, \omega_{H1}, \omega_{H2}$) for the proposed dual-passband filter was discovered in [2]. The relationship is established by the frequency transformation.

By applying the frequency transformation in (3-2), the two lower passband limits ω_{L1} and ω_{L2} on de-normalised frequency domain can be mapped to -1 on normalised frequency domain; similarly, the two higher passband limits ω_{H1} and ω_{H2} can be mapped to 1 (see Figure 3.3). Taken into consideration that (3-2) is an odd function, it can be expressed as:

$$D(-\omega_{L1}) = D(-\omega_{L2}) = D(\omega_{H1}) = D(\omega_{H2}) = 1 \tag{3-12}$$

Let

$$VD(\omega) = D(\omega) - 1 \tag{3-13}$$

Then, it can be easily observed that $-\omega_{L1}$, $-\omega_{L2}$, ω_{H1} and ω_{H2} are the zeros of $VD(\omega)$. Meanwhile, $VD(\omega)$ can be also expressed as,

$$VD(\omega) = \frac{ZD(\omega)}{PD(\omega)} = \frac{\omega^4 + z_3\omega^3 + z_2\omega^2 + z_1\omega + z_0}{p_3\omega^3 + p_2\omega^2 + p_1\omega + p_0} \tag{3-14}$$

The coefficient of the highest order term has been normalised. $ZD(\omega)$ is the numerator, $PD(\omega)$ is the denominator, z_i (i=0,1,2,3) is the coefficient of the polynomial $ZD(\omega)$, p_i (i=0,1,2,3) is the coefficient of the polynomial $PD(\omega)$. $ZD(\omega$, plays an important role in establishing the relationship between the interim parameters (ω_{o1} , ω_{o2} , b_1 , b_2) and the passband specifications (ω_{L1} , ω_{L2} , ω_{H1} , ω_{H2}), because z_i (i=0,1,2,3) can be analytically derived from two separated ways.

One way of deriving z_i (i=0,1,2,3) is by combining the (3-2), (3-13) and (3-14), which leads to the result shown in (3-15); z_i (i=0,1,2,3) are expressed in terms of the interim parameters ($\omega_{o1}, \omega_{o2}, b_1, b_2$) [2],

$$
\begin{aligned}
z_3 &= -\frac{\omega_{o1}}{b_1} \\
z_2 &= -{\omega_{o1}}^2 - {\omega_{o2}}^2 - \frac{\omega_{o1}}{b_1} - \frac{\omega_{o2}}{b_2} \\
z_1 &= \frac{\omega_{o1}}{b_1} \cdot {\omega_{o2}}^2 \\
z_0 &= {\omega_{o1}}^2 \cdot {\omega_{o2}}^2
\end{aligned}
\tag{3-15}
$$

At the same time, since $-\omega_{L1}$, $-\omega_{L2}$, ω_{H1} and ω_{H2} are the roots of $VD(\omega)$, they are also the roots of $ZD(\omega)$. Therefore z_i (i=0,1,2,3) can also be derived in another way, which are expressed in terms of passband specifications ($\omega_{L1}, \omega_{L2}, \omega_{H1}, \omega_{H2}$) [2]. The result is shown in (3-16):

$$
\begin{aligned}
z_3 &= \omega_{L1} + \omega_{L2} - \omega_{H1} - \omega_{H2} \\
z_2 &= \omega_{L1} \cdot \omega_{L2} + \omega_{H1} \cdot \omega_{H2} - \left(\omega_{L1} + \omega_{L2}\right) \cdot \left(\omega_{H1} + \omega_{H2}\right) \\
z_1 &= \omega_{H1} \cdot \omega_{H2} \cdot \left(\omega_{L1} + \omega_{L2}\right) - \omega_{L1} \cdot \omega_{L2} \cdot \left(\omega_{H1} + \omega_{H2}\right) \\
z_0 &= \omega_{L1} \cdot \omega_{L2} \cdot \omega_{H1} \cdot \omega_{H2}
\end{aligned}
\tag{3-16}
$$

So far, the relationship between the passband specifications ($\omega_{L1}, \omega_{L2}, \omega_{H1}, \omega_{H2}$) and the interim parameters ($\omega_{o1}, \omega_{o2}, b_1, b_2$) has been established through z_i (i=0,1,2,3). As long as the passband specifications ($\omega_{L1}, \omega_{L2}, \omega_{H1}, \omega_{H2}$) are given, the interim parameters (ω_{o1}, ω_{o2}, b_1, b_2) can be obtained.

(3-15) can be re-written in the form of (3-17), which describes the interim parameters (ω_{o1}, ω_{o2}, b_1, b_2) in terms of z_i (i=0,1,2,3),

$$\begin{aligned}
\omega_{o1} &= \sqrt{-\frac{z_0 \cdot z_3}{z_1}} \\
\omega_{o2} &= \sqrt{-\frac{z_1}{z_3}} \\
b_1 &= \sqrt{-\frac{z_0}{z_1 \cdot z_3}} \\
b_2 &= \frac{z_1 \cdot z_3^{\,2}}{z_1 \cdot z_2 \cdot z_3 - z_1^{\,2} - z_0 \cdot z_3^{\,2}} \cdot \sqrt{-\frac{z_1}{z_3}}
\end{aligned} \tag{3-17}$$

At this stage, the interim parameters ($\omega_{o1}, \omega_{o2}, b_1, b_2$) can be synthesised directly from the desired passband specifications ($\omega_{L1}, \omega_{L2}, \omega_{H1}, \omega_{H2}$).

3.2.2 Generalised Topology for Dual-Passband Filter with Chebyshev Response

Now, let us consider a more generalised dual-passband filter which contains 2n resonators. The topology is shown below in Figure 3.5.

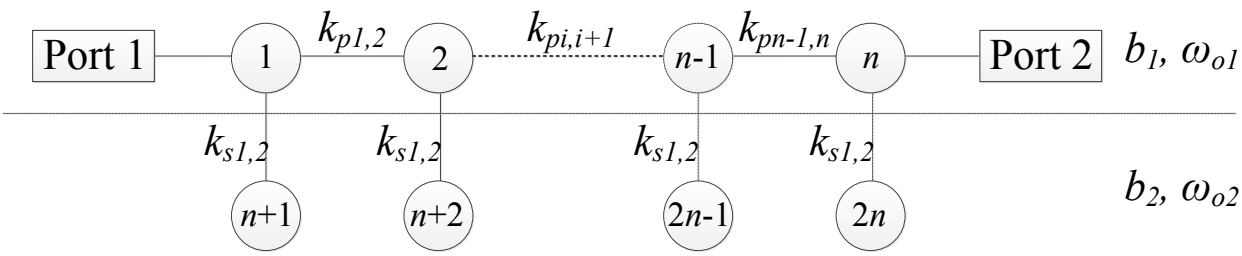

Figure 3.5 Generalised topology of the dual-passband filter with Chebyshev response

Resonator 1 to n are the bandpass resonators, all of them are resonating at ω_{o1}; resonator n+1 to 2n are the bandstop resonators, all of them are resonating at ω_{o2}. There are n identical multi-passband resonator sections in this 2n^{th} order filter. The section is the periodic unit of the dual-passband filter; it can be seen as the basic building blocks of the structure [3]. For generalised dual-passband filter topology, the frequency transformation in (3-2) is still valid; the response of this generalised topology still has two passbands, but each passband will have an n^{th} order Chebyshev response.

For the generalised 2n^{th} order dual-passband filter with Chebyshev response, (3-7), (3-8) and (3-10) are still valid; k_p (coupling between bandpass resonators) and Q_{eL} (external Q-factor to load) can be re-written in more generalise forms, which are given below in (3-18) and (3-19).

$$k_{pi,i+1} = \frac{J_{i,i+1}}{b_1} = \frac{1}{b_1\sqrt{g_i \cdot g_{i,i+1}}} \quad (i=1,2,\ldots,n\text{-}1) \tag{3-18}$$

$$Q_{eL} = \frac{b_1}{J_{nL}^{\ 2}} = b_1 \cdot g_n \cdot g_{n+1} \tag{3-19}$$

3.2.3 The Verification

Two examples are given to validate the synthesis technique and to demonstrate the practical design procedure. A 4th order symmetrical dual-passband filter which is based on the topology shown in Figure 3.4(a) is synthesised step by step in example 1. This is followed by another design of a 10th order asymmetrical dual-passband filter, which is given in example 2 to show the flexibility of this synthesis technique.

3.2.3.1 Example 1: A 4th Order Even Dual-Passband Filter with Chebyshev Response

The topology is given in Figure 3.4(a), so it is not repeated here. The two passband of this filter are arbitrarily chosen at 9.13-9.59GHz and 10.06-10.52GHz, but the bandwidths are equal. The maximum return loss for both passband is chosen to be 20dB. The passband specifications and the corresponding interim parameters are given in Table 3.1,

Passband specifications	**Interim parameters**
$\omega_{L1} = 9.13GHz$	$\omega_{o1} = 9.78GHz$
$\omega_{H1} = 9.59GHz$	$\omega_{o2} = 9.82GHz$
$\omega_{L2} = 10.06GHz$	$b_1 = 10.52$
$\omega_{H2} = 10.52GHz$	$b_2 = 14.36$

Table 3.1 The passband specifications and interim parameters for Example 1

Below are the *g*-values of a standard 2nd order lowpass prototype Chebyshev filter with 20dB return loss, which are given in Table 3.2. The *S*-parameters are given in Figure 3.6.

g_0	g_1	g_2	g_3
1	0.6648	0.5445	1.2210

Table 3.2 The *g*-values of a 2nd order Chebyshev filter with passband return loss at 20dB

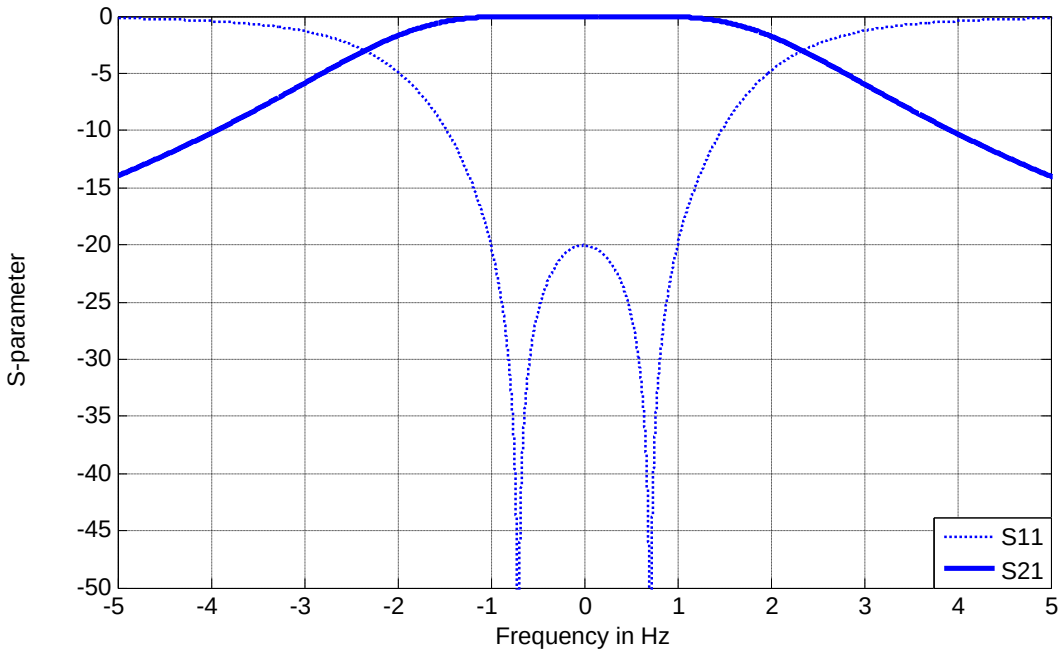

Figure 3.6 A 2nd order lowpass prototype Chebyshev response with 20dB return loss

As shown in Figure 3.6 above, the reflection zeros are placed at ±0.7071, while the transmission zeros are placed at ±∞. This lowpass response will be transformed into the desired two frequency bands which are given in Table 3.1.

With the above information, the dual-passband filters can now be synthesised. According to (3-6), (3-7) and (3-8), the coupling coefficients can be calculated; $k_{p1,2}$ is 0.1579, $k_{s1,2}$ is 0.0813, k_1 is -0.0041 and k_2 is 0.0041. They can be presented in a coupling matrix shown below,

$$[M]=\begin{pmatrix} -0.0041 & 0.1579 & 0.0813 & 0 \\ 0.1579 & -0.0041 & 0 & 0.0813 \\ 0.0813 & 0 & 0.0041 & 0 \\ 0 & 0.0813 & 0 & 0.0041 \end{pmatrix} \tag{3-20}$$

Also, according to (3-10) and (3-11), the external Q-factors ($Q_{eS}=Q_{eL}$) are obtained as 6.99.

The S-parameters are plotted using the characteristic polynomials. This is done by substituting (3-2) into (2-32), which is shown in (3-21). The ripple constant ε is defined by (2-33). The polynomial P and F are obtained by fitting curves to transmission zeros and reflection zeros of the lowpass prototype, respectively; the polynomial E can be obtained from **(2-35)**, once P and F are known.

$$\begin{aligned} S11(s) &= \frac{F_n\left(jD(\omega)\right)}{E_n\left(jD(\omega)\right)} \\ S21(s) &= \frac{P_n\left(jD(\omega)\right)}{\varepsilon \cdot E_n\left(jD(\omega)\right)} \end{aligned} \tag{3-21}$$

The S-Parameters are shown in Figure 3.7.

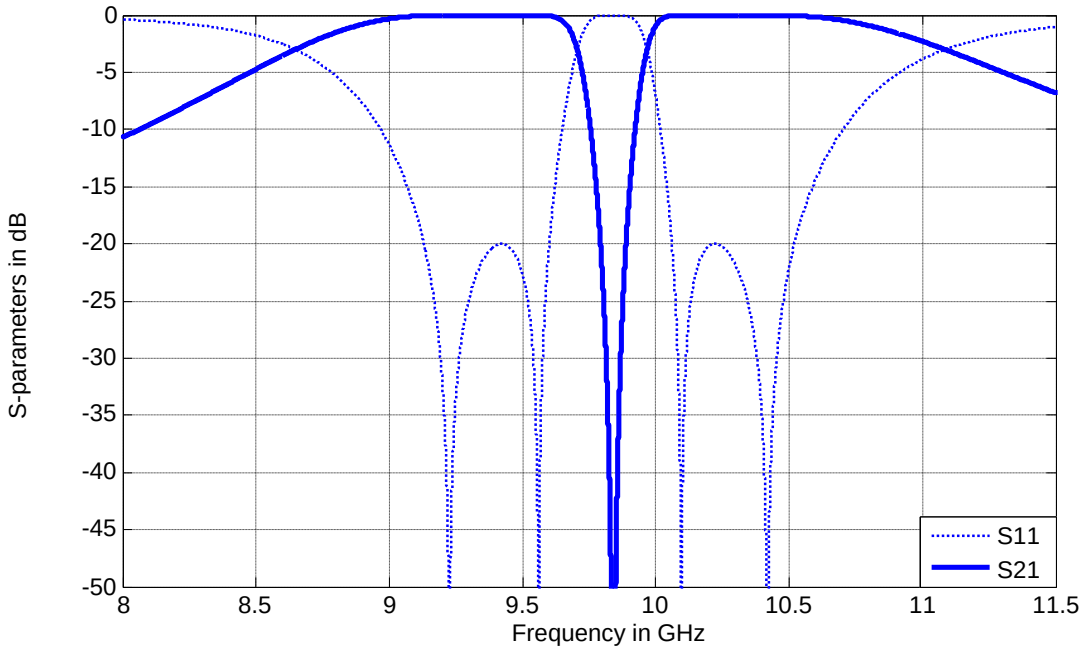

Figure 3.7 The *S*-parameter of a 4th order symmetrical dual-passband filter with Chebyshev response (Passband 1: 9.13 ~ 9.59 GHz, Passband 2: 10.06 ~ 10.52 GHz)

3.2.3.2 Example 2: A 10th Order Asymmetrical Dual-Passband Filter with Chebyshev Response

To be distinct from the previous example, the second one is a 10th order dual-passband filter, with passband return loss at 25dB; the topology is shown in Figure 3.8. The two passbands are arbitrarily chosen at 8.5-9.5GHz and 10.5-11GHz, with unequal bandwidths.

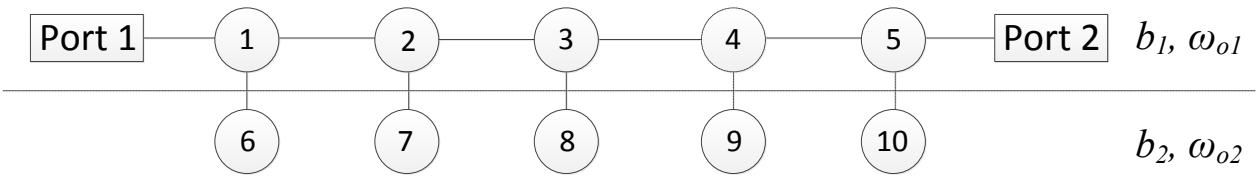

Figure 3.8 The topology of a 10th order dual-passband filter

Passband specifications	**Interim parameters**
$\omega_{L1} = 8.5GHz$	$\omega_{o1} = 9.47GHz$
$\omega_{H1} = 9.5GHz$	$\omega_{o2} = 10.19GHz$
$\omega_{L2} = 10.5GHz$	$b_1 = 6.32$
$\omega_{H2} = 11GHz$	$b_2 = 7.34$

Table 3.3 The passband specifications and interim parameters for Example 2

The *g*-values of the lowpass prototype 5th order Chebyshev filter with 25dB passband return loss is given in Table 3.4; the corresponding lowpass response is shown in Figure 3.9.

g_0	g_1	g_2	g_3	g_4	g_5	g_6
1	0.7956	1.3246	1.6202	1.3246	0.7956	1

Table 3.4 The *g*-values of a 5th order Chebyshev filter with passband return loss at 25dB

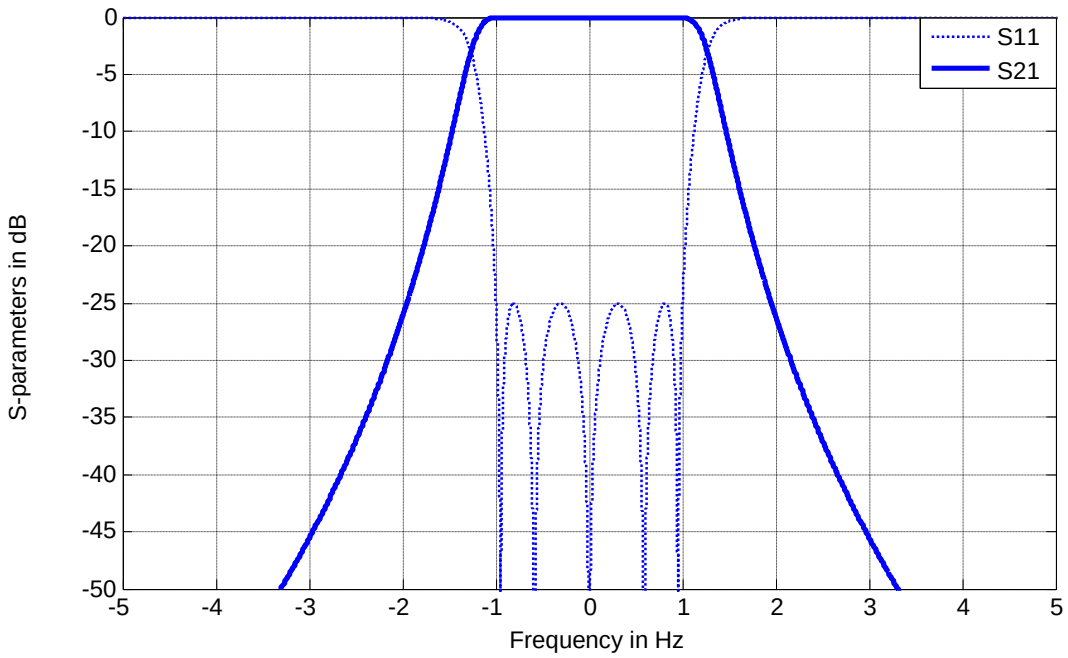

Figure 3.9 A 5th order lowpass prototype Chebyshev response with 25dB return loss

For the above lowpass prototype response, the five reflection zeros are placed at ±0.9511, ±0.5878 and 0, while the transmission zeros are still at ±∞. This lowpass response will be transformed into the desired two frequency bands which are given in Table 3.3.

According to (3-7), (3-8) and (3-18), the coupling matrix can be obtained as below,

$$[M]=\begin{pmatrix} -0.0417 & 0.1542 & 0 & 0 & 0 & 0.1468 & 0 & 0 & 0 & 0 \\ 0.1542 & -0.0417 & 0.1081 & 0 & 0 & 0 & 0.1468 & 0 & 0 & 0 \\ 0 & 0.1081 & -0.0417 & 0.1081 & 0 & 0 & 0 & 0.1468 & 0 & 0 \\ 0 & 0 & 0.1081 & -0.0417 & 0.1542 & 0 & 0 & 0 & 0.1468 & 0 \\ 0 & 0 & 0 & 0.1542 & -0.0417 & 0 & 0 & 0 & 0 & 0.1468 \\ 0.1468 & 0 & 0 & 0 & 0 & 0.1010 & 0 & 0 & 0 & 0 \\ 0 & 0.1468 & 0 & 0 & 0 & 0 & 0.1010 & 0 & 0 & 0 \\ 0 & 0 & 0.1468 & 0 & 0 & 0 & 0 & 0.1010 & 0 & 0 \\ 0 & 0 & 0 & 0.1468 & 0 & 0 & 0 & 0 & 0.1010 & 0 \\ 0 & 0 & 0 & 0 & 0.1468 & 0 & 0 & 0 & 0 & 0.1010 \end{pmatrix} \tag{3-22}$$

Also, according to (3-10) and (3-19), the external Q-factor ($Q_{eS} = Q_{eL}$) is 5.03.

The S-parameters are plotted using the same method shown in example 1; the results are given in Figure 3.10.

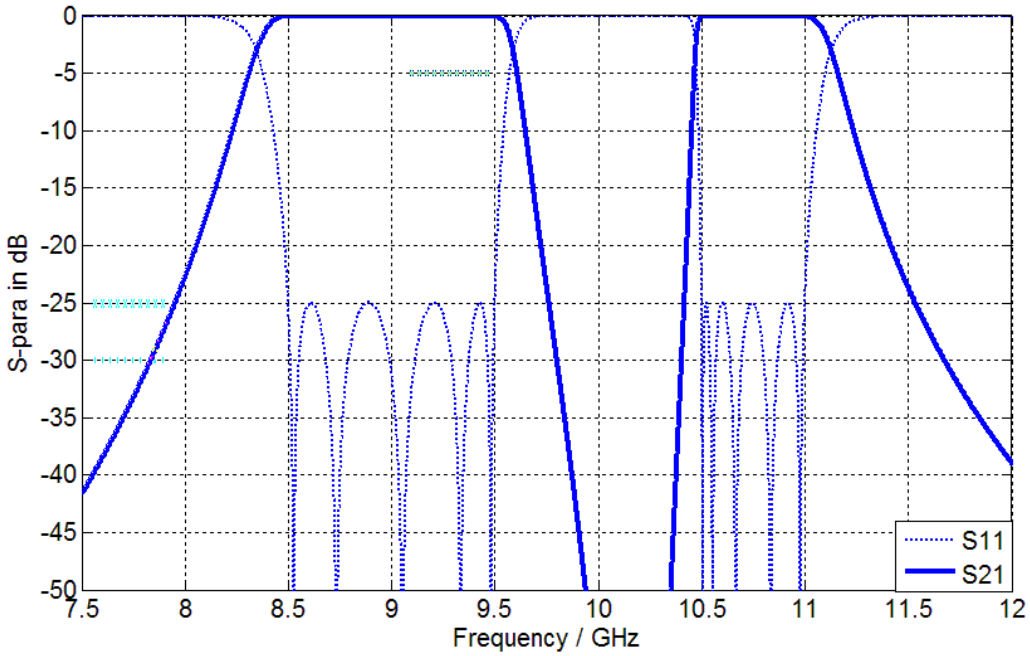

Figure 3.10 The S-parameter of a 10th order uneven dual-passband filter with Chebyshev response (Passband 1: 8.5 ~ 9.5 GHz, Passband 2: 10.5 ~ 11 GHz)

3.2.4 Conclusion

The full synthesis procedure is shown in a flowchart in Figure 3.11. For each step, a MATLAB computation takes less than 1 second to get all the results using a Core i5 processor computer with 3 GB usable memory (this includes plotting the *S*-parameter which contains 20002 points).

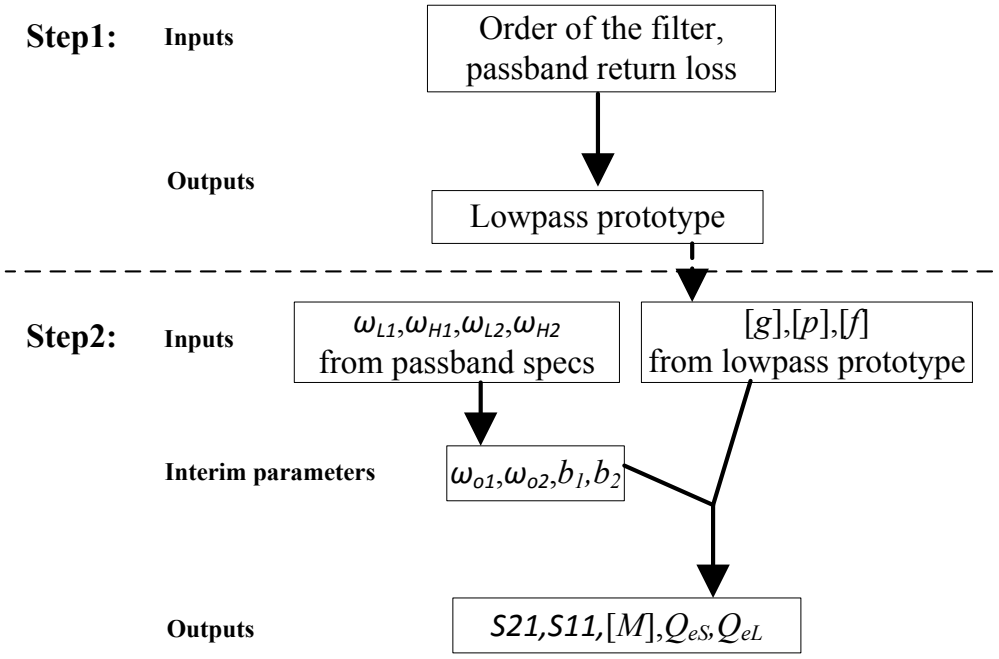

Figure 3.11 The flowchart of the dual-passband filter synthesis procedure

The first step has been discussed in Chapter 2. For the second step, the input variables are [*p*], [*f*], [*g*], and the passband specifications (ω_{L1}, ω_{L2}, ω_{H1}, ω_{H2}), where [*p*] is a matrix that contains the positions of transmission zeros of the lowpass prototype response. In this case, because it is an all-pole Chebyshev response, all the transmission zeros are at infinity. The transmission zeros mentioned here are for the lowpass prototype response. They are not the transmission zeros of the de-normalised response, i.e. the dual-passband filter response. The transmission zeros of the de-normalised responses are generated by the bandstop resonators. [*f*] is a matrix that contains the positions of reflection zeros of the lowpass prototype; [*g*] is a matrix that contains the *g*-values of the lowpass prototype. The interim parameters (ω_{o1}, ω_{o2},

b_1, b_2) which define the frequency transformation are synthesised directly from the passband specifications. The final outputs include *S*-parameters and design parameters.

3.3 Triple-Passband Filter Synthesis Techniques

Similar to the previous section, two analytical synthesis techniques which synthesise triple-passband filters with Chebyshev response are discussed in this section. The two synthesis techniques involve two different forms of frequency transformations which correspond to different topologies of multi-passband resonator sections, but both of them produce triple-passband response. Finite order filter examples will be given first to help the theory explanation, and then follows by a discussion on a more generalised filter topology. At the end of this section, design examples are given for verification.

3.3.1 Triple-Passband Synthesis Technique 1

Similar to that of the dual-passband filter, the triple-passband synthesis technique 1 also follows the two steps; the only difference is that, for the second step, the frequency transformation maps the lowpass prototype response into three frequency bands. Therefore, the discussion below only focuses on the second step. Figure 3.12 gives an illustrative view of the mapping procedure for the triple-passband synthesis technique 1, where ω_{L1}, ω_{H1}, ω_{L2}, ω_{H2}, ω_{L3} and ω_{H3} are the passbands specifications. ω_{o2} and ω_{o3} are the frequency points of the transmission zeros in the de-normalised response. The three passbands don't need to have equal bandwidth. They can have arbitrary passband centre frequencies and bandwidths.

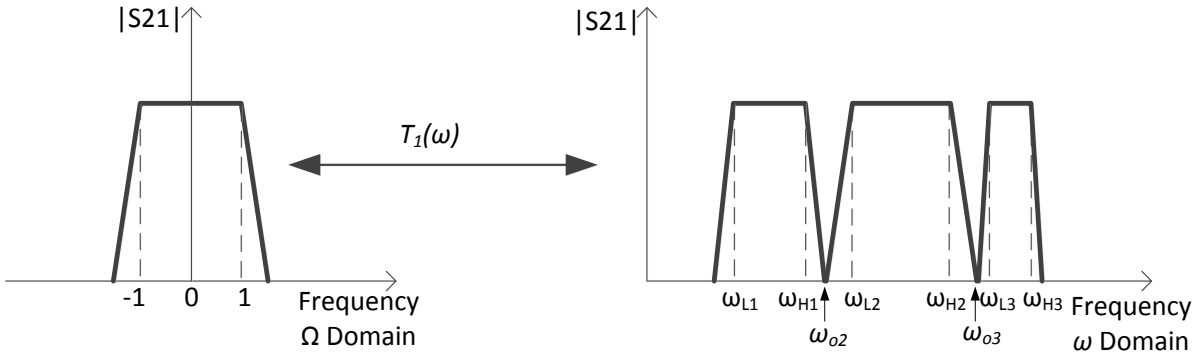

Figure 3.12 Lowpass to triple-passband frequency transformation procedure (Technique 1)

The frequency transformation is given below [3],

$$\Omega = T_1(\omega) = b_1\left(\frac{\omega}{\omega_{o1}} - \frac{\omega_{o1}}{\omega}\right) - \frac{1}{b_2\left(\frac{\omega}{\omega_{o2}} - \frac{\omega_{o2}}{\omega}\right)} - \frac{1}{b_3\left(\frac{\omega}{\omega_{o3}} - \frac{\omega_{o3}}{\omega}\right)} \tag{3-23}$$

All the notations in (3-23) are defined under the same way as the previous dual-passband example. b_1, ω_{o1}, b_2, ω_{o2}, b_3 and ω_{o3} are the interim parameters that define the frequency transformation .

A 6th order triple-passband filter with Chebyshev response is used as an example here to explain the synthesis procedure. The topology of the proposed 6th order triple-passband filter is shown in Figure 3.13(a), the equivalent circuits are given in Figure 3.13 (b) and Figure 3.13(c).

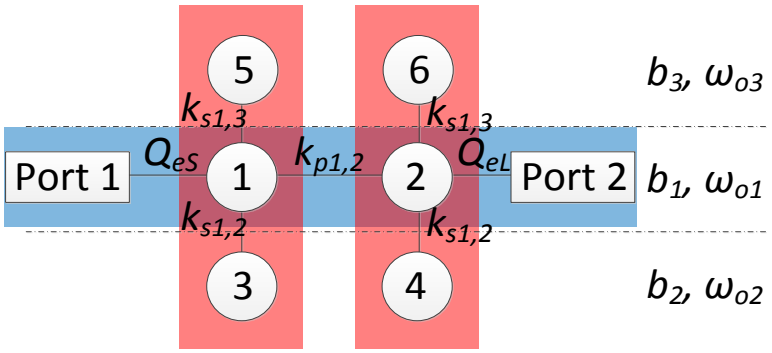

(a)

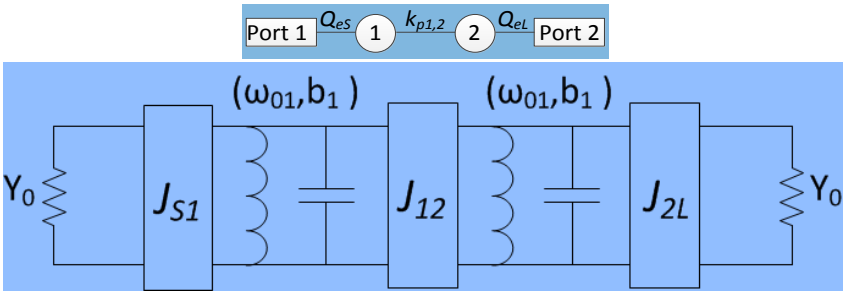

(b)

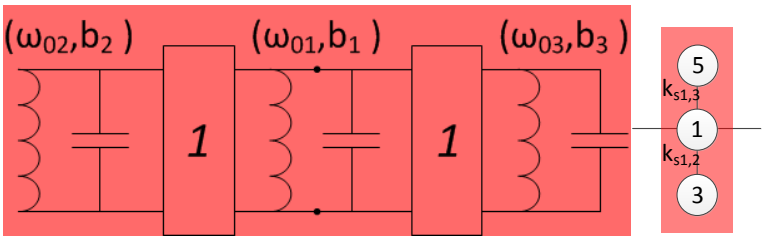

(c)

Figure 3.13 (a) The topology of a 6th order triple-passband filter, (b) The equivalent circuit for bandpass resonators and ports, (c) The equivalent circuit for multi-passband resonator section

Figure 3.13(a) shows a 6th order triple-passband filter topology. Resonator 1 and 2 are the bandpass resonators resonating at ω_{o1}; resonator 3 and 4 are the bandstop resonators resonating at ω_{o2}; resonator 5 and 6 are the bandstop resonators resonating at ω_{o3}. The bandpass resonators and ports are shown in blue, while the multi-passband resonator sections are shown in red. In this triple-passband filter, each multi-passband resonator section has two bandstop resonators, which are not resonating at the same frequency, directly coupled to the same bandpass resonator. Q_{eS} and Q_{eL} are the external Q-factors of the source and load, respectively. $k_{p1,2}$ represents the coupling between the bandpass resonators. $k_{s1,2}$ represents the coupling between the bandpass resonator and the bandstop resonator resonating at ω_{o2}. $k_{s1,3}$ represents the coupling between the bandpass resonator and the bandstop resonator resonating at ω_{o3}.

Figure 3.13(b) shows the equivalent circuit of the blue part in Figure 3.13(a), which produces a 2nd order all-pole chebyshev response. This part shares the same equivalent circuit as the one given in Figure 3.4(b), so it is not discussed again here.

Figure 3.13(c) shows the equivalent circuit of the multi-passband resonator section. The black nodes imply the points where the current section connected with the adjacent ones. b_2 is the susceptance slope parameter of the bandstop resonator resonating at ω_{o2}; b_3 is the susceptance slope parameter of the bandstop resonator resonating at ω_{o3}.

The susceptance slope parameter b_i (i=1,2,3) and the resonant frequency ω_{oi} (i=1,2,3) are defined by (3-3) and (3-4).

The corresponding coupling matrix of this 6th order triple-passband filter is given below,

$$[M]=\begin{pmatrix} k_1 & k_{p1,2} & k_{s1,2} & 0 & k_{s1,3} & 0 \\ k_{p1,2} & k_1 & 0 & k_{s1,2} & 0 & k_{s1,3} \\ k_{s1,2} & 0 & k_2 & 0 & 0 & 0 \\ 0 & k_{s1,2} & 0 & k_2 & 0 & 0 \\ k_{s1,3} & 0 & 0 & 0 & k_3 & 0 \\ 0 & k_{s1,3} & 0 & 0 & 0 & k_3 \end{pmatrix} \tag{3-24}$$

$k_{s1,3}$ can be calculated through

$$k_{s1,3}=\frac{1}{\sqrt{b_1 \cdot b_3}} \tag{3-25}$$

All other elements in matrix (3-24) and the external Q-factors can be synthesized by (3-6) to (3-11) and (3-25).

Although in [3], a similar triple-passband topology had been investigated, there were no equations presented the relationship between the interim parameters ($\omega_{o1}, \omega_{o2}, \omega_{o3}, b_1, b_2, b_3$)

and the passband specifications ($\omega_{L1}, \omega_{L2}, \omega_{H1}, \omega_{H2}, \omega_{L3}, \omega_{H3}$). The corresponding equations are first presented here.

The equations are obtained in a similar way that shown in dual-passband filter synthesis. The de-normalised lower passband limits ω_{L1}, ω_{L2} and ω_{L3} are mapped to -1 on the normalised frequency domain; the de-normalised higher passband limits ω_{H1}, ω_{H2} and ω_{H3} are mapped to 1 on the normalised frequency domain (see Figure 3.12). The frequency transformation $T_1(\omega)$ is an odd function, it can be expressed as:

$$T_1(-\omega_{L1}) = T_1(-\omega_{L2}) = T_1(-\omega_{L3}) = T_1(\omega_{H1}) = T_1(\omega_{H2}) = T_1(\omega_{H3}) = 1 \qquad (3\text{-}26)$$

Let

$$VT_1(\omega) = T_1(\omega) - 1 \qquad (3\text{-}27)$$

$VT_1(\omega)$ can be written as,

$$VT_1(\omega) = \frac{ZT_1(\omega)}{PT_1(\omega)} = \frac{\omega^6 + z_5\omega^5 + z_4\omega^4 + z_3\omega^3 + z_2\omega^2 + z_1\omega + z_0}{p_5\omega^5 + p_4\omega^4 + p_3\omega^3 + p_2\omega^2 + p_1\omega + p_0} \qquad (3\text{-}28)$$

where $ZT_1(\omega)$ is the numerator, $PT_1(\omega)$ is the denominator, z_i (i=0,1,2,3,4,5) are the coefficient of the polynomial $ZT_1(\omega)$, p_i (i=0,1,2,3,4,5) are the coefficient of the polynomial $PT_1(\omega)$. $ZT_1(\omega)$ can be analytically derived from two ways.

One way of deriving z_i (i=0,1,2,3,4,5) is by combining the (3-23), (3-27) and (3-28), which gives the results shown in (3-29); z_i (i=0,1,2,3,4,5) are function of the interim parameters ($\omega_{o1}, \omega_{o2}, \omega_{o3}, b_1, b_2, b_3$),

$$
\begin{aligned}
z_5 &= -\frac{\omega_{o1}}{b_1} \\
z_4 &= -{\omega_{o1}}^2 - {\omega_{o2}}^2 - {\omega_{o3}}^2 - \frac{\omega_{o1}\cdot\omega_{o2}}{b_1\cdot b_2} - \frac{\omega_{o1}\cdot\omega_{o3}}{b_1\cdot b_3} \\
z_3 &= \frac{\omega_{o1}}{b_1}\cdot{\omega_{o2}}^2 + \frac{\omega_{o1}}{b_1}\cdot{\omega_{o3}}^2 \\
z_2 &= {\omega_{o1}}^2\cdot{\omega_{o2}}^2 + {\omega_{o2}}^2\cdot{\omega_{o3}}^2 + {\omega_{o1}}^2\cdot{\omega_{o3}}^2 + \frac{\omega_{o1}\cdot\omega_{o2}\cdot{\omega_{o3}}^2}{b_1\cdot b_2} + \frac{\omega_{o1}\cdot\omega_{o3}\cdot{\omega_{o2}}^2}{b_1\cdot b_3} \\
z_1 &= -\frac{\omega_{o1}}{b_1}\cdot{\omega_{o2}}^2\cdot{\omega_{o3}}^2 \\
z_0 &= -{\omega_{o1}}^2\cdot{\omega_{o2}}^2\cdot{\omega_{o3}}^2
\end{aligned}
\tag{3-29}
$$

Because $-\omega_{L1}, -\omega_{L2}, -\omega_{L3}, \omega_{H1}, \omega_{H2}, \omega_{H3}$ are the roots of $VT_1(\omega)$, therefore they are the roots of $ZT_1(\omega)$. Hence, z_i (i=0,1,2,3,4,5) can be derived from the passband specifications, i.e. $\omega_{L1}, \omega_{L2}, \omega_{H1}, \omega_{H2}, \omega_{L3}, \omega_{H3}$. They are shown in (3-30):

$$
\begin{aligned}
z_5 &= -\omega_{H1} - \omega_{H2} - \omega_{H3} + \omega_{L1} + \omega_{L2} + \omega_{L3} \\
z_4 &= \omega_{H1}\cdot\omega_{H2} + \omega_{H2}\cdot\omega_{H3} + \omega_{H1}\cdot\omega_{H3} + \omega_{L1}\cdot\omega_{L2} + \omega_{L2}\cdot\omega_{L3} \\
&\quad +\omega_{L1}\cdot\omega_{L3} - (\omega_{L1} + \omega_{L2} + \omega_{L3})\cdot(\omega_{H1} + \omega_{H2} + \omega_{H3}) \\
z_3 &= \omega_{H1}\cdot\omega_{H2}\cdot(-\omega_{H3} + \omega_{L1} + \omega_{L2} + \omega_{L3}) - \omega_{L1}\cdot\omega_{L2}\cdot(\omega_{H1} + \omega_{H2} + \omega_{H3} - \omega_{L3}) \\
&\quad +\omega_{H3}\cdot(\omega_{H1} + \omega_{H2})\cdot(\omega_{L1} + \omega_{L2} + \omega_{L3}) - \omega_{L3}\cdot(\omega_{L1} + \omega_{L2})\cdot(\omega_{H1} + \omega_{H2} + \omega_{H3}) \\
z_2 &= -\omega_{H1}\cdot\omega_{H2}\cdot\omega_{H3}\cdot(\omega_{L1} + \omega_{L2} + \omega_{L3}) - \omega_{L1}\cdot\omega_{L2}\cdot\omega_{L3}\cdot(\omega_{H1} + \omega_{H2} + \omega_{H3}) \\
&\quad +(\omega_{L1}\cdot\omega_{H1}\cdot\omega_{H2} + \omega_{L1}\cdot\omega_{H1}\cdot\omega_{H3} + \omega_{L1}\cdot\omega_{H2}\cdot\omega_{H3})\cdot(\omega_{L2} + \omega_{L3}) \\
&\quad +(\omega_{H1}\cdot\omega_{H2} + \omega_{H2}\cdot\omega_{H3} + \omega_{H1}\cdot\omega_{H3})\cdot\omega_{L2}\cdot\omega_{L3} \\
z_1 &= -\omega_{H1}\cdot\omega_{H2}\cdot\omega_{H3}\cdot(\omega_{L1}\cdot\omega_{L2} + \omega_{L2}\cdot\omega_{L3} + \omega_{L1}\cdot\omega_{L3}) \\
&\quad +\omega_{L1}\cdot\omega_{L2}\cdot\omega_{L3}\cdot(\omega_{H1}\cdot\omega_{H2} + \omega_{H2}\cdot\omega_{H3} + \omega_{H1}\cdot\omega_{H3}) \\
z_0 &= -\omega_{L1}\cdot\omega_{L2}\cdot\omega_{L3}\cdot\omega_{H1}\cdot\omega_{H2}\cdot\omega_{H3}
\end{aligned}
\tag{3-30}
$$

The relationship between passband specifications ($\omega_{L1}, \omega_{L2}, \omega_{L3}, \omega_{H1}, \omega_{H2}, \omega_{H3}$) and the interim parameters ($\omega_{o1}, \omega_{o2}, \omega_{o3}, b_1, b_2, b_3$) can be established by equating z_i (i=0,1,2,3,4,5) in (3-29) and (3-30).

By re-arranging (3-29), the interim parameters ($\omega_{o1}, \omega_{o2}, \omega_{o3}, b_1, b_2, b_3$) can be expressed in terms of z_i (i=0,1,2,3,4,5); the equations are given in (3-31)

$$
\begin{aligned}
\omega_{o1} &= \sqrt{-\frac{z_0 \cdot z_5}{z_1}} \\
\omega_{o2} &= \sqrt{\frac{-z_3 + \sqrt{z_3^{\,2} - 4 z_5 \cdot z_1}}{2 z_5}} \\
\omega_{o3} &= \sqrt{\frac{-z_3 - \sqrt{z_3^{\,2} - 4 z_5 \cdot z_1}}{2 z_5}} \\
b_1 &= \sqrt{-\frac{z_0}{z_1 \cdot z_5}} \\
b_2 &= \frac{\dfrac{\omega_{o1} \cdot \omega_{o2} \cdot (\omega_{o3}^{\,2} - \omega_{o2}^{\,2})}{b_1}}{z_2 - (\omega_{o1}^{\,2} \cdot \omega_{o2}^{\,2} + \omega_{o2}^{\,2} \cdot \omega_{o3}^{\,2} + \omega_{o1}^{\,2} \cdot \omega_{o3}^{\,2}) + \dfrac{(\omega_{o1}^{\,2} + \omega_{o2}^{\,2} + \omega_{o3}^{\,2} + z_4) \cdot \dfrac{\omega_{o1} \cdot \omega_{o3} \cdot \omega_{o2}^{\,2}}{b_1}}{\dfrac{\omega_{o1} \cdot \omega_{o3}}{b_1}}} \\
b_3 &= \frac{\dfrac{\omega_{o1} \cdot \omega_{o3}}{b_1}}{-\omega_{o1}^{\,2} - \omega_{o2}^{\,2} - \omega_{o3}^{\,2} - \dfrac{\omega_{o1} \cdot \omega_{o2}}{b_1 \cdot b_2} - z_4}
\end{aligned}
\qquad \text{(3-31)}
$$

At this stage, with the desired passband specifications ($\omega_{L1}, \omega_{L2}, \omega_{L3}, \omega_{H1}, \omega_{H2}, \omega_{H3}$), the relevant interim parameters ($\omega_{o1}, \omega_{o2}, \omega_{o3}, b_1, b_2, b_3$) can be synthesised. Meanwhile, the frequency transformation in (3-23) is fully defined as well. A design example using this synthesis technique is given in Section 3.3.4, but before that, the 2nd synthesis technique for triple-passband filter is given in the following section.

3.3.2 Triple-Passband Synthesis Technique 2

Another 6th order triple-passband filter with Chebyshev response is used as an example here to show a different approach of triple-passband synthesis. The mapping process is shown in Figure 3.14. What should be noted is that, unlike the first triple-passband synthesis technique, the positions of the transmission zeros are not the resonant frequencies of the bandstop resonators any more.

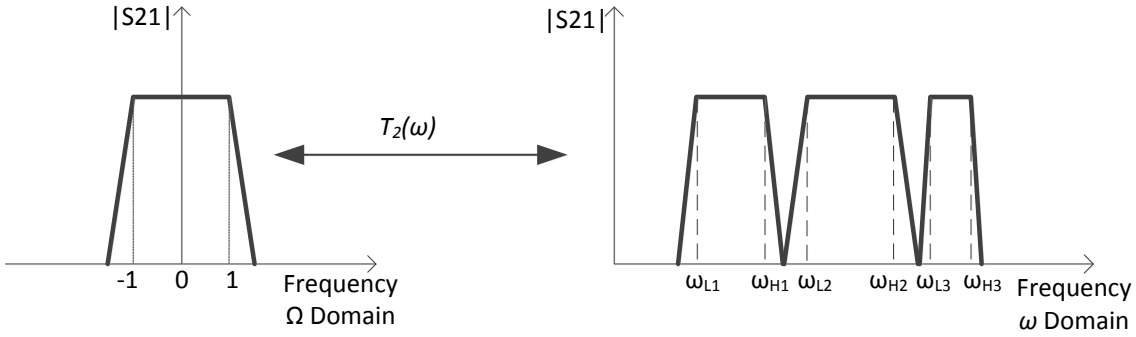

Figure 3.14 Lowpass to triple-passband frequency transformation procedure (Technique 2)

All the notations in the above figure are defined in the same way as the previous example. The three passbands can still have arbitrary passband centre frequencies and bandwidths.

The corresponding frequency transformation for the second triple-passband synthesis technique is given below,

$$\Omega = T_2(\omega) = b_1\left(\frac{\omega}{\omega_{o1}} - \frac{\omega_{o1}}{\omega}\right) - \frac{1}{b_2\left(\frac{\omega}{\omega_{o2}} - \frac{\omega_{o2}}{\omega}\right) - \frac{1}{b_3\left(\frac{\omega}{\omega_{o3}} - \frac{\omega_{o3}}{\omega}\right)}} \tag{3-32}$$

The topology of this 6th order triple-passband filter is shown in Figure 3.15(a); Figure 3.15(b) and Figure 3.15(c) are the equivalent circuits of the topology.

In Figure 3.15(a), $k_{s2,3}$ is the coupling between bandstop resonators. All the other notations have the same definitions as the previous examples.

Figure 3.15(b) shows the equivalent circuit of the blue part, which is same as the one shown in Figure 3.4(b).

Figure 3.15(c) is the equivalent circuit of the corresponding multi-passband resonator section. The positions of the black nodes are different from that in Figure 3.13(c), which implies that the bandstop resonators are series connected, and only one bandstop resonator is directly connected to the bandpass resonator.

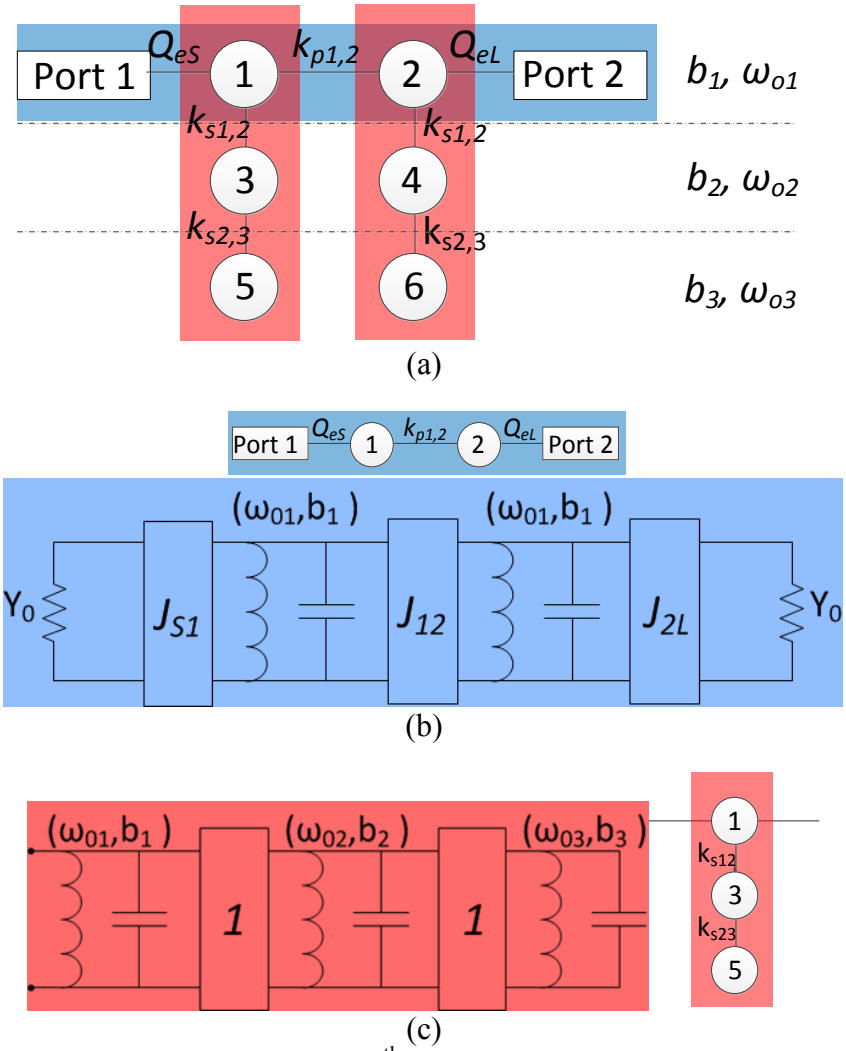

Figure 3.15 (a) The topology of another 6th order triple-passband filter, (b) The equivalent circuit for bandpass resonators and ports, (c) The equivalent circuit for multi-passband resonator section

The relevant coupling matrix of this 6th order triple-passband filter shown in Figure 3.15 is given in (3-33),

$$[M]=\begin{pmatrix} k_1 & k_{p1,2} & k_{s1,2} & 0 & 0 & 0 \\ k_{p1,2} & k_1 & 0 & k_{s1,2} & 0 & 0 \\ k_{s1,2} & 0 & k_2 & 0 & k_{s2,3} & 0 \\ 0 & k_{s1,2} & 0 & k_2 & 0 & k_{s2,3} \\ 0 & 0 & k_{s2,3} & 0 & k_3 & 0 \\ 0 & 0 & 0 & k_{s2,3} & 0 & k_3 \end{pmatrix} \tag{3-33}$$

$k_{s2,3}$ can be calculated through

$$k_{s2,3}=\frac{1}{\sqrt{b_2 \cdot b_3}} \tag{3-34}$$

The elements in matrix (3-33) and the external *Q*-factors can be synthesized through (3-6) to (3-11) and (3-34).

The relationship between interim parameters (ω_{o1} , ω_{o2} , ω_{o3} , b_1 , b_2 , b_3) and the passband specifications (ω_{L1} , ω_{L2} , ω_{H1} , ω_{H2} , ω_{L3} , ω_{H3}) for this triple-passband topology can be derived using the similar method shown previously. The equation $VT_2(\omega)$ can be expressed as,

$$VT_2(\omega)=T_2(\omega)-1=VT_2(\omega)=\frac{ZT_2(\omega)}{PT_2(\omega)}=\frac{\omega^6+z_5\omega^5+z_4\omega^4+z_3\omega^3+z_2\omega^2+z_1\omega+z_0}{p_5\omega^5+p_4\omega^4+p_3\omega^3+p_2\omega^2+p_1\omega+p_0} \tag{3-35}$$

Because the derivation process is similar to the previous examples, only the results are presented. z_i (*i*=0,1,2,3,4,5) can be expressed only with the interim parameters (ω_{o1} , ω_{o2} , ω_{o3} , b_1 , b_2 , b_3); the results are shown below in (3-36).

$$
\begin{aligned}
z_5 &= -\frac{\omega_{o1}}{b_1} \\
z_4 &= -{\omega_{o1}}^2 - {\omega_{o2}}^2 - {\omega_{o3}}^2 - \frac{\omega_{o2}\cdot\omega_{o3}}{b_2\cdot b_3} - \frac{\omega_{o1}\cdot\omega_{o2}}{b_1\cdot b_2} \\
z_3 &= \frac{\omega_{o1}}{b_1}\cdot{\omega_{o2}}^2 + \frac{\omega_{o1}}{b_1}\cdot{\omega_{o3}}^2 + \frac{\omega_{o1}\cdot\omega_{o2}\cdot\omega_{o3}}{b_1\cdot b_2\cdot b_3} \\
z_2 &= {\omega_{o1}}^2\cdot{\omega_{o2}}^2 + {\omega_{o2}}^2\cdot{\omega_{o3}}^2 + {\omega_{o1}}^2\cdot{\omega_{o3}}^2 + \frac{{\omega_{o1}}^2\cdot\omega_{o2}\cdot\omega_{o3}}{b_2\cdot b_3} + \frac{\omega_{o1}\cdot\omega_{o2}\cdot{\omega_{o3}}^2}{b_1\cdot b_2} \\
z_1 &= -\frac{\omega_{o1}}{b_1}\cdot{\omega_{o2}}^2\cdot{\omega_{o3}}^2 \\
z_0 &= -{\omega_{o1}}^2\cdot{\omega_{o2}}^2\cdot{\omega_{o3}}^2
\end{aligned}
\tag{3-36}
$$

z_i (i=0,1,2,3,4,5) can also be expressed in the form of passband specifications ($\omega_{L1}, \omega_{L2}, \omega_{H1}, \omega_{H2}, \omega_{L3}, \omega_{H3}$). The equations are given in (3-30).

By re-arranging (3-36), the interim parameters ($\omega_{o1}, \omega_{o2}, \omega_{o3}, b_1, b_2, b_3$) can be expressed in terms of z_i (i=0,1,2,3,4,5) [4],

$$
\begin{aligned}
\omega_{o1} &= \sqrt{-\frac{z_0\cdot z_5}{z_1}} \\
\omega_{o2} &= \sqrt{\frac{{z_1}^2\cdot z_4\cdot z_5 - z_0\cdot z_1\cdot{z_5}^2 - {z_1}^2\cdot z_3}{z_0\cdot z_3\cdot{z_5}^2 + {z_1}^2\cdot z_5 - z_1\cdot z_2\cdot{z_5}^2}} \\
\omega_{o3} &= \sqrt{\frac{z_1}{z_5\cdot{\omega_{o2}}^2}} \\
b_1 &= \sqrt{-\frac{z_0}{z_1\cdot z_5}} \\
b_2 &= \sqrt{\frac{z_1\cdot{z_5}^2}{\left(\frac{z_0\cdot z_3}{z_1} + \frac{z_1}{z_5} - z_2\right)\cdot\left(z_4\cdot z_5 - \frac{z_0\cdot{z_5}^2}{z_1} - z_3\right)}} \\
b_3 &= \frac{\omega_{o1}\cdot\omega_{o2}\cdot\omega_{o3}}{b_1\cdot b_2\left[z_3 + z_5\cdot\left({\omega_{o2}}^2 + {\omega_{o3}}^2\right)\right]}
\end{aligned}
\tag{3-37}
$$

Therefore, as long as the passband specifications are given, the frequency transformation in (3-32) can be fully defined. An example is given in Section 3.3.4, but before that the

generalised topology for triple-passband filters with Chebyshev response are presented in the following section.

3.3.3 Generalised Topology for Triple-Passband Filter with Chebyshev Response

Generalised topologies for both type of triple-passband filter that have 3*n* resonators are presented here in Figure 3.16 and Figure 3.17.

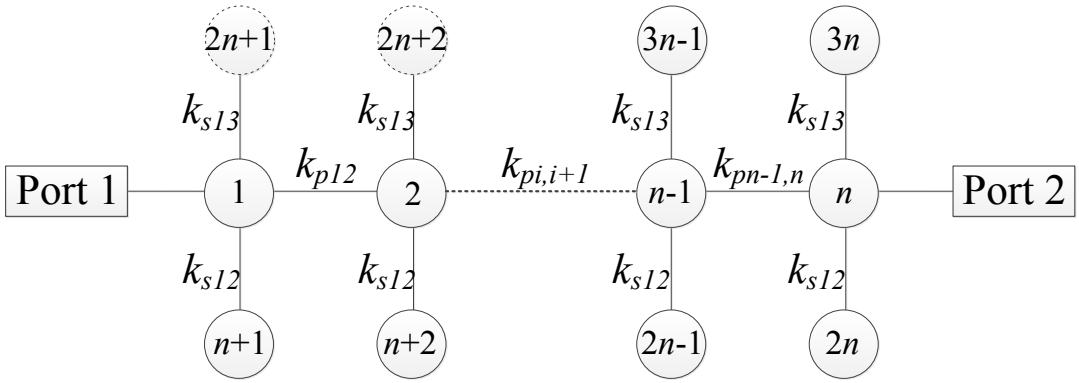

Figure 3.16 Generalised topology for triple-passband synthesis technique 1

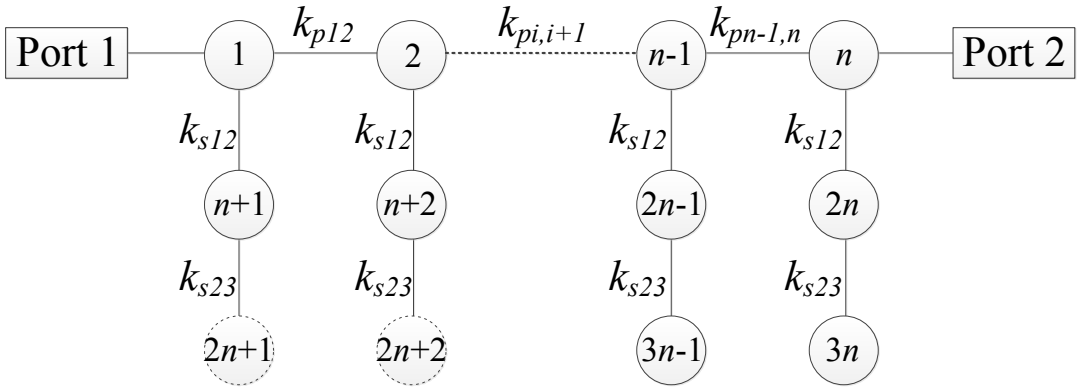

Figure 3.17 Generalised topology for triple-passband synthesis technique 2

For both triple-passband filter topologies, the only difference is that they have different multi-passband resonator sections. Both types of sections have one bandpass resonator and two bandstop resonators, but the way they coupled are different. The frequency transformation in

(3-23) and (3-32) are still valid for the two generalised topologies. It should be noted that each passband now has the shape of n^{th} order all-pole Chebyshev response.

For both generalised triple-passband topologies, (3-18) defines the coupling between bandpass resonators; (3-7), (3-25) and (3-34) define the couplings between bandpass and bandstop resonators; (3-10) and (3-19) define the external Q-factors.

3.3.4 Example Filters

The design examples of both 6th order triple-passband filters are given in this section, in order to verify the synthesis theory. For comparison, the identical passband specifications (ω_{L1}, ω_{L2}, ω_{L3}, ω_{H1}, ω_{H2}, ω_{H3}) are applied in both designs. The syntheses are implemented in MATLAB. A flowchart can be used to summarise both syntheses and is given in Figure 3.18.

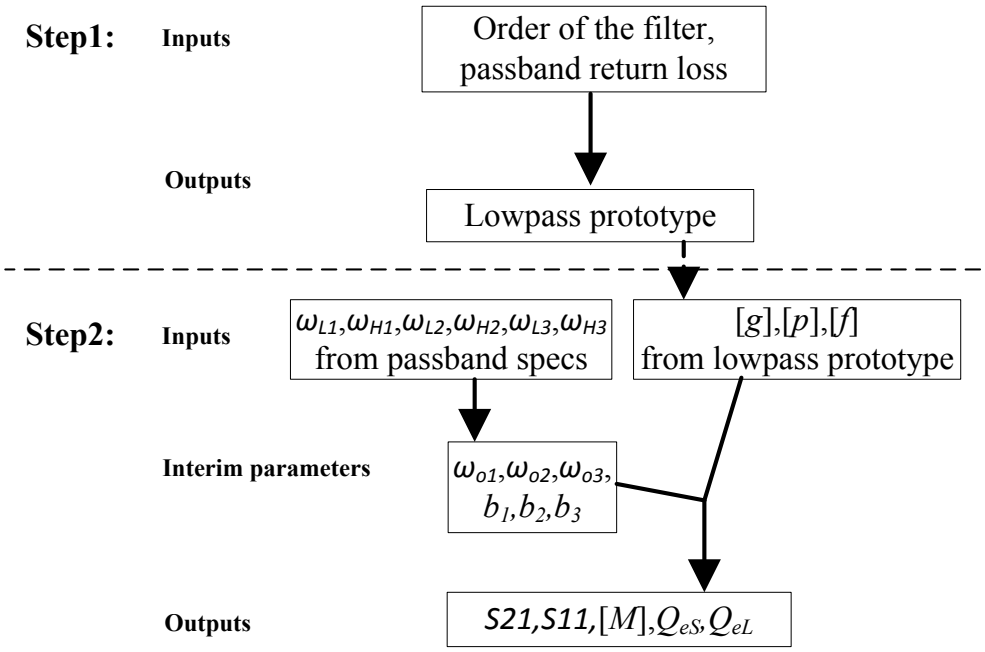

Figure 3.18 The flowchart for both triple-passband filter synthesis techniques

3.3.4.1 Example 3: The Design of A 6th Order Triple-Passband Filter Using Triple-Passband Synthesis Technique 1

This example uses the 6th order triple-passband filter topology shown in Section 3.3.1 (see Figure 3.13). The three passbands are arbitrarily chosen at 9.1-9.4GHz, 9.5-9.8GHz and 9.9-10.1GHz. The design uses the 2nd order lowpass prototype Chebyshev filter which is given in Section 3.2.3.1 (refer to Figure 3.6 and Table 3.2). The interim parameters can be directly synthesised from the desired passband specifications. They are given in Table 3.5.

Passband specifications	**Interim parameters**
$\omega_{L1} = 9.1GHz$	$\omega_{o1} = 9.57GHz$
$\omega_{H1} = 9.4GHz$	$\omega_{o2} = 9.44GHz$
$\omega_{L2} = 9.5GHz$	$\omega_{o3} = 9.87GHz$
$\omega_{H2} = 9.8GHz$	$b_1 = 11.97$
$\omega_{L3} = 9.9GHz$	$b_2 = 85.78$
$\omega_{H3} = 10.1GHz$	$b_3 = 112.06$

Table 3.5 The passband specifications and interim parameters for Example 3

According to (3-6) to (3-8) and (3-25), the coupling matrix is calculated as follow,

$$[M] = \begin{pmatrix} -0.0029 & 0.1389 & 0.0312 & 0 & 0.0273 & 0 \\ 0.1389 & -0.0029 & 0 & 0.0312 & 0 & 0.0273 \\ 0.0312 & 0 & -0.0307 & 0 & 0 & 0 \\ 0 & 0.0312 & 0 & -0.0307 & 0 & 0 \\ 0.0273 & 0 & 0 & 0 & 0.0590 & 0 \\ 0 & 0.0273 & 0 & 0 & 0 & 0.0590 \end{pmatrix} \quad (3\text{-}38)$$

Also, according to (3-10) and (3-11), the external Q-factors are both 7.96. The S-parameters are below shown in Figure 3.19.

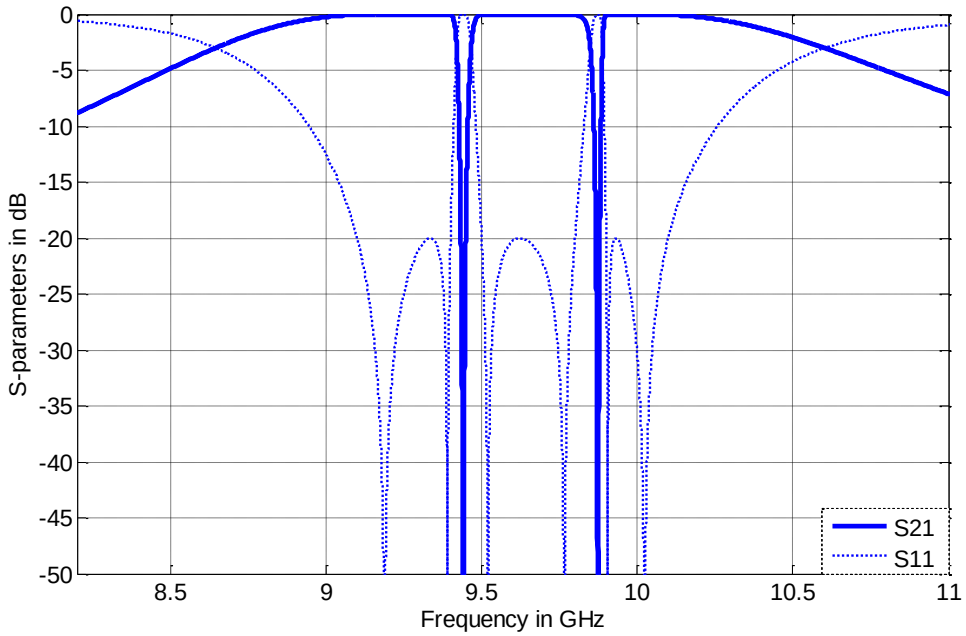

Figure 3.19 The *S*-parameter of a 6th order triple-passband filter with Chebyshev response using the triple-passband synthesis technique 1 (Passband 1: 9.1 ~ 9.4 GHz, Passband 2: 9.5 ~ 9.8 GHz, Passband 3: 9.9 ~ 10.1 GHz)

3.3.4.2 Example 4: The Design of A 6th Order Triple-Passband Filter Using Triple-Passband Synthesis Technique 2

The topology of this 6th order triple-passband filter can be found in Section 3.3.2 (Figure 3.15). For comparison, this design uses the same passband specifications and the lowpass prototype which are used in Example 3. Although the desired filter specifications remain the same, the interim parameters synthesised by the 2nd technique are not the same. The unchanged passband specifications and the new interim parameters are given in Table 3.6,

Passband specifications	**Interim parameters**
$\omega_{L1} = 9.1GHz$	$\omega_{o1} = 9.57GHz$
$\omega_{H1} = 9.4GHz$	$\omega_{o2} = 9.63GHz$
$\omega_{L2} = 9.5GHz$	$\omega_{o3} = 9.68GHz$
$\omega_{H2} = 9.8GHz$	$b_1 = 11.97$
$\omega_{L3} = 9.9GHz$	$b_2 = 48.58$
$\omega_{H3} = 10.1GHz$	$b_3 = 10.42$

Table 3.6 The passband specifications and interim parameters for Example 4

According to (3-6) to (3-8) and (3-34), the coupling matrix is calculated as,

$$[M]=\begin{pmatrix} -0.0029 & 0.1389 & 0.0415 & 0 & 0 & 0 \\ 0.1389 & -0.0029 & 0 & 0.0415 & 0 & 0 \\ 0.0415 & 0 & 0.0082 & 0 & 0.0444 & 0 \\ 0 & 0.0415 & 0 & 0.0082 & 0 & 0.0444 \\ 0 & 0 & 0.0444 & 0 & 0.0201 & 0 \\ 0 & 0 & 0 & 0.0444 & 0 & 0.0201 \end{pmatrix} \tag{3-39}$$

According to (3-10) and (3-11), the external Q-factors ($Q_{eS} = Q_{eL}$) are both 7.96. The relevant S-parameters are plotted in Figure 3.20.

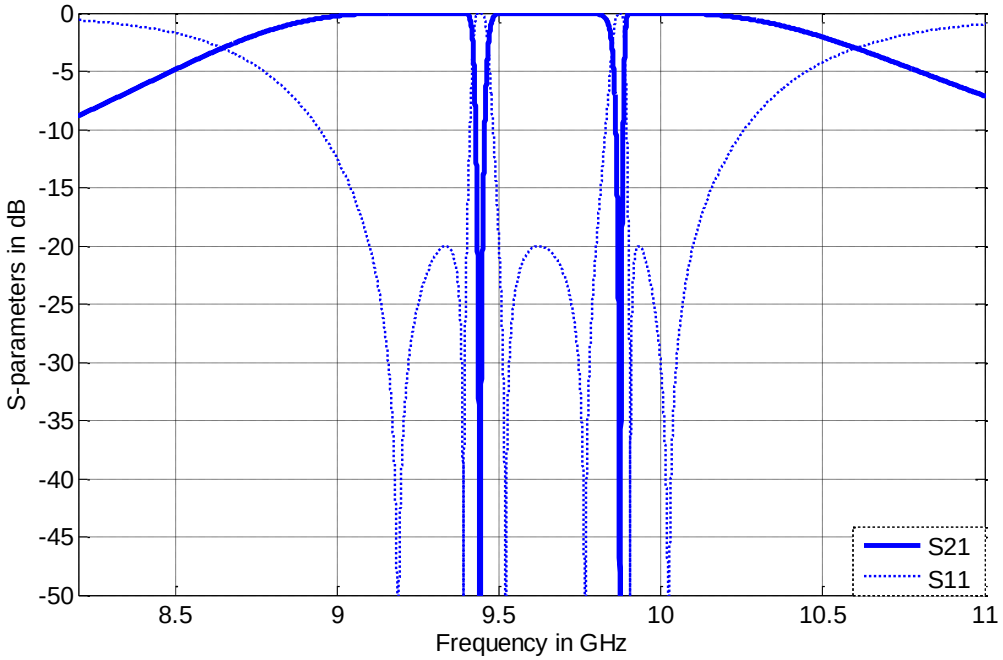

Figure 3.20 The S-parameter of a 6th order triple-passband filter with Chebyshev response using the triple-passband synthesis technique 2 (Passband 1: 9.1 ~ 9.4 GHz, Passband 2: 9.5 ~ 9.8 GHz, Passband 3: 9.9 ~ 10.1 GHz)

It can be found that, given the same passband specifications and the same lowpass prototype, both synthesis techniques can produce identical triple-passband responses, but the topologies behind may not be the same.

3.4 Generalised Multi-Passband Synthesis Technique Based on Multi-passband resonator section

Given the above dual-passband and triple-passband examples, the generalised multi-passband filters can be synthesised with a similar routine. To make things clear, the synthesis techniques for multi-passband filter will be discussed from the multi-passband resonator section point of view, since it is the basic building block for the generalised multi-passband filter discussed here.

3.4.1 Introduction of Generalised Multi-Passband Filter Synthesis

In order to give a more straight-forward explanation of the generalised multi-passband filter synthesis technique, a comparison between the conventional bandpass filter design method and the proposed multi-passband filter synthesis technique is given. As shown in Figure 3.21, the bandpass filter is obtained by applying the well-known conventional lowpass to bandpass frequency transformation $B(\omega)$ (given in (3-1)) to the lowpass prototype filter. The black circles represent the lowpass resonators; while the white circles are the bandpass resonators.

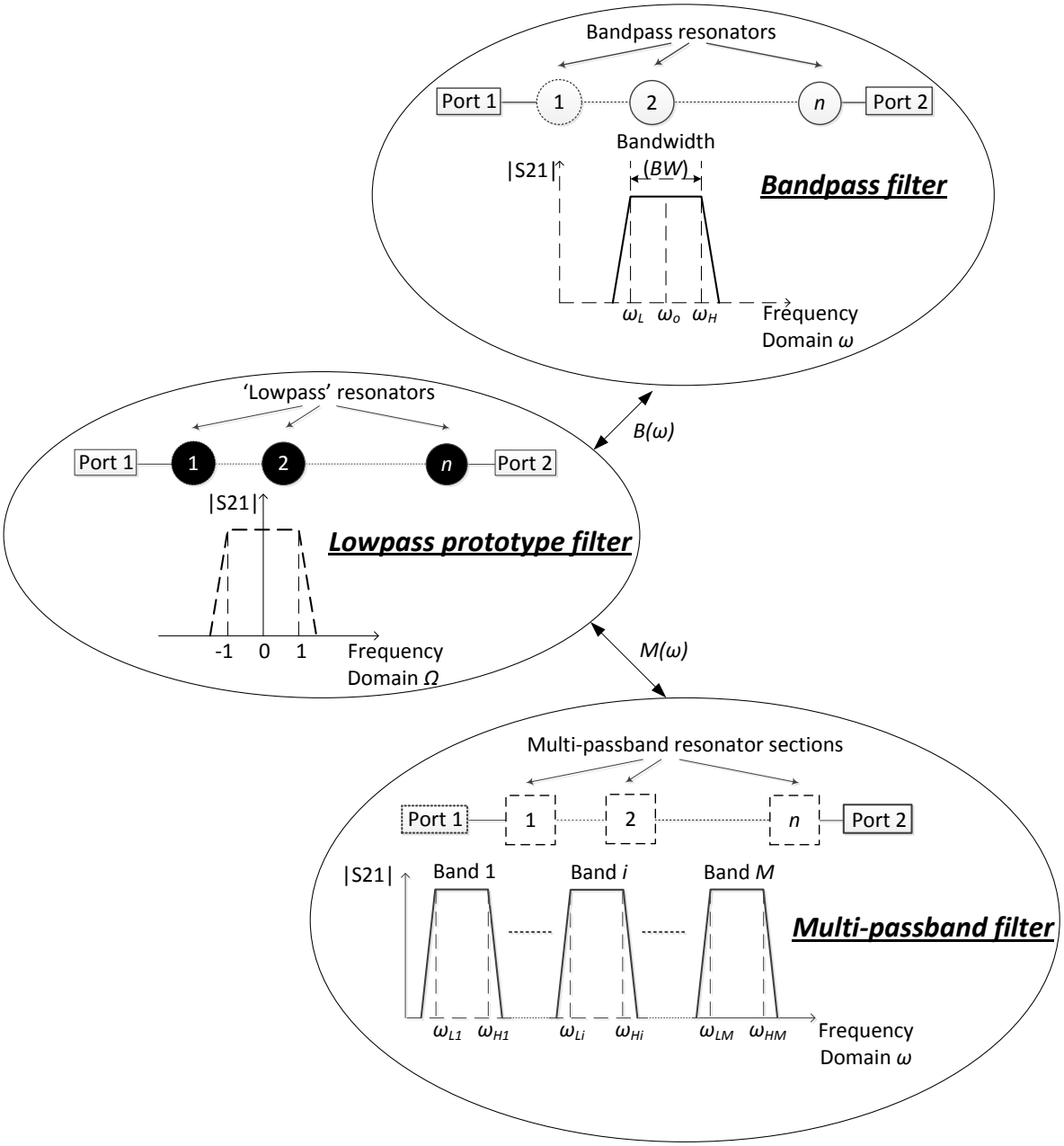

Figure 3.21 The schematic of frequency transformation

By applying the lowpass to multi-passband frequency transformation $M(\omega)$, the lowpass prototype filter will be transformed into a multi-passband filter. This is physically realised by replacing the lowpass resonators into multi-passband resonator sections which are denoted by dashed squares in Figure 3.21.

The generalised multi-passband resonator sections can be broadly categorised into three major types, which are shown in Figure 3.22. For the first type, all bandstop resonators are

directly connected to the bandpass resonator; it is named as parallel coupled resonator section. For the second type, the bandstop resonators have an inline layout and only one bandstop resonator is directly connected to the bandpass resonator; it is named as the series coupled resonator section. The third one is the mixed coupled resonator section which contains both parallel and series couple resonator at the same time. The bigger circles represent bandpass resonators; the smaller circles represent bandstop resonators; the solid lines stand for couplings between resonators; the dashed lines represent the unshown re-occurring parts.

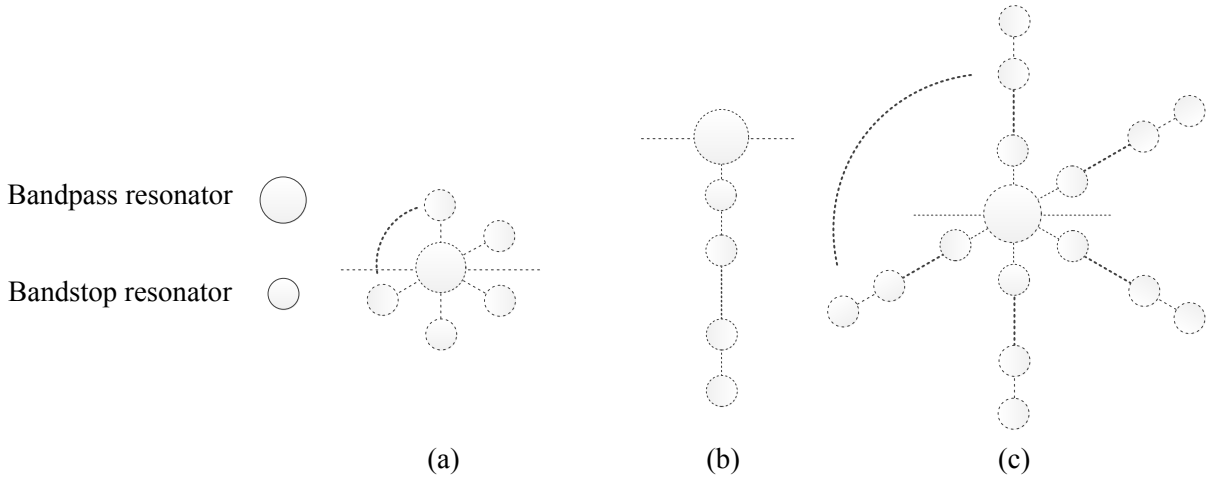

Figure 3.22. Different kind of multi-passband resonator sections: (a) parallel section, (b) series section, (c) mixed section

The multi-passband filters discussed here are built up with these sections. For each section, there is only one bandpass resonator, but the number of bandstop resonator is not limited. Within one particular multi-passband filter, all the sections share the same topology; the repeating sections are connected through the inverters between bandpass resonators. It is worth mentioning that it is actually the multi-passband resonator section that ultimately determines the frequency transformation and the number of passband for this multi-passband synthesis technique [2].

3.4.2 Parallel Coupled Resonator Section

Figure 3.23 shows a generalised multi-passband filter which is built up by parallel coupled resonator section. Resonator 1 to n are the bandpass resonators. If it is transformed from an n^{th} order lowpass prototype Chebyshev filter, then each passband of this multi-passband filter will have the same in-band and out-of band response of the n^{th} order Chebyshev filter.

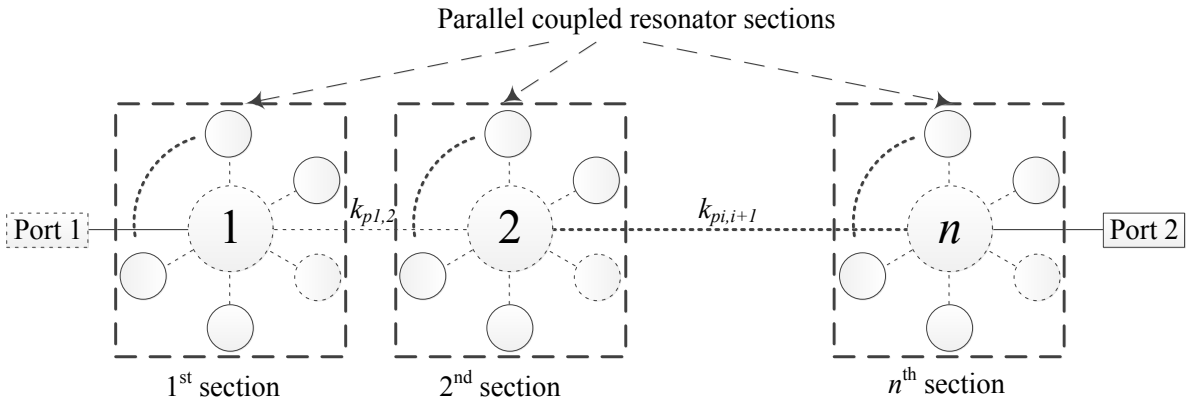

Figure 3.23 The topology of a generalised multi-passband filter which is built up by parallel coupled resonator section

The couplings between bandpass resonators $k_{pi,i+1}$ (i=1,2,...,n-1) can be calculated by (3-18).

Figure 3.24 presents a detailed picture of the 1st parallel coupled resonator section of the multi-passband filter that is shown in Figure 3.23. The multi-passband filter is made up of n sections like this. It shows a generalised topology of a single parallel coupled resonator section. M is the number of resonators in one parallel coupled resonator section. M could be any positive integers. In each resonator section, the bandpass resonator is directly coupled to M-1 bandstop resonators. So there will be $M \times n$ resonators in total for the multi-passband filter. ω_{oi} and b_i (i=1,2,3,…,M) are the resonant frequency and susceptance slope parameter for the i^{th} resonator, respectively. When i=1, the resonator is a bandpass resonator; when i=2,3,…,M, the resonator is a bandstop resonator. Within one multi-passband filter, all the parallel coupled resonator sections must share the same layout and interim parameters.

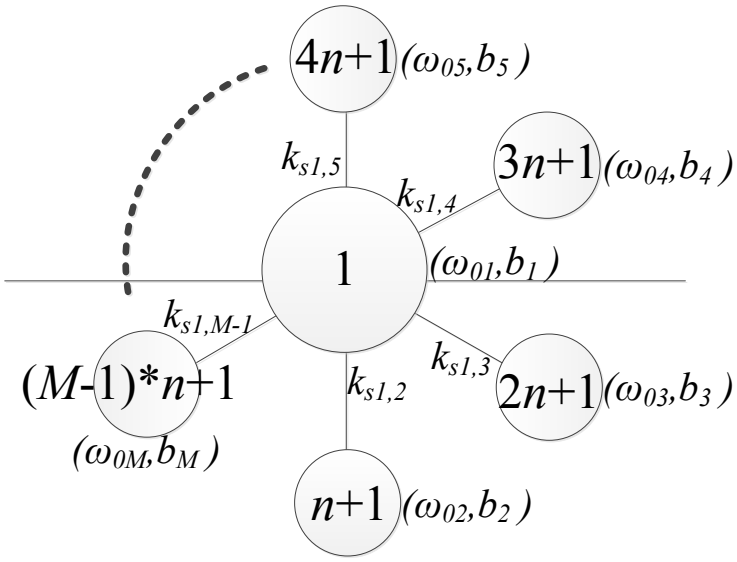

Figure 3.24 1st parallel coupled resonator section (*n* is the order of the each passband, *M* is the total number of passbands)

The couplings between the bandpass resonator and all bandstop resonators are calculated by,

$$k_{s1,i} = \frac{1}{\sqrt{b_1 \cdot b_i}} \quad (i=2,3,\ldots,M\text{-}1) \tag{3-40}$$

The generalised frequency transformation $M_P(\omega)$ for the multi-passband filter built by this generalised parallel coupled resonator sections is given below,

$$\Omega = M_P(\omega) = b_1\left(\frac{\omega}{\omega_{o1}} - \frac{\omega_{o1}}{\omega}\right) - \frac{1}{b_2\left(\frac{\omega}{\omega_{o2}} - \frac{\omega_{o2}}{\omega}\right)} - \frac{1}{b_3\left(\frac{\omega}{\omega_{o3}} - \frac{\omega_{o3}}{\omega}\right)} - \frac{1}{b_4\left(\frac{\omega}{\omega_{o4}} - \frac{\omega_{o4}}{\omega}\right)} - \frac{1}{b_5\left(\frac{\omega}{\omega_{o5}} - \frac{\omega_{o5}}{\omega}\right)} \cdots\cdots - \frac{1}{b_M\left(\frac{\omega}{\omega_{oM}} - \frac{\omega_{oM}}{\omega}\right)} \tag{3-41}$$

By applying the above frequency transformation, the lowpass prototype response can be mapped into *M* arbitrary frequency bands. Figure 3.25 gives an illustrative picture of this procedure, where ω_{Li} and ω_{Hi} (i=1,2,…,M) are the lower and higher passband limits for band *i*, respectively. ω_{oi} (i=2,3,…,M) are positions of the transmission zeros in the de-normalised response. There are *M* passbands in total for this multi-passband filter. It should be noted that this filter could have a large number of couplings to each bandpass resonator, which may make practical implementation difficult.

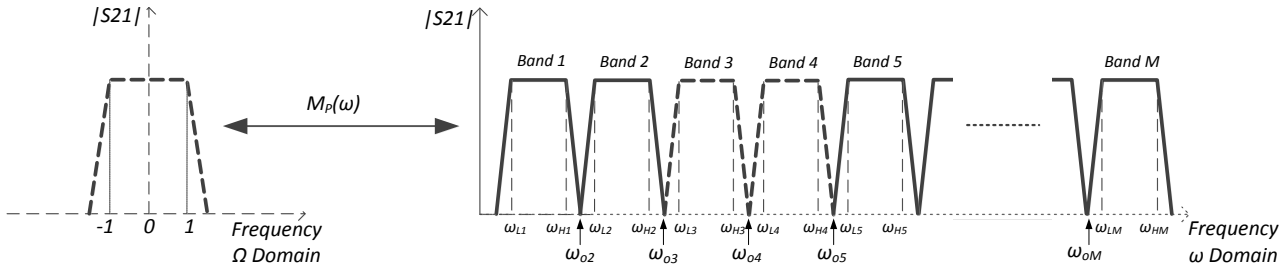

Figure 3.25 Schematic S21 for multi-passband synthesis technique with parallel coupled resonator section

3.4.3 Series Coupled Resonator Section

Figure 3.26 below is the topology of a generalised multi-passband filter based on series coupled resonator section. Again, the resonators from 1 to *n* are the bandpass resonators. All other resonators are bandstop resonators.

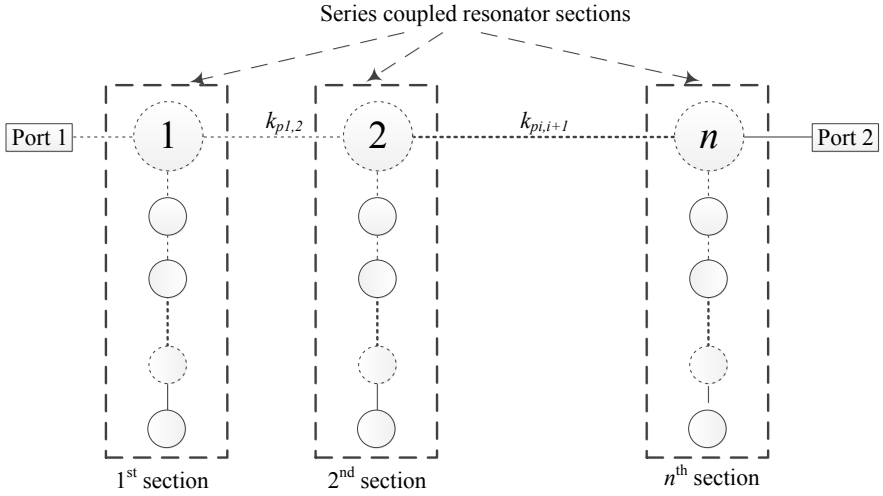

Figure 3.26 The topology of a generalised multi-passband filter built up by series coupled resonator section

Figure 3.27 shows the detail layout of the 1st series coupled resonator section in Figure 3.26. Similarly, in the multi-passband filter, there are *n* identical sections like this; each section contains one bandpass resonator resonating at ω_{o1} and *M*-1 bandstop resonators resonating at ω_{oi} (*i*=2,3,…,*M*),. There are $M \times n$ resonators in this multi-passband filter, as well.

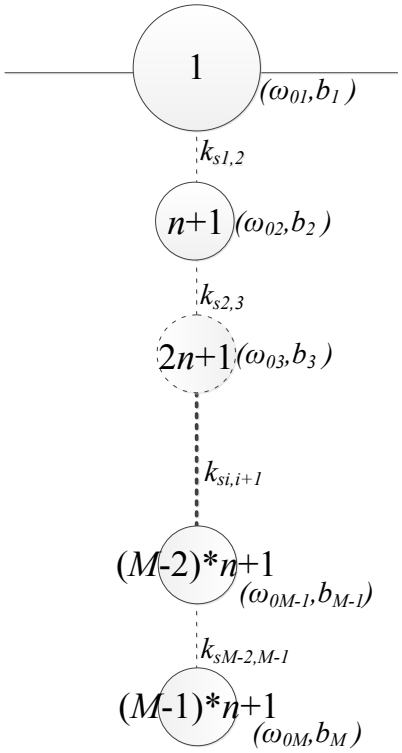

Figure 3.27 1st series coupled resonator section (*n* is the order of each passband, *M* is the total number of passbands)

The couplings between the resonators in one section is defined by,

$$k_{si,i+1} = \frac{1}{\sqrt{b_i \cdot b_{i+1}}} \quad (i=1,2,\ldots,M\text{-}2) \tag{3-42}$$

The generalised frequency transformation $M_S(\omega)$ for this series coupled resonator section based multi-passband filter is given below,

$$\Omega = M_S(\omega) = b_1\left(\frac{\omega}{\omega_{o1}} - \frac{\omega_{o1}}{\omega}\right) - \cfrac{1}{b_2\left(\frac{\omega}{\omega_{o2}} - \frac{\omega_{o2}}{\omega}\right) - \cfrac{1}{b_3\left(\frac{\omega}{\omega_{o3}} - \frac{\omega_{o3}}{\omega}\right) - \ddots - \cfrac{1}{b_{M-1}\left(\frac{\omega}{\omega_{oM-1}} - \frac{\omega_{oM-1}}{\omega}\right) - \cfrac{1}{b_M\left(\frac{\omega}{\omega_{oM}} - \frac{\omega_{oM}}{\omega}\right)}}}} \tag{3-43}$$

The de-normalising procedure for this kind of multi-passband filter is illustrated in Figure 3.28.

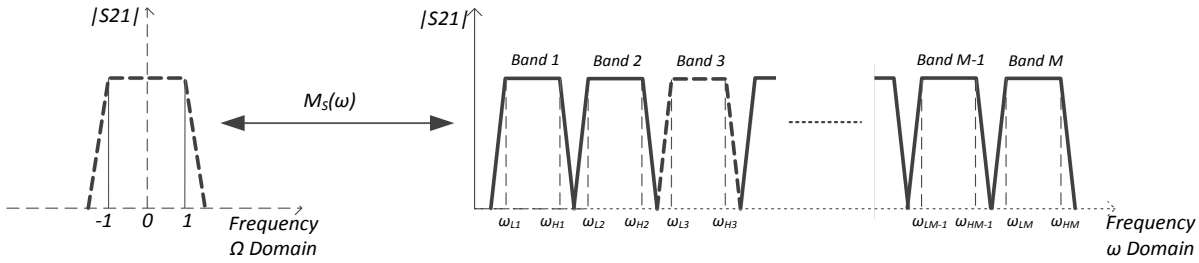

Figure 3.28 Schematic S21 for multi-passband synthesis technique with series coupled resonator section

There are M passbands in total for this multi-passband filter, as well. But ω_{oi} (i=2,3,…,M) are not the positions of the transmission zeros in the de-normalised response any more.

3.4.4 Mixed Coupled Resonator Section

Figure 3.29 shows the generalised multi-passband filter made up by mixed coupled resonator sections which is a combination of both parallel and series coupled resonator section. Resonator 1 to n are still bandpass resonators, all other resonators are bandstop resonators.

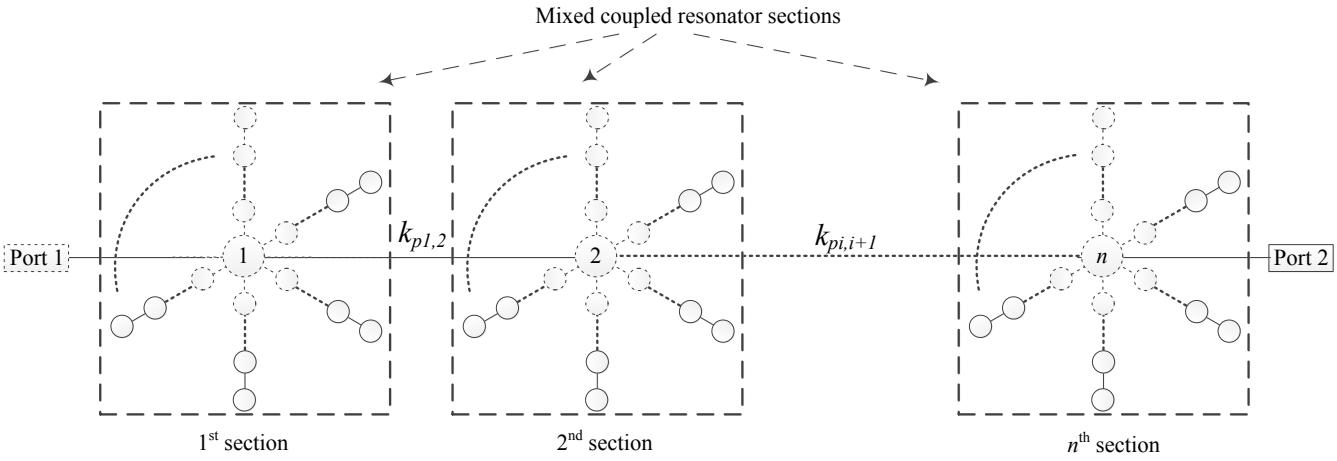

Figure 3.29 The topology of a generalised multi-passband filter which is built up by mixed coupled resonator section

Because of the complicity in numbering, an intuitive example topology of a mixed couple resonator section is given in Figure 3.30 rather than a generalised topology, but it still gives a good explanation of the structure.

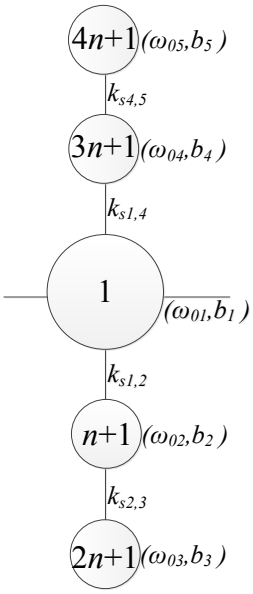

Figure 3.30 An example of the 1st mixed coupled resonator section (five-passband)

In Figure 3.30, resonator 1 is the bandpass resonator; all the other four resonators are bandstop resonators. Two bandstop resonators (resonator n+1 and 3n+1) are directly coupled to the bandpass resonator; while the other two bandstop resonators (resonator 2n+1 and 4n+1) are indirectly connected to the bandpass resonator through the adjacent bandstop resonators. The inter resonator coupling in this mixed coupled section can be calculated using (3-40) and (3-42). With this specific section, a five-passband filter can be made with arbitrary required passband specifications. The corresponding frequency transformation for this five-passband filter is given in (3-44); once the passband specifications are given, the frequency transformation can be fully defined.

$$\Omega = F(\omega) = b_1\left(\frac{\omega}{\omega_{o1}} - \frac{\omega_{o1}}{\omega}\right) - \frac{1}{b_2\left(\frac{\omega}{\omega_{o2}} - \frac{\omega_{o2}}{\omega}\right) - \frac{1}{b_3\left(\frac{\omega}{\omega_{o3}} - \frac{\omega_{o3}}{\omega}\right)}} - \frac{1}{b_4\left(\frac{\omega}{\omega_{o4}} - \frac{\omega_{o4}}{\omega}\right) - \frac{1}{b_5\left(\frac{\omega}{\omega_{o5}} - \frac{\omega_{o5}}{\omega}\right)}} \quad (3\text{-}44)$$

The de-normalising procedure by applying frequency transformation in (3-44) is presented in Figure 3.31,

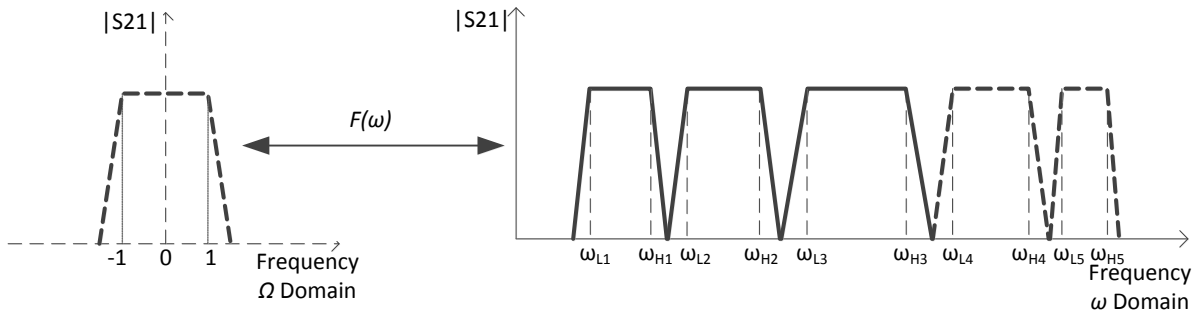

Figure 3.31 Lowpass to five-passband frequency transformation procedure

For the generalised mixed couple resonator section which has M resonators, the corresponding frequency transformation can be obtained in following way. First, there is a term $b_1\left(\frac{\omega}{\omega_{o1}} - \frac{\omega_{o1}}{\omega}\right)$, which corresponds the bandpass resonators; then, if a single bandstop resonator is directly connected to the bandpass resonator, a term of $-\frac{1}{b_i\left(\frac{\omega}{\omega_{oi}} - \frac{\omega_{oi}}{\omega}\right)}$ (i is an integer between 2 and M) will be added into the frequency transformation; and if there is a set of series coupled bandstop resonators connected to the bandpass resonator, a new term which has the form of the second term given in (3-43) will be added into the frequency transformation. Finally, there should be in total M pairs of interim parameters in this frequency transformation, which define all the M resonators in the mixed coupled resonator section.

To verify the generalised multi-passband synthesis technique, three five-passband filters are given in next section as examples. They use the mixed coupled resonator section which is shown in Figure 3.30 as the basic building blocks, (3-44) as the frequency transformation.

3.5 The Verification of Generalised Multi-Passband Synthesis Technique

To validate the multi-passband synthesis technique, three examples of the five-passband filter are given. The first example is a 10th order five-passband filter with Chebyshev response which is used to present the detailed synthesis procedure; it produces five even bandwidth passband. To show the flexibility of the design technique, it is then followed by two concise examples. Both have uneven passband bandwidths which are chosen arbitrarily; one is another 10th order five-passband filter with Chebyshev response; the other one is a 20th order five-passband filter with quasi-elliptic response.

3.5.1 Example 5: A 10th Order Five-Passband Filter with Chebyshev Response (Even Bandwidth)

Figure 3.32(a) shows a 10th order five-passband filter which is built up with the mixed coupled resonator sections shown in Figure 3.30, the corresponding equivalent circuits are shown in Figure 3.32(b) and Figure 3.32(c). Red sections are multi-passband resonator section, while the blue section is the section of bandpass resonators.

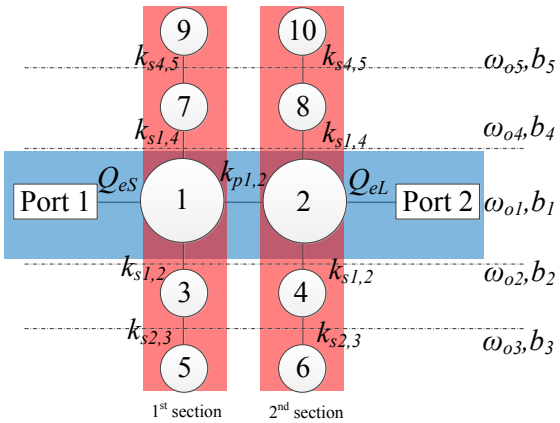

(a)

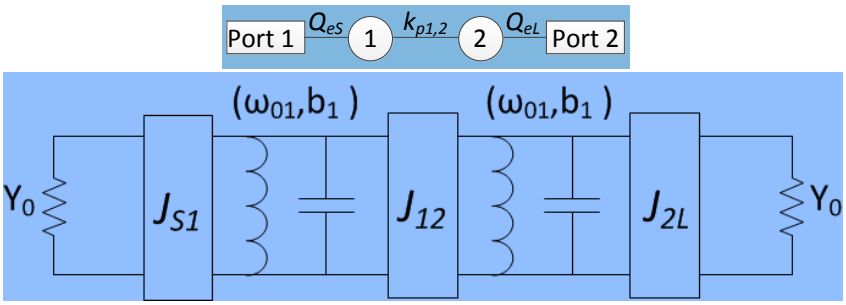

(b)

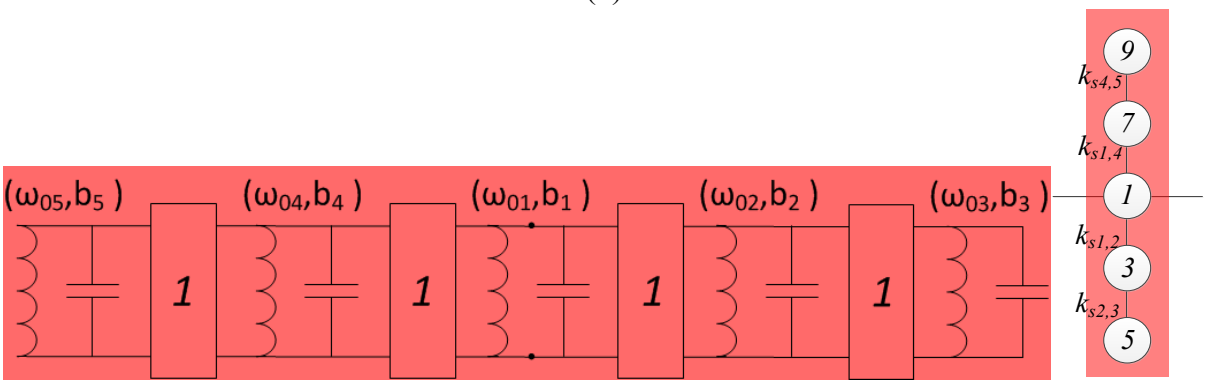

(c)

Figure 3.32 (a) The topology of the 10th order five-passband filter, (b) The equivalent circuit for bandpass resonators and ports, (c) The equivalent circuit for multi-passband resonator section

All the notations and parameters here are named using the same routine as the previous examples. The coupling matrix for this 10th order five-passband filter is

$$[M]=\begin{pmatrix} k_1 & k_{p1,2} & k_{s1,2} & 0 & 0 & 0 & k_{s1,4} & 0 & 0 & 0 \\ k_{p1,2} & k_1 & 0 & k_{s1,2} & 0 & 0 & 0 & k_{s1,4} & 0 & 0 \\ k_{s1,2} & 0 & k_2 & 0 & k_{s2,3} & 0 & 0 & 0 & 0 & 0 \\ 0 & k_{s1,2} & 0 & k_2 & 0 & k_{s2,3} & 0 & 0 & 0 & 0 \\ 0 & 0 & k_{s2,3} & 0 & k_3 & 0 & 0 & 0 & 0 & 0 \\ 0 & 0 & 0 & k_{s2,3} & 0 & k_3 & 0 & 0 & 0 & 0 \\ k_{s1,4} & 0 & 0 & 0 & 0 & 0 & k_4 & 0 & k_{s4,5} & 0 \\ 0 & k_{s1,4} & 0 & 0 & 0 & 0 & 0 & k_4 & 0 & k_{s4,5} \\ 0 & 0 & 0 & 0 & 0 & 0 & k_{s4,5} & 0 & k_5 & 0 \\ 0 & 0 & 0 & 0 & 0 & 0 & 0 & k_{s4,5} & 0 & k_5 \end{pmatrix} \quad (3\text{-}45)$$

All the couplings in matrix (3-45) and the external Q-factors can be calculated from b_i, ω_{oi}, (i=1,2,3,4,5) and g-values by applying (3-6), (3-8), (3-10), (3-11), (3-40) and (3-42). The frequency transformation procedure is shown in Figure 3.31. The synthesis details are given below. As $F(\omega)$ is the frequency transformation, it maps the passband limits in de-normalised

frequency domain onto ±1 in normalised frequency domain. Therefore, (3-46) can be written as,

$$\begin{aligned} &F\left(-\omega_{L1}\right)=F\left(-\omega_{L2}\right)=F\left(-\omega_{L3}\right)=F\left(-\omega_{L4}\right)=F\left(-\omega_{L5}\right) \\ &=F\left(\omega_{H1}\right)=F\left(\omega_{H2}\right)=F\left(\omega_{H3}\right)=F\left(\omega_{H4}\right)=F\left(\omega_{H5}\right)=1 \end{aligned} \tag{3-46}$$

Let

$$VF(\omega)=F(\omega)-1 \tag{3-47}$$

$VF(\omega)$ can also be expressed as,

$$VF(\omega)=\frac{ZF(\omega)}{PF(\omega)}=\frac{\omega^{10}+z_9\omega^9+z_8\omega^8+z_7\omega^7+z_6\omega^6+z_5\omega^5+z_4\omega^4+z_3\omega^3+z_2\omega^2+z_1\omega+z_0}{p_9\omega^9+p_8\omega^8+p_7\omega^7+p_6\omega^6+p_5\omega^5+p_4\omega^4+p_3\omega^3+p_2\omega^2+p_1\omega+p_0} \tag{3-48}$$

By combining (3-44), (3-47) and (3-48), the polynomial *ZF*'s coefficients z_i (*i*=0,1,…,9) can be expressed in terms of ω_{oi} and b_i (*i*=1,2,3,4,5)

$$z_9 = -\frac{\omega_{o1}}{b_1}$$

$$z_8 = -\omega_{o1}^{\ 2} - \omega_{o2}^{\ 2} - \omega_{o3}^{\ 2} - \omega_{o4}^{\ 2} - \omega_{o5}^{\ 2} - \frac{\omega_{o1}\cdot\omega_{o2}}{b_1\cdot b_2} - \frac{\omega_{o2}\cdot\omega_{o3}}{b_2\cdot b_3} - \frac{\omega_{o1}\cdot\omega_{o4}}{b_1\cdot b_4} - \frac{\omega_{o4}\cdot\omega_{o5}}{b_4\cdot b_5}$$

$$z_7 = \frac{\omega_{o1}}{b_1}\cdot\omega_{o2}^{\ 2} + \frac{\omega_{o1}}{b_1}\cdot\omega_{o3}^{\ 2} + \frac{\omega_{o1}}{b_1}\cdot\omega_{o4}^{\ 2} + \frac{\omega_{o1}}{b_1}\cdot\omega_{o5}^{\ 2} + \frac{\omega_{o1}\cdot\omega_{o4}\cdot\omega_{o5}}{b_1\cdot b_4\cdot b_5} + \frac{\omega_{o1}\cdot\omega_{o2}\cdot\omega_{o3}}{b_1\cdot b_2\cdot b_3}$$

$$z_6 = \omega_{o1}^{\ 2}\cdot\omega_{o2}^{\ 2} + \omega_{o2}^{\ 2}\cdot\omega_{o3}^{\ 2} + \omega_{o1}^{\ 2}\cdot\omega_{o3}^{\ 2} + \omega_{o1}^{\ 2}\cdot\omega_{o4}^{\ 2} + \omega_{o2}^{\ 2}\cdot\omega_{o4}^{\ 2} + \omega_{o3}^{\ 2}\cdot\omega_{o4}^{\ 2} + \omega_{o1}^{\ 2}\cdot\omega_{o5}^{\ 2} + \omega_{o2}^{\ 2}\cdot\omega_{o5}^{\ 2}$$
$$+\omega_{o3}^{\ 2}\cdot\omega_{o5}^{\ 2} + \omega_{o4}^{\ 2}\cdot\omega_{o5}^{\ 2} + \frac{\omega_{o1}\cdot\omega_{o2}\cdot\left(\omega_{o3}^{\ 2}+\omega_{o4}^{\ 2}+\omega_{o5}^{\ 2}\right)}{b_1\cdot b_2} + \frac{\omega_{o1}\cdot\omega_{o4}\cdot\left(\omega_{o2}^{\ 2}+\omega_{o3}^{\ 2}+\omega_{o5}^{\ 2}\right)}{b_1\cdot b_4}$$
$$+\frac{\omega_{o2}\cdot\omega_{o3}\cdot\left(\omega_{o1}^{\ 2}+\omega_{o4}^{\ 2}+\omega_{o5}^{\ 2}\right)}{b_2\cdot b_3} + \frac{\omega_{o4}\cdot\omega_{o5}\cdot\left(\omega_{o1}^{\ 2}+\omega_{o2}^{\ 2}+\omega_{o3}^{\ 2}\right)}{b_4\cdot b_5} + \frac{\omega_{o1}\cdot\omega_{o2}\cdot\omega_{o3}\cdot\omega_{o4}}{b_1\cdot b_2\cdot b_3\cdot b_4}$$
$$+\frac{\omega_{o1}\cdot\omega_{o2}\cdot\omega_{o4}\cdot\omega_{o5}}{b_1\cdot b_2\cdot b_4\cdot b_5} + \frac{\omega_{o2}\cdot\omega_{o3}\cdot\omega_{o4}\cdot\omega_{o5}}{b_2\cdot b_3\cdot b_4\cdot b_5}$$

$$z_5 = -\frac{\omega_{o1}}{b_1}\cdot\left(\omega_{o2}^{\ 2}\cdot\omega_{o3}^{\ 2} + \omega_{o2}^{\ 2}\cdot\omega_{o4}^{\ 2} + \omega_{o3}^{\ 2}\cdot\omega_{o4}^{\ 2} + \omega_{o2}^{\ 2}\cdot\omega_{o5}^{\ 2} + \omega_{o3}^{\ 2}\cdot\omega_{o5}^{\ 2} + \omega_{o4}^{\ 2}\cdot\omega_{o5}^{\ 2}\right)$$
$$-\frac{\omega_{o1}\cdot\omega_{o2}\cdot\omega_{o3}\cdot\left(\omega_{o4}^{\ 2}+\omega_{o5}^{\ 2}\right)}{b_1\cdot b_2\cdot b_3} - \frac{\omega_{o1}\cdot\omega_{o4}\cdot\omega_{o5}\cdot\left(\omega_{o2}^{\ 2}+\omega_{o3}^{\ 2}\right)}{b_1\cdot b_4\cdot b_5} - \frac{\omega_{o1}\cdot\omega_{o2}\cdot\omega_{o3}\cdot\omega_{o4}\cdot\omega_{o5}}{b_1\cdot b_2\cdot b_3\cdot b_4\cdot b_5}$$

$$z_4 = -\omega_{o1}^{\ 2}\cdot\omega_{o2}^{\ 2}\cdot\omega_{o3}^{\ 2} - \omega_{o1}^{\ 2}\cdot\omega_{o2}^{\ 2}\cdot\omega_{o5}^{\ 2} - \omega_{o2}^{\ 2}\cdot\omega_{o3}^{\ 2}\cdot\omega_{o5}^{\ 2} - \omega_{o1}^{\ 2}\cdot\omega_{o3}^{\ 2}\cdot\omega_{o5}^{\ 2} - \omega_{o1}^{\ 2}\cdot\omega_{o2}^{\ 2}\cdot\omega_{o4}^{\ 2}$$
$$-\omega_{o2}^{\ 2}\cdot\omega_{o3}^{\ 2}\cdot\omega_{o4}^{\ 2} - \omega_{o1}^{\ 2}\cdot\omega_{o3}^{\ 2}\cdot\omega_{o4}^{\ 2} - \omega_{o1}^{\ 2}\cdot\omega_{o4}^{\ 2}\cdot\omega_{o5}^{\ 2} - \omega_{o2}^{\ 2}\cdot\omega_{o4}^{\ 2}\cdot\omega_{o5}^{\ 2} - \omega_{o3}^{\ 2}\cdot\omega_{o4}^{\ 2}\cdot\omega_{o5}^{\ 2}$$
$$-\frac{\omega_{o1}\cdot\omega_{o2}\cdot\left(\omega_{o3}^{\ 2}\cdot\omega_{o4}^{\ 2}+\omega_{o3}^{\ 2}\cdot\omega_{o5}^{\ 2}+\omega_{o4}^{\ 2}\cdot\omega_{o5}^{\ 2}\right)}{b_1\cdot b_2} - \frac{\omega_{o2}\cdot\omega_{o3}\cdot\left(\omega_{o1}^{\ 2}\cdot\omega_{o5}^{\ 2}+\omega_{o1}^{\ 2}\cdot\omega_{o4}^{\ 2}+\omega_{o4}^{\ 2}\cdot\omega_{o5}^{\ 2}\right)}{b_2\cdot b_3}$$
$$-\frac{\omega_{o1}\cdot\omega_{o4}\cdot\left(\omega_{o2}^{\ 2}\cdot\omega_{o3}^{\ 2}+\omega_{o2}^{\ 2}\cdot\omega_{o5}^{\ 2}+\omega_{o3}^{\ 2}\cdot\omega_{o5}^{\ 2}\right)}{b_1\cdot b_4} - \frac{\omega_{o4}\cdot\omega_{o5}\cdot\left(\omega_{o1}^{\ 2}\cdot\omega_{o2}^{\ 2}+\omega_{o2}^{\ 2}\cdot\omega_{o3}^{\ 2}+\omega_{o1}^{\ 2}\cdot\omega_{o3}^{\ 2}\right)}{b_4\cdot b_5}$$
$$-\frac{\omega_{o1}\cdot\omega_{o2}\cdot\omega_{o3}\cdot\omega_{o4}\cdot\omega_{o5}^{\ 2}}{b_1\cdot b_2\cdot b_3\cdot b_4} - \frac{\omega_{o1}\cdot\omega_{o2}\cdot\omega_{o3}^{\ 2}\cdot\omega_{o4}\cdot\omega_{o5}}{b_1\cdot b_2\cdot b_4\cdot b_5} - \frac{\omega_{o1}^{\ 2}\cdot\omega_{o2}\cdot\omega_{o3}\cdot\omega_{o4}\cdot\omega_{o5}}{b_2\cdot b_3\cdot b_4\cdot b_5}$$

$$z_3 = \frac{\omega_{o1}}{b_1}\cdot\left(\omega_{o2}^{\ 2}\cdot\omega_{o3}^{\ 2}\cdot\omega_{o4}^{\ 2} + \omega_{o2}^{\ 2}\cdot\omega_{o3}^{\ 2}\cdot\omega_{o5}^{\ 2} + \omega_{o2}^{\ 2}\cdot\omega_{o4}^{\ 2}\cdot\omega_{o5}^{\ 2} + \omega_{o3}^{\ 2}\cdot\omega_{o4}^{\ 2}\cdot\omega_{o5}^{\ 2}\right)$$
$$+\frac{\omega_{o1}\cdot\omega_{o2}^{\ 2}\cdot\omega_{o3}^{\ 2}\cdot\omega_{o4}\cdot\omega_{o5}}{b_1\cdot b_4\cdot b_5} + \frac{\omega_{o1}\cdot\omega_{o2}\cdot\omega_{o3}\cdot\omega_{o4}^{\ 2}\cdot\omega_{o5}^{\ 2}}{b_1\cdot b_2\cdot b_3}$$

$$z_2 = \omega_{o1}^{\ 2}\cdot\omega_{o2}^{\ 2}\cdot\omega_{o3}^{\ 2}\cdot\omega_{o4}^{\ 2} + \omega_{o1}^{\ 2}\cdot\omega_{o2}^{\ 2}\cdot\omega_{o3}^{\ 2}\cdot\omega_{o5}^{\ 2} + \omega_{o1}^{\ 2}\cdot\omega_{o2}^{\ 2}\cdot\omega_{o4}^{\ 2}\cdot\omega_{o5}^{\ 2} + \omega_{o2}^{\ 2}\cdot\omega_{o3}^{\ 2}\cdot\omega_{o4}^{\ 2}\cdot\omega_{o5}^{\ 2}$$
$$+\omega_{o1}^{\ 2}\cdot\omega_{o3}^{\ 2}\cdot\omega_{o4}^{\ 2}\cdot\omega_{o5}^{\ 2} + \frac{\omega_{o1}\cdot\omega_{o2}\cdot\omega_{o3}^{\ 2}\cdot\omega_{o4}^{\ 2}\cdot\omega_{o5}^{\ 2}}{b_1\cdot b_2} + \frac{\omega_{o1}^{\ 2}\cdot\omega_{o2}\cdot\omega_{o3}\cdot\omega_{o4}^{\ 2}\cdot\omega_{o5}^{\ 2}}{b_2\cdot b_3} + \frac{\omega_{o1}\cdot\omega_{o2}^{\ 2}\cdot\omega_{o3}^{\ 2}\cdot\omega_{o4}\cdot\omega_{o5}^{\ 2}}{b_1\cdot b_4}$$
$$+\frac{\omega_{o1}^{\ 2}\cdot\omega_{o2}^{\ 2}\cdot\omega_{o3}^{\ 2}\cdot\omega_{o4}\cdot\omega_{o5}}{b_4\cdot b_5}$$

$$z_1 = -\frac{\omega_{o1}}{b_1}\cdot\omega_{o2}^{\ 2}\cdot\omega_{o3}^{\ 2}\cdot\omega_{o4}^{\ 2}\cdot\omega_{o5}^{\ 2}$$

$$z_0 = -\omega_{o1}^{\ 2}\cdot\omega_{o2}^{\ 2}\cdot\omega_{o3}^{\ 2}\cdot\omega_{o4}^{\ 2}\cdot\omega_{o5}^{\ 2}$$

(3-49)

Since $-\omega_{Li}$ and ω_{Hi} (i=1,2,3,4,5) are the roots of Equation (3-47), z_i (i=0,1,…,9) can also be analytically derived from equation below,

$$\omega^{10}+z_9\omega^9+z_8\omega^8+z_7\omega^7+z_6\omega^6+z_5\omega^5+z_4\omega^4+z_3\omega^3+z_2\omega^2+z_1\omega+z_0 = (\omega+\omega_{L1})\cdot(\omega+\omega_{L2})\cdot(\omega+\omega_{L3})\cdot(\omega+\omega_{L4})\cdot(\omega+\omega_{L5})\cdot(\omega-\omega_{H1})\cdot(\omega-\omega_{H2})\cdot(\omega-\omega_{H3})\cdot(\omega-\omega_{H4})\cdot(\omega-\omega_{H5}) \quad (3\text{-}50)$$

It can be observed that, by expanding the right part of (3-50), z_i (i=0,1,…,9) can be derived easily, and can be expressed only in terms of ω_{Li} and ω_{Hi} (i=1,2,3,4,5). Because of the extremely large volume of terms in it, the result will not be presented here.

As long as the passband specification of ω_{Li} and ω_{Hi} (i=1,2,3,4,5) are known, z_i (i=0,1,…,9) can be obtained from (3-50). Then, by substituting them into (3-49), the interim parameters of ω_{oi} and b_i (i=1,2,3,4,5) can be solved. Hence, the frequency transformation (3-44) is fully defined. Then, if the lowpass prototype for this 10th order five-passband filter is given, the matrix in (3-44) and external Q-factors can also be fully derived as well. A numerical example is given below for validation.

This example is based on the topology shown in Figure 3.32(a). The five passbands of this filter are 8.20 ~ 8.67 GHz, 9.13 ~ 9.60 GHz, 10.06 ~ 10.52 GHz, 11.00 ~ 11.46 GHz and 11.92 ~ 12.40 GHz. It is transformed from the 2nd order lowpass prototype Chebyshev given in Section 3.2.3.1 (refer to Figure 3.6 and Table 3.2). The passband specifications and corresponding interim parameters are given in Table 3.7.

Passband specifications	**Interim parameters**
$\omega_{L1} = 8.20GHz$	$\omega_{o1} = 10.04GHz$
$\omega_{H1} = 8.67GHz$	$\omega_{o2} = 9.32GHz$
$\omega_{L2} = 9.13GHz$	$\omega_{o3} = 9.29GHz$
$\omega_{H2} = 9.60GHz$	$\omega_{o4} = 11.20GHz$
$\omega_{L3} = 10.06GHz$	$\omega_{o5} = 11.39GHz$
$\omega_{H3} = 10.52GHz$	$b_1 = 4.29$
$\omega_{L4} = 11.00GHz$	$b_2 = 8.05$
$\omega_{H4} = 11.46GHz$	$b_3 = 10.68$
$\omega_{L5} = 11.92GHz$	$b_4 = 10.32$
$\omega_{H5} = 12.40GHz$	$b_5 = 13.09$

Table 3.7 The passband specifications and interim parameters for Example 5

According to (3-6), (3-8), (3-40) and (3-42), the coupling matrix is calculated below,

$$[M] = \begin{pmatrix} -0.0087 & 0.3874 & 0.1701 & 0 & 0 & 0 & 0.1503 & 0 & 0 & 0 \\ 0.3874 & -0.0087 & 0 & 0.1701 & 0 & 0 & 0 & 0.1503 & 0 & 0 \\ 0.1701 & 0 & -0.1577 & 0 & 0.1079 & 0 & 0 & 0 & 0 & 0 \\ 0 & 0.1701 & 0 & -0.1577 & 0 & 0.1079 & 0 & 0 & 0 & 0 \\ 0 & 0 & 0.1079 & 0 & -0.1641 & 0 & 0 & 0 & 0 & 0 \\ 0 & 0 & 0 & 0.1079 & 0 & -0.1641 & 0 & 0 & 0 & 0 \\ 0.1503 & 0 & 0 & 0 & 0 & 0 & 0.2104 & 0 & 0.0860 & 0 \\ 0 & 0.1503 & 0 & 0 & 0 & 0 & 0 & 0.2104 & 0 & 0.0860 \\ 0 & 0 & 0 & 0 & 0 & 0 & 0.0860 & 0 & 0.2442 & 0 \\ 0 & 0 & 0 & 0 & 0 & 0 & 0 & 0.0860 & 0 & 0.2442 \end{pmatrix} \tag{3-51}$$

According to Equation (3-10) and (3-11), the external Q-factors ($Q_{eS} = Q_{eL}$) are both 2.85.

The *S*-parameters are plotted in Figure 3.33.

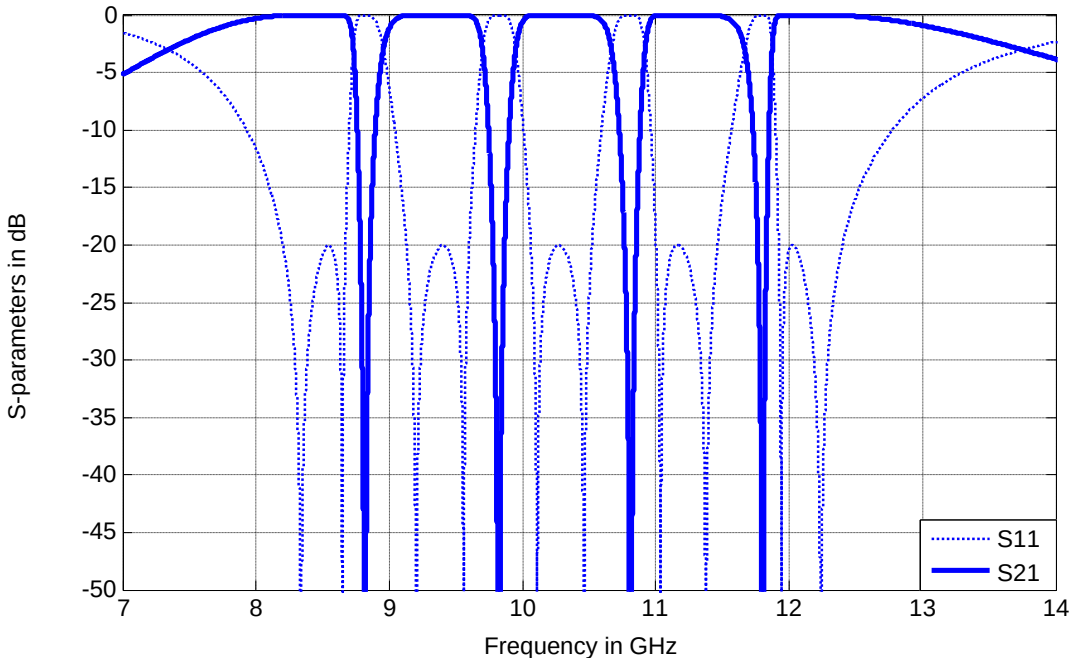

Figure 3.33 The *S*-parameter of a 10th order even bandwidth five-passband filter with Chebyshev response (Passband 1: 8.20 ~ 8.67 GHz, Passband 2: 9.13 ~ 9.60 GHz, Passband 3: 10.06 ~ 10.52 GHz, Passband 4: 11.00 ~ 11.46 GHz, Passband 5: 11.92 ~ 12.40 GHz)

The corresponding group delay for the above response is given below in Figure 3.34.

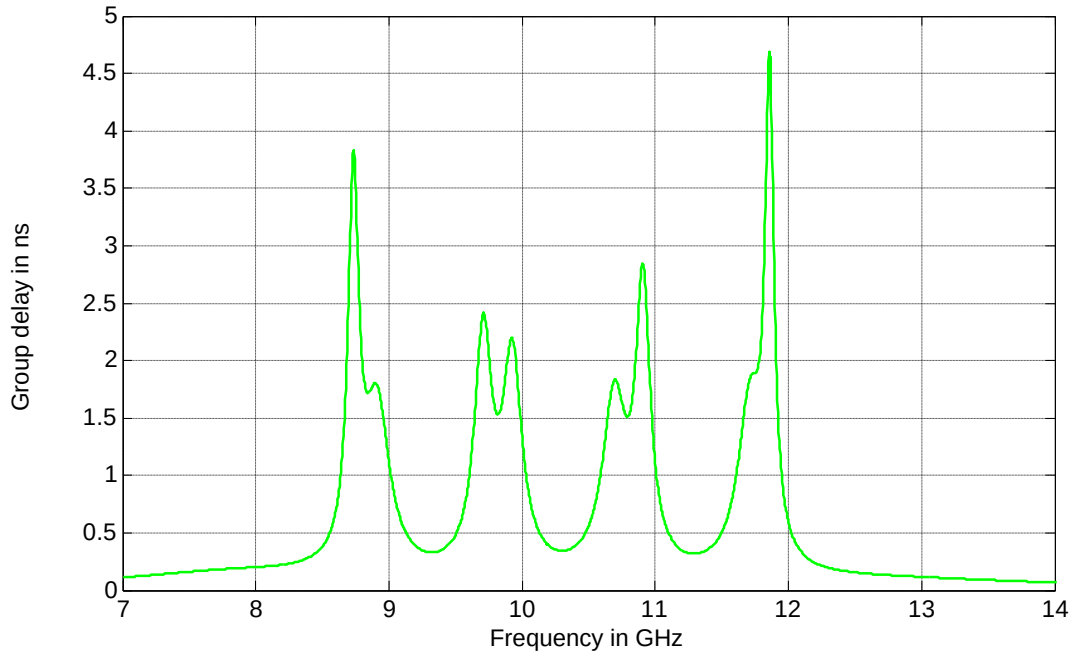

Figure 3.34 The group delay of the 10th order even bandwidth five-passband filter with Chebyshev response.

3.5.2 Example 6: A 10th Order Five-Passband Filter with Chebyshev Response (Uneven Bandwidth)

This example is also based on the 10th order topology given in Figure 3.32(a), but with uneven bandwidths. It is also transformed from the same lowpass prototype shown in Section 3.2.3.1 (refer to Figure 3.6 and Table 3.2). The passband specifications and corresponding interim parameters are given in Table 3.8

Passband specifications	**Interim parameters**
ω_{L1}=9.20 GHz	ω_{o1}=9.94 GHz
ω_{H1}=9.29 GHz	ω_{o2}=9.59 GHz
ω_{L2}=9.41 GHz	ω_{o3}=9.43 GHz
ω_{H2}=9.67 GHz	ω_{o4}=10.35 GHz
ω_{L3}=9.80 GHz	ω_{o5}=10.43 GHz
ω_{H3}=10.17 GHz	b_1=9.22
ω_{L4}=10.25 GHz	b_2=51.88
ω_{H4}=10.48 GHz	b_3=12.16
ω_{L5}=10.57 GHz	b_4=78.94
ω_{H5}=10.70 GHz	b_5=13.30

Table 3.8 The passband specifications and interim parameters for Example 6

According to (3-6), (3-8), (3-40) and (3-42) the coupling matrix is calculated as,

$$[M]=\begin{pmatrix} 0.0037 & 0.1803 & 0.0457 & 0 & 0 & 0 & 0.0371 & 0 & 0 & 0 \\ 0.1803 & 0.0037 & 0 & 0.0457 & 0 & 0 & 0 & 0.0371 & 0 & 0 \\ 0.0457 & 0 & -0.0680 & 0 & 0.0398 & 0 & 0 & 0 & 0 & 0 \\ 0 & 0.0457 & 0 & -0.0680 & 0 & 0.0398 & 0 & 0 & 0 & 0 \\ 0 & 0 & 0.0398 & 0 & -0.1017 & 0 & 0 & 0 & 0 & 0 \\ 0 & 0 & 0 & 0.0398 & 0 & -0.1017 & 0 & 0 & 0 & 0 \\ 0.0371 & 0 & 0 & 0 & 0 & 0 & 0.0846 & 0 & 0.0309 & 0 \\ 0 & 0.0371 & 0 & 0 & 0 & 0 & 0 & 0.0846 & 0 & 0.0309 \\ 0 & 0 & 0 & 0 & 0 & 0 & 0.0309 & 0 & 0.1000 & 0 \\ 0 & 0 & 0 & 0 & 0 & 0 & 0 & 0.0309 & 0 & 0.1000 \end{pmatrix} \tag{3-52}$$

Also, according to (3-10) and (3-19), the external Q-factors ($Q_{eS}=Q_{eL}$) are both 6.13. The S-parameters and the group delay are plotted in Figure 3.35 and Figure 3.37, respectively.

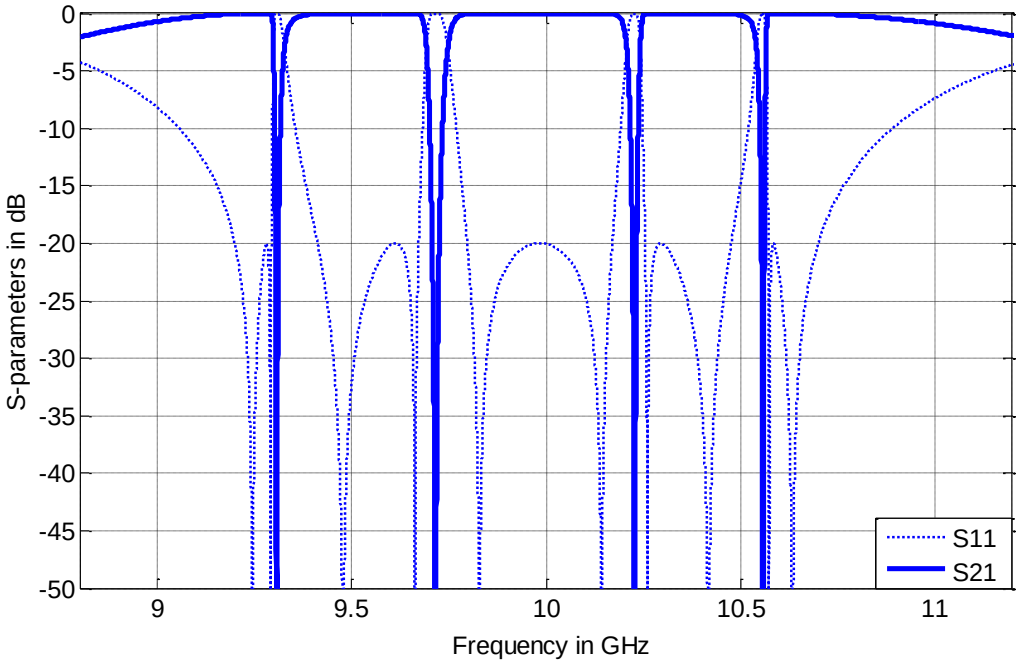

Figure 3.35 The *S*-parameter of a 10th order uneven bandwidth five-passband filter with Chebyshev response (Passband 1: 9.20~ 9.29 GHz, Passband 2: 9.41 ~ 9.67 GHz, Passband 3: 9.80 ~ 10.17 GHz, Passband 4: 10.25 ~ 10.48 GHz, Passband 5: 10.57 ~ 10.70 GHz)

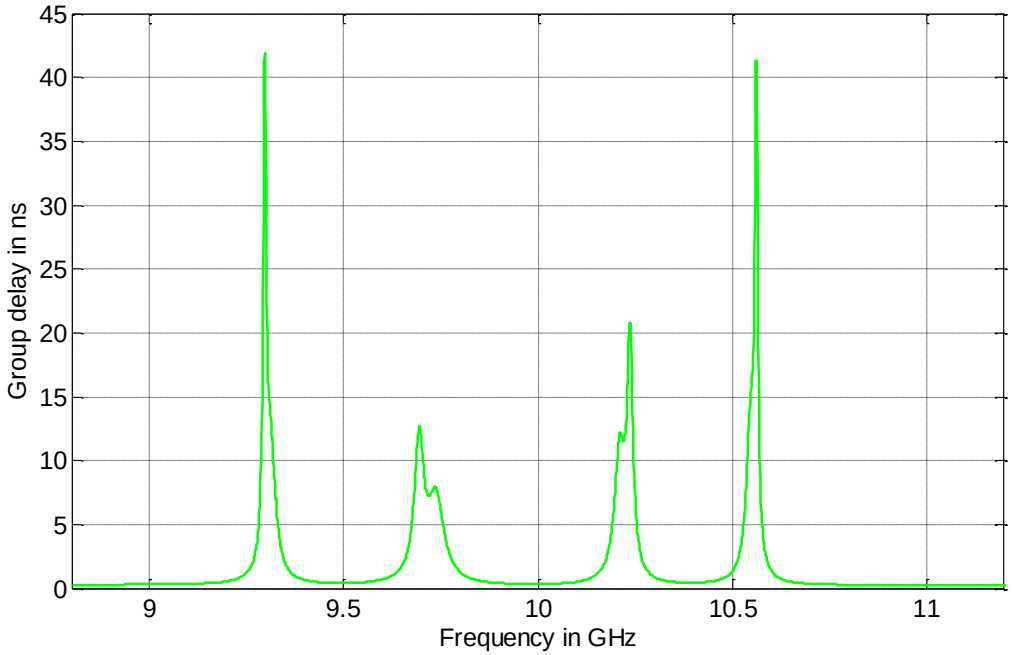

Figure 3.36 The group delay of the uneven bandwidth five-passband filter

It can be found that the delay near the edges of the stopbands is greater than that of the previous example. This is inevitable due to the smaller *FBW* which causes sharper slopes of the *S*21. It extends well into the passbands [7].

3.5.3 Example 7: A 20th Order Five-Passband Filter with Quasi-Elliptic Response (Uneven Bandwidth)

Usually there are two ways to increase the selectivity of the passband. One way is to increase the order of the filter; the other one is to introduce transmission zeros to the sideband, which makes the attenuation goes down more quickly. Given the fact that, the filters with very large orders may be difficult to implement, the second method is used. As shown in Appendix I, by introducing cross-coupling, a cascaded quadruplet (CQ) structure can produce a quasi-elliptic response. In this example, the five-passband filter is transformed from the lowpass prototype quasi-elliptic filter given in Appendix I. From topology point of view, this means that, the four lowpass resonators are replaced by the mixed coupled resonator sections shown in Figure 3.30. The de-normalised 20th order five-passband filter has a topology shown in Figure 3.37. For comparison, the passband specifications are designed to be the same as that in example 6, i.e. the interim parameters are same as well (refer to Table 3.8). Therefore, this 20th order filter shares the exactly same mixed coupled resonator sections with the 10th order filter in example 6, but there are four of them now.

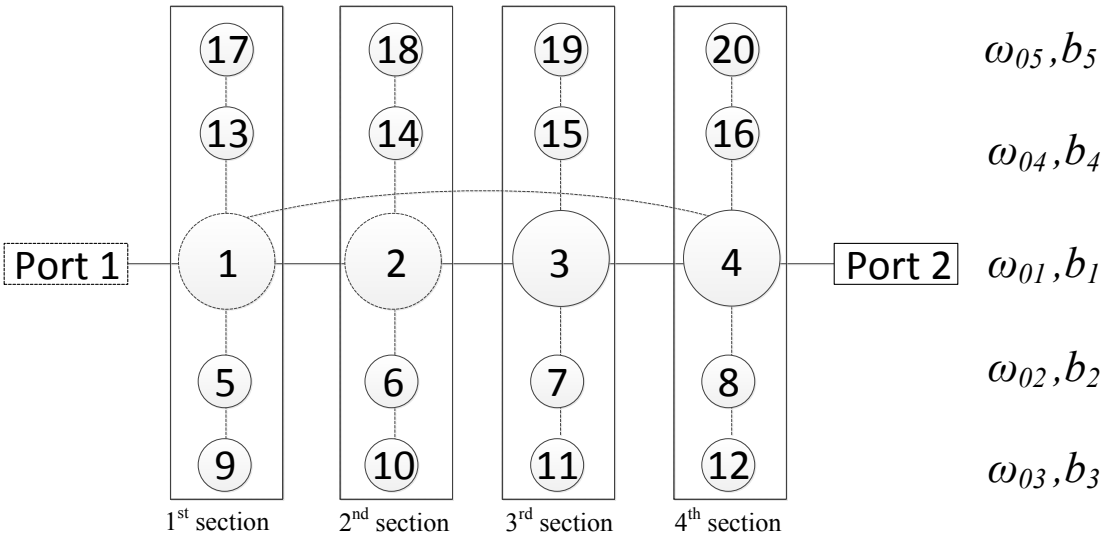

Figure 3.37 The topology of a 20th order five-passband filter (each passband has a 4th order quasi-elliptic response)

According to (3-8), (3-18) and (3-42), the coupling matrix is calculated as,

$$[M]=\begin{pmatrix}
0.0037 & 0.0901 & 0 & -0.0321 & 0.0457 & 0 & 0 & 0 & 0 & 0 & 0 & 0 & 0.0371 & 0 & 0 & 0 & 0 & 0 & 0 & 0 \\
0.0901 & 0.0037 & 0.0883 & 0 & 0 & 0.0457 & 0 & 0 & 0 & 0 & 0 & 0 & 0 & 0.0371 & 0 & 0 & 0 & 0 & 0 & 0 \\
0 & 0.0883 & 0.0037 & 0.0901 & 0 & 0 & 0.0457 & 0 & 0 & 0 & 0 & 0 & 0 & 0 & 0.0371 & 0 & 0 & 0 & 0 & 0 \\
-0.0321 & 0 & 0.0901 & 0.0037 & 0 & 0 & 0 & 0.0457 & 0 & 0 & 0 & 0 & 0 & 0 & 0 & 0.0371 & 0 & 0 & 0 & 0 \\
0.0457 & 0 & 0 & 0 & -0.0680 & 0 & 0 & 0 & 0.0398 & 0 & 0 & 0 & 0 & 0 & 0 & 0 & 0 & 0 & 0 & 0 \\
0 & 0.0457 & 0 & 0 & 0 & -0.0680 & 0 & 0 & 0 & 0.0398 & 0 & 0 & 0 & 0 & 0 & 0 & 0 & 0 & 0 & 0 \\
0 & 0 & 0.0457 & 0 & 0 & 0 & -0.0680 & 0 & 0 & 0 & 0.0398 & 0 & 0 & 0 & 0 & 0 & 0 & 0 & 0 & 0 \\
0 & 0 & 0 & 0.0457 & 0 & 0 & 0 & -0.0680 & 0 & 0 & 0 & 0.0398 & 0 & 0 & 0 & 0 & 0 & 0 & 0 & 0 \\
0 & 0 & 0 & 0 & 0.0398 & 0 & 0 & 0 & -0.1017 & 0 & 0 & 0 & 0 & 0 & 0 & 0 & 0 & 0 & 0 & 0 \\
0 & 0 & 0 & 0 & 0 & 0.0398 & 0 & 0 & 0 & -0.1017 & 0 & 0 & 0 & 0 & 0 & 0 & 0 & 0 & 0 & 0 \\
0 & 0 & 0 & 0 & 0 & 0 & 0.0398 & 0 & 0 & 0 & -0.1017 & 0 & 0 & 0 & 0 & 0 & 0 & 0 & 0 & 0 \\
0 & 0 & 0 & 0 & 0 & 0 & 0 & 0.0398 & 0 & 0 & 0 & -0.1017 & 0 & 0 & 0 & 0 & 0 & 0 & 0 & 0 \\
0.0371 & 0 & 0 & 0 & 0 & 0 & 0 & 0 & 0 & 0 & 0 & 0 & 0.0846 & 0 & 0 & 0 & 0.0309 & 0 & 0 & 0 \\
0 & 0.0371 & 0 & 0 & 0 & 0 & 0 & 0 & 0 & 0 & 0 & 0 & 0 & 0.0846 & 0 & 0 & 0 & 0.0309 & 0 & 0 \\
0 & 0 & 0.0371 & 0 & 0 & 0 & 0 & 0 & 0 & 0 & 0 & 0 & 0 & 0 & 0.0846 & 0 & 0 & 0 & 0.0309 & 0 \\
0 & 0 & 0 & 0.0371 & 0 & 0 & 0 & 0 & 0 & 0 & 0 & 0 & 0 & 0 & 0 & 0.0846 & 0 & 0 & 0 & 0.0309 \\
0 & 0 & 0 & 0 & 0 & 0 & 0 & 0 & 0 & 0 & 0 & 0 & 0.0309 & 0 & 0 & 0 & 0.1000 & 0 & 0 & 0 \\
0 & 0 & 0 & 0 & 0 & 0 & 0 & 0 & 0 & 0 & 0 & 0 & 0 & 0.0309 & 0 & 0 & 0 & 0.1000 & 0 & 0 \\
0 & 0 & 0 & 0 & 0 & 0 & 0 & 0 & 0 & 0 & 0 & 0 & 0 & 0 & 0.0309 & 0 & 0 & 0 & 0.1000 & 0 \\
0 & 0 & 0 & 0 & 0 & 0 & 0 & 0 & 0 & 0 & 0 & 0 & 0 & 0 & 0 & 0.0309 & 0 & 0 & 0 & 0.1000
\end{pmatrix} \tag{3-53}$$

Also, according to (3-10) and (3-19), the external Q-factors ($Q_{eS}=Q_{eL}$) are both 8.92. The S-parameters and group delay are plotted in Figure 3.38 and Figure 3.39, respectively.

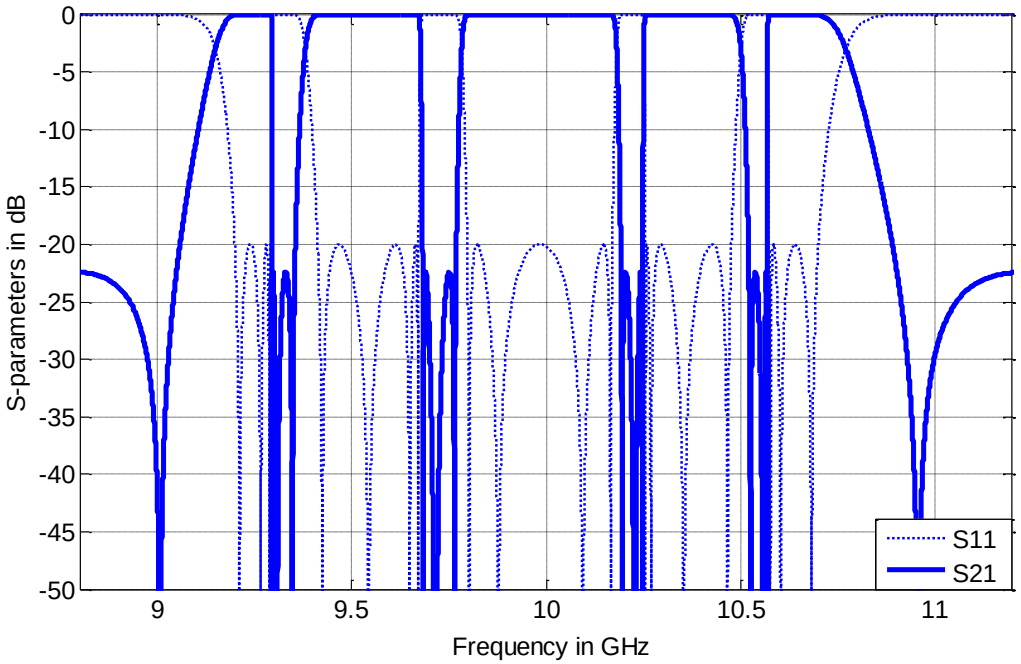

Figure 3.38 The S-parameter of a 20th order uneven bandwidth five-passband filter with quasi-elliptic response (Passband 1: 9.20~ 9.29 GHz, Passband 2: 9.41 ~ 9.67 GHz, Passband 3: 9.80 ~ 10.17 GHz, Passband 4: 10.25 ~ 10.48 GHz, Passband 5: 10.57 ~ 10.70 GHz)

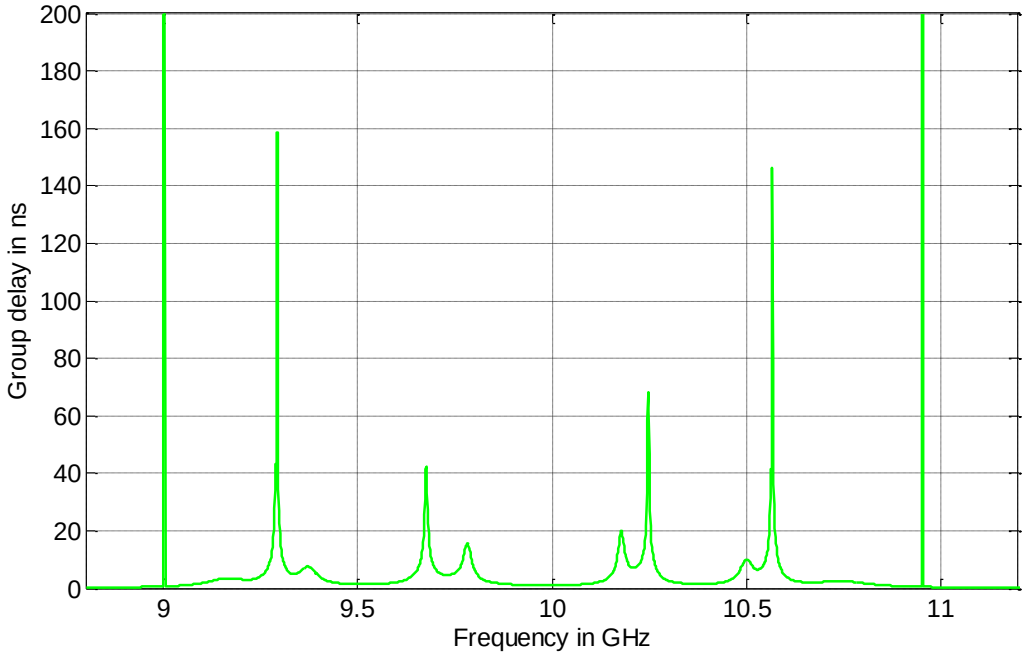

Figure 3.39 The group delay of a 20th order uneven bandwidth five-passband filter with quasi-elliptic response

The above group delay is larger than that in Example 6, because the slope of *S*21 near stopband edges is sharper. It reaches infinity at the positions of transmission zeros.

Because the 20th order five-passband filter has the exactly same multi-passband resonator section as the 10th order five-passband filter in example 6, they should have the same passband specifications. Therefore, a comparison of the two responses is given in Figure 3.40. The blue line is the S11 for the 10th order five-band filter with Chebyshev response. The red line is the S11 for the 20th order five-band filter with quasi-elliptic response. A dashed line is placed horizontally on -20dB as a reference line for passband.

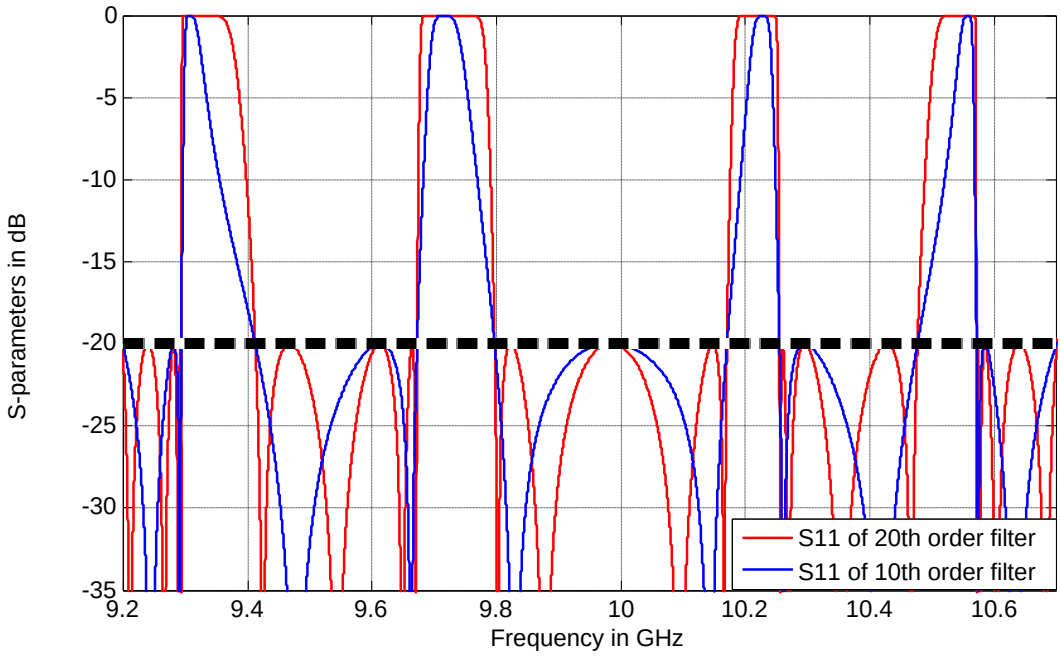

Figure 3.40 The *S*11 comparison between the 20th order five-passband filter and the 10th order five-passband filter (Passband 1: 9.20~ 9.29 GHz, Passband 2: 9.41 ~ 9.67 GHz, Passband 3: 9.80 ~ 10.17 GHz, Passband 4: 10.25 ~ 10.48 GHz, Passband 5: 10.57 ~ 10.70 GHz)

Reference:

1. Hong, J.-S. and M.J. Lancaster, *Microstrip Filters for RF/Microwave Applications* 2001: John Wiley and Sons Ltd, United Kingdom.
2. Giuseppe Macchiarella, S.T., "Design Techniques for Dual-passband Filters," *IEEE TRANSACTION ON MICROWAVE THEORY AND TECHNIQUES* , 2005. **53**(11): p. 7.
3. Xiao-Ping Chen, K.W., Zhao-Long Li, "Dual-Band and Triple-Band Substrate Integrated Waveguide Filters With Chebyshev and Quasi-Elliptic Responses," *IEEE TRANSACTION ON MICROWAVE THEORY AND TECHNIQUES* , 2007. **55**(12): p. 10.
4. Hao Di, B.W., Xin Lai and Chang-Hong Liang, "Synthesis and Realization of Novel Triple-passband Filter Based on Frequency Transformation," *APMC Microwave Conference*, 2009. p. 4.
5. Matthaei, G.L., L. Young, and E.M.T. Jones, *Microwave filters, impedance-matching networks, and coupling structures* 1964: McGraw-Hill.
6. Nedelchev, M.V. and I.G. Iliev, "Synthesis of Microwave Filters by Coupling Matrix Optimization," ICEST, 2011. **1**: p. 167-170.
7. Huang, F., "Dual-Band Superconducting Spiral Filters Including Narrow Bandstop Notches," *IEEE TRANSACTION ON MICROWAVE THEORY AND TECHNIQUES* , 2009. **57**(5): p. 8.

CHAPTER 4 RECTANGULAR WAVEGUIDE IMPLEMENTATION OF MULTI-PASSBAND FILTERS

There are many ways to implement a filter topology in real world. The rectangular waveguide is one of them. In this chapter, the five-passband filters discussed in the previous chapter with uneven bandwidth are implemented in the form of rectangular waveguide. To begin with, a discussion on the fundamental theory of rectangular waveguide is given in Section 4.1. This section describes the two basic building blocks of the rectangular waveguide circuit, which are the resonator and the coupling iris. The procedure of interpreting the theoretical coupling values into the real circuit is also illustrated within this section. Section 4.2 will discuss the design of the 10^{th} order five-passband filter with Chebyshev response. It is fabricated and measured; the results are given and analysed in this section. A 20^{th} order five-passband filter with quasi-elliptic response will be presented in Section 4.3.

4.1 The rectangular waveguide filter

4.1.1 Rectangular Waveguide

As its name indicates, a waveguide is a device that guides the energy of microwave signal along a pre-set path. There are many physical forms of transmission lines, including rectangular waveguide, coaxial cable, micro-strip, etc. They satisfy the design requirements for a range of applications. For low frequency (below 100MHz) applications, lumped element circuits work well, but for high frequency (above 1GHz) applications, as the lumped element circuit size is comparable to the wavelength of electromagnetic wavelength, it may have a significant power loss due to radiation and high current density; here waveguide circuits overcome these problems [1].

Free space between a transmitter and a receiver can also be considered as a waveguide in a more general sense, because it provides channels for wireless communication [2]. However, for earth to space satellite communication, the transmission through the atmosphere has to be taken into consideration. RF and microwave communications are exploited here mainly because the atmosphere is almost transparent to these frequencies (30MHz ~30GHz). Within the RF and microwave region of the frequency spectrum, X-band (8.0 to 12.0 GHz) is a frequency band that is widely used in satellite communication and other communication systems, such as radar. The reason behind is that, it offers a good compromise in performance features such as, interference resilience, rain resilience, compact terminal size, good data rates and good remote coverage, which are especially suitable for wireless communication use [3]. Among the waveguide forms that can be used at X-band frequency, rectangular waveguide is a good choice, as it provides high *Q*-factor, low insertion loss and good shielding which meets high performance requirements for communication applications [2]. Although X-band is used widely in this thesis, of course the design principles apply to all other frequency bands for rectangular waveguide circuits as well.

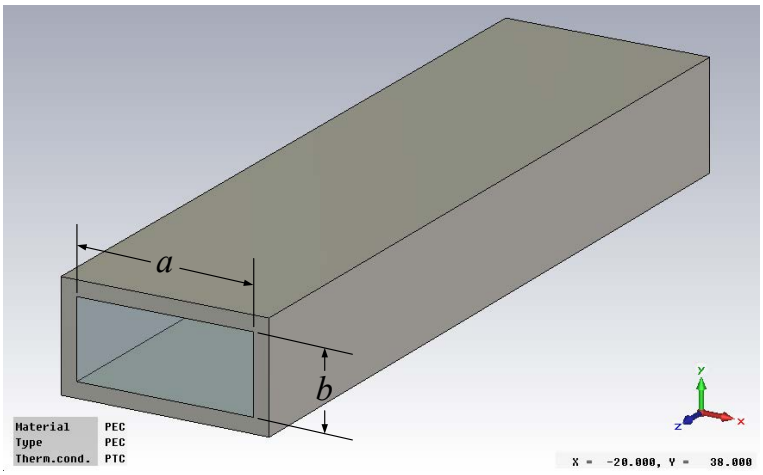

Figure 4.1 The configuration of a rectangular waveguide

As shown in Figure 4.1, the typical geometric structure of a rectangular waveguide is a hollow metal tube with rectangular transverse cross-section; *a* is the dimension in *x* direction

(width), b is the dimension in y direction (height). For a standard WR90 X-band rectangular waveguide, a is 22.86mm (0.900inches), b is 10.16mm (0.400inches).

As stated in [4], the transverse electromagnetic (TEM) mode does not exist in a rectangular waveguide, because there is only one conductor; but transverse electric (TE) mode and transverse magnetic (TM) mode can be supported by a rectangular waveguide. For each mode ($TE_{m,n}$ or $TM_{m,n}$), there is a cut-off frequency f_c where propagation is only possible above this frequency [4]. f_c is defined by,

$$f_c = \frac{1}{2\pi\sqrt{\mu\varepsilon}}\sqrt{\left(\frac{m\pi}{a}\right)^2 + \left(\frac{n\pi}{b}\right)^2} \tag{4-1}$$

here μ is the permeability, ε is the permittivity of the filling material; m and n represents the mode number in x and y directions, respectively. When the waveguide is filled up with vacuum, (4-1) can be re-written as,

$$f_c = \frac{c}{2}\sqrt{\left(\frac{m}{a}\right)^2 + \left(\frac{n}{b}\right)^2} \tag{4-2}$$

Here, $c = 1/\sqrt{\mu_0\varepsilon_0}$ is the speed of light in vacuum (μ_0 and ε_0 are permeability and permittivity of vacuum, respectively). When it is filled up with air, (4-1) can also provide a very good approximation, since the speed of light in air is very close to c. Usually, a standard rectangular waveguide has a width about twice the length of its height ($a \approx 2b$). This makes the $TE_{1,0}$ mode have the lowest cut-off frequency among all the modes, and also means that it is the dominant mode in the rectangular waveguide. It can be easily found from (4-2) that the $TE_{2,0}$ mode has the second lowest cut-off frequency. The band between these two cut-off frequencies is normally the operating frequency band of a waveguide, as only $TE_{1,0}$ mode exists within this band. There are reasons for the dimensions of rectangular waveguide to have the arrangement of $a \approx 2b$. When b is between $a/2$ and a, $TE_{0,1}$ mode will become the

second lowest mode; this will reduce the useful bandwidth of the rectangular waveguide. When *b* is smaller than *a*/2, it will reduce the power-handling capability of the waveguide [2].

Figure 4.2 shows the electromagnetic (EM) field and surface current of the $TE_{1,0}$ mode inside a rectangular waveguide.

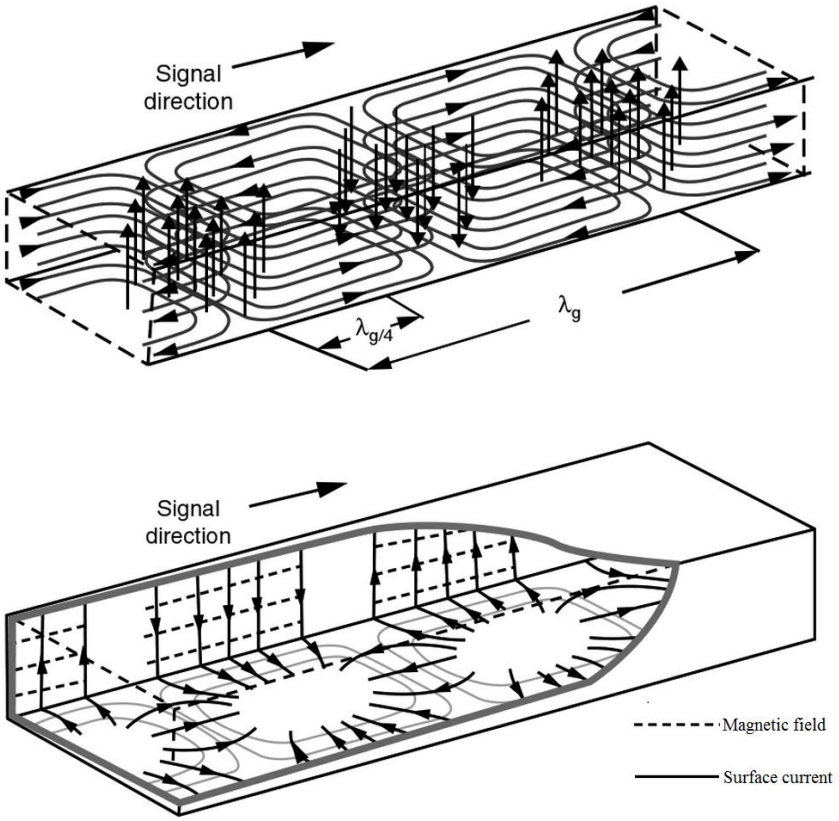

Figure 4.2 The EM field and surface current of $TE_{1,0}$ mode inside a rectangular waveguide (reproduced from [5])

In Figure 4.2, λ_g is the guided wavelength for the case of $TE_{1,0}$ mode, and it can be calculated by [4],

$$\lambda_g = \frac{2\pi}{\beta_{1,0}} = \frac{2\pi}{\sqrt{\omega^2 \mu\varepsilon - \left(\frac{\pi}{a}\right)^2}} \tag{4-3}$$

here $\beta_{1,0}$ is the propagation constant for $TE_{1,0}$ mode and can be calculated from the more generalized version of $\beta_{m,n}$ [4],

$$\beta_{m,n} = \sqrt{\omega^2 \mu\varepsilon - \left(\frac{m\pi}{a}\right)^2 - \left(\frac{n\pi}{b}\right)^2} \tag{4-4}$$

Because practical filters are made up of non-perfect conductor materials, α_c is introduced to describe the attenuation caused by conductor loss and for $TE_{1,0}$ mode is given by [4],

$$\alpha_c = \frac{R_s}{a^3 b \beta_{1,0} k\eta}\left(2b\pi^2 + a^3 k^2\right) \cdot 8.686 \quad \text{dB/m} \tag{4-5}$$

here $R_s = \sqrt{\omega\mu/2\sigma}$ is the surface resistance of the waveguide inner walls (σ is the conductivity of the waveguide material); $k = \omega\sqrt{\mu\varepsilon}$ is the wave number; $\eta = \sqrt{\mu/\varepsilon}$ is the intrinsic impedance for the filling material of the waveguide.

4.1.2 Rectangular Waveguide Resonator

As mentioned previously, rectangular waveguide cavity resonator is one of the building elements for rectangular waveguide filter circuits. The geometry of a resonator is shown in Figure 4.3.

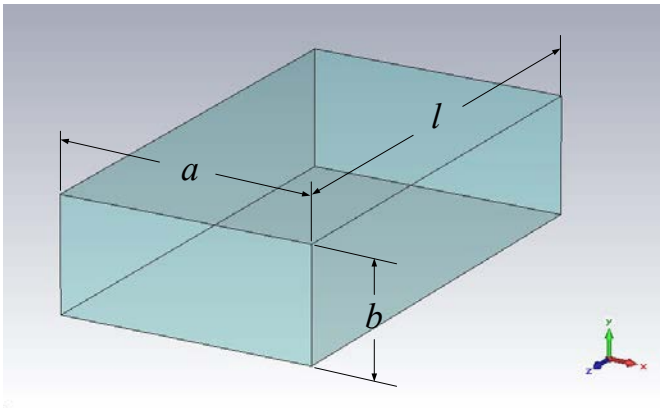

Figure 4.3 The geometric structure of a rectangular waveguide resonator, the blue indicates the air inside the resonator which is surrounded by conductor material

As discussed previously for the waveguide, *a* is the width in *x* direction, *b* is the height in *y* direction; now *l* is the length in *z* direction (for resonator that compatible with WR90 standard, *a* is 22.86mm, *b* is 10.16mm; when *l* is 20mm gives a frequency of 10GHz). Generally, there are two important parameters that describe a practical resonator, which are

resonant frequency f_0 and the unloaded Q-factor Q_u. The electric energy and magnetic energy transform between each other in cycles within a resonator; the number of these cycles per second is f_0. The intrinsic loss of a resonator is characterised by Q_u, which is a value that only determined by the physical dimension and the materials of the cavity resonator [6].

4.1.2.1 Centre Frequency

In a rectangular waveguide resonator, the transverse electric fields (for either $TE_{m,n}$ mode or $TM_{m,n}$ mode) is defined as [4],

$$\overline{E_t}(x,y,z) = \bar{e}(x,y)\left[A^+ e^{-j\beta_{m,n}z} + A^- e^{j\beta_{m,n}z}\right] \tag{4-6}$$

in which $\bar{e}(x,y)$ is a matrix in x and y directions which describes the transverse variation. A^+ and A^- represents the amplitude of waves that travels in $+z$ and $-z$ directions. $\beta_{m,n}$ is the propagation constant which is defined in (4-4).

By applying the boundary conditions that $z = 0$ and $z = l$ to equation (4-6), it is interesting to find that $A^+ = -A^-$ when $z = 0$, $\beta_{m,n} \cdot l = k \cdot \pi$ (k = 1,2,3…) when $z = l$. Recalling (4-3), the latter formula can be re-written as,

$$l = k \cdot \frac{\pi}{\beta_{m,n}} = k \cdot \frac{\lambda_g}{2} \qquad (k = 1,2,3,...) \tag{4-7}$$

This indicates that the cavity length d must be integral multiple of the half guided wavelength λ_g of the propagated wave. Therefore, the modes in the resonator can be represented as $TE_{m,n,k}$ mode or $TM_{m,n,k}$ mode (k represents the mode number in z direction; in this thesis k=1); the centre frequency of a rectangular waveguide resonator can be obtained from [4].

$$f_0 = \frac{1}{2\pi\sqrt{\mu\varepsilon}}\sqrt{\left(\frac{m\pi}{a}\right)^2 + \left(\frac{n\pi}{b}\right)^2 + \left(\frac{k\pi}{d}\right)^2} \tag{4-8}$$

Generally speaking, $TE_{1,0,1}$ mode is the dominant mode of the rectangular waveguide resonator. The EM field of $TE_{1,0,1}$ mode inside a cavity are shown in Figure 4.4.

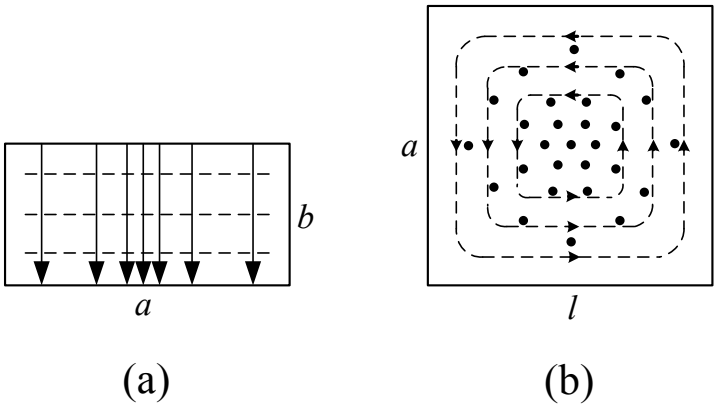

Figure 4.4 EM field configuration of $TE_{1,0,1}$ mode, (a) front view of a resonator, (b) top view of a resonator

Figure 4.4(a) shows the front of the resonator, the dashed line represents the magnetic field; the solid line represents the electric field with the arrow indicating the direction. Figure 4.4(b) shows the top view, where the dashed line means the anti-clockwise magnetic field, while the dots stand for the electric fields pointing out of the page.

4.1.2.2 Unloaded *Q*-factor

The unloaded *Q*-factor Q_u is a quantity that characterises the performance of a resonator in terms of stored energy and dissipated energy. For a resonator, a higher Q_u usually indicates lower loss and vice versa. There is a general equation given below which defines the Q_u of a resonator with arbitrary form [7],

$$Q_u = \omega \frac{Time\text{-}average \quad energy \quad stored \quad in \quad resonator}{Average \quad power \quad dissipated \quad in \quad resoantor} \tag{4-9}$$

A number of mechanisms can cause the loss in a resonator; by nature, they are categorised into three groups, which are: conductor loss Q_c, dielectric loss Q_d and radiation loss Q_r. The Q_u is defined as the sum of all these three losses [7],

$$\frac{1}{Q_u} = \frac{1}{Q_c} + \frac{1}{Q_d} + \frac{1}{Q_r} \tag{4-10}$$

For a closed rectangular waveguide cavity filled up with vacuum or air ($TE_{1,0,1}$ mode), its Q_d and Q_r can be considered as infinity; the only contribution to Q_u is Q_c which can be obtained from [4],

$$Q_c = \frac{(kad)^3 b\eta}{2\pi^2 R_s \left(2a^3 b + 2bd^3 + a^3 d + ad^3\right)} \tag{4-11}$$

This implies that, for such a waveguide resonator, Q_u is only determined by the conductor material and the dimension of the cavity.

4.1.3 The Physical Implementation of Coupling

During the design of a coupled-resonator filter, the physical implementation is usually based on given coupling matrix and external Q-factors that produce the desired response. Therefore, in order to realise the couplings in real circuits, they have to be interpreted into some particular physical form. This can be done with the help of an EM simulator. For the case of rectangular waveguide circuit, the coupling iris is the element to realise these couplings. The iris has different forms; Figure 4.5 shows the four that commonly use.

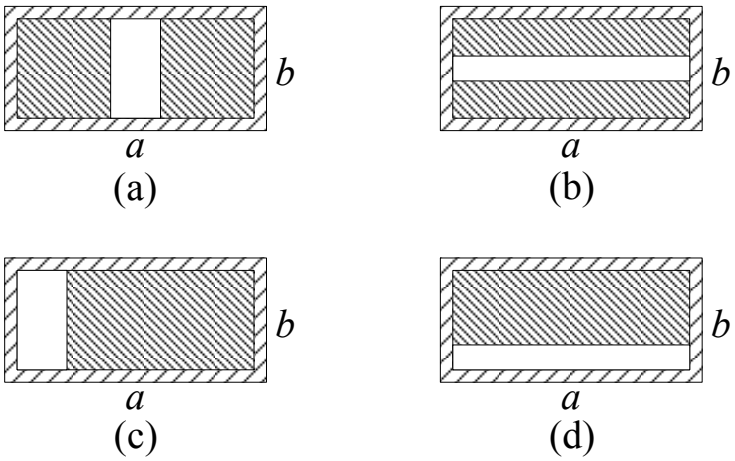

Figure 4.5 Coupling iris in different forms: (a) symmetrical inductive iris, (b) symmetrical capacitive iris, (c) asymmetrical inductive iris, (d) asymmetrically capacitive iris

The coupling strength is determined by the dimension of the coupling iris. For each iris, the dimensions can be determined individually with the help of EM simulator. In the following sections, the way to extract the dimensions of coupling iris is going to be investigated step by step.

4.1.3.1 External *Q*-Factor (Q_e)

The extraction procedure for Q_e is usually done with the help of an EM simulator. In this thesis, Computer Simulation Technology Microwave Studio (CST mws) was the EM simulation software that chosen for the microwave filter design [8]. As shown in Figure 4.6, a waveguide structure has been modelled in CST mws to extract the Q_e. This model was based on asymmetrical inductive irises. *wr*1 and *wr*2 were the widths of the two coupling irises, *t* was the thickness of both the irises.

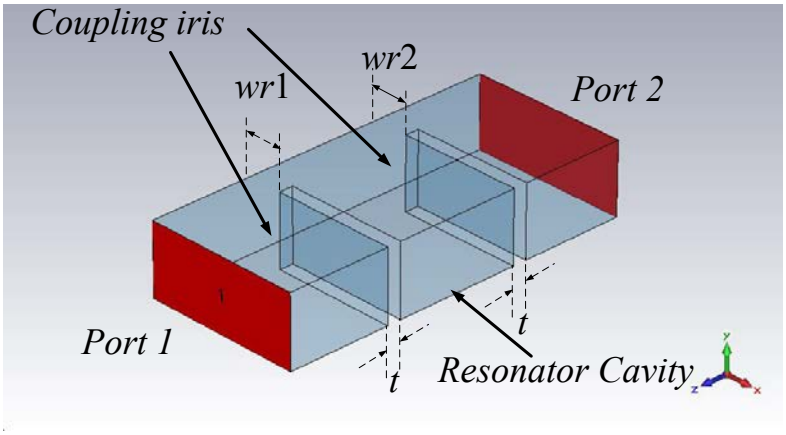

Figure 4.6 The structure modelled in CST for extracting Q_e

When a resonator is connected with external ports, the loaded *Q*-factor Q_L can be obtained from *S*21 [7],

$$Q_L = \frac{f_0}{BW_{3dB}} \tag{4-12}$$

Figure 4.7 was the simulated *S*21 response of the loaded single cavity resonator shown in Figure 4.6. It shows how the centre frequency f_0 and the 3dB bandwidth BW_{3dB} can be extracted from the *S*21.

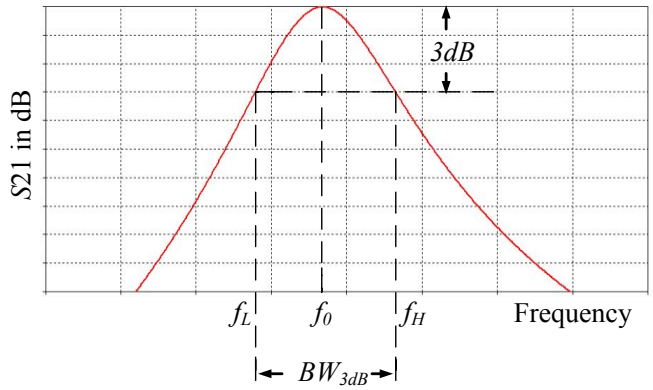

Figure 4.7 The $S21$ of the loaded resonator.

According to [4], Q_L can be defined in terms of Q_u and Q_e,

$$\frac{1}{Q_L} = \frac{1}{Q_u} + \frac{1}{Q_e} \tag{4-13}$$

The cavity resonator discussed here satisfies the following conditions:

- filled up with vacuum, so $\frac{1}{Q_d} = 0$,
- closed cavity, there is no radiation slot, so $\frac{1}{Q_r} = 0$,
- the conducting material is perfect electric conductor (PEC), so $\frac{1}{Q_c} = 0$.

Therefore, $\frac{1}{Q_u} = 0$, which makes $Q_e = Q_L = \frac{f_0}{BW_{3dB}}$.

For the model shown in Figure 4.6, the resonator is loaded with two external ports, therefore Q_e is defined by Q_{e1} and Q_{e2} which are ultimately controlled by $wr1$ and $wr2$, respectively.

$$\frac{1}{Q_e} = \frac{1}{Q_{e1}} + \frac{1}{Q_{e2}} \tag{4-14}$$

The narrower the iris is, the larger the external Q-factor will be. Consequently, when $wr2$ is very small, i.e. the coupling is very weak at port 2; then Q_{e2} can be considered close to infinity ($\frac{1}{Q_{e2}} \to 0$). This means that Q_{e1} plays the dominant role in controlling Q_e ($Q_e \approx Q_{e1}$).

Because $wr1$ controls Q_{e1}, $wr1$ also controls Q_e. A relationship between Q_e and $wr1$ is

obtained in Figure 4.8, when $wr2$ is 0.05mm (Q_{e2} is above 10^6), cavity length d is 18mm and iris thickness t is 2mm.

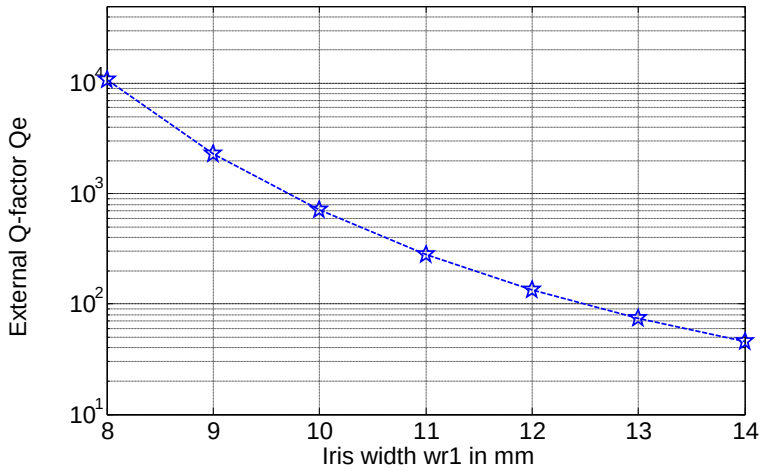

Figure 4.8 The relationship between Q_e and $wr1$

4.1.3.2 Inter-Resonator Coupling Coefficient (k_c)

The coupling coefficient k_c can be extracted with the EM simulator as well. Figure 4.9 shows a resonator pair coupled by asymmetrical inductive iris which was modelled in CST mws as an example for this purpose. In this particular example, k_c is controlled by $wr12$.

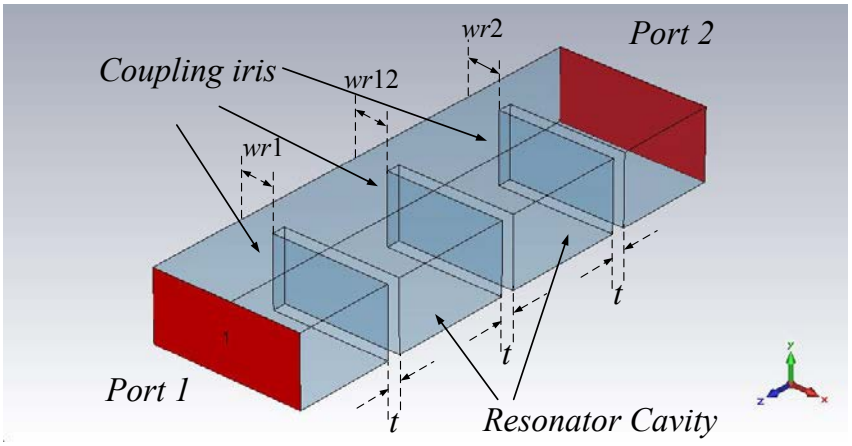

Figure 4.9 The structure modelled in CST for extracting k_c

To get a more accurate result, the couplings to external ports should be very weak ($wr1$ and $wr2$ should be small). A general equation for the extraction of k_c is given in [9].

$$k_c = \pm\frac{1}{2}\left(\frac{f_{01}}{f_{02}}+\frac{f_{02}}{f_{01}}\right)\cdot\sqrt{\left(\frac{f_1^2-f_2^2}{f_1^2+f_2^2}\right)^2+\left(\frac{f_{01}^2-f_{02}^2}{f_{01}^2+f_{02}^2}\right)^2} \tag{4-15}$$

f_{01} and f_{02} are the centre frequency of the two resonators. f_1 and f_2 are the two frequency peaks shown in Figure 4.10.

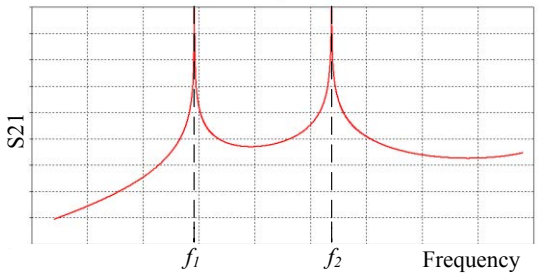

Figure 4.10 A typical S21 of the coupled resonator pair

(4-15) can be simplified when the two resonators are synchronously tuned ($f_{01} = f_{02}$), which gives [10],

$$k_c = \pm\left(\frac{f_1^2-f_2^2}{f_1^2+f_2^2}\right) \tag{4-16}$$

The wider the iris is, the larger the k_c will be. The relationship between k_c and $wr12$ is given in Figure 4.11; both $wr1$ and $wr2$ are set small to ensure weak external couplings ($wr1$=$wr2$=0.1mm, cavity length d for both resonator is 18mm, and iris thickness t is 2mm).

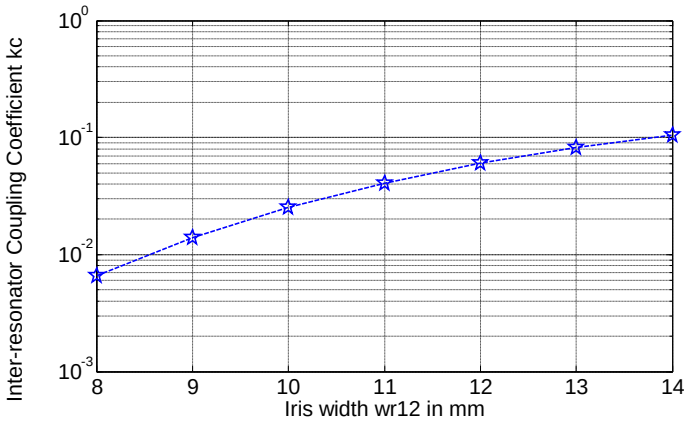

Figure 4.11 The relationship between k_c and r_{12}

For the asynchronously tuned case, if the difference between f_{01} and f_{02} is small, (4-16) can still provide a good approximation [9].

4.1.3.3 Resonator Length

The coupling matrix is discussed in Chapter 2, and self-coupling is introduced to represent the frequency shift of the resonator. According to [11], self-coupling $M_{i,i}$ can be directly obtained from,

$$M_{i,i} = \left(\frac{f_{0i}}{f_0} - \frac{f_0}{f_{0i}} \right) \tag{4-17}$$

in which f_0 is the centre frequency of the filter; f_{0i} is the centre frequency of the i^{th} resonator. It is interesting to find that, $M_{i,i}$ is zero when $f_{0i} = f_0$ (synchronously tuned), negative when $f_{0i} < f_0$ and positive when $f_{0i} > f_0$ (asynchronously tuned). For asynchronously tuned case, $M_{i,i}$ can be obtained in terms of the centre frequency f_0 and the length of the i^{th} resonator l_i. For the i^{th} resonator with $TE_{1,0,1}$ as the dominant mode, the cavity length l_i is $\lambda_{gi}/2$; the guided wavelength λ_{gi} is defined in [4], where a is the width of the cavity resonator, c is the speed of light.

$$\lambda_{gi} = 2l_i = \frac{2ac}{\sqrt{4a^2 f_{0i}^2 + c^2}} \tag{4-18}$$

Substituting (4-17) into (4-18), the relationship between $M_{i,i}$ and the i^{th} cavity resonator is given [12],

$$l_i = \frac{ac}{\sqrt{4a^2 f_0^2 \left(\frac{M_{i,i}}{2} + \sqrt{\left(\frac{M_{i,i}}{2} \right)^2 + 1} \right)^2 + c^2}} \tag{4-19}$$

Hence, the resonator length can be determined from the self-couplings.

4.2 A 10th Order Five-Passband Rectangular Waveguide Filter with Chebyshev Response

The 10th order five-passband filter implemented here is the one shown in Example 6 in Section 3.5.2. Its topology is shown in Figure 4.12.

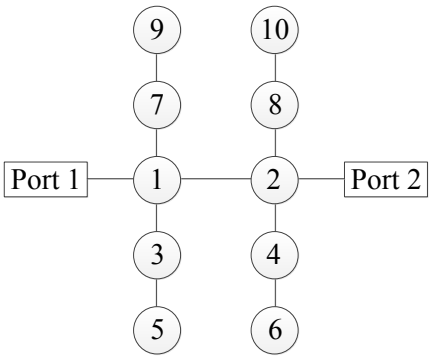

Figure 4.12 The topology of the 10th order five-passband filter

4.2.1 The Physical Configuration of The 10th Order Five-Passband Filter

All couplings are fulfilled by capacitive irises. The filter configuration is given in Figure 4.13.

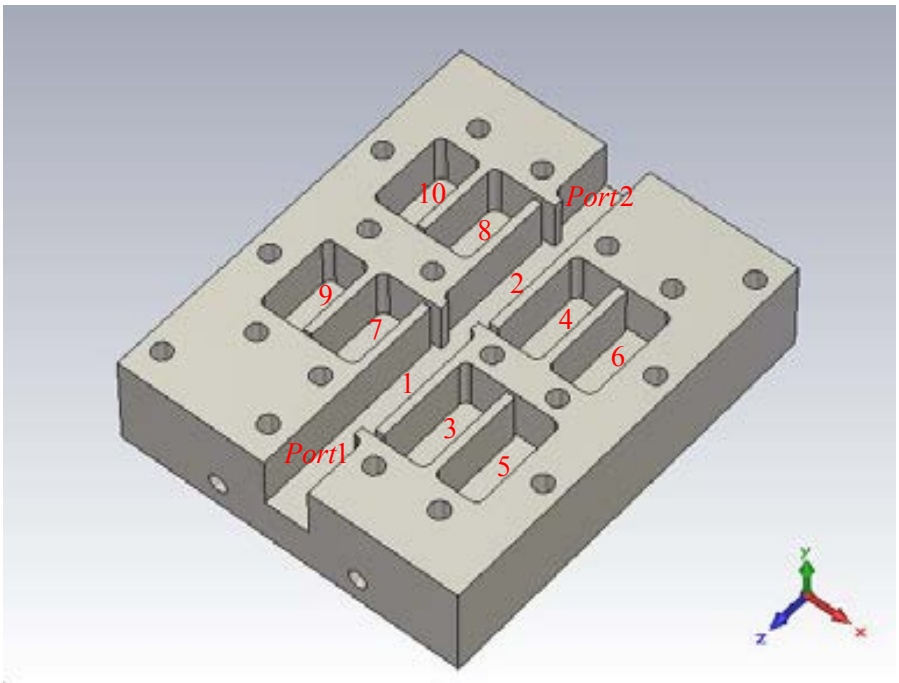

Figure 4.13 The 3D view of the 10th order five-passband rectangular waveguide filter (lower half)

The filter is symmetrical in the E-plane (*x*-*z* plane). In order to facilitate the milling by CNC machine, it has to be cut through the E-plane; this means the filter will be assembled from

two parts including a lower half and an upper half. Figure 4.13 shows the lower half of the filter. There are 10 cavities inside the filter acting as the 10 resonators. They are numbered in red together with the two ports which meet the WR90 standard. The cylindrical holes are for assembly screws.

The filter's physical dimensions are labelled and named in Figure 4.14.

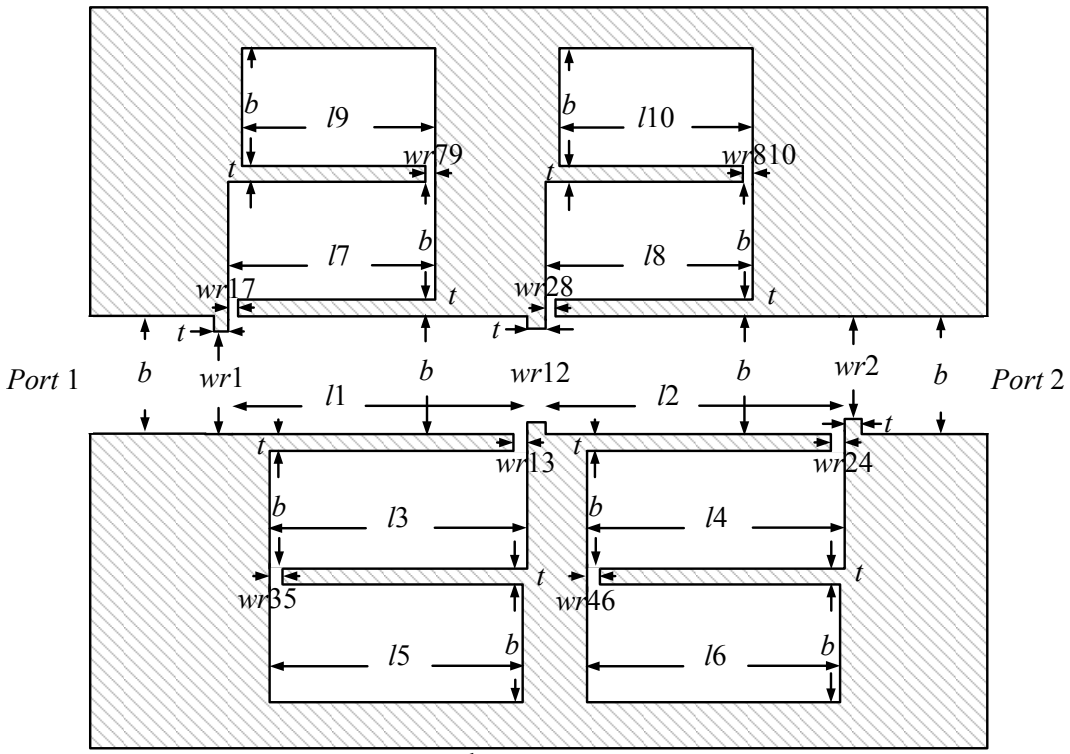

Figure 4.14 The configuration of the 10th order five-passband rectangular waveguide filter (*x-z* plane cross sectional view)

Because Figure 4.14 is the top view, the dimension of *a* cannot be shown in the figure; it is perpendicular to this *x-z* plane. Since the coupling matrix and external *Q*-factors are given in Section 3.5.2, the dimensions of each iris and resonator can be obtained.

4.2.2 The Optimised Dimensions and Responses

When putting all the components together, further fine optimisation on the structure dimensions can be done by using the embedded optimiser in CST mws [8]. The dimensions of the resonator length *l* and iris width *wr* are further optimised in order to accurately meet

the required specification. The physical dimension before the optimisation and the one after the optimisation are all listed in Table 4.1. The filter is fabricated based on the optimised dimension. The final optimised results simulated by CST are given in Figure 4.15 and compared with the theoretical ones calculated by MATLAB. In order to illustrate the necessity of optimisation, the initial simulated results are compared with the optimised simulated results in Figure 4.16; they are corresponded to the dimensions given in Table 4.1. It takes no more than a week to obtain the optimised results from the initial dimension.

	a	*b*	*t*	*l*1	*l*2	*l*3
Dimension before optimisation(mm)	22.86	22.86	2.0	29.0	29.0	23.0
Dimension after optimisation(mm)	22.86	10.16	2.0	29.1	29.1	23.2
	*l*4	*l*5	*l*6	*l*7	*l*8	*l*9
Dimension before optimisation(mm)	23.0	23.0	23.0	20.0	20.0	19.0
Dimension after optimisation(mm)	23.2	23.1	23.1	19.7	19.7	18.9
	*l*10	*wr*1	*wr*2	*wr*12	*wr*13	*wr*35
Dimension before optimisation(mm)	19.0	7.0	7.0	6.0	1.3	1.0
Dimension after optimisation(mm)	18.9	8.0	8.0	7.0	1.2	0.8
	*wr*17	*wr*79	*wr*24	*wr*46	*wr*28	*wr*810
Dimension before optimisation(mm)	1.2	0.6	1.3	1.0	1.2	0.6
Dimension after optimisation(mm)	1.0	0.6	1.2	0.8	1.0	0.6

Table 4.1 Dimensions of the proposed 10^{th} order five-passband rectangular waveguide filter

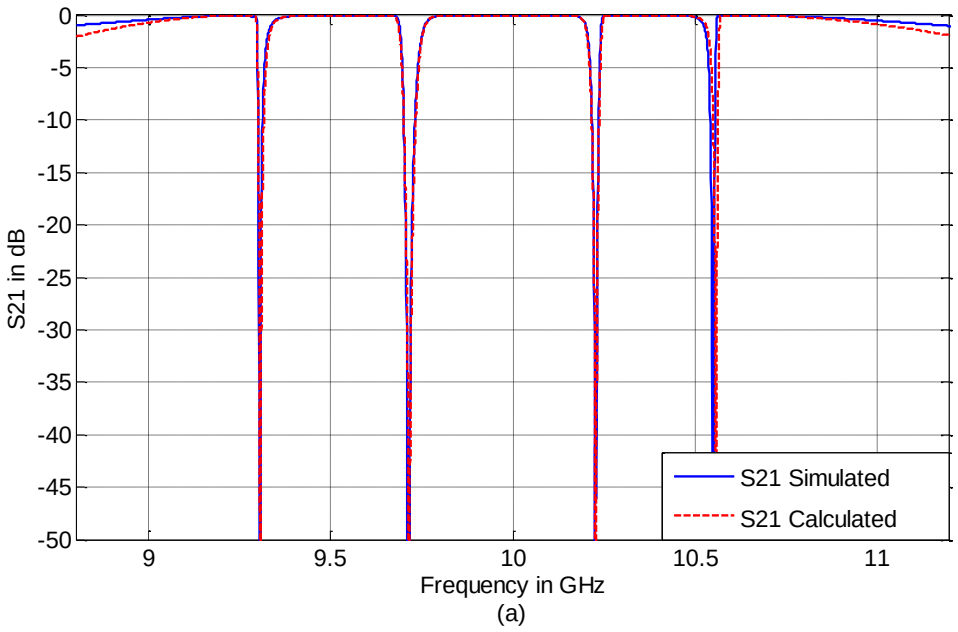

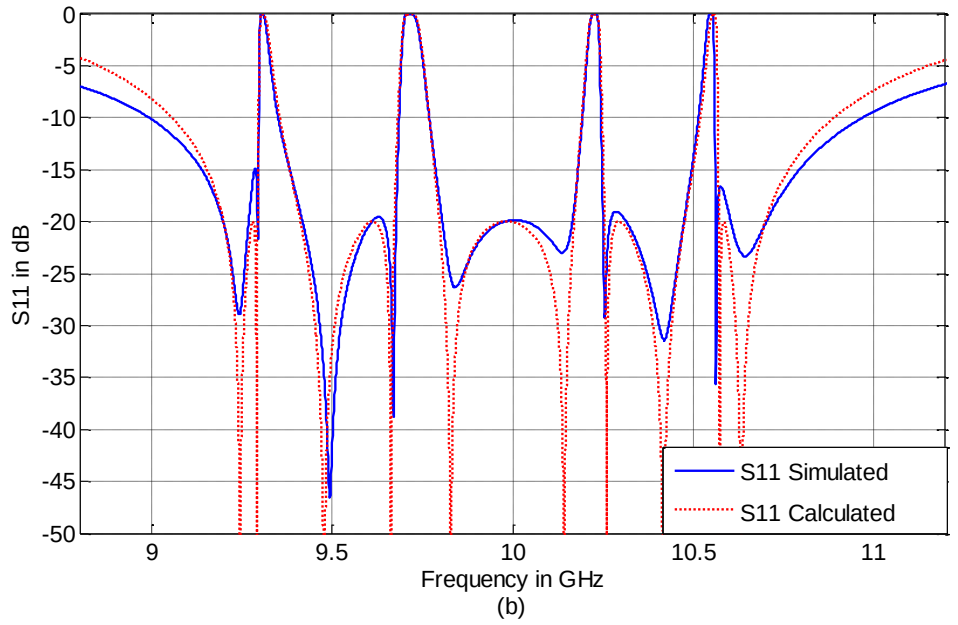

Figure 4.15 *S*-parameters comparison between the CST simulated results and MATLAB calculated results (a) *S*21, (b) *S*11 (Passband 1: 9.20 ~ 9.29 GHz, Passband 2: 9.41 ~ 9.67 GHz, Passband 3: 9.80 ~ 10.17 GHz, Passband 4: 10.25 ~ 10.48 GHz, Passband 5: 10.57 ~ 10.70 GHz)

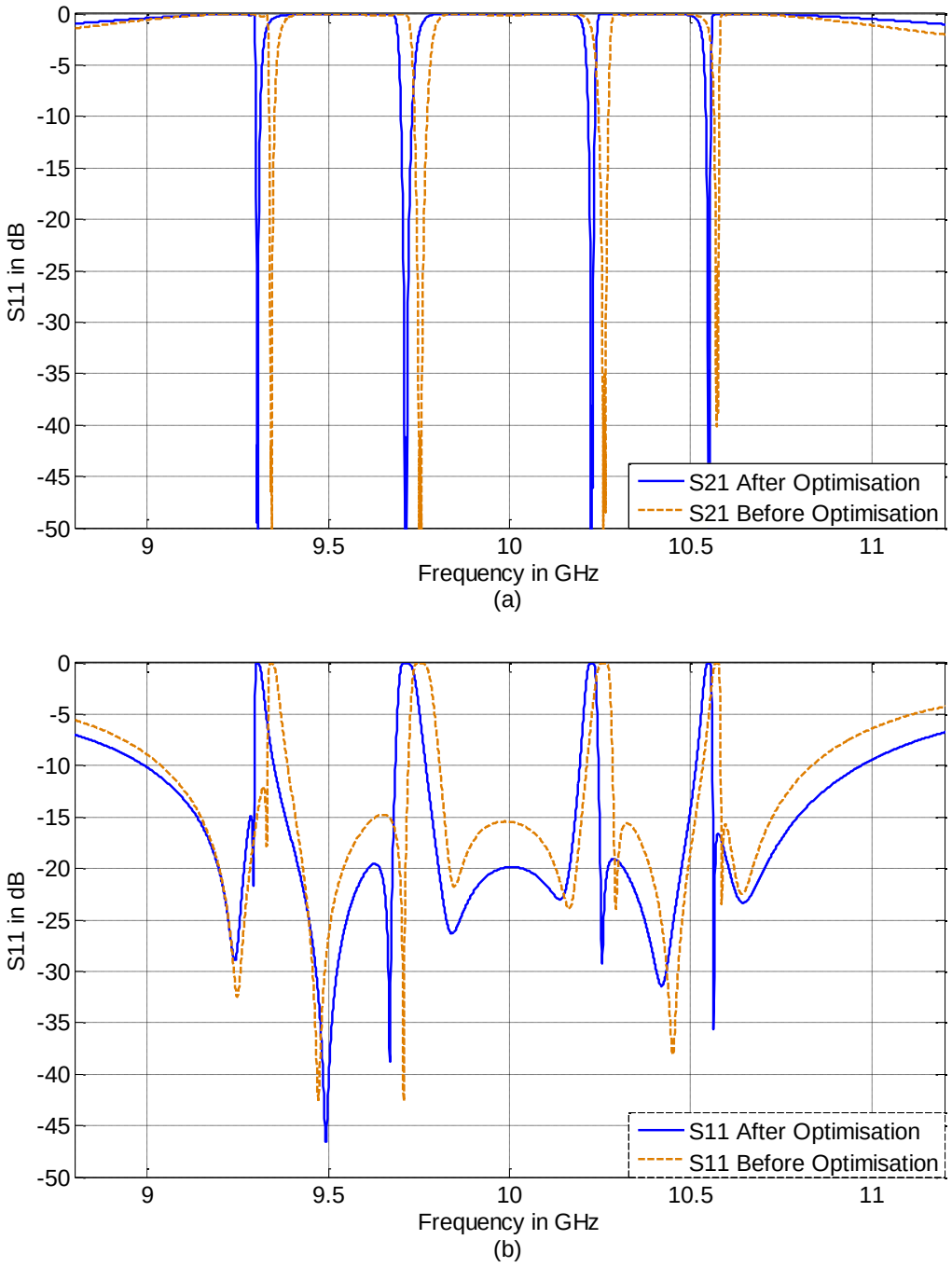

Figure 4.16 *S*-parameters comparison between the initial simulated results and the optimised results (a) *S*21, (b) *S*11

4.2.3 Fabrications and Measurement

The photos of the fabricated filter are given in Figure 4.17.

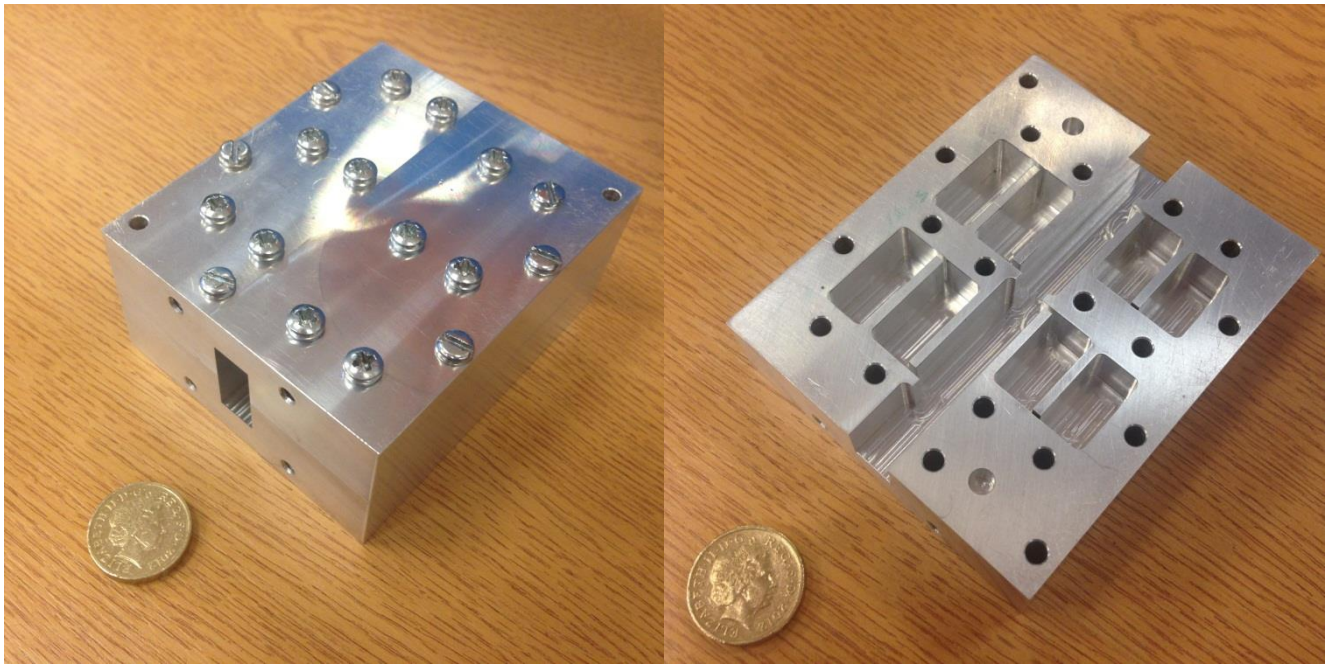

(a) (b)

Figure 4.17 Photos of the fabricated 10^{th} order five-passband rectangular waveguide filter. (a) full filter, (b) lower half of the filter

The filter is fabricated using aluminium with an electrical conductivity of 3.56×10^7 S/m. The measured results are given in Figure 4.18 together with the simulated results for the purpose of comparison. The measured *S*21 has a 0.07dB mid-band insertion loss.

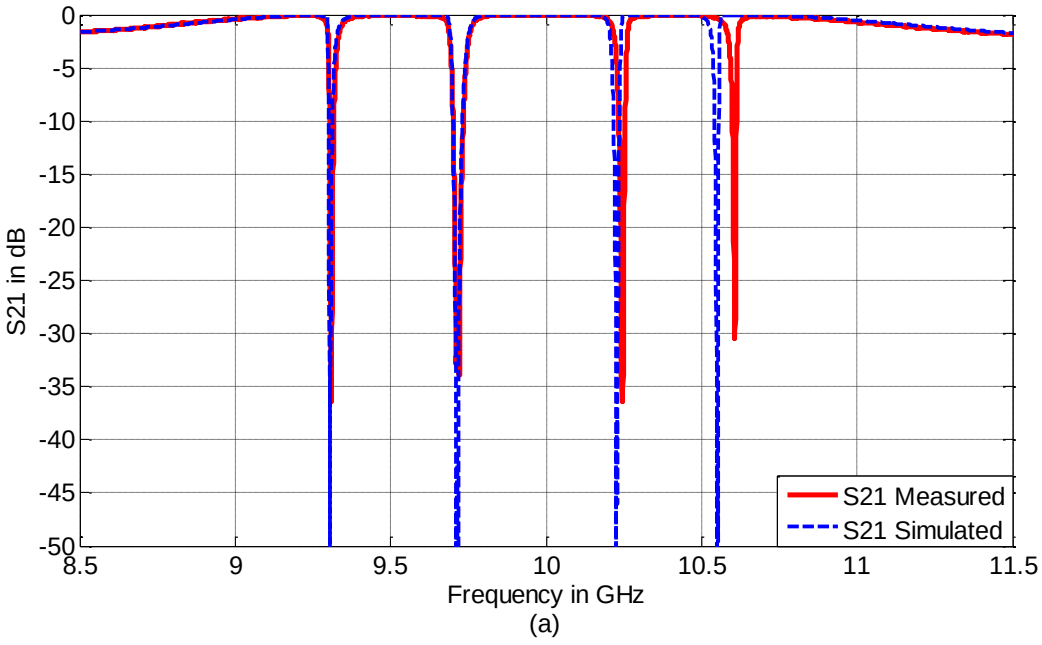

(a)

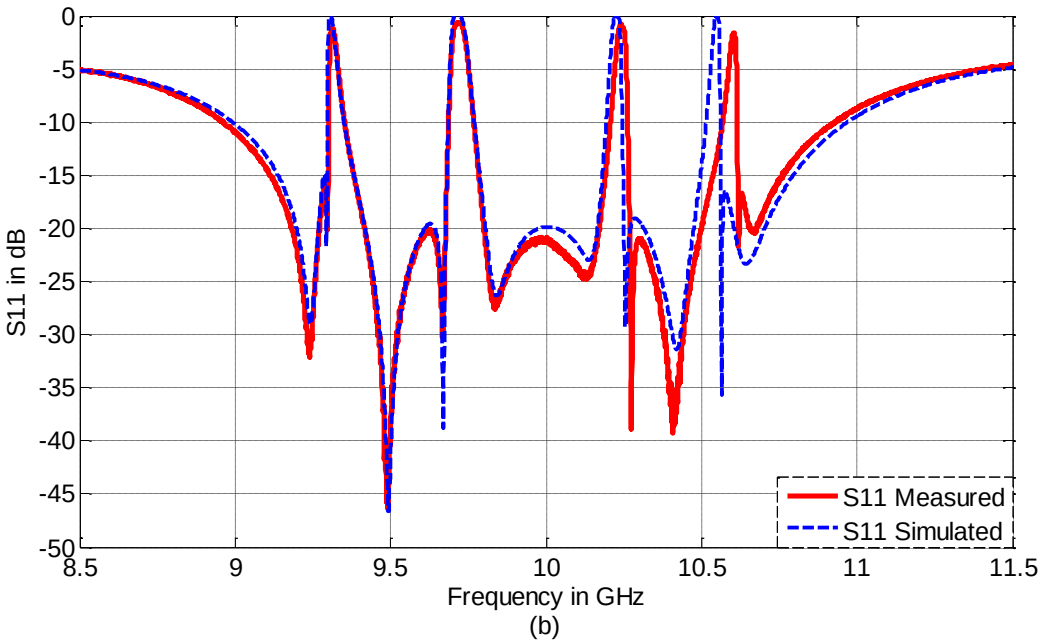

Figure 4.18 *S*-parameters comparison between the measured results and CST simulated results. (a) *S*21, (b) *S*11

4.2.4 Measured Result Analysis

The measured full passbands area is about 15MHz below the simulated one. In general, the measured *S*-parameters show good agreement with the simulated ones, except for the region of band 4 and band 5, which is between 10.2GHz to 10.7GHz. This is due to the fabrication errors in iris79 and iris810, which change the values of *wr*79 and *wr*810. The errors can be measured using a vernier caliper; both irises are about 0.12mm larger than the proposed widths. The defects can be recognised by eyes if observed closely. The close-up shot for the defect irises are given in Figure 4.19, and are labelled with red circles.

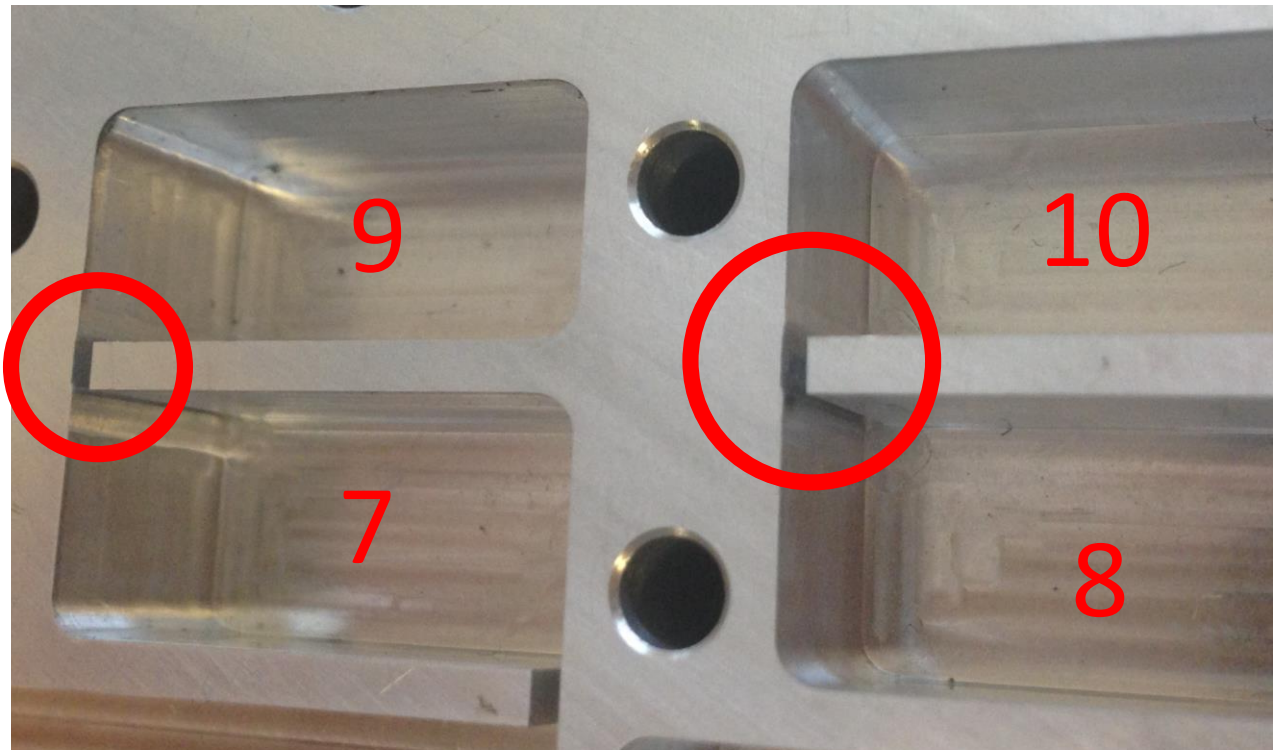

Figure 4.19 Close-up shot of the defect irises

Updated simulated responses are given in Figure 4.20, which considers the fabrication errors. Besides *wr*79 and *wr*810, *l*1 and *l*2 also artificially increase by 0.2mm to make the full passbands area move down by 15MHz. The updated simulated responses show very good agreement with the measured responses.

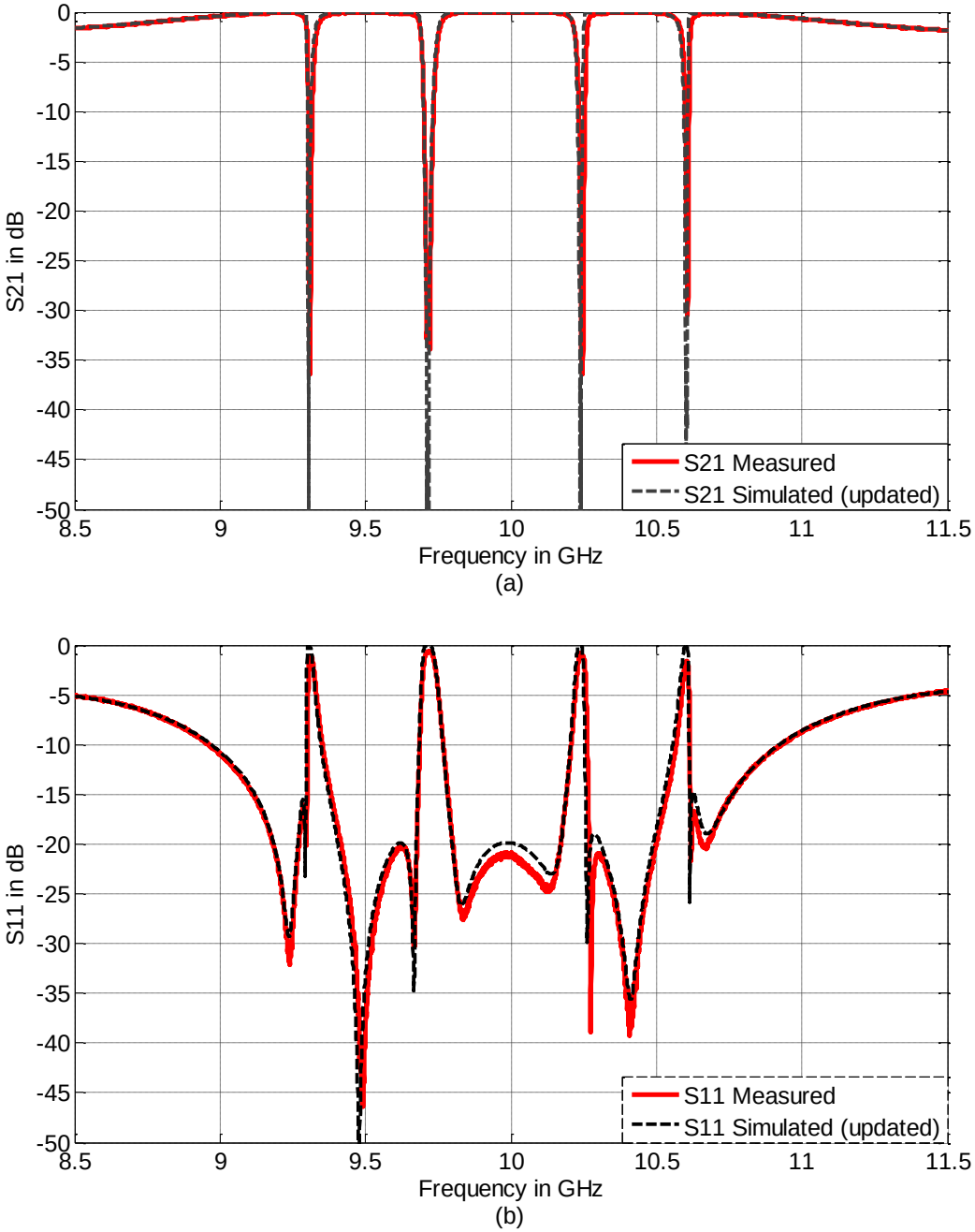

Figure 4.20 *S*-parameters comparison between the measured results and the updated CST simulated results. (a) *S*21, (b) *S*11

The corresponding updated dimension values are given in red in Table 4.2.

	a	*b*	*t*	*l*1	*l*2	*l*3
Dimension (mm)	22.86	10.16	2.0	29.3	29.3	23.2
	*l*4	*l*5	*l*6	*l*7	*l*8	*l*9
Dimension (mm)	23.2	23.1	23.1	19.7	19.7	18.9
	*l*10	*wr*1	*wr*2	*wr*12	*wr*13	*wr*35
Dimension (mm)	18.9	8.0	8.0	7.0	1.2	0.8
	*wr*17	*wr*79	*wr*24	*wr*46	*wr*28	*wr*810
Dimension (mm)	1.0	0.72	1.2	0.8	1.0	0.72

Table 4.2 Dimensions of the updated 10th order five-passband rectangular waveguide filter

4.3 A 20th Order Five-Passband Rectangular Waveguide Filter with Quasi-Elliptic Response

The 20th order five-passband filter implemented here is the Example 7 in Section 3.5.3. It has a topology which is shown in Figure 4.21. The dashed line between resonator 1 and 4 indicates the cross-coupling.

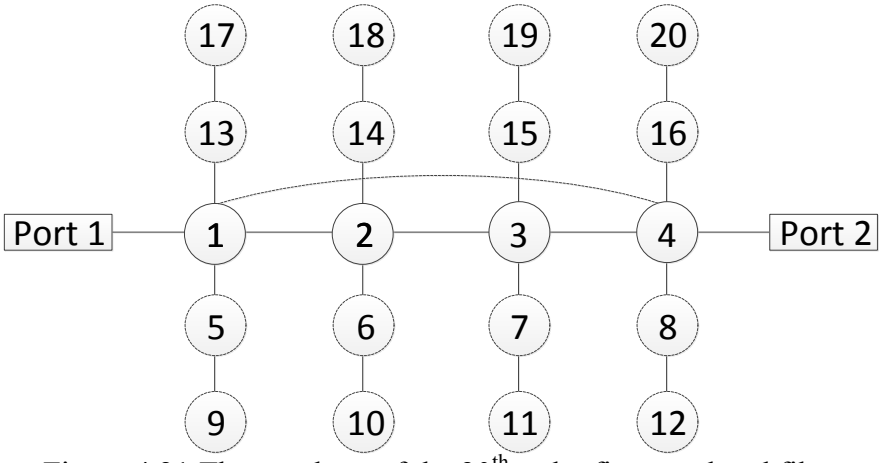

Figure 4.21 The topology of the 20th order five-passband filter

4.3.1 The Physical Configuration of The 20th Order Five-Passband Filter

Figure 4.22 shows the configuration of the lower half of this 20th order filter. There are 20 cavity resonators inside this filter; they together with the two ports are labelled and numbered in red. The two ports are WR90 standard waveguide ports. All couplings are fulfilled by capacitive irises except for the cross coupling between resonator 1 and 4 which is fulfilled by inductive iris. This filter is also symmetrical to the E-plane (*y*-*z* plane in this case). Therefore, for milling, it is also has to be cut through the E-plane.

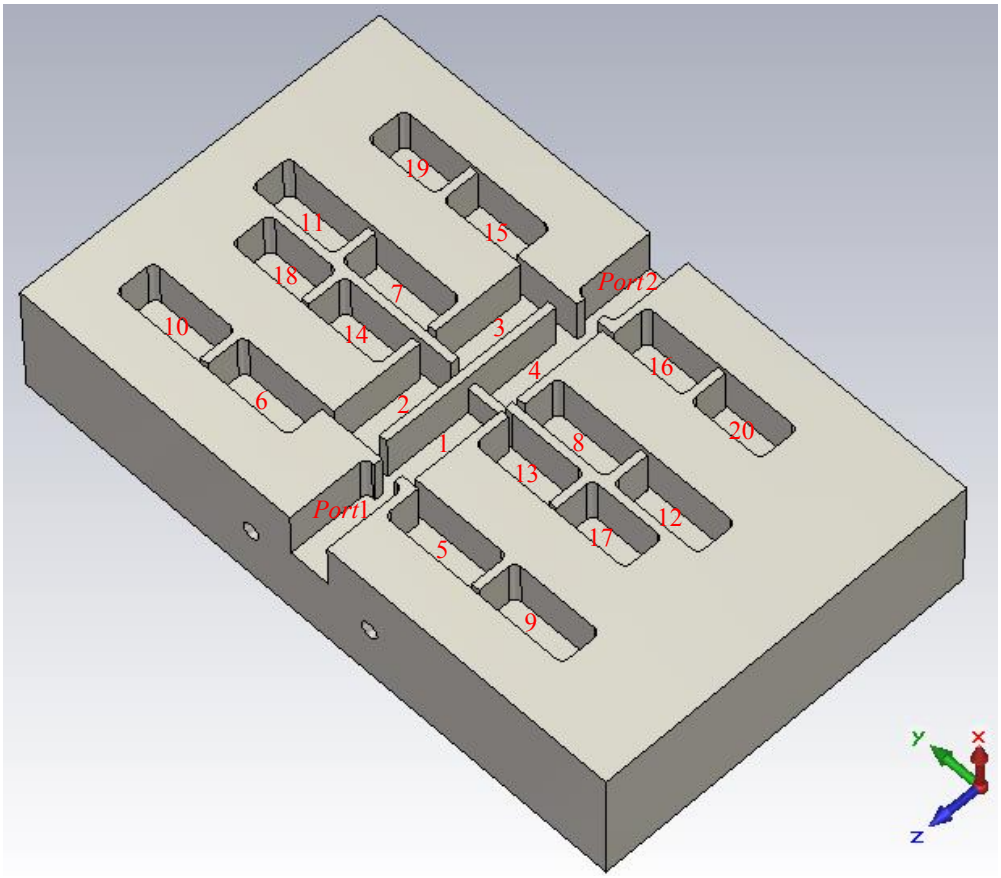

Figure 4.22 The 3D view of the 10th order five-passband rectangular waveguide filter (lower half)

The physical dimensions of the filter are labelled and named on the figure as shown in Figure 4.23. The only inductive iris is a symmetrical inductive iris, named *wr*14 and are labelled in red. The width of it cannot be shown in this configuration, as it is perpendicular to this plane.

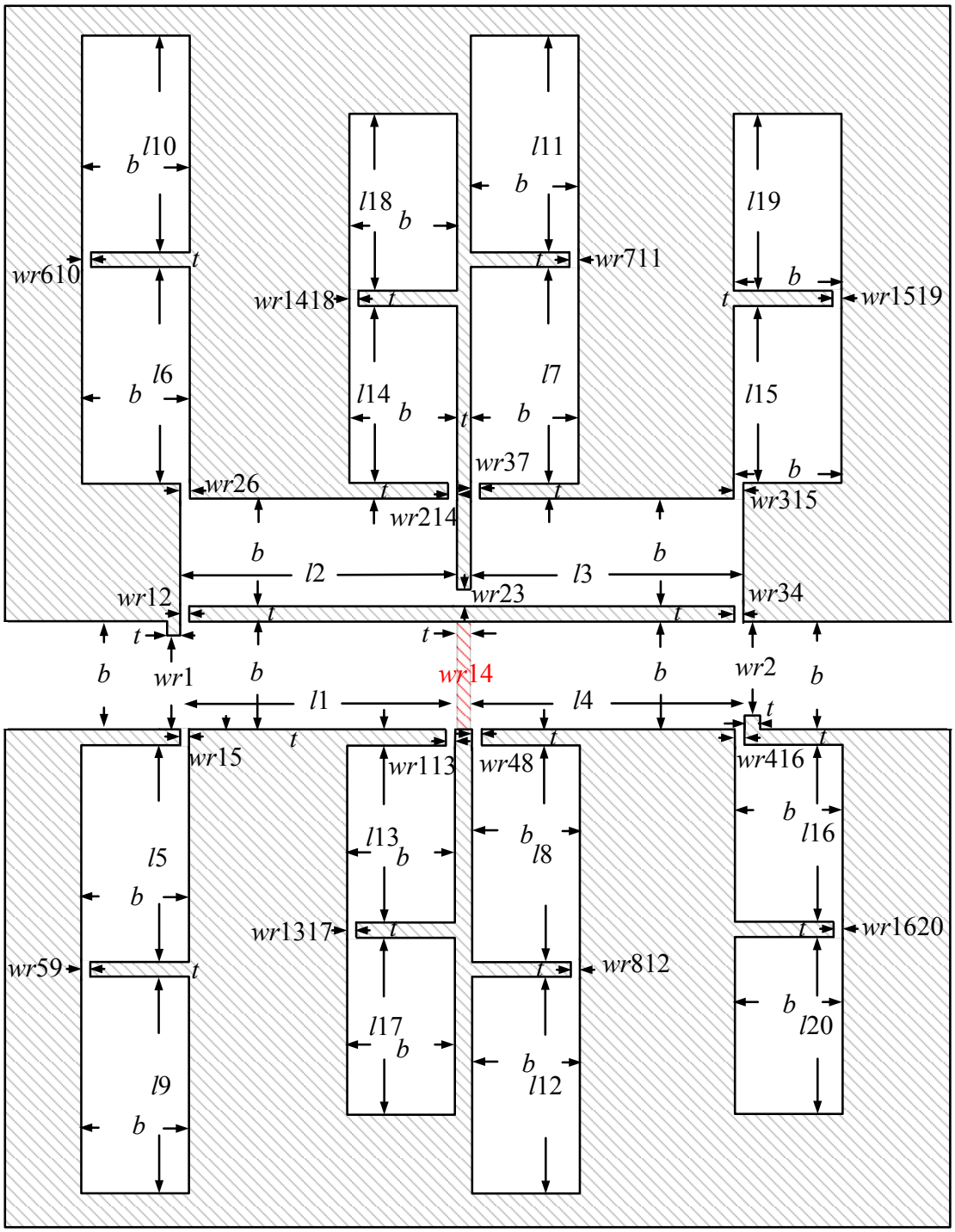

Figure 4.23 The configuration of the 20th order five-passband rectangular waveguide filter (*y*-*z* plane cross sectional view)

4.3.2 The Optimised Dimensions and Response

The optimisation procedure for this 20th order filter follows the same procedure of the previous 10th order filter. Similarly, only the dimensions of the resonator length *l* and iris

width *wr* are further optimised in order to meet the specification accurately. The optimised results simulated by CST are given in Figure 4.24 and compared with the theoretical ones calculated by MATLAB.

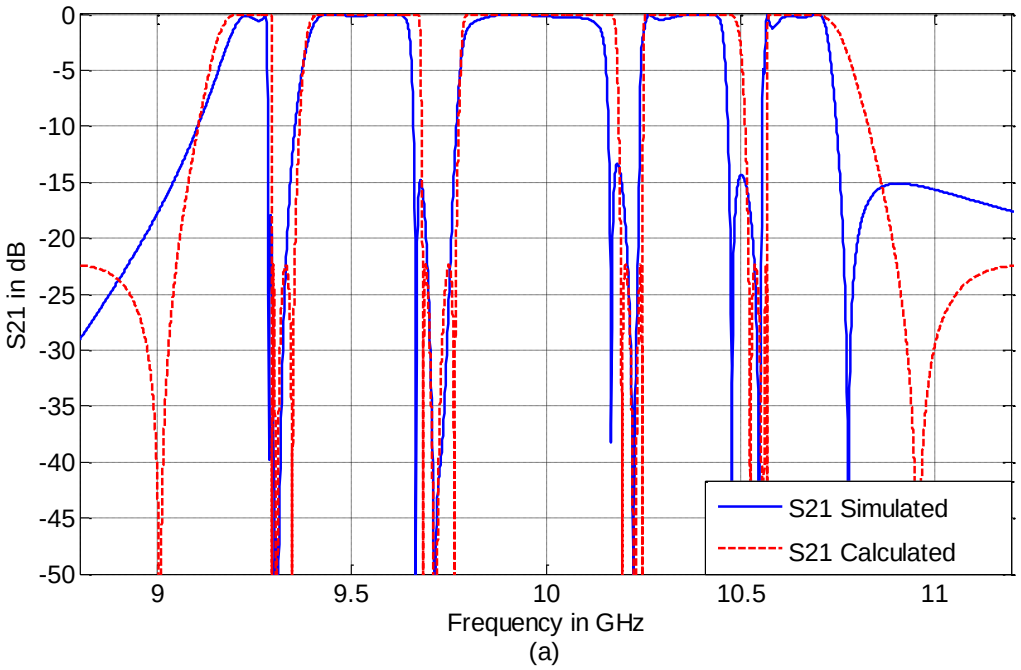

(a)

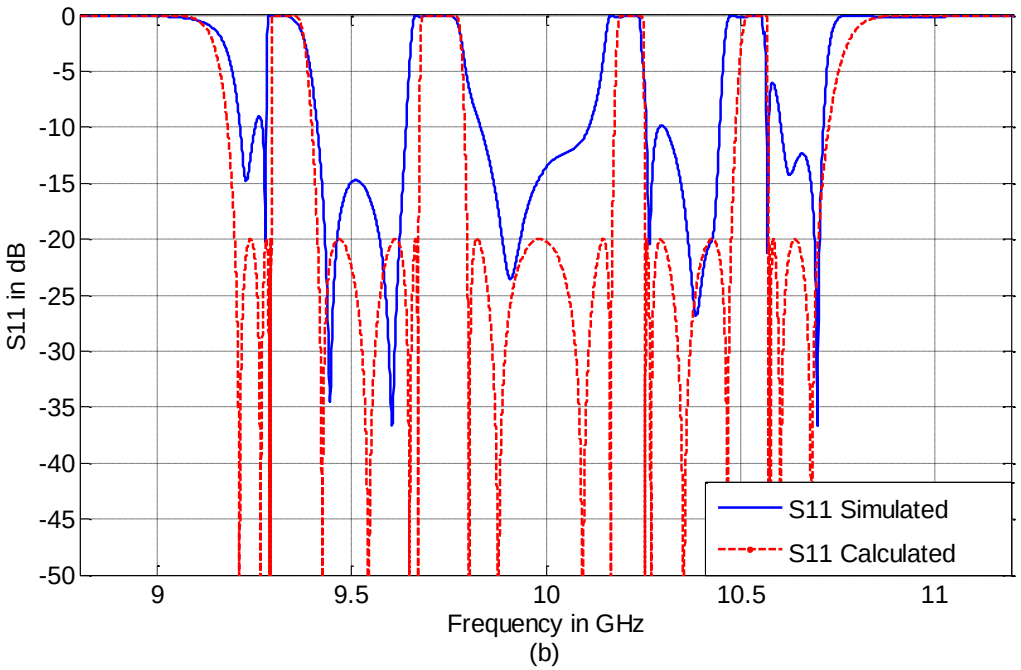

(b)

Figure 4.24 *S*-parameters comparison between the CST simulated results and MATLAB calculated results (a) *S*21, (b) *S*11 (Passband 1: 9.20 ~ 9.29 GHz, Passband 2: 9.41 ~ 9.67 GHz, Passband 3: 9.80 ~ 10.17 GHz, Passband 4: 10.25 ~ 10.48 GHz, Passband 5: 10.57 ~ 10.70 GHz)

The physical dimensions are given in Table 4.3.

	a	*b*	*t*	*l*1	*l*2	*l*3	*l*4	*l*5	*l*6
Dimension (mm)	22.86	10.16	2.0	25.0	25.0	25.0	25.0	23.1	23.1
	*l*7	*l*8	*l*9	*l*10	*l*11	*l*12	*l*13	*l*14	l15
Dimension (mm)	23.1	23.1	23.5	23.5	23.5	23.5	19.7	19.7	19.7
	*l*16	*l*17	*l*18	l19	*l*20	*wr*1	*wr*2	*wr*12	*wr*23
Dimension (mm)	19.7	19.0	19.0	19.0	19.0	5.5	5.5	3.5	2.6
	*wr*34	*wr*14	*wr*15	*wr*59	*wr*113	*wr*1317	*wr*26	*wr*610	*wr*214
Dimension (mm)	3.5	7.5	1.2	0.8	1.0	0.6	1.2	0.8	1.0
	*wr*1418	*wr*37	*wr*711	*wr*315	*wr*1519	*wr*48	*wr*812	*wr*416	*wr*1620
Dimension (mm)	0.6	1.2	0.8	1.0	0.6	1.2	0.8	1.0	0.6

Table 4.3 Dimensions of the updated 10th order five-passband rectangular waveguide filter

For this 20th order filter, the match between the simulated responses and theoretical calculated ones are not as good as that of the 10th order filter. The reason is, due to the higher order of the filter, the freedom of resonator layout has to be compromised to some extent. Consequently, this introduces some additional cross couplings between non-adjacent resonators. For this 20th order filter design, ideally, there should be no couplings between resonator 8 and 13, resonator 1 and 8, resonator 4 and 13; but in practise, there are unwanted couplings between them through the path of iris48—iris14—iris113 as these three irises are geometrically close. For example, if artificially set $M_{8,13}$, $M_{1,8}$, $M_{4,13}$ to be -0.12, -0.1, -0.1, respectively, a new $S11$ can be calculated. It is shown in Figure 4.25, together with the previous simulated $S11$ for comparison. As can be seen from the figure, these additional cross couplings do play key roles in causing the mismatch between the calculated results and simulated results.

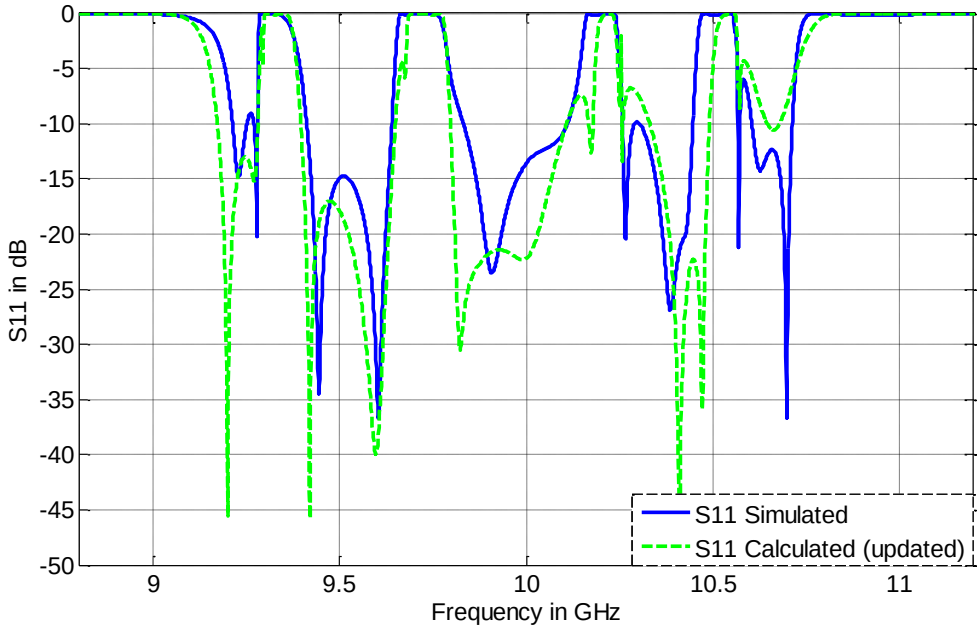

Figure 4.25 *S*11 comparison for simulated result from CST and updated calculated results from MATLAB

4.3.3 Fabrications and Measurement

The 20th order five-passband rectangular waveguide filter is fabricated based on the dimensions given in Table 4.3. The photos of the fabricated 20th order filter are given in Figure 4.26.

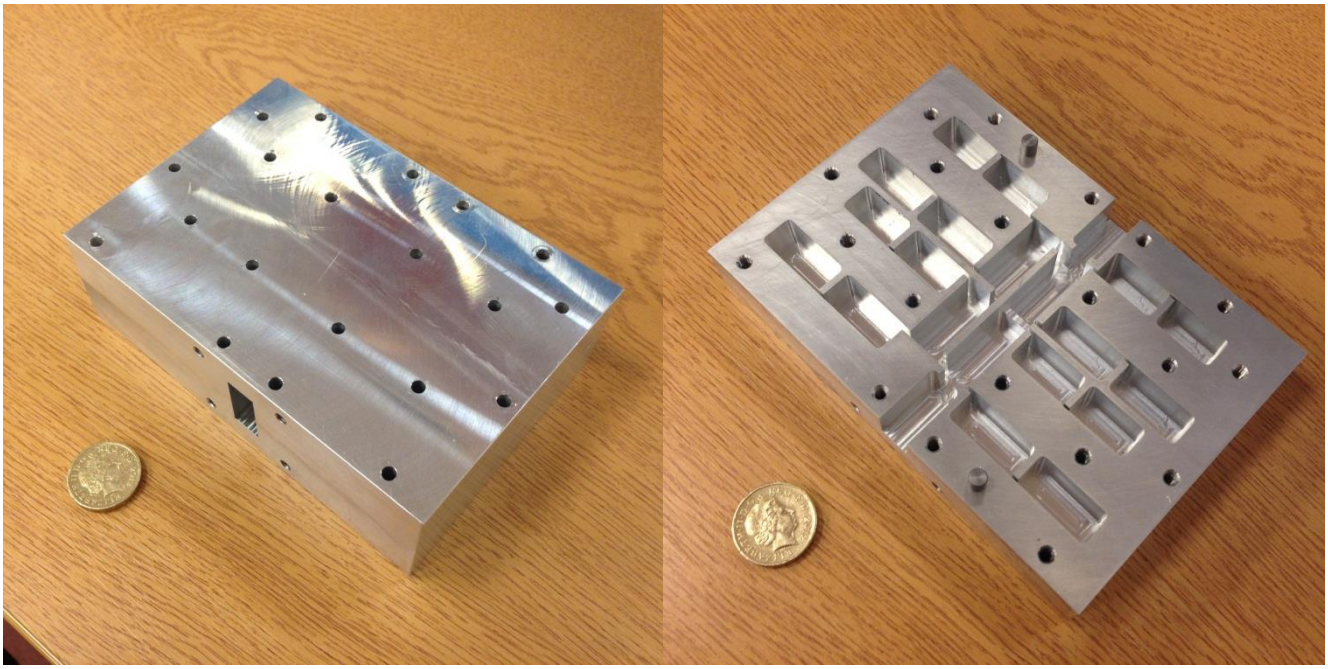

(a) (b)

Figure 4.26 Photos of the fabricated 20th order five-passband rectangular waveguide filter. (a) full filter, (b) lower half of the filter

The filter is fabricated using aluminium as well (electric conductivity is 3.56×10^7 S/m). The measured results are given in Figure 4.27, together with the simulated ones. The measured *S*21 has a 0.4dB mid-band insertion loss.

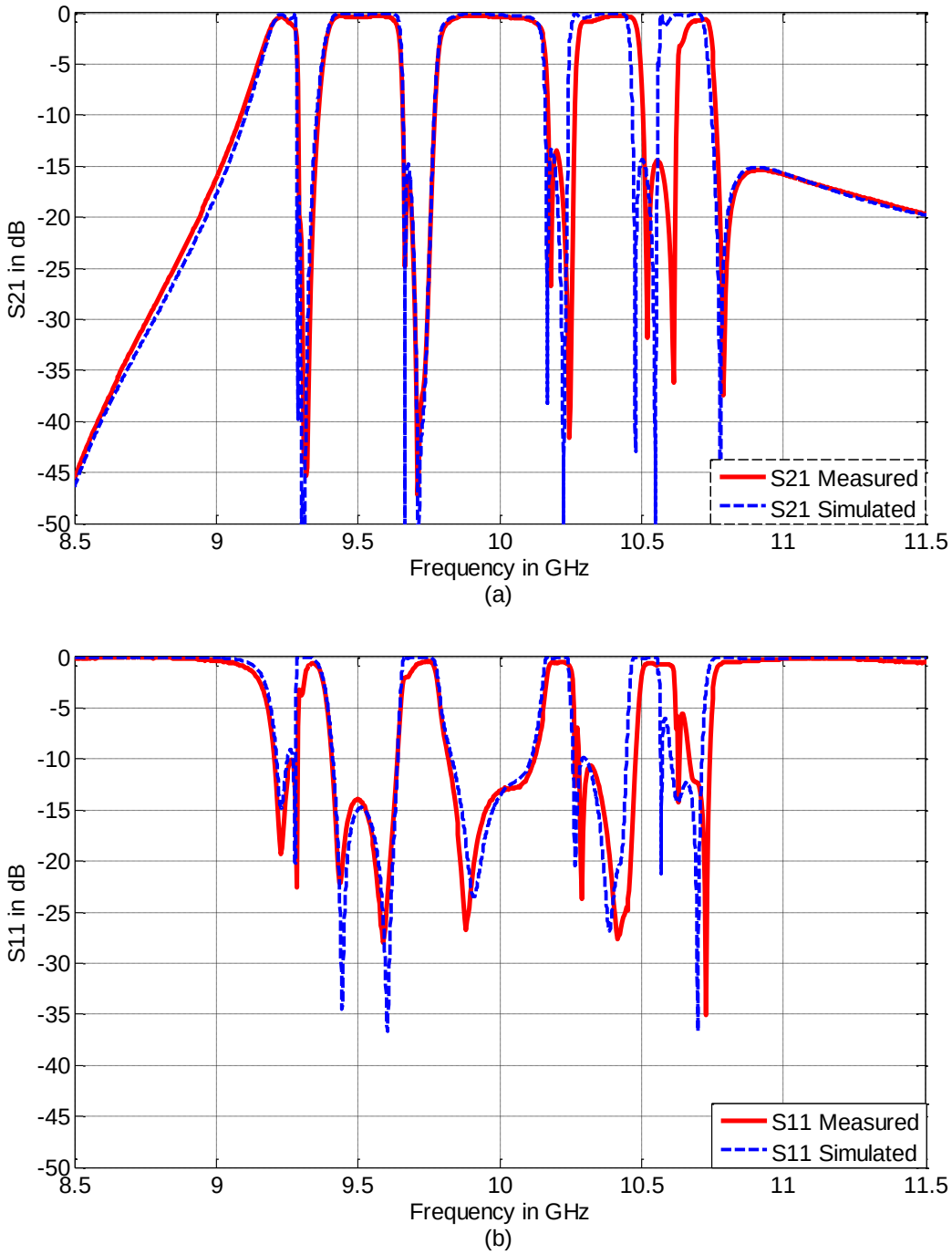

Figure 4.27 *S*-parameters comparison between the measured results and CST simulated results. (a) *S*21, (b) *S*11

4.3.4 Measured Result Analysis

The measured result has the same issue as the previous 10th order filter. It shows good agreement with the simulated one in general, except for the region of band 4 and band 5. This is also due to the similar fabrication errors on particular irises, which affect the values of *wr*1317, *wr*1418, *wr*1519 and *wr*1620. The widths of these irises are again about 0.12mm larger than the proposed widths. The close-up shot for the defect irises are given in Figure 4.28, and are labelled with red circles.

All the defects are found on the smallest irises, which are 0.6mm in width. The reason is that, during the milling procedure, a smaller size drill is used to mill these smallest irises, but the drill is a defected one.

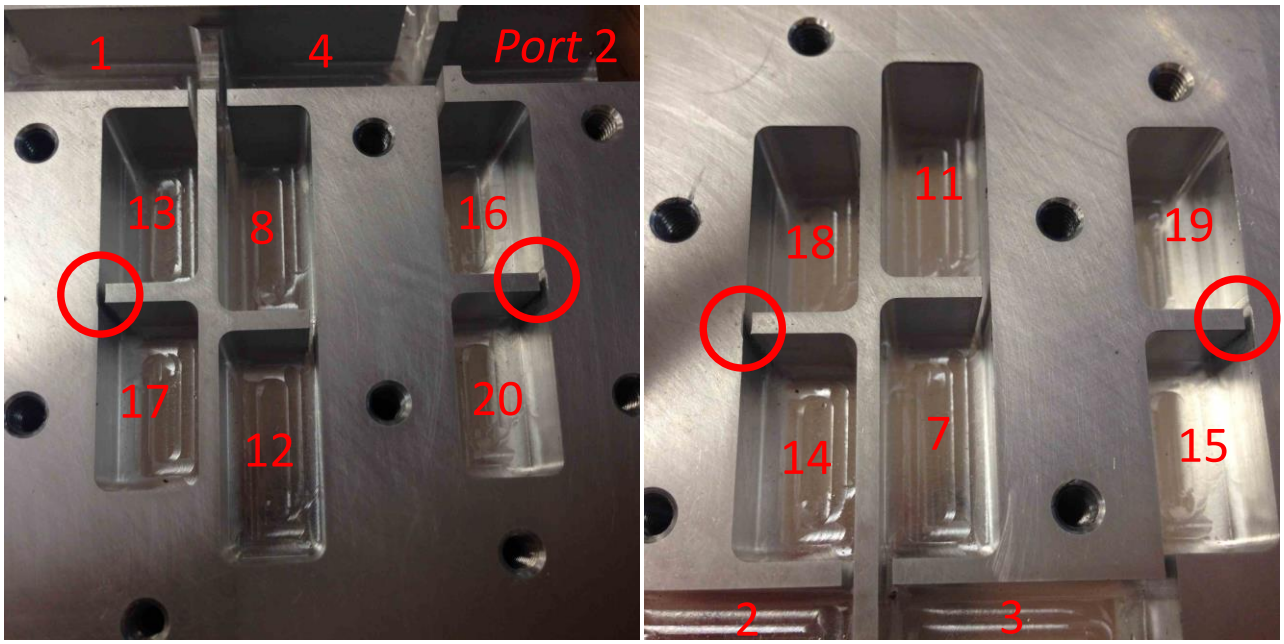

(a) (b)

Figure 4.28 Close-up shot, (a) defects for iris 1317 and 1620, (b) defects for iris 1418 and 1519

Updated simulated responses are given in Figure 4.29, which considers the fabrication errors. The new dimension values are listed in Table 4.4; the updated values are shown in red. The updated simulated responses show very good agreement with the measured responses.

	a	*b*	*t*	*l*1	*l*2	*l*3	*l*4	*l*5	*l*6
Dimension (mm)	22.86	10.16	2.0	25.0	25.0	25.0	25.0	23.1	23.1
	*l*7	*l*8	*l*9	*l*10	*l*11	*l*12	*l*13	*l*14	l15
Dimension (mm)	23.1	23.1	23.5	23.5	23.5	23.5	19.7	19.7	19.7
	*l*16	*l*17	*l*18	l19	*l*20	*wr*1	*wr*2	*wr*12	*wr*23
Dimension (mm)	19.7	19.0	19.0	19.0	19.0	5.5	5.5	3.5	2.6
	*wr*34	*wr*14	*wr*15	*wr*59	*wr*113	*wr*1317	*wr*26	*wr*610	*wr*214
Dimension (mm)	3.5	7.5	1.2	0.8	1.0	0.72	1.2	0.8	1.0
	*wr*1418	*wr*37	*wr*711	*wr*315	*wr*1519	*wr*48	*wr*812	*wr*416	*wr*1620
Dimension (mm)	0.72	1.2	0.8	1.0	0.72	1.2	0.8	1.0	0.72

Table 4.4 Dimensions of the updated 10th order five-passband rectangular waveguide filter

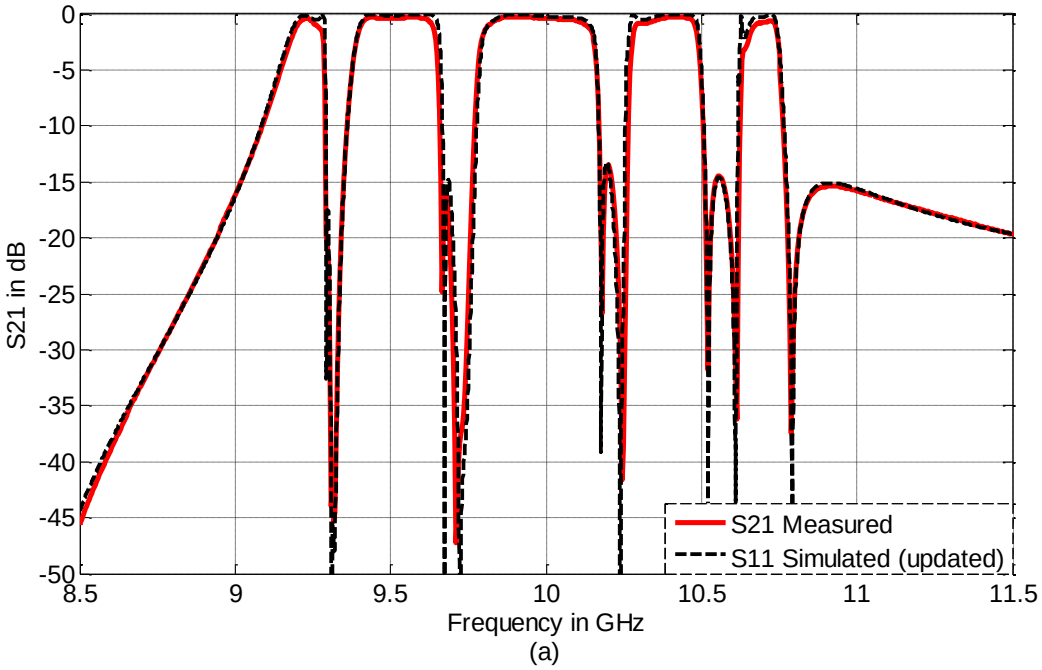

(a)

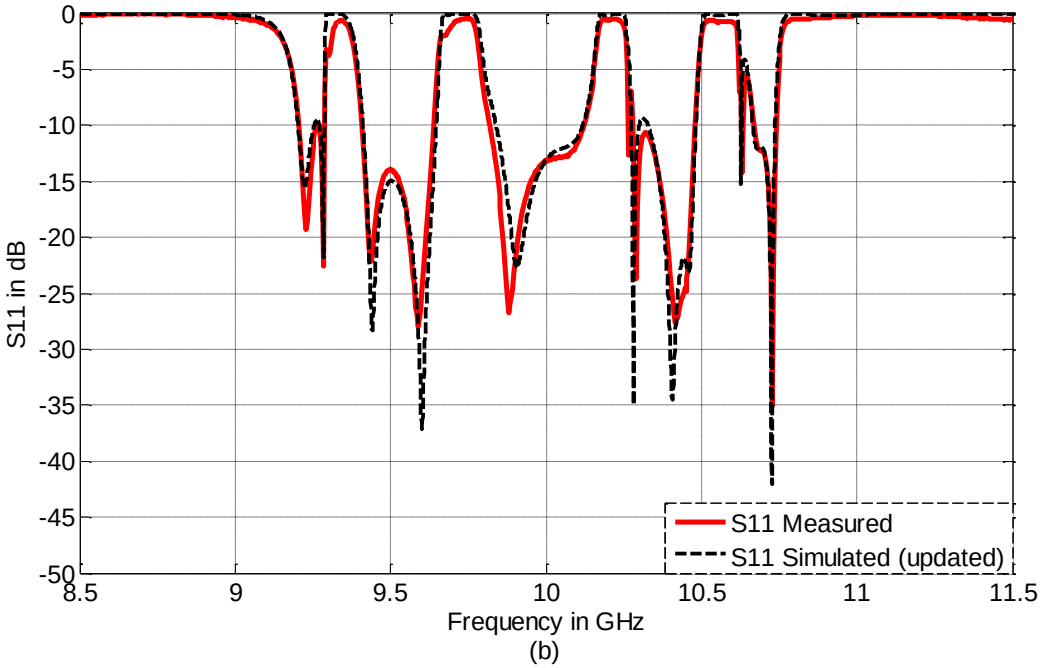

Figure 4.29 *S*-parameters comparison between the measured results and the updated CST simulated results. (a) *S*21, (b) *S*11

References:

1. Cronin, N.J., *Microwave and Optical Waveguides* 1995: Taylor & Francis.
2. Sorrentino, R. and G. Bianchi, *Microwave and RF Engineering* 2010: Wiley.
3. Chambers, J., *Commercial X-Band: The Technical + Operational Advantages*, in *Milsat Magazine* 2013, Satnews.
4. Pozar, D.M., *Microwave Engineering (Third Edition)* 2005: John Wiley & Sons, Inc.
5. Sorrentino, R. and G. Bianchi, *Ingegneria delle microonde e radiofrequenze* 2005: McGraw-Hill Companies.
6. Cameron, R.J., R. Mansour, and C.M. Kudsia, *Microwave Filters for Communication Systems: Fundamentals, Design and Applications* 2007: Wiley.
7. Hong, J.-S. and M.J. Lancaster, *Microstrip Filters for RF/Microwave Applications* 2001: John Wiley and Sons Ltd, United Kingdom.
8. *CST Microwave Studio 2013*, CST - Computer Simulation Technology AG.
9. Hong, J.S., "Couplings of asynchronously tuned coupled microwave resonators," *IEE Proceedings on Microwaves, Antennas and Propagation*, 2000. **147**(5): p. 354-358.
10. Lancaster, M.J., *passive microwave device applications of high-temperature superconductors.* 1997.
11. Nedelchev, M.V. and I.G. Iliev, "Synthesis of Microwave Filters by Coupling Matrix Optimization," ICEST, 2011. **1**: p. 167-170.
12. Xia, W., "Diplexers and Multiplexers Design by using Coupling Matrix Optimisation," in 2015, University of Birmingham: Birmingham. p. 129.

CHAPTER 5 TUNABLE BANDPASS FILTER DESIGN BASED ON RECTANGULAR WAVEGUIDE CIRCUIT

The tunable bandpass filter discussed in this chapter has the flexibility in tuning both centre frequency and bandwidth. A new structure for coupling tuning based on rectangular waveguide filter is investigated in this chapter. To begin with, the design of new coupling tuning structure is given in Section 5.1. It is followed by Section 5.2, where a frequency tuning element is discussed. Lastly but not least, a 3rd order X-band rectangular waveguide tunable bandpass filter is implemented and measured in Section 5.3 for validation.

The main novelties and advantages of the coupling tuning structure presented in this chapter is that it maintains the unloaded Q-factor of the resonator during the full tuning range, which significantly reduced the insertion loss and distortion of the filter response compared to most designs so far [1-36], which were using technologies like switched capacitor, varactors and elaborate MEMS structures for coupling tuning. With this new tuning structure, the tunable filter achieves a good compromise between tuning flexibilities and performance over its tuning range. Since it is a mechanically tuning structure, it improves the reliability and also reduces the fabrication cost of the filter.

5.1 Coupling Tuning Structure

A novel coupling tuning structure is presented here for the first time. This section has two parts. The first part shows a coupling tuning structure without chokes. In the second part, chokes are integrated and compared to the first model without chokes. It shows that the chokes improve the performance of the tuning structure by maintaining the unloaded Q-factor Q_u of the waveguide resonator.

5.1.1 Coupling Structure without Chokes

Figure 5.1 shows the structure of a tunable waveguide resonator with two coupling tuners; an expanded picture is also given to show the gaps between coupling tuner and waveguide main body (the gaps in the picture are enlarged for clearer illustration; its actual size are smaller).

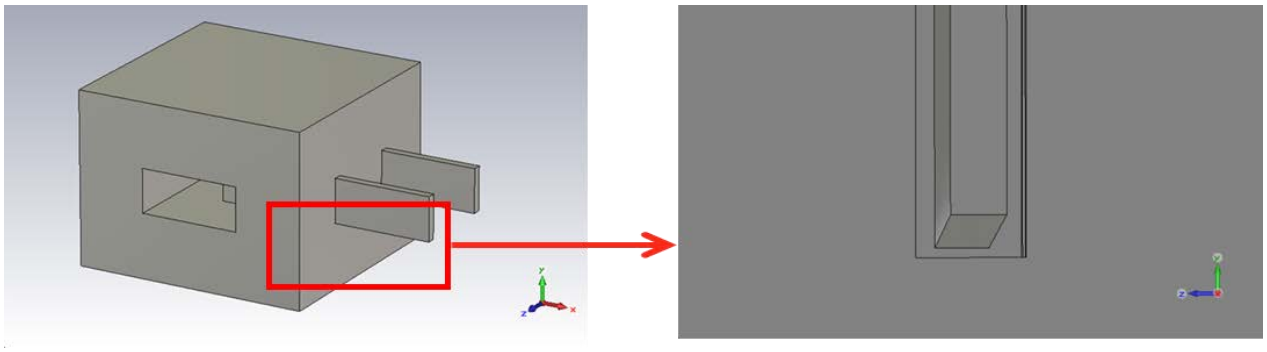

(a) (b)

Figure 5.1 (a) The perspective 3D view of a single resonator cavity with coupling tuners, (b) expanded side view focus near the coupling tuner

In order to present the inside structure, the H-plane cross sectional view of this tunable waveguide resonator is given in Figure 5.2.

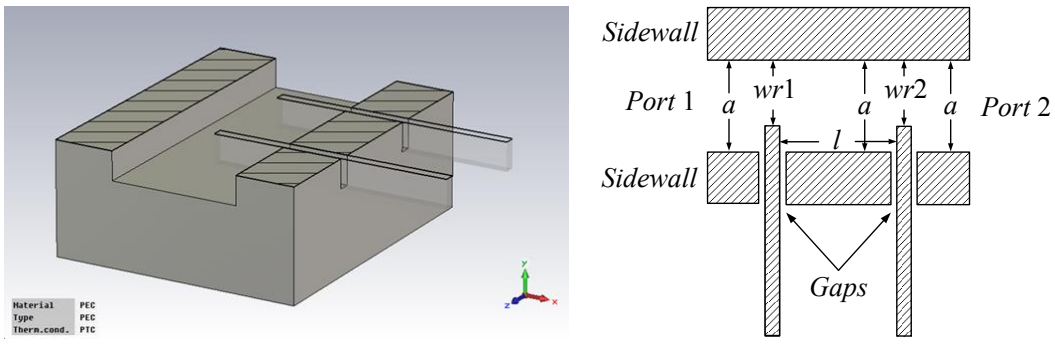

(a) (b)

Figure 5.2 (a) The H-plane cross sectional view, (b) schematic of the waveguide resonator

It is a WR90 standard rectangular waveguide resonator, the cavity width a is 22.86mm, the height b is 10.16mm (perpendicular to H-plane, not shown in Figure 5.2), the length l is 18mm. The widths of the iris1 and iris2 are named as $wr1$ and $wr2$, respectively. The width of

the sidewall is set as 10mm which is the average quarter guided wavelength for X-band microwave. The reason behind is to make the sidewall as a $\lambda_g/4$ transmission line which may reduce the energy leakage caused by the gaps between the tuners and the holes they reside in.

The loss caused by the gaps has been investigated. When the gaps between coupling tuners and the holes are set to be 0.05mm, a set of *S*21s can be obtained from simulation and these are shown in Figure 5.3. In simulation, the building material for this model is PEC and the structure contains and is surrounded by vacuum. The two coupling tuners are moving together (*wr*1 and *wr*2 are same all the time); the widths of both irises change from 8mm to 13mm with a step of 1mm. It should be noted that, the Q_L is not linear against the *wr*; the Q_L is more sensitive to the change of *wr* when Q_L is larger.

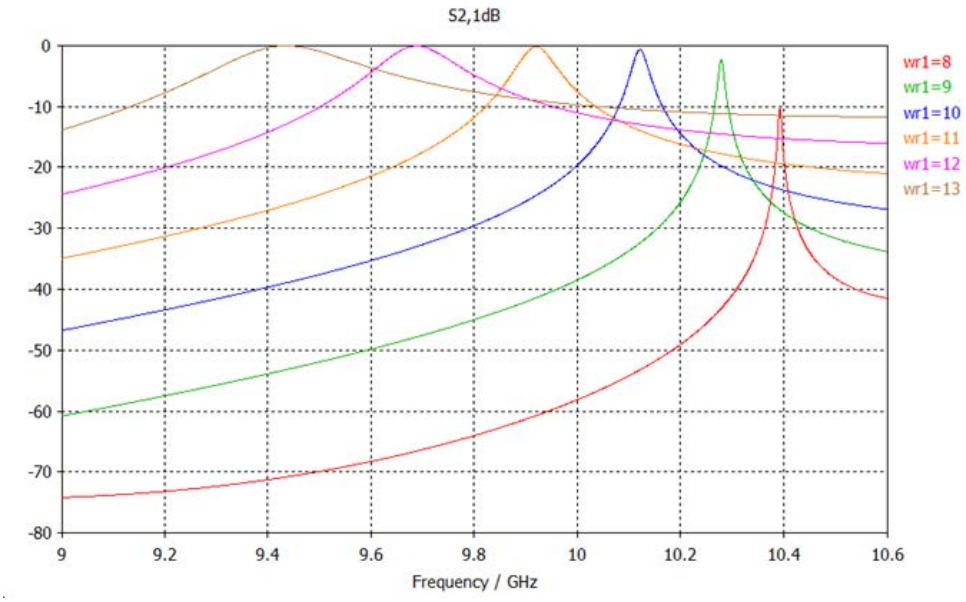

Figure 5.3 A set of *S*21s when gaps are 0.05mm

It is obvious that, there is insertion loss for this model. It is more significant when Q_L is larger, less significant but still exist when Q_L is low. This can be explained by additional losses in the cavity. Referring to (4-10), this means that the unloaded *Q*-factor Q_u is not infinite. From (5-1) below, Q_u can be defined in terms of and Q_L and $S21(f_0)$ [37],

$$Q_u = \frac{Q_L}{1 - S21(f_0)} \tag{5-1}$$

Because the structure is built up by PEC and filled up with vacuum, there is no conductor loss or dielectric loss. The only contribution to the Q_u is the radiation loss caused by the gaps. Therefore, for convenience, the radiation Q-factor caused by gaps (denoted as Q_{gap}) is used to quantitate the radiation loss through the gaps; larger Q_{gap} means lower loss. A relationship between Q_{gap} and iris width can be obtained in Figure 5.4.

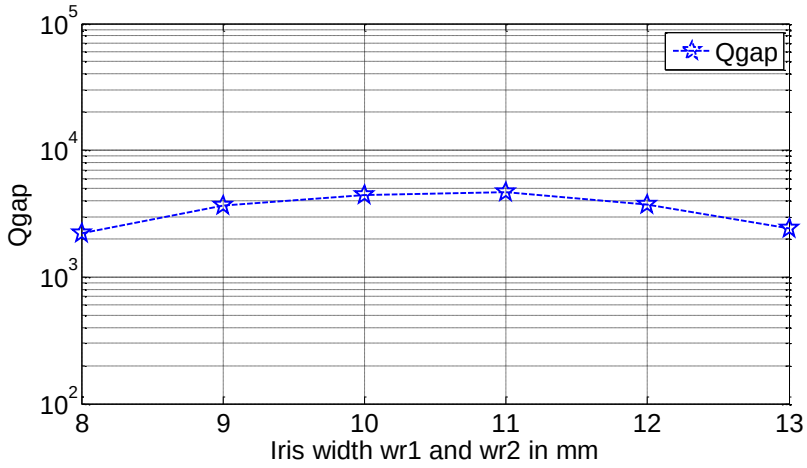

Figure 5.4 The relationship between Q_{gap} and wr when gaps are 0.05mm

As shown above, Q_{gap} is a little higher when $wr1$ and $wr2$ are between 10 and 11 (correspond to the $S21$s with frequency near 10GHz). The value of Q_{gap} is between 2400 and 4700 with an average value of 3500.

By repeating the above method with different gap sizes, a relationship between Q_{gap} (average value) and gap size can be obtained in Figure 5.5.

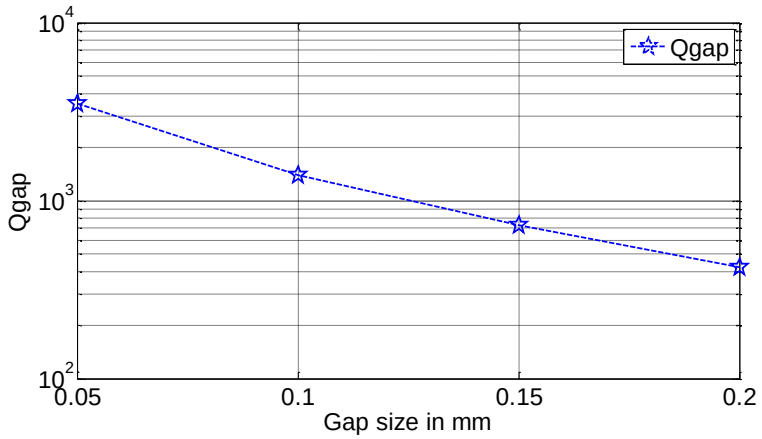

Figure 5.5 The relationship between Q_{gap} and gap size

When the gap size increases, the value of Q_{gap} will decrease. Considering the manufacturing error (the accuracy of a CNC machine about is 0.01 to 0.02mm) and assembling error, the practical gap size for design is taken as 0.1mm, therefore Q_{gap} is about 1000. As Q_{gap} is sensitive to the gap size, this result is not good enough for a resonator involving tuning elements. Besides, Q_{gap} is lower than the conductor Q-factor Q_c of aluminium cavity which is around 2000, when the gap size is larger than 0.07mm.

5.1.2 Coupling Structure with Chokes

In order to increase Q_{gap}, two chokes are integrated into the sidewall. They cannot be seen from outside, so an H-plane cross sectional view is shown in Figure 5.6. The dimensions of cavity and two coupling tuners remain the same as the previous model. The size of choke is optimised by EM simulator. The initial value was $7.5\times17\times10.16$ mm (at x,y,z direction respectively), which is based on the quarter wavelength of the guided wave of 10GHz. The final optimised value is $6.57\times12\times12$ mm (at x,y,z direction respectively).

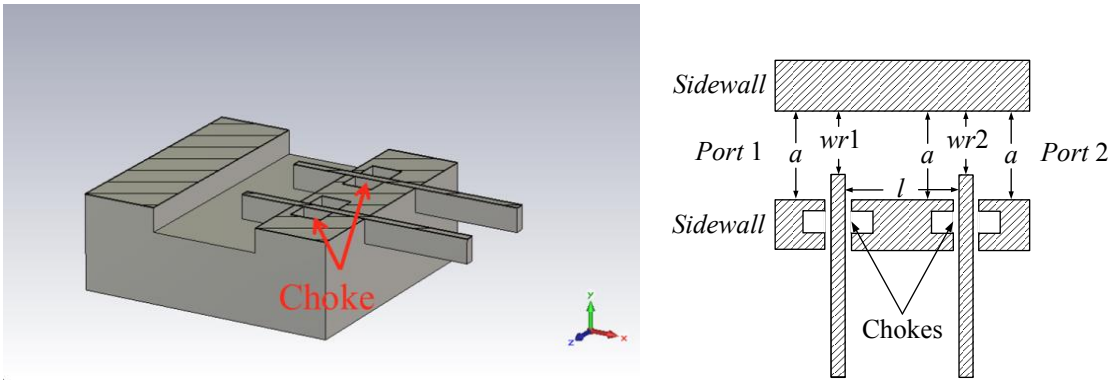

(a) (b)

Figure 5.6 (a) The H-plane cross sectional view with chokes, (b) schematic of the tunable waveguide resonator with chokes

Again, when the gap size is 0.05mm, *wr*1 and *wr*2 are moved synchronously from 8mm to 13mm with 1mm per step, a set of *S*21s can be obtained in Figure 5.7.

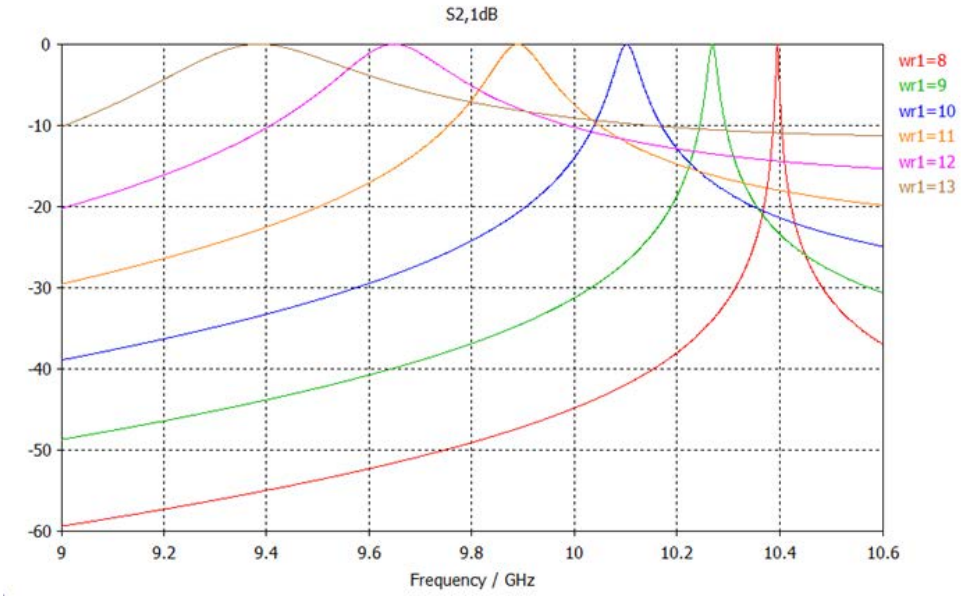

Figure 5.7 A set of S21 when gap is 0.05mm (with choke)

In the figure above, the insertion loss does not change significantly with *wr*1 and *wr*2 compared with that in Figure 5.3, but variation still exists and is from 0.05 to 0.0001 dB. If there is no gap, the insertion loss will be 0dB. A relationship between Q_{gap} and *wr* can be obtained as below.

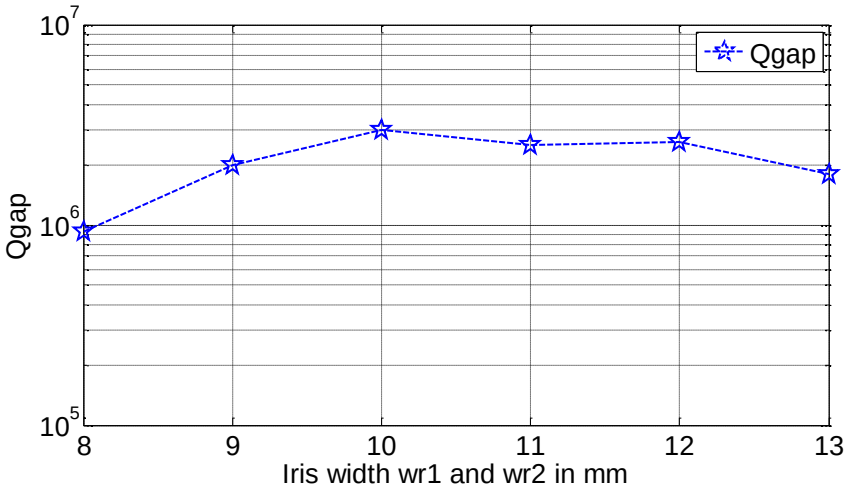

Figure 5.8 The relationship between Q_{gap} and *wr* when gap size is 0.05mm (with choke)

In the figure, Q_{gap} is above 10^6 with an average value of 1.76×10^6. It is about a factor of 1000 above the non-choke case. A relationship between Q_{gap} (average value) and gap size can be obtained by repeating the procedure with different gap size; the results are shown in Figure 5.9 together with the results without choke.

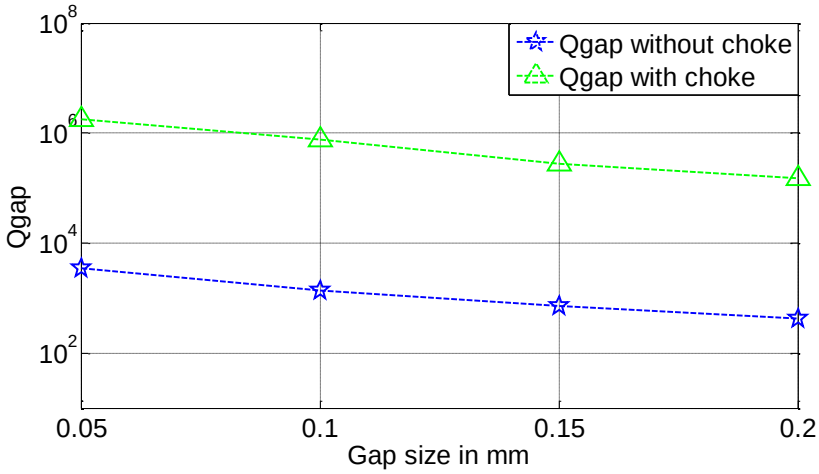

Figure 5.9 The relationship between Q_{gap} and gap size (choke and without choke)

The Q_{gap} curve for the resonator with chokes follows the same trend compared to the one without chokes. With the integration of choke, though it is still sensitive to the gap size, the loss caused by the gap is now far smaller than the loss caused by conductor material (aluminium or copper). For an X-band waveguide circuit, as long as the gap size is smaller than 0.2mm, the effect of Q_{gap} to the response is negligible if a choke is used [38].

To verify the simulations, a model was fabricated with the gap size of 0.1mm; its photos were shown in Figure 5.10. In Figure 5.10(a), the resonator was disassembled from several parts; the metallic parts were the upper half and lower half of the main body, while the white solid was the dielectric bearing for the coupling tuner, which was made of PTFE. Figure 5.10(b) shows the assembled resonator.

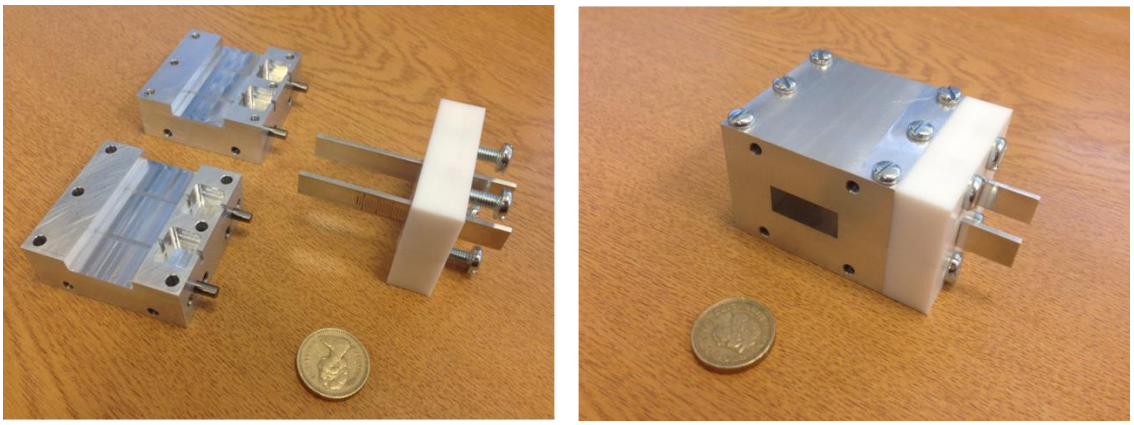

(a) (b)

Figure 5.10 The fabricated tunable waveguide resonator with chokes, (a) disassembled, (b) assembled

The fabrication material was Aluminium with an electrical conductivity of 3.56×10^7 S/m. The measured results were given together with the simulated responses (in this simulation, the material was aluminium with an electrical conductivity of 3.56×10^7 S/m) for comparison in Figure 5.11. From right to left, the *S*21 corresponds to *wr* changing from 8 to 13mm.

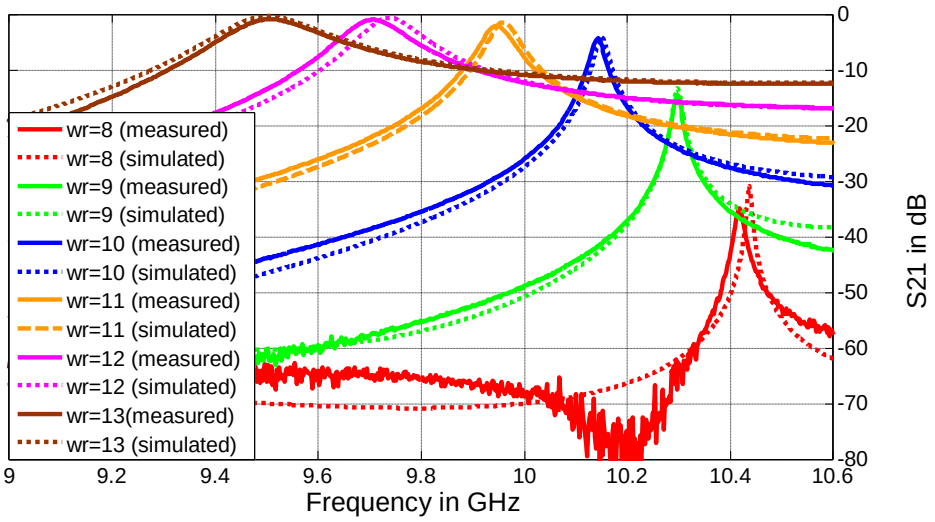

Figure 5.11 The measured S21 of the fabricated single resonator cavity with choke

The main contribution to insertion loss was the conductor loss of the aluminium ($Q_c \approx 2000$ for one resonator). By analysing the results above, the relationship between Q_e and wr is shown in Figure 5.12; the relationship between f_0 and wr is shown in Figure 5.13.

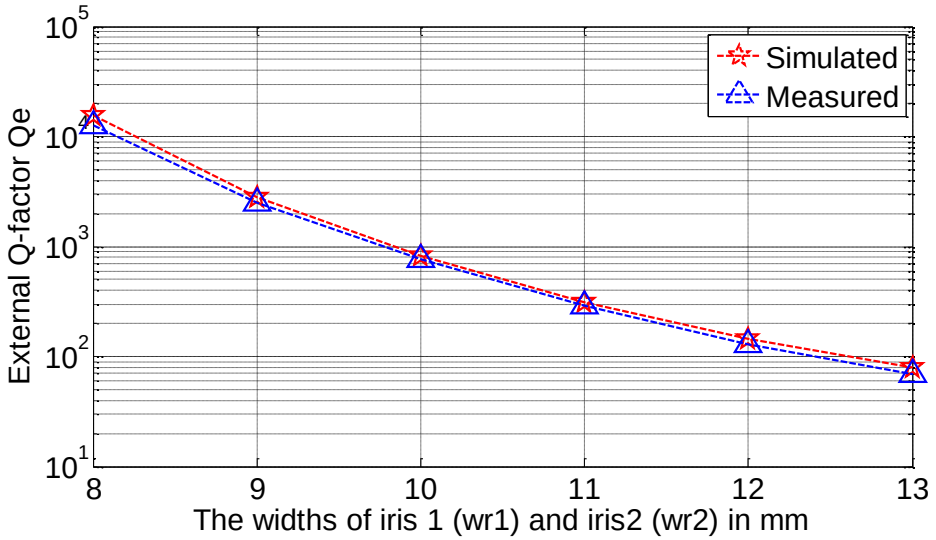

Figure 5.12 The simulated results and measure results for Q_e vs wr

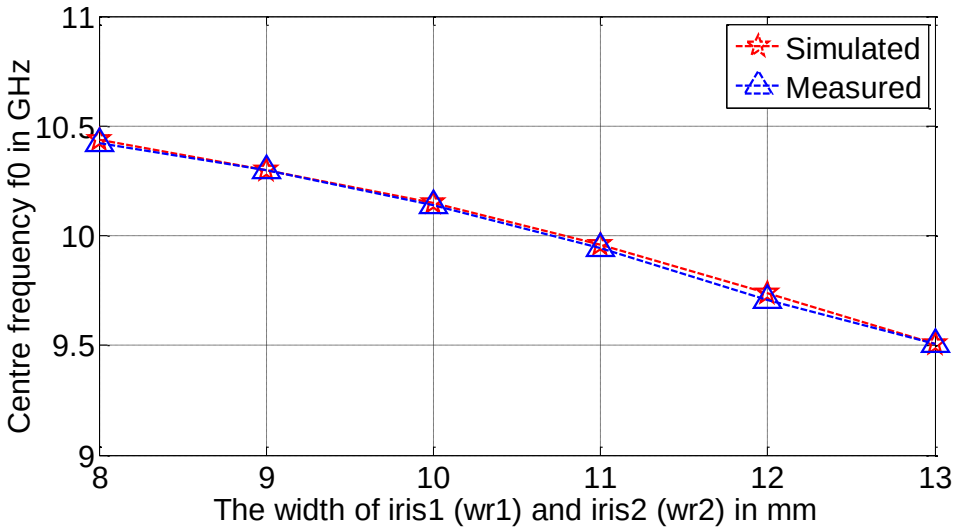

Figure 5.13 The simulated results and measure results for f_0 vs wr

For measured results, with the widths of both irises changing from 8 to 13mm, Q_e changes from 59 to 12000. For a particular iris, Q_e and k_c have a relationship, and one of them can be calculated, once the other one is known [39]. The equivalent k_c for this tunable resonator changes from 0.005 to 0.08, which covers many cases for narrow band Chebyshev filter design. The centre frequency shifts from 10.4GHz to 9.5GHz. But by integrating the frequency tuner which will be discussed in next section, the frequency shift can be compensated.

5.2 Frequency Tuning Structure

The frequency tuner design was based on the tuning structure which was discussed in [40, 41]. As shown in Figure 5.14, an x-direction cylindrical rod is the frequency tuner for this waveguide resonator. The tuner has a diameter d of 3.8mm and is placed at the centre of the cavity. The cavity has the same dimension of the models in previous section. The insertion depth of the frequency tuner is denoted as fr. The maximum value for fr is 22.86mm. When the gap between frequency tuner and main body is 0.1mm, the radiation Q-factor caused by

this gap is around 10^6. This value remains above 10^5, as long as the gap size is smaller than 0.2mm.

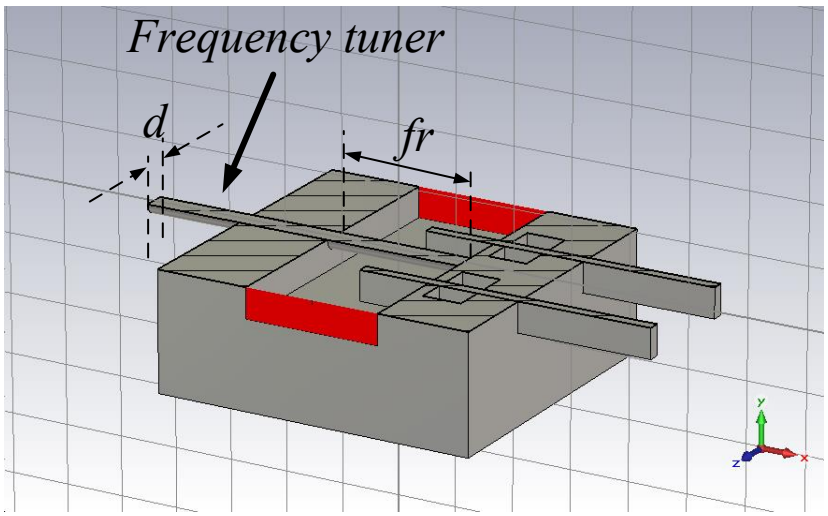

Figure 5.14 The waveguide resonator with frequency tuner

According to [41], for $TE_{1,0,1}$ mode, the frequency tuning range increases if d/b increases (b=10.16mm for WR90 waveguide), but the ratio should be kept smaller than 0.4 to avoid additional resonance and excitation of other modes [41]. When the widths of both irises are kept at 10mm, a set of S21s can be obtained by tuning fr. The simulated results are given in Figure 5.15.

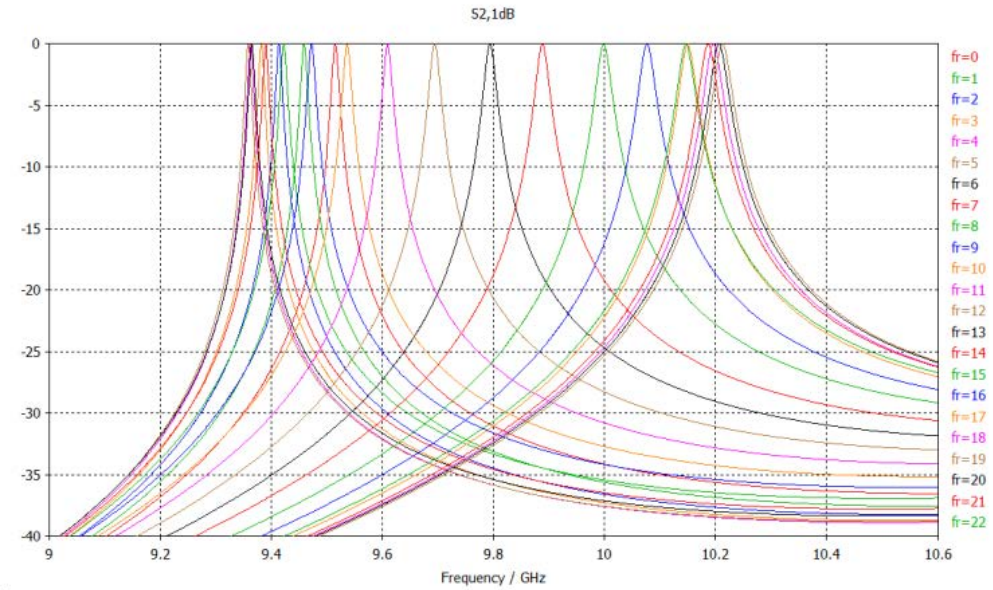

Figure 5.15 A set of S21s when fr changes from 0 to 22mm

The analysed result based on the above responses are given below, Figure 5.16 shows the relationship between f_0 and fr. Figure 5.17 shows the curve of Q_L vs fr.

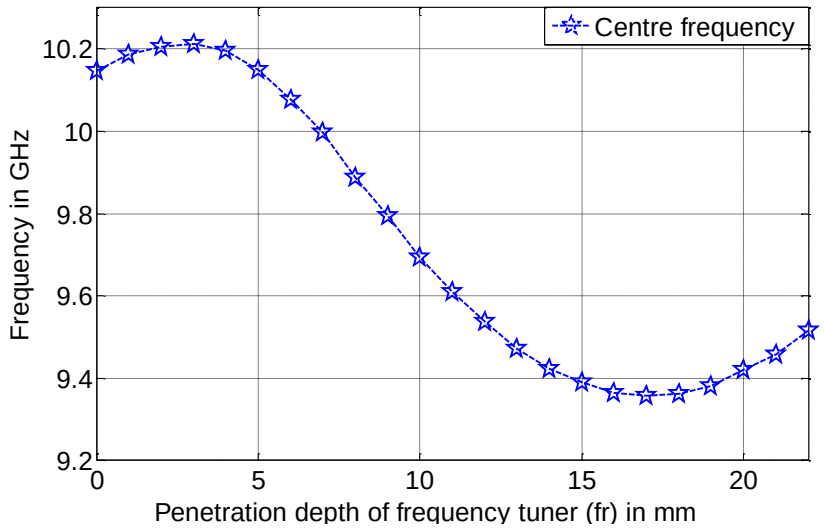

Figure 5.16 Centre frequency f_0 vs insertion depth of frequency tuner fr (widths of both irises are fixed at 10mm)

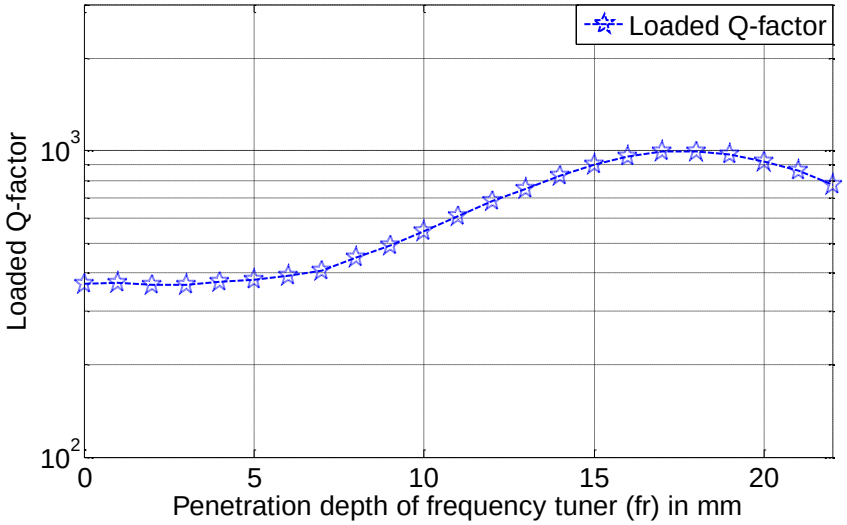

Figure 5.17 Q_L vs fr (widths of both irises are fixed at 10mm)

The frequency tuning range is from 9.3GHz to 10.2GHz, the maximum difference is 0.9GHz. Q_L increases slightly as the frequency tuner penetrates more into the cavity [41].

In next section, a fully tunable bandpass filter is designed and implemented in rectangular waveguide, based on the proposed frequency tuner and coupling tuner.

5.3 Design of A 3rd Order Tunable Bandpass Filter

A 3rd order tunable bandpass filter is presented in this section. In order to achieve flexibility in both centre frequency and bandwidth, all the couplings in this filter can be tuned. The topology of the filter is given first, followed by the measured results.

5.3.1 The Filter Topology

The topology is given below in Figure 5.18, where the circles denote resonators, the lines denote couplings, $m_{i,j}$ is the coupling coefficient between resonator i and j, $m_{i,i}$ is the self-coupling of resonator, Q_{eS} and Q_{eL} are the external Q-factors at port 1 and port 2, respectively. The blue arrows mean tunable inter-resonator couplings and external Q-factors which are implemented by coupling tuners, the red arrows stand for tunable resonant frequencies which are carried out by frequency tuners.

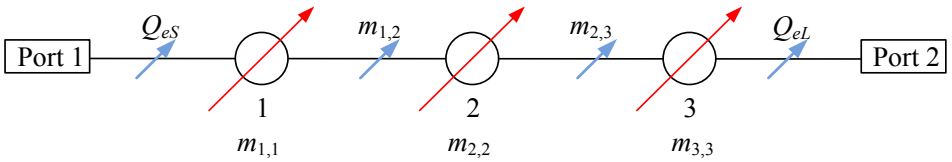

Figure 5.18 The topology of a 3rd order tunable filter

The fabricated filter is shown in Figure 5.19. The metal part is the main body of the filter; the plastic part is the dielectric bearing for the tuners. There are scales on the tuners, the unit scale is 1mm. The material for main body is aluminium and the material for dielectric bearing is C6 (a polymer with similar dielectric properties to PTFE, but harder).

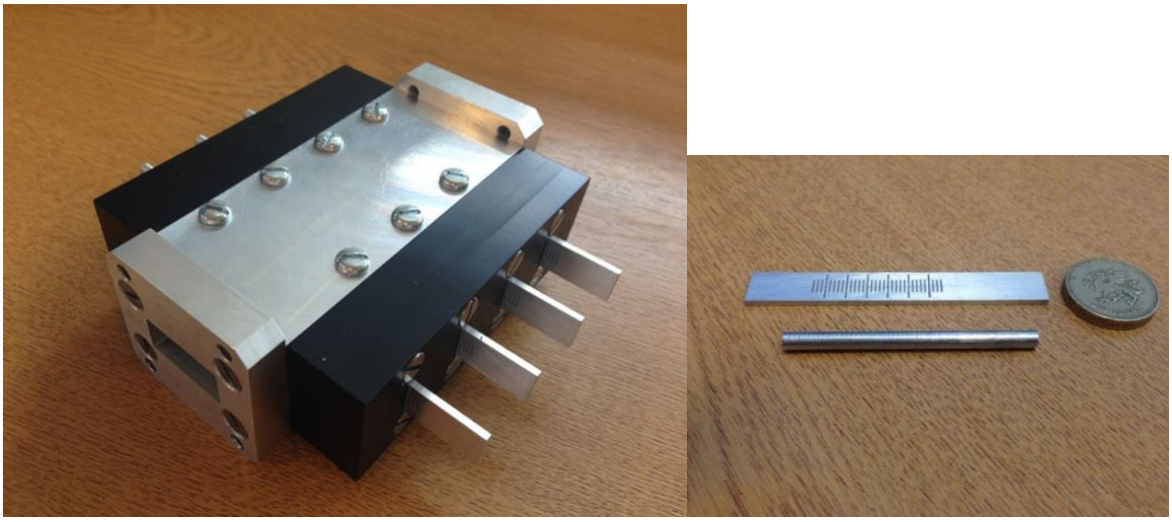

(a) (b)

Figure 5.19 The fabricated 3rd order tunable filter, (a) the full structure, (b) a coupling tuner and a frequency tuner

In order to illustrate the inside structure of the filter, an H-plane cross sectional view is given in Figure 5.20 (lower half of the main body and tuners). The figure shows 3 cavities, 3 frequency tuners and 4 coupling tuners of the filter, all of which are labelled and named. The dimensions of the cavities and the tuners are identical to that of the tunable waveguide resonator. The width, height and length for all three cavities are 22.86mm, 10.16mm and 18mm, respectively; the gaps around all tuners are 0.1mm.

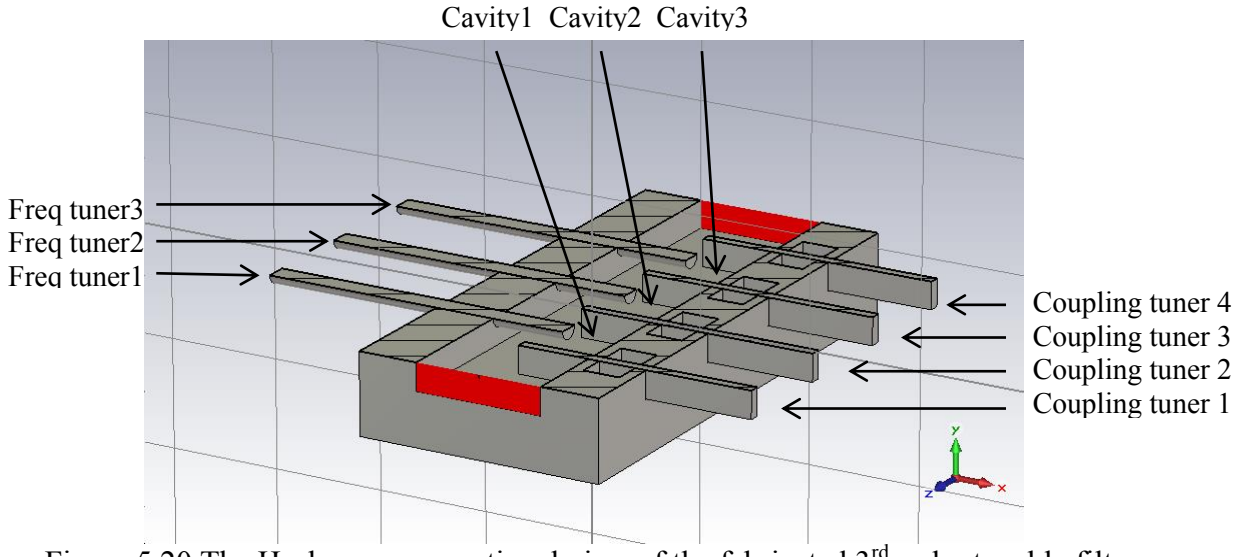

Figure 5.20 The H-plane cross-sectional view of the fabricated 3rd order tunable filter

The namings of the tunable parameters are shown below in Figure 5.21, where *wr*1, *wr*12, *wr*23 and *wr*2 are the widths of the irises, and *fr*1, *fr*2 and *fr*3 are the insertion depths of frequency tuners.

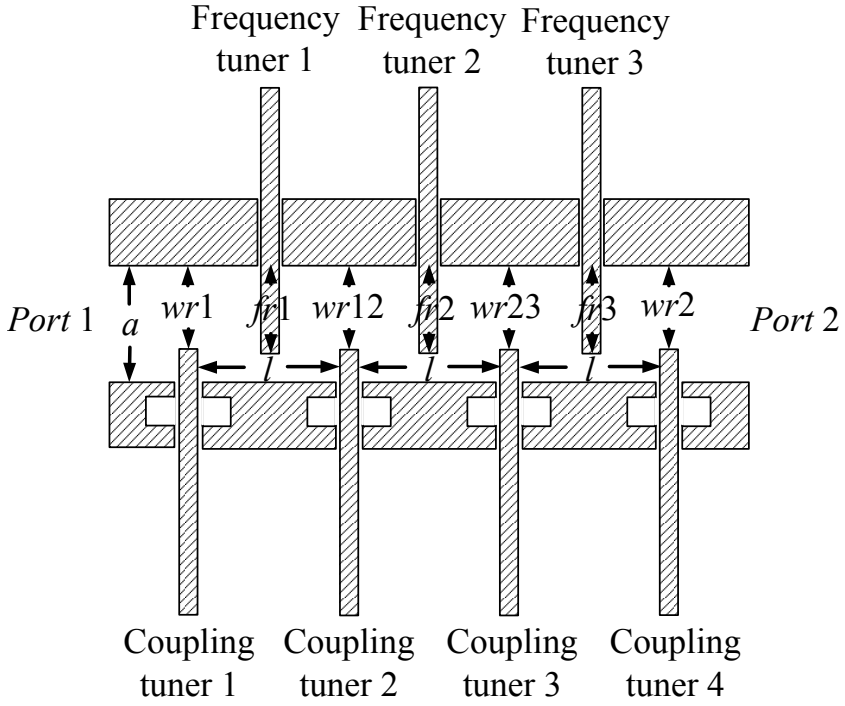

Figure 5.21 The H-plane cross-sectional view of the 3rd order tunable filter

5.3.2 The Lowpass Prototype Response

The design of the tunable filter is based on a 3rd order lowpass prototype Chebyshev with 15dB return loss level for passband. The lowpass prototype response is given below.

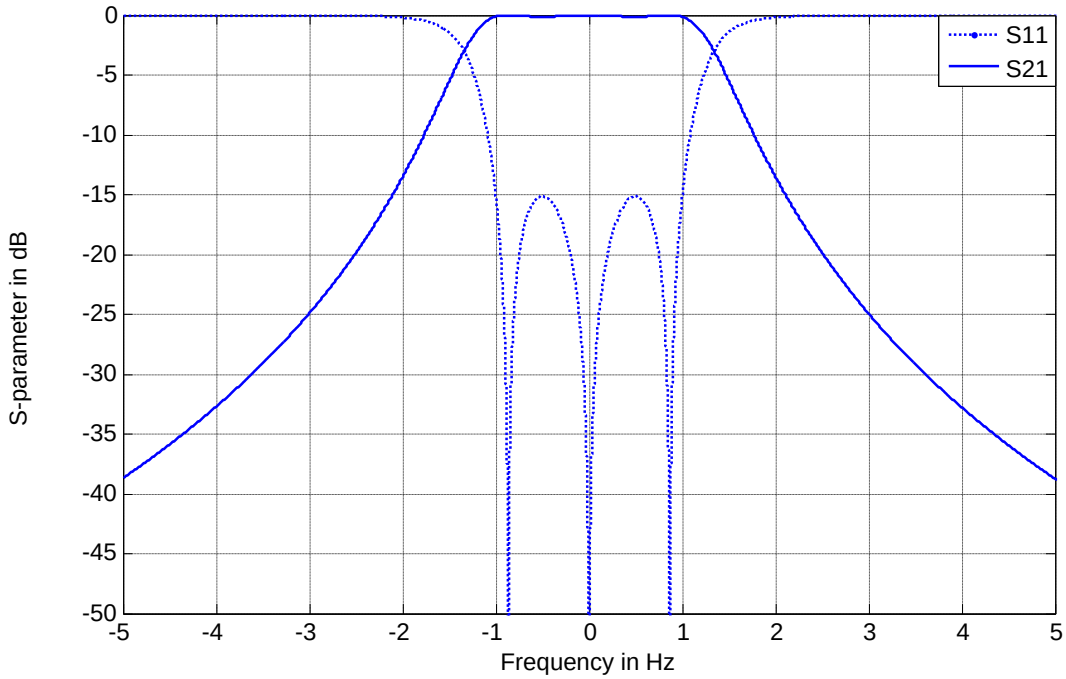

Figure 5.22 The lowpass prototype response of a 3rd order Chebyshev filter with 15dB return loss

The corresponding normalised coupling matrix and the normalised external Q-factors are given in (5-2).

$$[m]=\begin{pmatrix} 0 & 0.8835 & 0 \\ 0.8835 & 0 & 0.8835 \\ 0 & 0.8835 & 0 \end{pmatrix}, \qquad (5\text{-}2)$$
$$Q_{eS}=Q_{eL}=1.1104$$

5.3.3 Passband Bandwidth Tuning

The bandwidth tuning ability is mainly implemented by coupling tuners. However, the frequency tuners also play assistant roles, since the moving of the coupling tuners may cause the resonant frequency shift and need to be compensated by the frequency tuners. Due to the limited tuning range of frequency tuner, the widest tuning range for the bandwidth is achieved when f_0=9.5GHz, the FBW is from 0.9% to 3.8%. Because the filter can achieve continuous tuning, it is impossible to list all the responses, only selected responses are shown here. Table 5.1 shows the theoretically synthesised de-normalised coupling matrix and

external Q-factors at 9.5GHz. The corresponding theoretical calculated S-parameters are given in Figure 5.23.

f_0=9.5GHz		
FBW	**Coupling Matrix**	**External Q-factors**
0.9%	$[M]=\begin{pmatrix} 0 & 0.0080 & 0 \\ 0.0080 & 0 & 0.0080 \\ 0 & 0.0080 & 0 \end{pmatrix}$	$Q_{eS}=Q_{eL}=123.5$
2.1%	$[M]=\begin{pmatrix} 0 & 0.0186 & 0 \\ 0.0186 & 0 & 0.0186 \\ 0 & 0.0186 & 0 \end{pmatrix}$	$Q_{eS}=Q_{eL}=52.9$
3.8%	$[M]=\begin{pmatrix} 0 & 0.0336 & 0 \\ 0.0336 & 0 & 0.0336 \\ 0 & 0.0336 & 0 \end{pmatrix}$	$Q_{eS}=Q_{eL}=29.2$

Table 5.1 The coupling matrices and external Q-factors

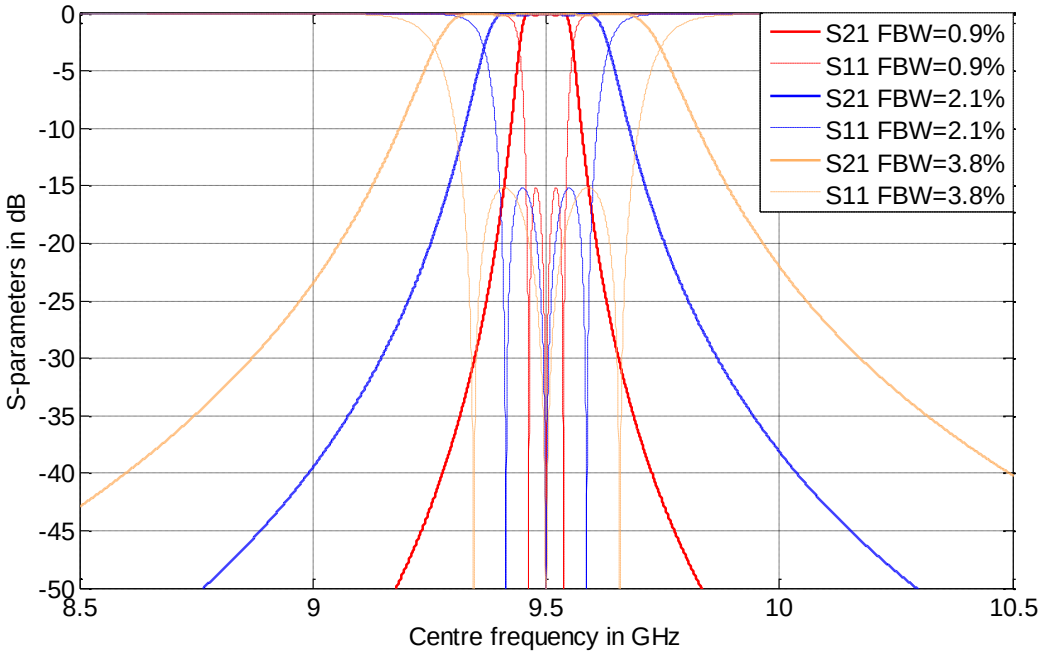

Figure 5.23 The calculated response of the 3rd order Chebyshev filter centred at 9.5GHz with *FBW* various from 0.9% to 3.8% (15dB passband return loss)

The coupling coefficients and external *Q*-factors in Table 5.1 can be interpreted into corresponding parameters of the tuners by using the methods shown in Section 4.1. They are good initial parameters; it is not difficult to obtain the desired *S*-parameters which are shown in Figure 5.24 and Figure 5.25. Figure 5.24 shows the simulated results when the filter is made of PEC; Figure 5.25 shows the simulated results when the filter is made of aluminium. The filling and background materials for both simulations are vacuum.

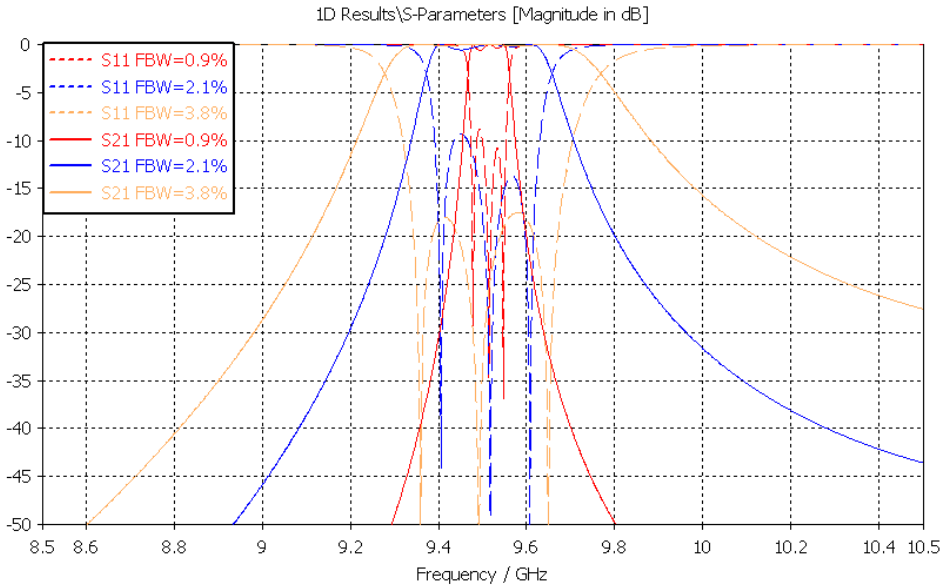

Figure 5.24 The simulated response of the filter centred near 9.5GHz with *FBW* various from 0.9% to 3.8% (PEC)

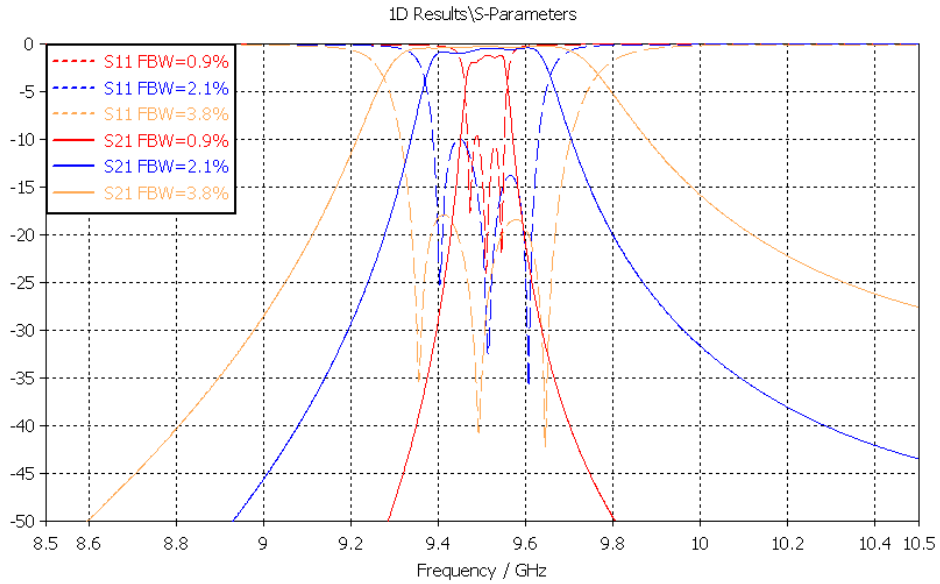

Figure 5.25 The simulated response of the filter centred near 9.5GHz with *FBW* various from 0.9% to 3.8% (Aluminium with electric conductivity of 3.56×10^7 S/m)

For PEC model, the mid-band insertion loss is smaller than 0.01dB. For aluminium model, the mid-band insertion loss is between 0.3dB to 1.6dB.

The corresponding tuning parameters for the above results are given in Table 5.2. As the tuning function is implemented by hand at current stage, the unit step is 0.5mm.

f_0=9.5GHz				
FBW	***wr*1=*wr*2 (mm)**	***wr*12=*wr*23 (mm)**	***fr*1=*fr*3 (mm)**	***fr*2 (mm)**
0.9%	12.5	9.5	10.5	13.5
2.1%	13.5	10.5	9	13
3.8%	14.5	11.5	4.5	10

Table 5.2 The corresponding tuning parameters

Figure 5.26 shows the measured results of the fabricated device.

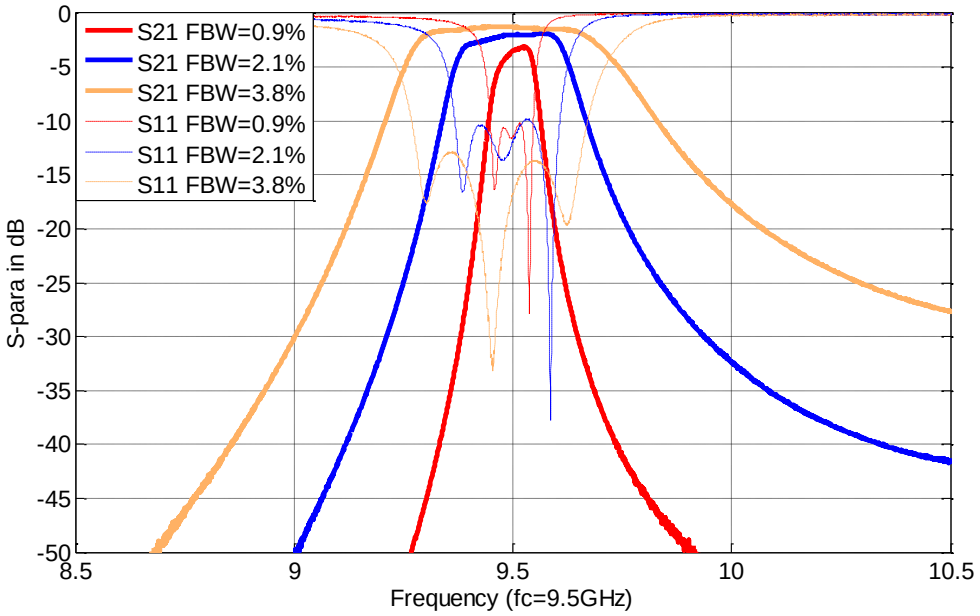

Figure 5.26 The measured response of the filter centred near 9.5GHz with *FBW* various from 0.9% to 3.8%

As shown in the figure above, the measured insertion loss increases from 1dB to 3dB as the *FBW* decreases from 3.8% to 0.9%. It is higher than that of the simulated results. The

insertion loss here is mainly due to the H-plane cutting and assembly errors. The misalignments between different parts may cut the surface current and increase the insertion loss. Also, as the *FBW* decreases, the Q_L increases. This can be explained by (5-1), which indicates when Q_u is fixed, the larger Q_L leads to higher insertion loss.

5.3.4 Passband Centre Frequency Tuning

In this section, the selected measured responses are categorised into 3 groups based on the positions of coupling tuners. For each group, the coupling tuners are fixed during the tuning; only the frequency tuners are moved to tune the centre frequency.

5.3.4.1 Group 1 (*FBW* from 3.4% to 3.8%)

In group 1, for the coupling tuners, *wr*1 and *wr*2 are both fixed at 14.5mm; *wr*12 and *wr*23 are fixed at 11.5mm. By only moving the frequency tuners, the *FBW* of the responses can be maintained between 3.4% and 3.8%. Figure 5.27 shows the corresponding *S*-parameters with different passband centre frequencies. The values of the tuning parameters can be found in Table 5.3.

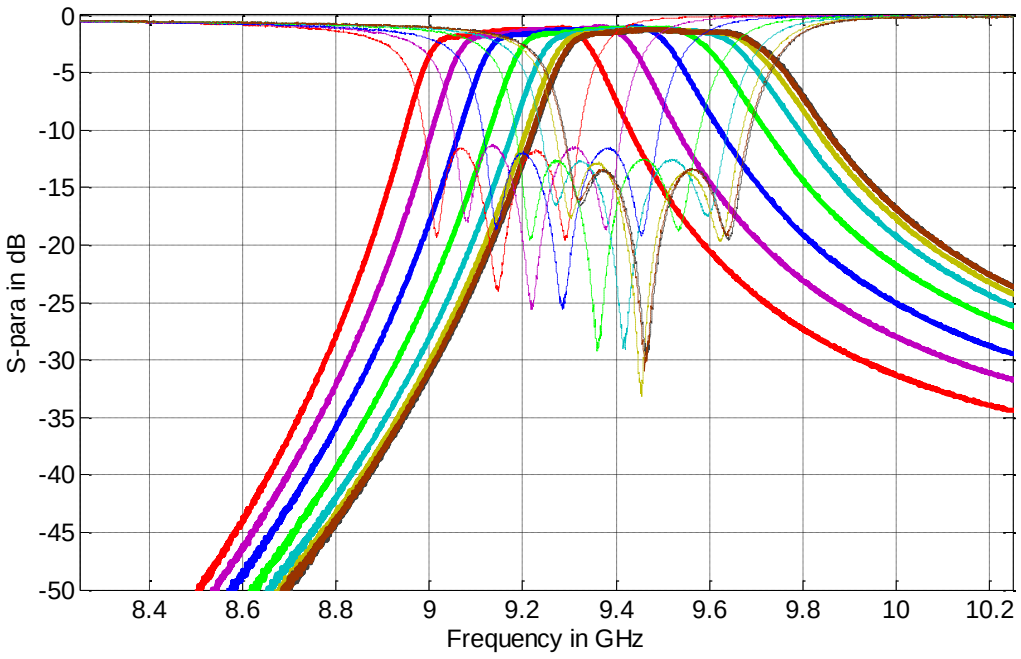

Figure 5.27 The measured response of the filter when *FBW* is from 3.4% to 3.8%

Group1							
***wr*1=*wr*2=14.5 mm**			***wr*12=*wr*23=11.5 mm**				
f_0 (GHz)	9.17	9.25	9.32	9.39	9.45	9.48	9.50
***fr*1=*fr*3 (mm)**	10.5	9.5	8.5	7.5	6.5	5.5	4.5
***fr*2 (mm)**	16.5	14	12.5	11.5	11	10.5	10
Absolute *BW* (GHz)	0.308	0.330	0.340	0.355	0.359	0.361	0.363
FBW	3.4%	3.5%	3.6%	3.7%	3.8%	3.8%	3.8%

Table 5.3 The corresponding parameters of tuners

5.3.4.2 Group 2 (*FBW* from 1.9% to 2.4%)

In group 2, *wr*1 and *wr*2 are both fixed at 13.5mm; *wr*12 and *wr*23 are fixed at 10.5mm. During the centre frequency tuning, the *FBW* remains between 1.9% and 2.4%. Figure 5.28 shows the corresponding *S*-parameters with different passband centre frequencies. The values of the tuning parameters can be found in Table 5.4.

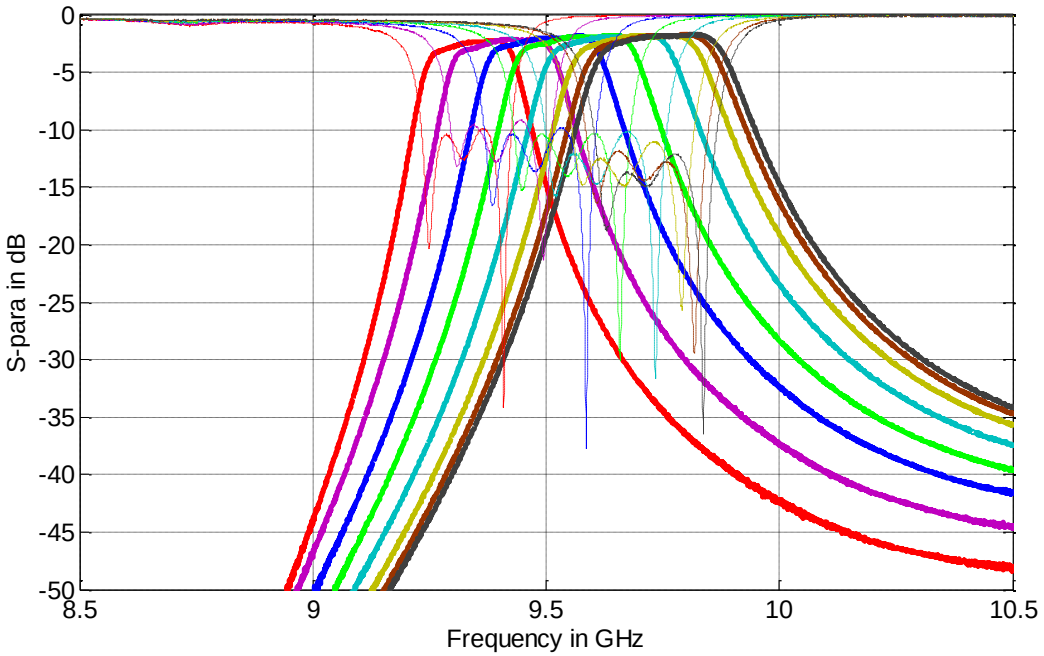

Figure 5.28 The measured response of the filter when *FBW* is from 1.9% to 2.4%

Group 2								
***wr*1=*wr*2=13.5 mm**				***wr*12=*wr*23=10.5 mm**				
f_0 (GHz)	9.34	9.42	9.50	9.57	9.65	9.70	9.73	9.75
***fr*1=*fr*3 (mm)**	11	10	9	8	7	6	5	4
***fr*2 (mm)**	18	14.5	13	12	11	10.5	10	10
Absolute *BW* (GHz)	0.178	0.195	0.220	0.226	0.232	0.233	0.237	0.237
FBW	1.9%	2.0%	2.1%	2.2%	2.3%	2.4%	2.4%	2.4%

Table 5.4 The corresponding parameters of tuners

5.3.4.3 Group 3 (*FBW* from 0.9% to 1.4%)

In group 3, *wr*1 and *wr*2 are both fixed at 12.5mm; *wr*12 and *wr*23 are fixed at 9.5mm. The *FBW* remains between 0.9% and 1.4%. Figure 5.29 shows the corresponding *S*-parameters with different passband centre frequencies. The values of the tuning parameters can be found in Table 5.5.

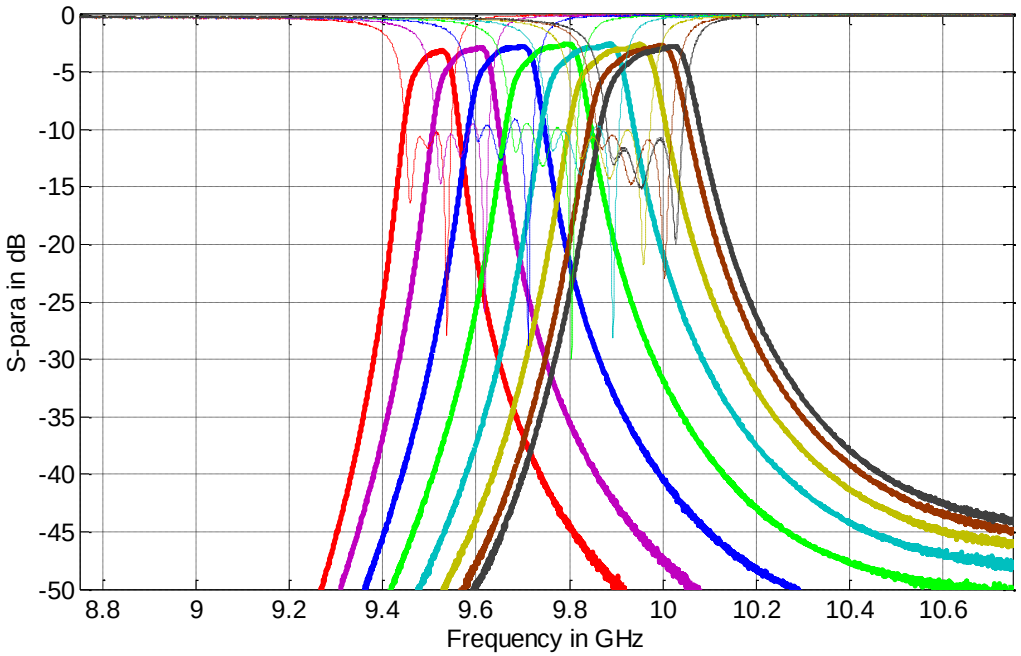

Figure 5.29 The measured response of the filter when *FBW* is from 0.9% to 1.4%

Group 3								
***wr*1=*wr*2=12.5 mm**				***wr*12=*wr*23=9.5 mm**				
f_0 (GHz)	9.51	9.58	9.66	9.76	9.84	9.90	9.95	9.98
***fr*1=*fr*3 (mm)**	10.5	9.5	8.5	7.5	6.5	5.5	4.5	4
***fr*2 (mm)**	13.5	12.5	11.5	10.5	10	9.5	9	8.5
Absolute *BW* (GHz)	0.087	0.102	0.110	0.116	0.127	0.135	0.140	0.139
FBW	0.9%	1.0%	1.1%	1.2%	1.3%	1.4%	1.4%	1.4%

Table 5.5 The corresponding parameters of tuners

5.3.5 Discussion

The filter achieves the maximum *FBW* tuning range of 0.9% to 3.8% at 9.5GHz. It also offers 400MHz range for centre frequency tuning when coupling tuners are fixed.

The passband is slightly uneven when the *BW* is narrow. This is caused by the mismatch of the coupling tuners. The external *Q*-factor Q_e changes along with the positions of coupling tuner 1 and 4. As shown in Figure 5.12, they have a non-linear relation. Q_e change per millimetre is smaller, when the value of Q_e is smaller; and vice versa. This means that Q_e is more sensitive to the positions of coupling tuner 1 and 4, when they are larger, i.e. *BW* is narrower. Consequently, the same scale errors of tuner position may cause more serious mismatch, when *BW* is narrower.

During the frequency tuning, as the frequency tuners penetrate more into the cavities, the *BW* increases along with the centre frequency. This is an inevitable effect, as the increase of the insertion depths of frequency tuners will increase the Q_L which eventually makes *BW* wider. If *BW* is strictly required to be constant during the frequency tuning, the above effect can be compensated by further fine tuning the coupling coefficients and external *Q*-factors. Such fine tunings might require more accurate and higher resolution manipulation of the tuners.

References:

1. Ming, Y., et al., "The Sound the Air Makes: High-Performance Tunable Filters Based on Air-Cavity Resonators," *IEEE Microwave Magazine,* 2014. **15**(5): p. 83-93.
2. Mansour, R.R., et al., "High-Q Tunable Filters: Challenges and Potential," *IEEE Microwave Magazine,* 2014. **15**(5): p. 70-82.
3. Manuel Sanchez-Renedo, R.G.-G., Jose I. Alonso, Cesar Briso-Rodriguez, "Tunable Combline Filter With Continuous Control of Center Frequency and Bandwidth," *IEEE TRANSACTION ON MICROWAVE THEORY AND TECHNIQUES* , 2005. **53**(1): p. 9.
4. Winter Dong, Y. and R.R. Mansour, "Tunable Dielectric Resonator Bandpass Filter With Embedded MEMS Tuning Elements," *IEEE Transaction on Microwave Theory and Techniques*, 2007. **55**(1): p. 154-160.
5. Huang, F., S. Fouladi, and R.R. Mansour, "High-Q Tunable Dielectric Resonator Filters Using MEMS Technology," *IEEE Transaction on Microwave Theory and Techniques,* 2011. **59**(12): p. 3401-3409.
6. Fengxi, H. and R. Mansour. "A novel varactor tuned dielectric resonator filter. in *2013 IEEE MTT-S International Microwave Symposium Digest (IMS)*. 2013.
7. Fouladi, S., et al., "High-Q Narrowband Tunable Combline Bandpass Filters Using MEMS Capacitor Banks and Piezomotors," *IEEE Transaction on Microwave Theory and Techniques,* 2013. **61**(1): p. 393-402.
8. Yassini, B., Y. Ming, and B. Keats, "A Ka-Band Fully Tunable Cavity Filter," *IEEE Transaction on Microwave Theory and Techniques*, 2012. **60**(12): p. 4002-4012.
9. Snyder, R.V. "A wide-band tunable filter technique based on double-diplexing and low-Q tuning elements," in *2000 IEEE MTT-S International Microwave Symposium Digest.*. 2000.
10. Yassini, B., et al., "A Ku-Band High-Q Tunable Filter With Stable Tuning Response," *IEEE Transaction on Microwave Theory and Techniques*, 2009. **57**(12): p. 2948-2957.
11. Kurudere, S. and V.B. Erturk, "Novel Microstrip Fed Mechanically Tunable Combline Cavity Filter," *IEEE Microwave and Wireless Components Letters,* 2013. **23**(11): p. 578-580.
12. Peng, W. and I. Hunter, "Electronically Tunable Filters," *IEEE Microwave Magazine*, 2009. **10**(6): p. 46-54.
13. Peng, W. and I.C. Hunter, "A New Class of Low-Loss High-Linearity Electronically Reconfigurable Microwave Filter," *IEEE Transaction on Microwave Theory and Techniques,* 2008. **56**(8): p. 1945-1953.
14. Alaa I. Abunjaileh, I.C.H., "Tunable Bandpass and Bandstop Filters Based on Dual-Band Combline Structures," *IEEE TRANSACTION ON MICROWAVE THEORY AND TECHNIQUES* , 2010. **58**(12): p. 10.
15. Rebeiz, G.M., et al., "Tuning in to RF MEMS," *IEEE Microwave Magazine*, 2009. **10**(6): p. 55-72.
16. Jia-Sheng, H., "Reconfigurable planar filters," *IEEE Microwave Magazine*, 2009. **10**(6): p. 73-83.
17. Naglich, E.J., D. Peroulis, and W.J. Chappell. "Wide spurious free range positive-to-negative inter-resonator coupling structure for reconfigurable filters," in *2013 IEEE MTT-S International Microwave Symposium Digest (IMS),*. 2013.
18. Sirci, S., et al. "Analog tuning of compact varactor-loaded combline filters in substrate integrated waveguide," in *2012 42nd European Microwave Conference (EuMC)*. 2012.

19. Mira, F., J. Mateu, and C. Collado, "Mechanical Tuning of Substrate Integrated Waveguide Resonators," *IEEE Microwave and Wireless Components Letters*, 2012. **22**(9): p. 447-449.
20. Armendariz, M., V. Sekar, and K. Entesari. "Tunable SIW bandpass filters with PIN diodes,". in *2010 European Microwave Conference (EuMC),*. 2010.
21. Joshi, H., et al., "High-Q Fully Reconfigurable Tunable Bandpass Filters," *IEEE Transaction on Microwave Theory and Techniques*, 2009. **57**(12): p. 3525-3533.
22. Torregrosa-Penalva, G., et al., "A simple method to design wide-band electronically tunable combline filters," *IEEE Transaction on Microwave Theory and Techniques*, 2002. **50**(1): p. 172-177.
23. Wen-Teng, L. and C.K.C. Tzuang, "K-band quasi-planar tapped combline filter and diplexer," *IEEE Transaction on Microwave Theory and Techniques*, 1993. **41**(2): p. 215-223.
24. Xu-Guang, W., C. Young-Ho, and Y. Sang-Won, "A Tunable Combline Bandpass Filter Loaded With Series Resonator," *IEEE Transaction on Microwave Theory and Techniques*, 2012. **60**(6): p. 1569-1576.
25. Matthaei, G.L., "Narrow-band, fixed-tuned, and tunable bandpass filters with zig-zag hairpin-comb resonators," *IEEE Transaction on Microwave Theory and Techniques*, 2003. **51**(4): p. 1214-1219.
26. Han-Ul, M., et al. "Size-reduced tunable hairpin bandpass filter using aperture coupling with enhanced selectivity and constant bandwidth," in *2008 IEEE MTT-S International Microwave Symposium Digest,*. 2008.
27. Xiu Yin, Z., et al., "RF Tunable Bandstop Filters With Constant Bandwidth Based on a Doublet Configuration,", *IEEE Transaction on Industrial Electronics,* 2012. **59**(2): p. 1257-1265.
28. Tsuzuki, G., et al. "Ultra-Selective Constant-Bandwidth Electromechanically Tunable HTS Filters," in *2006. IEEE MTT-S International Microwave Symposium Digest,*. 2006.
29. Psychogiou, D. and D. Peroulis, "Tunable VHF Miniaturized Helical Filters," *IEEE Transaction on Microwave Theory and Techniques*, 2014. **62**(2): p. 282-289.
30. Xiu Yin, Z., et al., "Low-Loss Frequency-Agile Bandpass Filters With Controllable Bandwidth and Suppressed Second Harmonic," *IEEE Transaction on Microwave Theory and Techniques*, 2010. **58**(6): p. 1557-1564.
31. Manh-Tai, N., W.D. Yan, and E.P.W. Horne. "Broadband tunable filters using high Q passive tunable ICs," in *2008 IEEE MTT-S International Microwave Symposium Digest,*. 2008.
32. Sirci, S., et al. "Varactor-loaded continuously tunable SIW resonator for reconfigurable filter design," in *2011 41st European Microwave Conference (EuMC),*. 2011.
33. Sekar, V., M. Armendariz, and K. Entesari, "A 1.2&1.6-GHz Substrate-Integrated-Waveguide RF MEMS Tunable Filter," *IEEE Transaction on Microwave Theory and Techniques*, 2011. **59**(4): p. 866-876.
34. Arif, M.S. and D. Peroulis, "All-Silicon Technology for High-Q Evanescent Mode Cavity Tunable Resonators and Filters," *Journal of Microelectromechanical Systems*, 2014. **23**(3): p. 727-739.
35. Da-Peng, W., C. Wen-quan, and P. Russer. "Tunable Substrate-Integrated Waveguide (SIW) Dual-Mode Square Cavity Filter with Metal Cylinders," in *IEEE MTT-S on International Microwave Workshop Series on Art of Miniaturizing RF and Microwave Passive Components,*. 2008.

36. Hyunseong, K., et al. "Silicon-based substrate-integrated waveguide-based tunable band-pass filter using interdigital MEMS capacitor," in *2013 Asia-Pacific Microwave Conference Proceedings (APMC),*. 2013.
37. Hong, J.-S. and M.J. Lancaster, *Microstrip Filters for RF/Microwave Applications* 2001: John Wiley and Sons Ltd, United Kingdom.
38. Bryan, J.G. and F.J. Rosenbaum, "A Wide-Band Nearly Constant Susceptance Waveguide Element (Correspondence)," *IEEE Transaction on Microwave Theory and Techniques*, 1971. **19**(11): p. 889-891.
39. Shang, X., W. Xia, and M.J. Lancaster, "The design of waveguide filters based on cross-coupled resonators," *Microwave and Optical Technology Letters*, 2014. **56**(1): p. 3-8.
40. Smullin, L.D., *Design of Tunable Resonant Cavities with Constant Bandwidth.* 1949.
41. Marcuvitz, N. and I.o.E. Engineers, *Waveguide Handbook* 1951: McGraw-Hill.

CHAPTER 6 TUNABLE NOTCH FILTER DESIGN BASED ON RECTANGULAR WAVEGUIDE CIRCUIT

Notch filters are widely used in industry and military applications, as they can suppress the unwanted jamming signals within the frequency spectrum. The Q-factor of the filter decides the sharpness of the rejection band. In order to achieve narrow and sharp notch, the Q-factor should be high. The tunable notch filter discussed in this chapter combines the tuning flexibility and high Q notch filter. The topology of the filter is based on the dual-passband filter topology investigated in Chapter 3. For such a dual-passband filter, when the stopband is much narrower than the passbands, it can be seen as a notch; meanwhile, the two passbands can be regarded as a single wide passband. In Section 6.1, a discussion on the topology selection for tunable notch filter is given. In Section 6.2, the lowpass prototype of a 4^{th} order tunable notch filter is investigated. In Section 6.3, the 4^{th} order lowpass prototype is transformed to X-band and implemented in the form of rectangular waveguide.

6.1 Topology Selection of Tunable Notch Filter

As proposed in Chapter 3, there are three major types of multi-passband resonator sections. In theory, no matter which type of the section is used, a multi-passband filter can always achieve the desired specifications. However, considered the practical design limitations, not all multi-passband filter topologies are suitable to be used as tunable notch filter design.

For a tunable filter, the independence of tuning parameter is very important. This means that one or one group of tuning parameters only controls one kind of filter specification, and does not control other specifications of the filter. If a tunable filter does not have good independence of the tuning parameters, it will be very difficult to tune.

The analysis in Appendix II reveals that, in order to achieve same flexibility, the filters with series coupled resonator sections or mixed coupled resonator sections are more difficult to tune than the one with parallel coupled resonator sections. This is because for the filters with parallel coupled resonator sections, each tuning parameter has a better independence. For example, the notch positions are controlled by the frequency of bandstop resonators, the passband centre frequency is controlled by the frequency of bandpass resonators. If one specification needs to be changed, only one or one group of parameters change. On the contrary, for the filter with non-parallel coupled resonator sections, even if just one kind of specification needs to change, all the parameters will need to be tuned. Hence, from this point of view, the topologies with parallel coupled resonator sections are more practical for tunable notch filter design.

However, besides the limitations in topologies, the physical configuration of coupling tuning structure also brings restrictions. The following conditions have to be considered:

- Each bandpass resonator can connect to maximally one bandstop resonator.
- There is no tuner between bandpass resonators and bandstop resonators; therefore the couplings between bandpass resonators and bandstop resonators cannot be tuned.

The conditions imply that, there is only one bandstop resonator in each multi-passband resonator section. It has to be a dual-passband topology.

Given the factors above, the generalised topology for tunable notch filter is illustrated below in Figure 6.1; all resonator frequencies are tunable, all couplings but the ones between bandpass resonators and bandstop resonators are tunable.

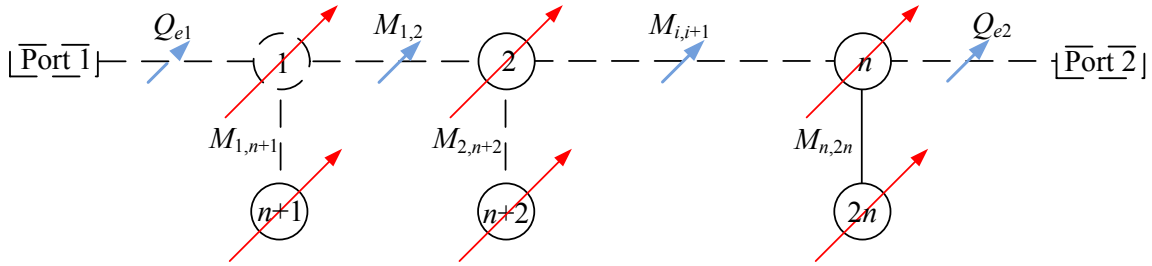

Figure 6.1 A generalised topology for tunable notch filter

6.2 A 4th Order Tunable Notch Filter

A 4th order tunable notch filter is discussed in this section as an example. The filter has a topology as shown in Figure 6.2.

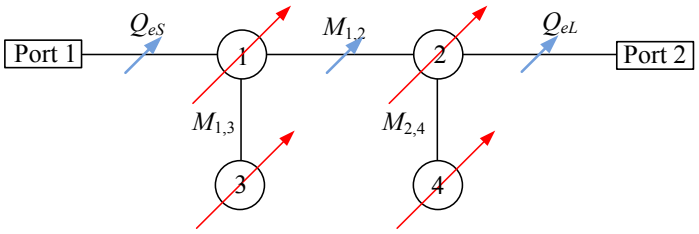

Figure 6.2 The topology of a 4th order tunable notch filter

The response and design parameters discussed in this section are in normalised lowpass frequency domain (Ω domain). They can be transformed to any required frequency bands. It is worth mentioning that, in order to control the responses directly by coupling matrix, the *S*-parameters shown in this chapter are plotted from the coupling matrix. This is different to that in Chapter 3, which uses characteristic polynomials to plot the *S*-parameters. A comparison between the *S*-parameters obtained from these two different approaches is given in Appendix III. As long as the *FBW* is small, the *S*-parameters can be considered accurate [1].

It should be noticed that the tunable notch filter can provide continuous tuning within its tuning range, but given the limited space, only the selected representative results are shown.

6.2.1 Notch Position Tuning

Figure 6.3 shows a set of *S*-parameters with varying notch positions. They are plotted from the design parameters given in Table 6.1. The passbands are centred at 0Hz with a width of 2Hz. The notch width is 0.2Hz. The solid lines are *S*21s, while the dotted line is *S*11. There are three *S*21s, displayed in red, blue and green, respectively; they have different notch positions but same centre frequency. In fact, besides the notch, only one of the *S*21s (red) can be seen, because they overlap with each other. For clearer illustration of the notch, only the red *S*11 is given in the figure, the other *S*11s have similar shapes.

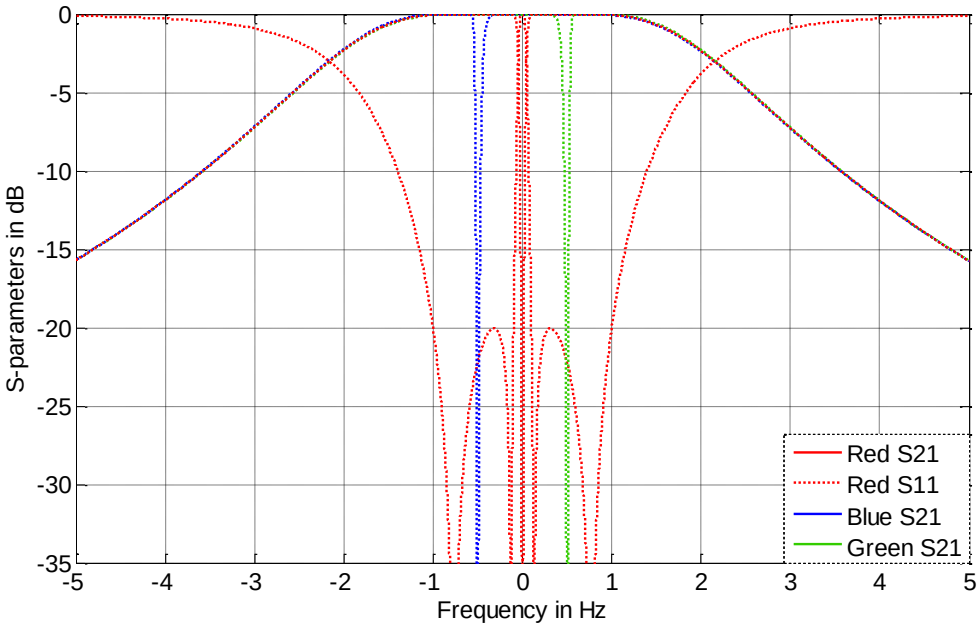

Figure 6.3 Fix centre frequency with varying notch positions

The couplings involved in the tuning are labelled in colour in Table 6.1. By only tuning the self-couplings (resonant frequencies) of bandstop resonators, the filter can effectively achieve tuning in notch position. The centre frequency and bandwidth remain unchanged during the notch position tuning.

	Notch position	**Coupling matrix**	**External *Q*-factor**

Red response	0Hz	$\begin{pmatrix} 0 & 1.4959 & 0.3162 & 0 \\ 1.4959 & 0 & 0 & 0.3162 \\ 0.3162 & 0 & 0 & 0 \\ 0 & 0.3162 & 0 & 0 \end{pmatrix}$	0.739
Blue response	-0.500Hz	$\begin{pmatrix} 0 & 1.4959 & 0.3162 & 0 \\ 1.4959 & 0 & 0 & 0.3162 \\ 0.3162 & 0 & -0.5000 & 0 \\ 0 & 0.3162 & 0 & -0.5000 \end{pmatrix}$	
Green response	0.500Hz	$\begin{pmatrix} 0 & 1.4959 & 0.3162 & 0 \\ 1.4959 & 0 & 0 & 0.3162 \\ 0.3162 & 0 & 0.5000 & 0 \\ 0 & 0.3162 & 0 & 0.5000 \end{pmatrix}$	

Table 6.1 The corresponding design parameters for notch position tuning

6.2.2 Passband Centre Frequency Tuning

Figure 6.4 shows a set of *S*-parameters with varying centre frequencies. The bandwidth is again 2Hz for this case, while the notch is placed at 0Hz and 0.2Hz wide. The three *S*21s each have different centre frequencies. The notch position is not changing during the tuning of centre frequency. The couplings involved in the tuning are labelled in colour in Table 6.2. The filter can achieve centre frequency tuning by only changing the resonant frequencies of the bandpass resonators.

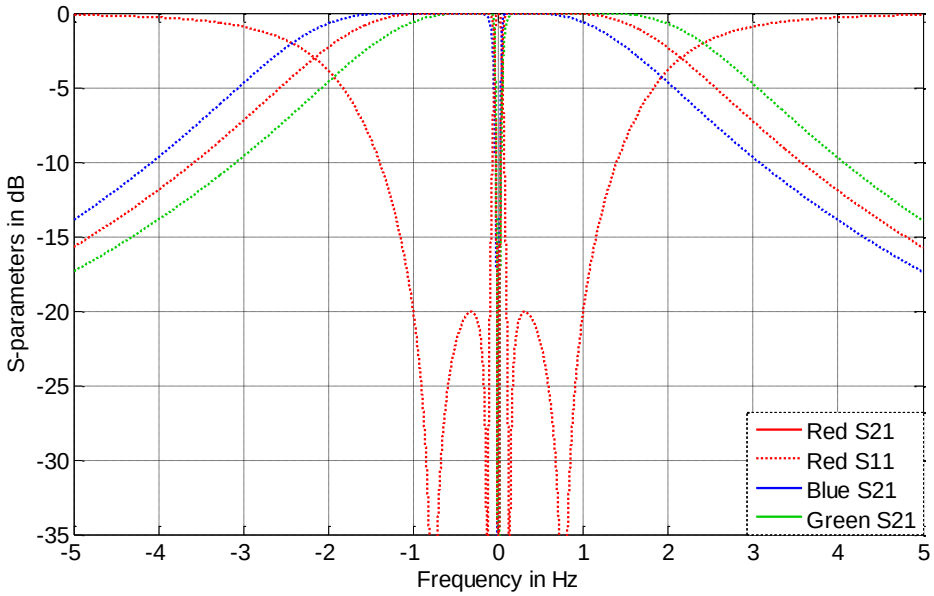

Figure 6.4 Fix notch with varying centre frequencies

	Passband centre frequency	Coupling matrix	External Q-factor
Red response	0Hz	$\begin{pmatrix} 0 & 1.4959 & 0.3162 & 0 \\ 1.4959 & 0 & 0 & 0.3162 \\ 0.3162 & 0 & 0 & 0 \\ 0 & 0.3162 & 0 & 0 \end{pmatrix}$	0.739
Blue response	-0.450Hz	$\begin{pmatrix} -0.5000 & 1.4959 & 0.3162 & 0 \\ 1.4959 & -0.5000 & 0 & 0.3162 \\ 0.3162 & 0 & 0 & 0 \\ 0 & 0.3162 & 0 & 0 \end{pmatrix}$	
Green response	0.450Hz	$\begin{pmatrix} 0.5000 & 1.4959 & 0.3162 & 0 \\ 1.4959 & 0.5000 & 0 & 0.3162 \\ 0.3162 & 0 & 0 & 0 \\ 0 & 0.3162 & 0 & 0 \end{pmatrix}$	

Table 6.2 The corresponding design parameters for centre frequency tuning

6.2.3 Notch Out of Passband

Figure 6.5 shows a special case when the frequencies of bandstop resonators are not in the passband region. The analytical multi-passband synthesis technique cannot produce the response with notch outside the passband. This is because the passband limits are the fundamental values that define the response and the design parameters; in other words, with passband limits given as input, the notch falls within the passband region in default.

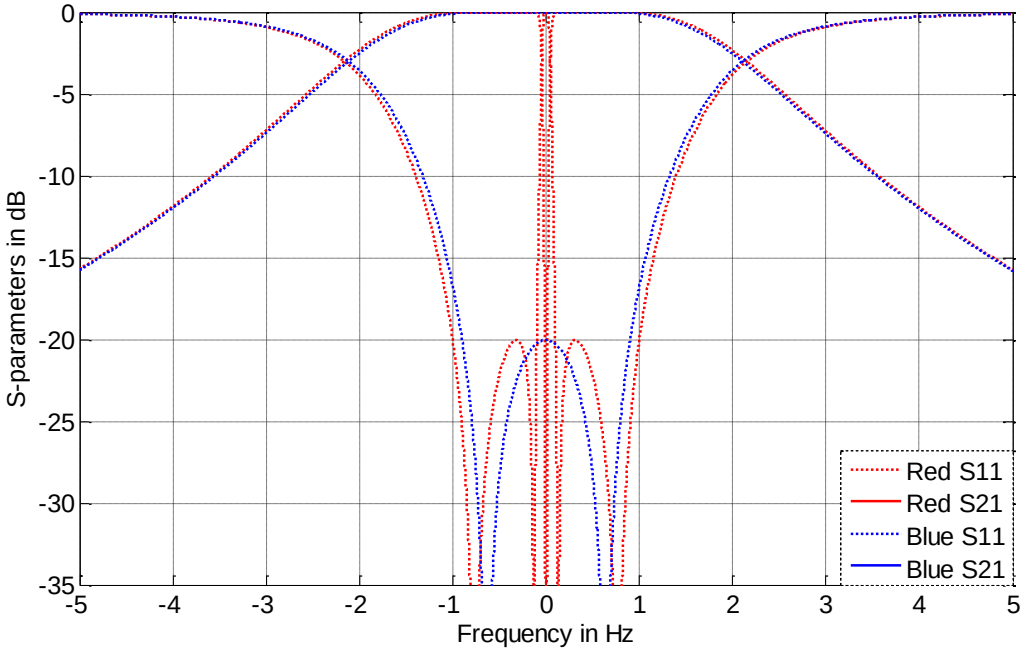

Figure 6.5 Responses with notch in and out of passband

The couplings involved in the tuning are labelled in colour in Table 6.3.

	Passband width	Coupling matrix	External Q-factor
Red response	2.000Hz	$\begin{pmatrix} 0 & 1.4959 & 0.3162 & 0 \\ 1.4959 & 0 & 0 & 0.3162 \\ 0.3162 & 0 & 0 & 0 \\ 0 & 0.3162 & 0 & 0 \end{pmatrix}$	0.739
Blue response	1.800Hz	$\begin{pmatrix} 0 & 1.4959 & 0.3162 & 0 \\ 1.4959 & 0 & 0 & 0.3162 \\ 0.3162 & 0 & -9.0000 & 0 \\ 0 & 0.3162 & 0 & -9.0000 \end{pmatrix}$	

Table 6.3 The corresponding design parameters

When the notch is tuned away from the passband, the passband is hardly affected by the notch. However, the bandstop resonators still create a transmission zero at their resonant frequency and at the same time, a very narrow passband is also introduced near the transmission zeros, which is shown in Figure 6.6 [2].

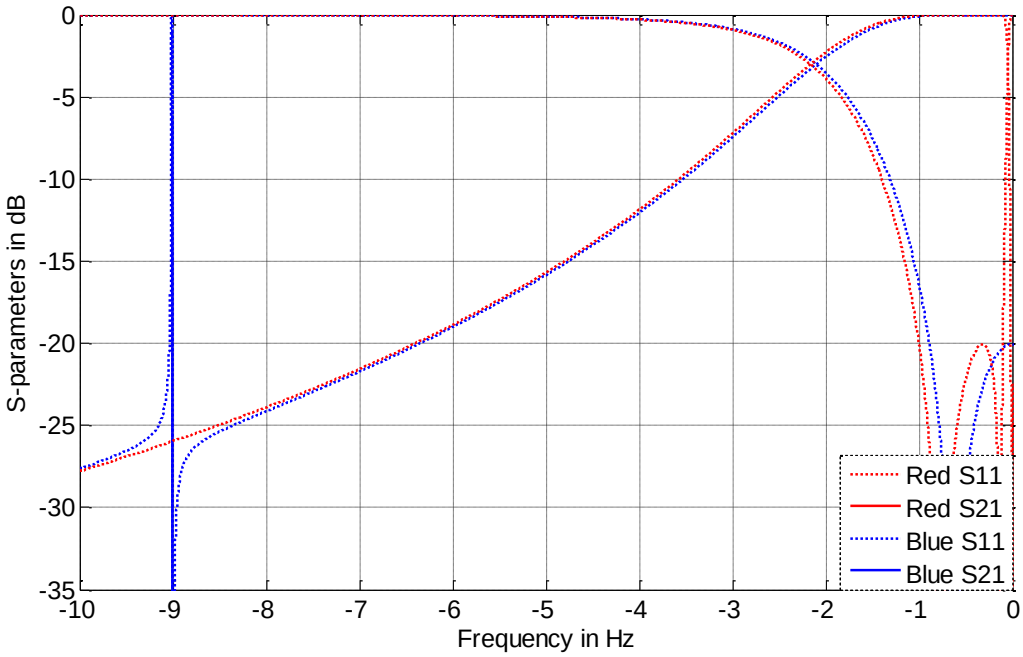

(a)

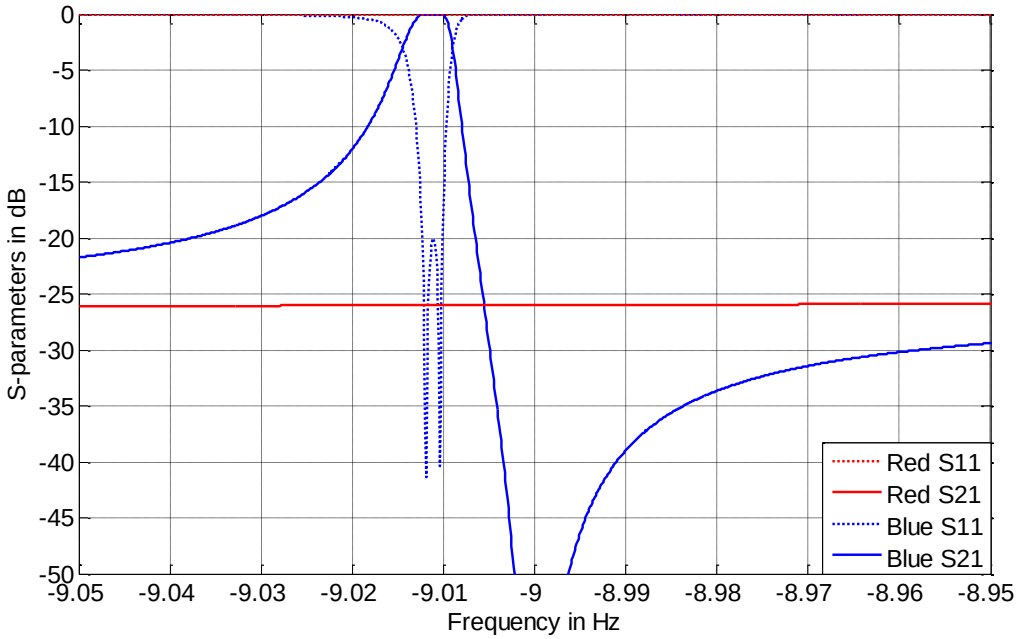

(b)

Figure 6.6 Left part of out-of-band response, (a) same scale with Figure 6.5, (b) an extended view near -9Hz

As long as the notch is tuned away from the passband, it will no longer affect the passband. The main passband of the blue response shown in Figure 6.5 has a 2nd order Chebyshev response with a bandwidth of 1.8Hz. The 0.2Hz difference between two bandwidths is the notch width. This difference can be compensated by adjusting the certain couplings, and is shown in the following section.

6.2.4 Passband Bandwidth Tuning

The green response below in Figure 6.7 is tuned from the blue response shown in Figure 6.5 by adjusting $M_{1,2}$ and external Q-factors. The relevant new coupling matrix for green response is given in Table 6.4. For the reason of comparison, the red response in Figure 6.5 is shown again in Figure 6.7.

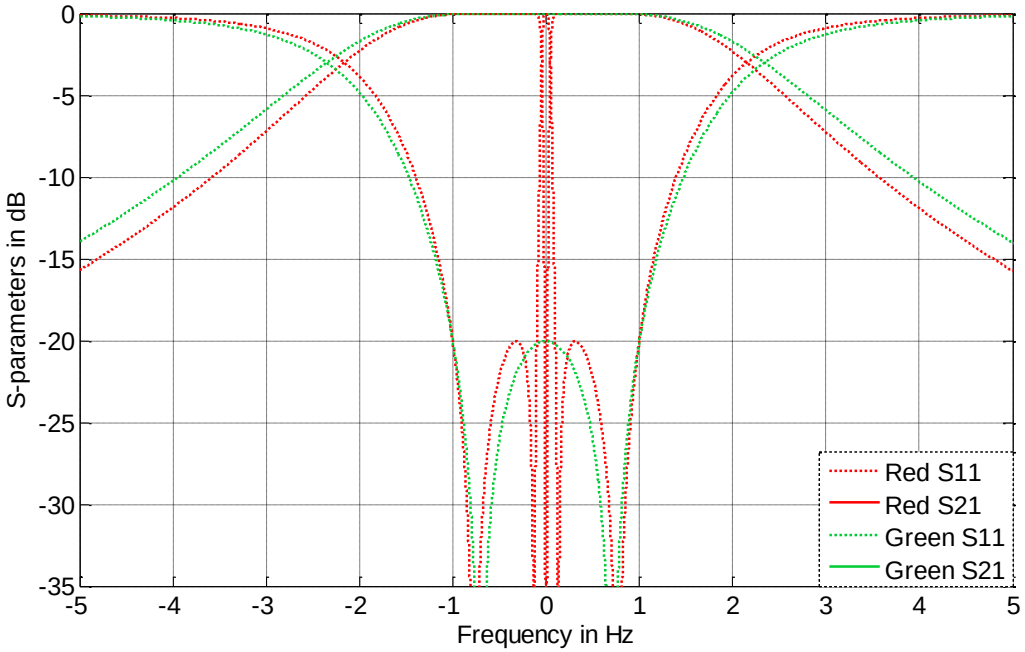

Figure 6.7 Responses with notch in and out of passband (bandwidth compensated)

	Passband bandwidth	**Coupling matrix**	**External *Q*-factor**
Red response	2.000Hz	$\begin{pmatrix} 0 & 1.4959 & 0.3162 & 0 \\ 1.4959 & 0 & 0 & 0.3162 \\ 0.3162 & 0 & 0 & 0 \\ 0 & 0.3162 & 0 & 0 \end{pmatrix}$	0.739
Green response	2.000Hz	$\begin{pmatrix} 0 & 1.6621 & 0.3162 & 0 \\ 1.6621 & 0 & 0 & 0.3162 \\ 0.3162 & 0 & -9.000 & 0 \\ 0 & 0.3162 & 0 & -9.000 \end{pmatrix}$	0.665

Table 6.4 The corresponding design parameters for passband bandwidth tuning

The bandwidth tuning can be achieved by only changing the external Q-factors and $M_{1,2}$. It can be found that, the coupling matrix and external Q-factors are very close to the synthesised values of a standard 2nd order lowpass prototype Chebyshev filter.

6.2.5 Multi-notch Response

The 4th order tunable notch filter can produce two notches by making the two bandstop resonators asynchronously tuned. In such case, each bandstop resonator controls one notch

independently. To give an example, the blue response in Figure 6.8 has two notches placed at -0.3Hz and 0.6Hz, respectively. The corresponding design parameters are given in Table 6.5.

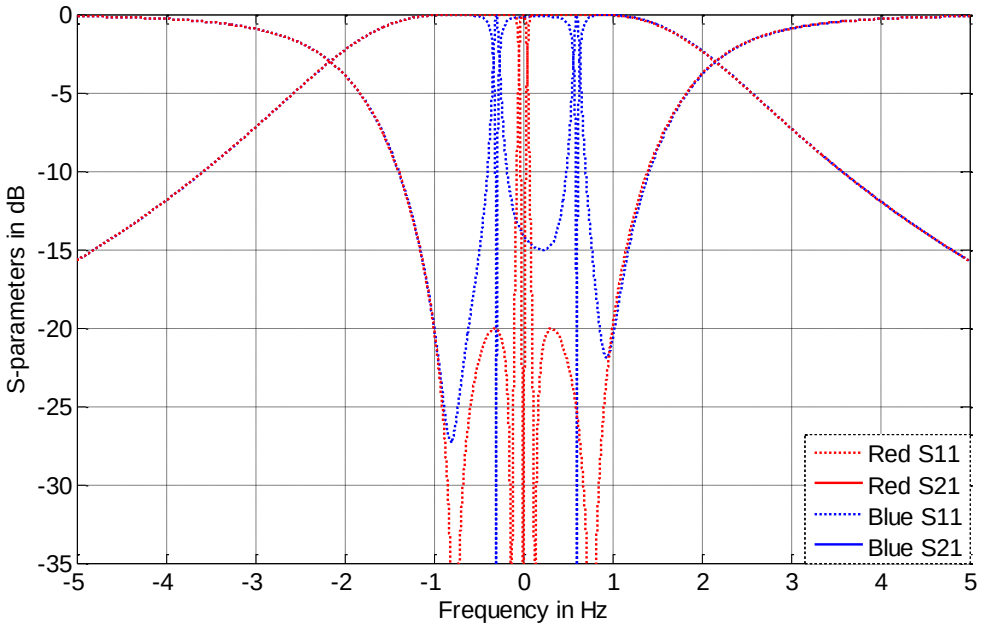

Figure 6.8 Response with split notches

	Notch position	**Coupling matrix**	**External *Q*-factor**
Red response	0Hz	$\begin{pmatrix} 0 & 1.4959 & 0.3162 & 0 \\ 1.4959 & 0 & 0 & 0.3162 \\ 0.3162 & 0 & 0 & 0 \\ 0 & 0.3162 & 0 & 0 \end{pmatrix}$	0.739
Blue response	-0.3Hz, 0.6Hz	$\begin{pmatrix} 0 & 1.4959 & 0.3162 & 0 \\ 1.4959 & 0 & 0 & 0.3162 \\ 0.3162 & 0 & -0.3000 & 0 \\ 0 & 0.3162 & 0 & 0.6000 \end{pmatrix}$ Or $\begin{pmatrix} 0 & 1.4959 & 0.3162 & 0 \\ 1.4959 & 0 & 0 & 0.3162 \\ 0.3162 & 0 & 0.6000 & 0 \\ 0 & 0.3162 & 0 & -0.3000 \end{pmatrix}$	

Table 6.5 The corresponding design parameters for two-notch tuning

In the table above, both coupling matrix are correct for the blue response. Compared with the red response (single notch), the notch width in blue response (two notches) decreases from 0.2Hz to 0.1Hz. The centre frequency and bandwidth are not affected by the notch splitting.

More notches could be introduced if the total order of the filter increases. Theoretically, there could be as many as n notches in a $2n^{th}$ order filter, but it should be noted that, the multi-notch response produced from such technique are not Chebyshev response any more.

6.3 The Implementation of A 4th Order Tunable Notch Filter

A 4th order tunable notch filter is implemented in the form of rectangular waveguide, with the tuning structure proposed in Chapter 5. It is designed to have a frequency tuning range of 810MHz which is from 8.670 to 9.480GHz. The passband bandwidth is tunable between 110MHz and 260MHz. The notch width is 43±3MHz.

6.3.1 The Rectangular Waveguide Structure

The rectangular waveguide realisation of the corresponding topology is given in Figure 6.9; it is an H-plane cross-sectional view showing the lower-half of the filter.

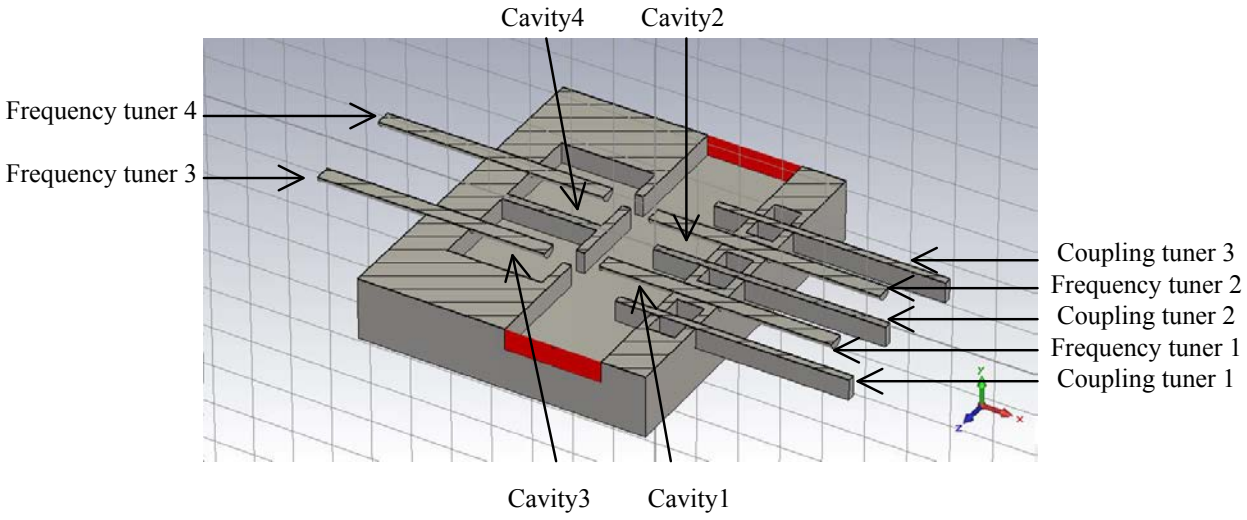

Figure 6.9 H-plane cross-sectional view of the 4th order tunable notch filter (lower-half)

There are four cavities and seven tuners in this filter. Among the four cavities, cavity 1 and 2 act as the two bandpass resonators, while the other two cavities act as two bandstop resonators. Among the seven tuners, coupling tuner 1, 2 and 3 controls the Q_{eS}, $M_{1,2}$ and Q_{eL}, respectively. Frequency tuner 1, 2, 3 and 4 control the frequencies of resonator 1, 2, 3 and 4, respectively. The dimensions of this filter are given in Figure 6.10. The dimensions of tuners and chokes, the gap size between the tuners and the main body is the same as that of the 3rd order tunable bandpass filter given in Chapter 5.

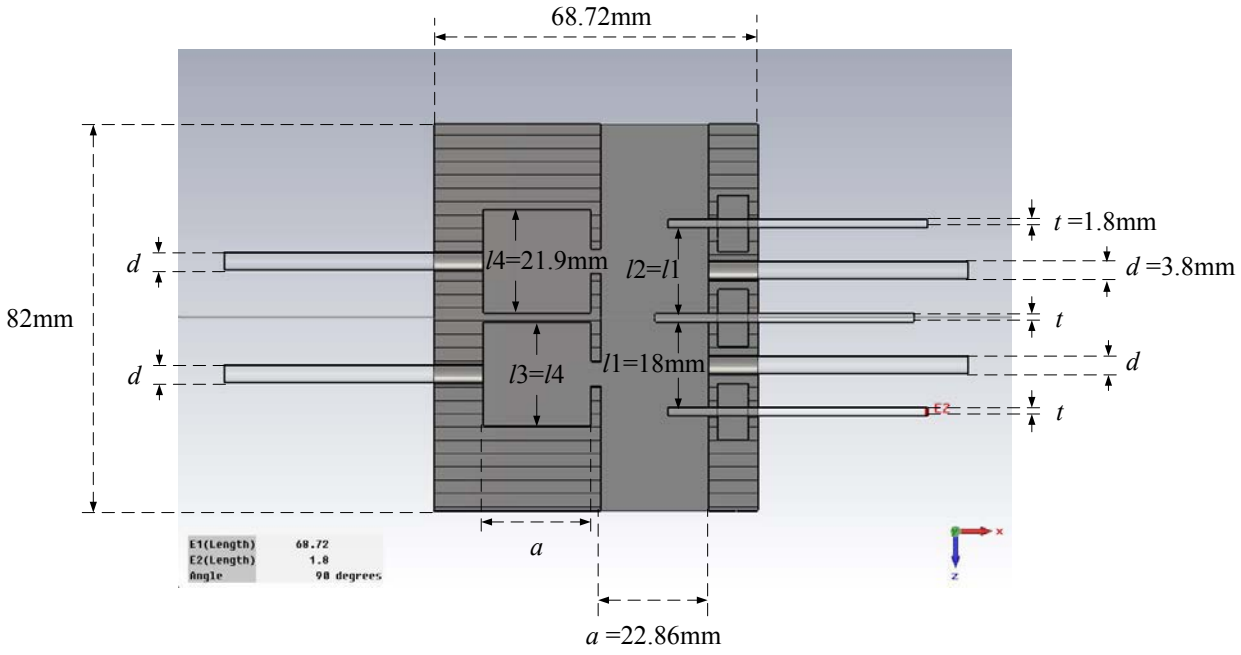

(Top view)

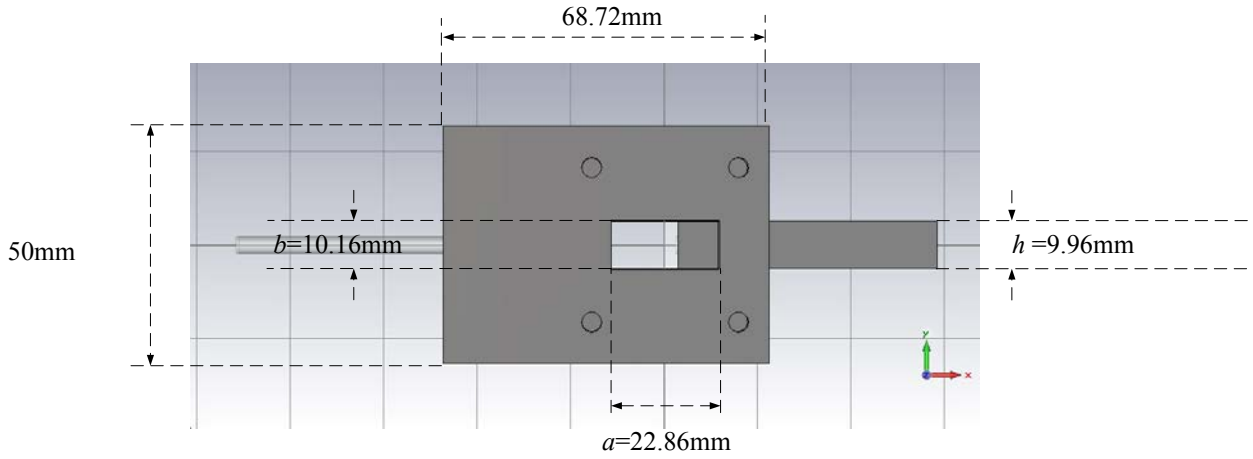

(Side view)

Figure 6.10 The 4th order tunable notch filter dimensions

6.3.2 Fabrication and Measurement

The filter is fabricated by a CNC milling machine. In order to facilitate the milling, the main body of the filter has to be cut through H-plane into two parts. The material used for main body is copper, which has an electrical conductivity of 5.96×10^7 S/m. The tuners are milled separately by the CNC machine. The material used for tuners is brass, which has an electrical conductivity of 2.74×10^7 S/m. The tuners are guided by dielectric polymer bearings. Photographs of the fabricated tunable notch filter are given in Figure 6.11 below.

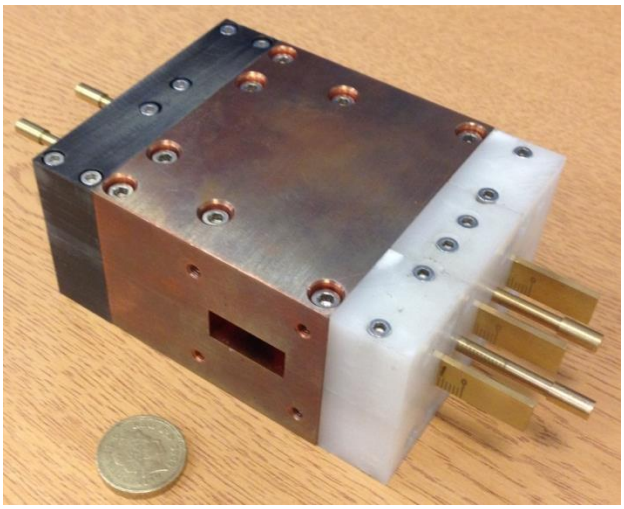

(a)

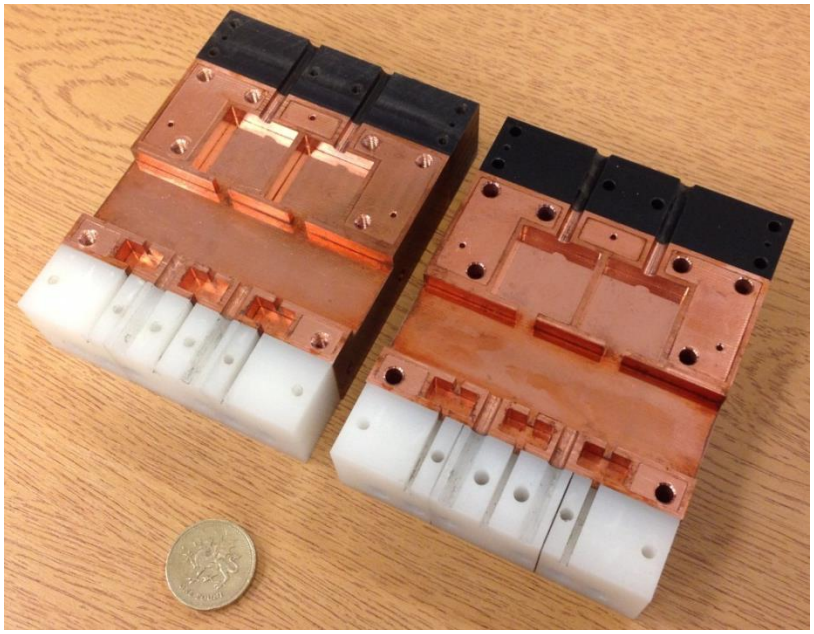

(b)

Figure 6.11 Fabricated rectangular waveguide tunable notch filter, (a) fully assembled filter; (b) disassembled filter main body

Because the filter can achieve continuous tuning, it is not possible to list all the measured results here. Hence, only some selected results are shown to illustrate the performance of the filter. By tuning functions, the results are categorised into five sections, which are centre frequency tuning with notch falling outside passband, centre frequency tuning with a fixed notch, notch position tuning with fixed centre frequency, multi-notch realisation and bandwidth tuning. All the relevant tuning parameters are named and labelled in Figure 6.12.

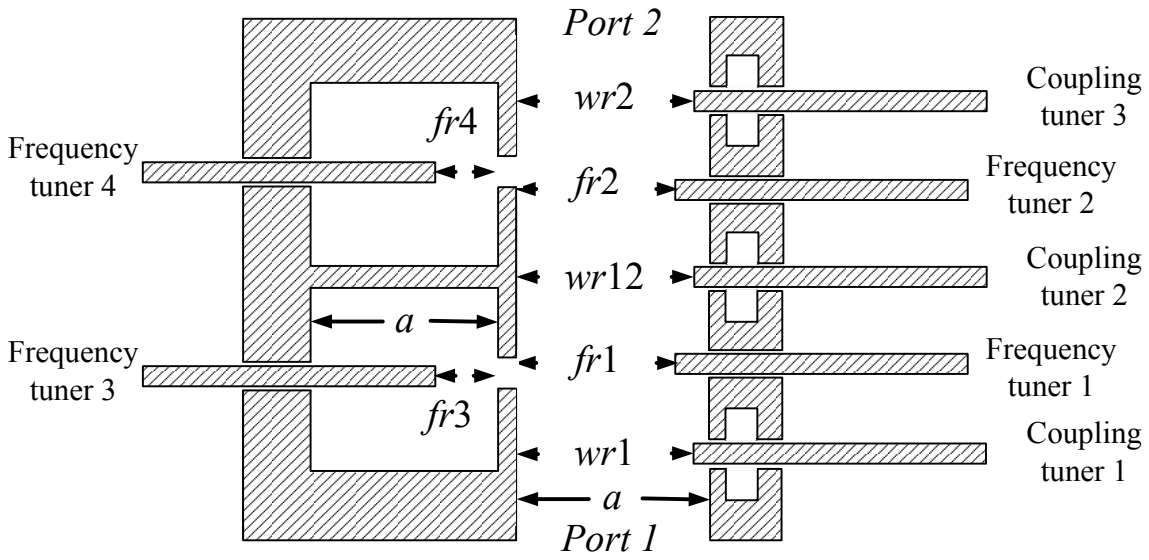

Figure 6.12 Naming of the tuning parameters in tunable notch filter (H-plane cross-sectional view)

6.3.2.1 Passband Centre Frequency Tuning with A Fixed Notch

Four selected responses are presented in different colours and shown in Figure 6.13. During the centre frequency tuning, the bandwidth remains at 255±5MHz, the notch is fixed at 8.807GHz, and only *fr*1 and *fr*2 change. The relevant tuning parameters are given in Table 6.6.

	Passband centre frequency	***wr*1=*wr*2**	***wr*12**	***fr*1= *fr*2**	***fr*3= *fr*4**
Red response	8.709GHz			5.5mm	

Blue response	8.746GHz	15.5mm	12.5mm	7.0mm	5.0mm
Green response	8.829GHz			8.5mm	
Purple response	8.878GHz			9.5mm	

Table 6.6 The corresponding tuning parameters for centre frequency tuning with fixed notch

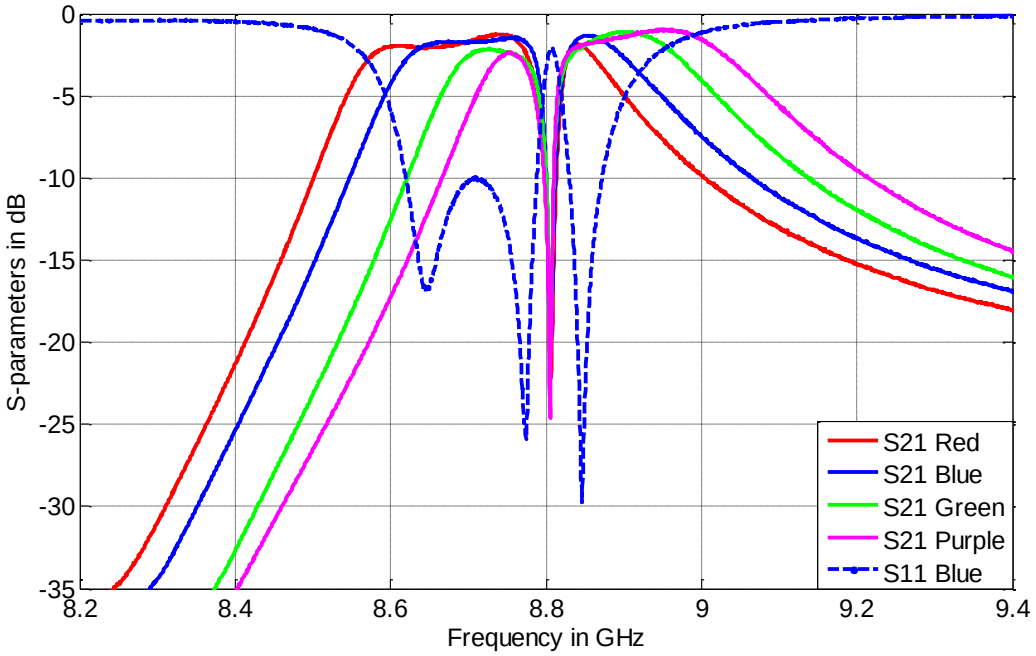

Figure 6.13 Centre frequency tuning with a fixed notch

Four *S*21s with different centre frequencies are shown in the figure above. For clearer view, only the *S*11 for blue response is shown, the other three *S*11s have similar shapes. Because the notch is in the passband, the filter behaves like a 4th order dual-passband filter. The average mid-band insertion loss for these responses is 1.5dB.

6.3.2.2 Passband Tuning with Notch Falling outside The Passband

A set of *S*-parameters are given in Figure 6.14. During the tuning, the bandwidth remains at 115±5MHz, and only *fr*1 and *fr*2 are involved. The relevant tuning parameters are given in Table 6.7

	Passband centre frequency	*wr*1=*wr*2	*wr*12	*fr*1= *fr*2	*fr*3= *fr*4
Red response	9.292GHz	14.0mm	11.0mm	14.0mm	5.0mm
Blue response	9.366GHz			15.0mm	
Green response	9.426GHz			16.0mm	
Purple response	9.480GHz			17.0mm	

Table 6.7 The corresponding parameters for passband tuning with notch falling outside the passband

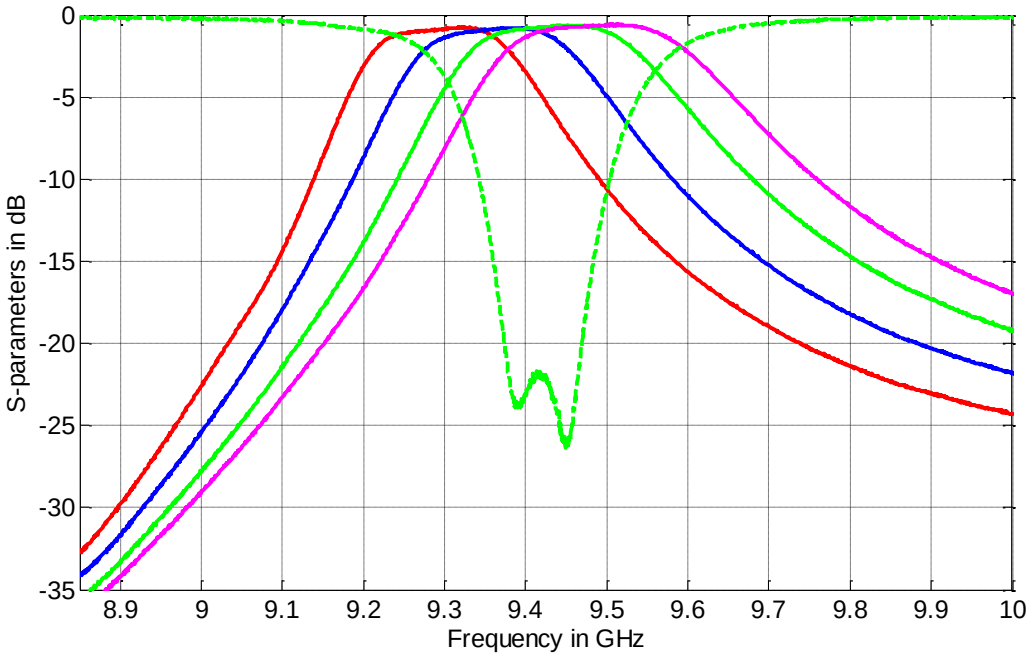

Figure 6.14 Centre frequency tuning with notch falling outside passband

Four *S*21s with different centre frequencies are given; the green *S*11 is given for reference. Because the notch falls outside the passband, there are only two reflection zeros on the passband. The average mid-band insertion loss is 0.9dB.

6.3.2.3 Passband Bandwidth Tuning

Two set of *S*-parameters with different bandwidth are given in Figure 6.15. During the tuning, the centre frequency is kept near 9.21GHz, with *fr*3 and *fr*4 fixed. The notch falls outside the passband. The relevant tuning parameters are given in Table 6.8.

	Passband bandwidth	***wr*1=*wr*2**	***wr*12**	***fr*1= *fr*2**	***fr*3= *fr*4**
Red response	116MHz	14.0mm	11.0mm	13.0mm	5.0mm
Blue response	236MHz	15.5mm	12.5mm	16.0mm	

Table 6.8 The corresponding parameters for passband bandwidth tuning

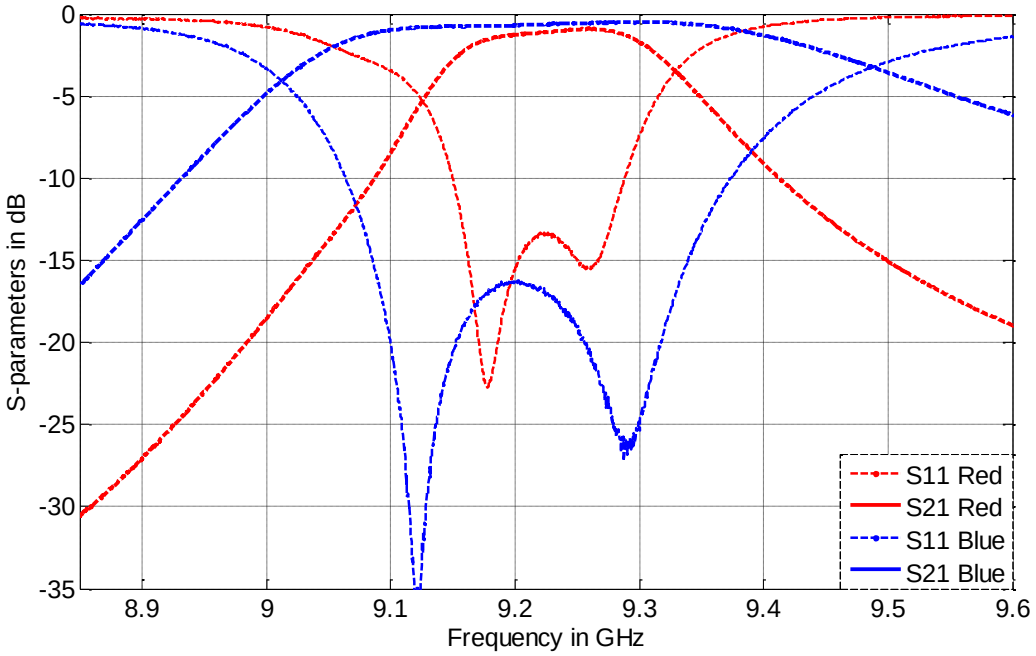

Figure 6.15 Passband bandwidth tuning

The passband bandwidth tuning is realised by tuning the Q_{eS}, Q_{eL} and $M_{1,2}$. This is physically achieved by adjusting the position of the three coupling tuners. *fr*1 and *fr*2 are tuned to compensate the frequency shift caused by the moving of coupling tuners. The average mid-band insertion loss is 0.6dB for blue response and 1.1dB for red response.

6.3.2.4 Notch Position Tuning with Fixed Passband Centre Frequency

Four *S*21s with varying notch positions are given in Figure 6.16. They have same bandwidth, which is 255MHz. The notch position tuning only involves *fr*3 and *fr*4. The relevant tuning parameters are given in Table 6.9.

	Notch position	***wr*1=*wr*2**	***wr*12**	***fr*1= *fr*2**	***fr*3= *fr*4**
Red response	9.061GHz	15.5mm	12.5mm	15.0mm	12.0mm
Green response	9.154GHz				13.0mm
Blue response	9.234GHz				14.0mm
Purple response	9.310GHz				15.0mm

Table 6.9 The corresponding parameters for notch tuning with fixed centre frequency

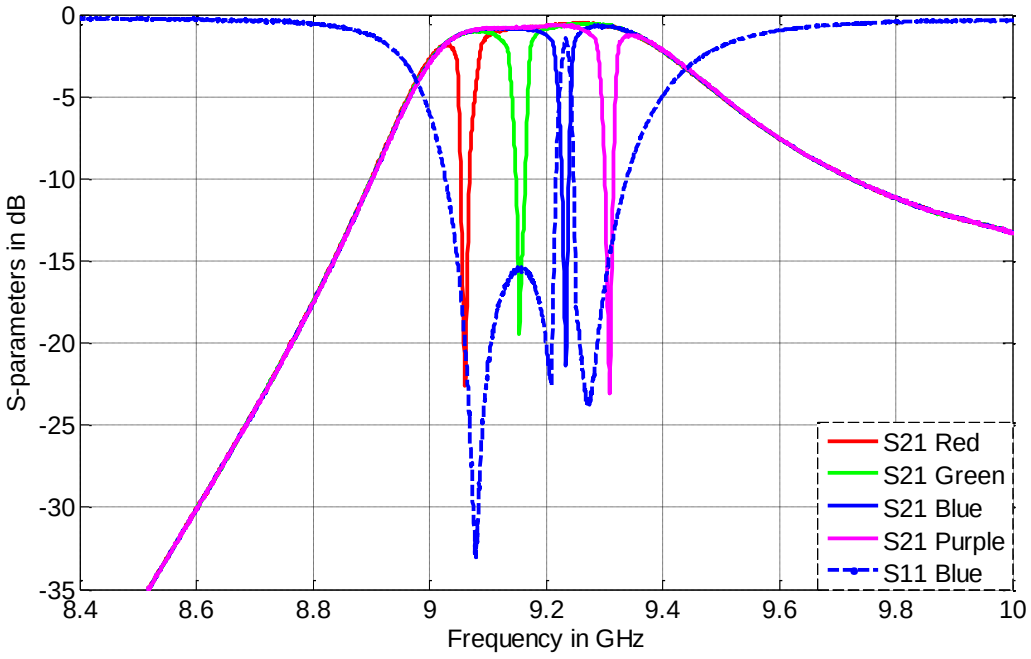

Figure 6.16 Notch position tuning with fixed centre frequency

During the tuning, the centre frequency and bandwidth do not change. The average mid-band insertion loss is 0.8dB.

6.3.2.5 Multi-Notch Realisation

Two set of *S*-parameters are given in Figure 6.17. As the frequencies of two bandstop resonators are tuned away from each other, the single notch splits into two separate ones. The two notches are individually controlled by *fr*3 and *fr*4. The centre frequency and bandwidth remain unchanged during the tuning. The relevant parameters are given in Table 6.10.

	Notch position(s)	***wr*1=*wr*2**	***wr*12**	***fr*1= *fr*2**	***fr*3**	***fr*4**
Red response	8.946GHz	15.5mm	12.0mm	10.0mm	10.5mm	
Blue response	8.902GHz & 8.985GHz				10.0mm	11.0mm

Table 6.10 The corresponding parameters for multi-notch realisation

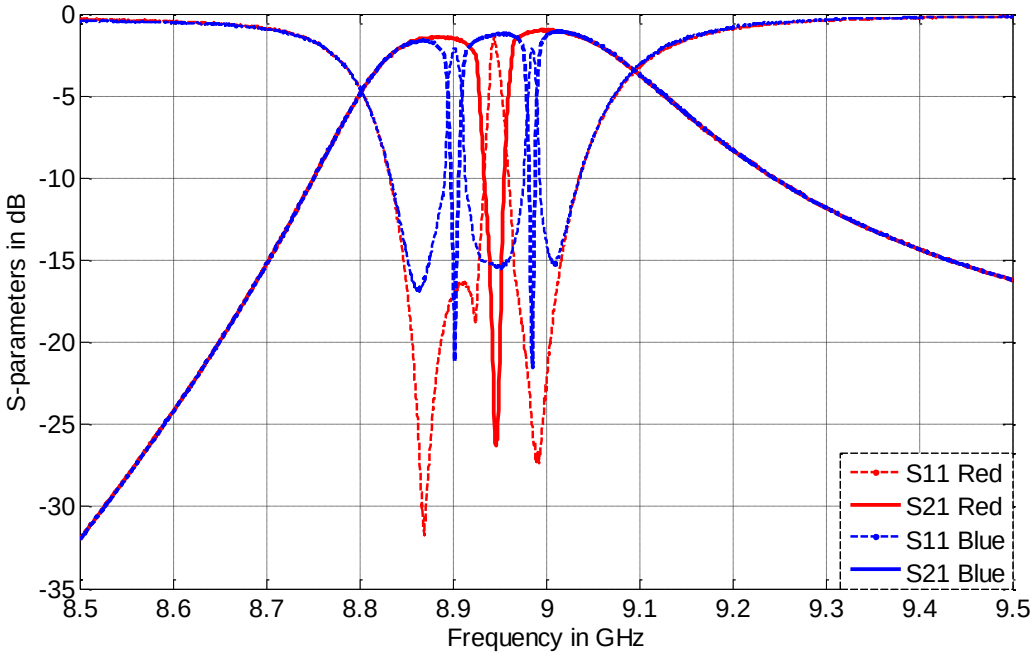

Figure 6.17 Multi-notch realisation

For the red response with single notch, the notch width is 40MHz; for the blue response, the two notches each have a width of 20MHz. The mid-band insertion loss is 1.5dB. The measured result confirms that, the total width of the two split notches is equal to the width of the single notch.

Reference:

1. *Hong, J.-S. and M.J. Lancaster, Microstrip Filters for RF/Microwave Applications 2001: John Wiley and Sons Ltd, United Kingdom.*
2. *Huang, F.,* "Dual-Band Superconducting Spiral Filters Including Narrow Bandstop Notches". *IEEE TRANSACTION ON MICROWAVE THEORY AND TECHNIQUES , 2009.* ***57****(5): p. 8.*

CHAPTER 7 CONCLUSION AND FUTURE WORK

7.1 Conclusion

The thesis investigates the design techniques of multi-passband filters and tunable filters. Both of them become more and more important in nowadays wireless communication industry, as they not only satisfy multi-functional applications, but also reduce the size and mass of the communication system.

A generalised analytical synthesis technique for multi-passband filter has been presented in Chapter 3. Starting with inline topologies, the generalised synthesis technique manages to produce multi-passband filters with Chebyshev response; examples of dual-passband, triple-passband and five-passband filters are presented. In order to increase the frequency selectivity, a topology with cross coupling is investigated; the design example of a 20^{th} order five-passband filter with quasi-elliptic response is presented. The lowpass to multi-passband frequency transformation is the key in the synthesis procedure. If the de-normalised response has M passbands, there will be in total M pairs of interim parameters ω_{oi}, b_i (i=1,2,…,M), which define the frequency transformation. The synthesis technique offer a way to analytically derive these M pairs of interim parameters directly from M pairs of passband limits ω_{Li}, ω_{Hi} (i=1,2,…,M). As long as the passband limits are known, the frequency transformation is determined. Physically, the lowpass to multi-passband frequency transformation is realised by the so called multi-passband resonator sections. Once the lowpass prototype is determined, each individual passband shape of the multi-passband filter is determined. Besides S-parameters, this synthesis technique also gives analytical solutions of the design parameters, including the coupling matrix and external Q-factors. They can be

analytically derived once the passband specification and the lowpass prototype are given. The synthesis details, relevant equations and expressions are presented in Chapter 3.

Following the synthesis technique, the implementations of the multi-passband filter are presented in Chapter 4. Two selected filter design examples are implemented in the form of rectangular waveguide. They are the 10^{th} order five-passband filter with Chebyshev response and the 20^{th} order five-passband filter with quasi-elliptic response. One thing that should be bear in mind is that, this synthesis technique is not limited to rectangular waveguide, but applies to all kinds of coupled resonator circuits. In Chapter 4, the fundamental knowledge and design technique of rectangular waveguide circuit are reviewed first; the relationships between rectangular waveguide circuit components (cavity resonator and iris) and the design parameters are given. A set of coupling matrix and external Q-factors can be interpreted into the topology of rectangular waveguide circuit. The individually obtained dimensions of each component are used as the initial value, and further overall structure optimisation is employed to match the desired filter specifications more accurately. Both the implementations of the 10^{th} order filter and the 20^{th} order filter follow this procedure. In general, the measured S-parameters show good agreements with the simulated ones.

Tunable bandpass filters are investigated in Chapter 5. A new coupling tuning structure based on rectangular waveguide is presented. In order to realise the tuning in the coupling coefficient, it physically changes the dimensions of the discontinuities between two adjacent cavity resonators in a rectangular waveguide filter. It can also be used for tuning the external Q-factors. However, due to the gap between the coupling tuner and the filter main body, radiation loss becomes an issue which reduces the unloaded Q-factor, and causes high insertion loss. To solve this problem, chokes are introduced. It increases the unloaded Q-factor by 10^3 times compared to the situation without chokes. The value of radiation Q-factor for a tunable resonator with chokes is therefore above 10^6. A 3^{rd} order fully tunable bandpass

filter is presented at the end of this chapter. The measured results show good agreements with the simulated ones. The filter has its maximum bandwidth tuning range at 9.5GHz, the corresponding *FBW* changes from 0.9% to 3.8%. Besides, it also offers a 400MHz tuning range for centre frequency, when the couplings are fixed.

The design of tunable notch filter is presented in Chapter 6. The topology of the tunable notch filter is based on the dual-passband filter topology. For such a topology, the frequencies of bandstop resonators control the position of the notch, and the frequencies of bandpass resonators control the centre frequency of the passband. Each tuning parameter in this filter controls one kind of filter specification. This feature makes the filter easy to tune. A 4^{th} order tunable notch filter is given as an example to illustrate the design. It achieves tuning flexibilities in centre frequency, notch position and passband width. The filter is successfully implemented in rectangular waveguide.

7.2 Future work

At current stage, the generalised synthesis technique for multi-passband filter is a pure analytical approach. This means though the results can be efficiently obtained from the relevant expressions, they have to follow certain rules. For example, the multi-passband filter obtained from the analytical synthesis technique has the same in-band and out-of-band response for every passband. It is not possible to make passband 1 having a 2^{nd} order Chebyshev response, while making passband 2 having a 4^{th} order quasi-elliptic response. However, such case might be solved by combining the analytical approach with optimisation methods. Such hybrid algorithm may use the analytical synthesis technique to obtain a set of good starting values and then use certain optimisation method to get a more flexible solution. Besides, the matrix rotation and reduction technique may also be combined with the current analytical synthesis technique, as for some cases, the synthesised filter topologies might be difficult to realise in real circuit.

Since the tunable filters are currently tuned by hand, the accuracy is limited. This can be improved by integrating step motor driving system, which offers more precisely control of tuners. Furthermore, based on such driving system, it might be possible to control the filter through a programmable chip. By uploading the measured results and the corresponding tuning parameters into the chip in advance, the filter may tune itself automatically once the desired specifications are provided.

Appendix I: Quasi-Elliptic Response Obtained by Coupling Matrix Optimisation

The quasi-elliptic response discussed here is produced by a cascade quadruplet (CQ) structure which has 4 resonators. The topology is given in Figure I.1. The dashed line stands for cross coupling between resonator 1 and 4, while the solid lines stand for the direct couplings. Resonator 1 and 4 connect to the two ports.

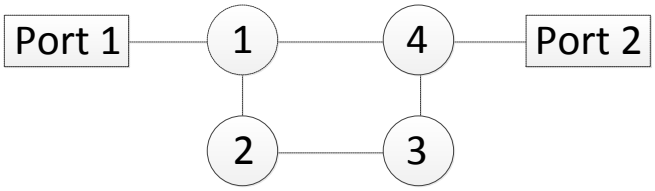

Figure I.1 The topology of the CQ structure

1. The flowchart of coupling matrix optimisation

In order to give a straight forward explanation on coupling matrix optimisation, a flowchart that describes the full optimisation process is given below in Figure I.2. Generally, there are two key elements in this optimisation method. They are the starting values and the cost function. Given the starting values, the coupling matrix [M] and external Q-factor Q_e can be initialised. The cost function (CF) is evaluated within every iteration. As long as CF satisfies the pre-set stopping conditions, the optimisation stops. If CF manages to converge before reaching the maximum iteration times, the valid result is obtained. This optimisation method is programmable in MATLAB. The algorithm is based on the default MATLAB function *fmincon*, which is a powerful tool for searching local optimum.

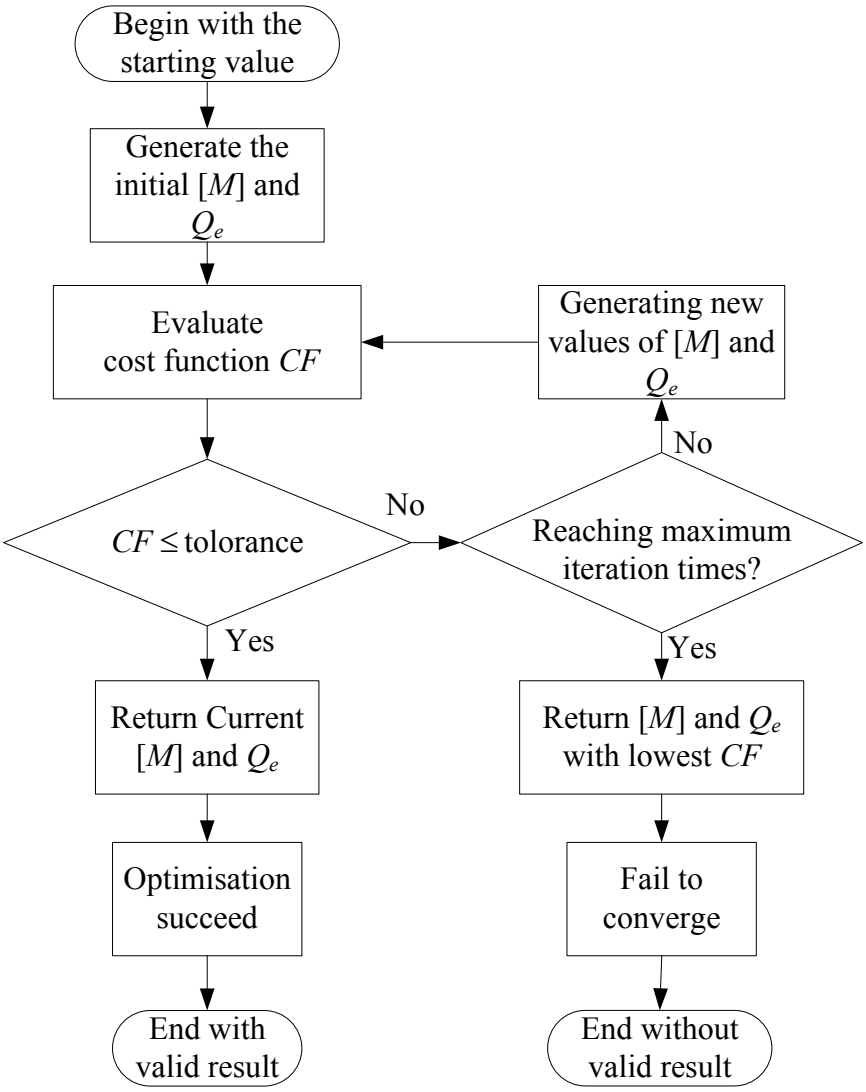

Figure I.2 The flowchart of coupling matrix optimisation method

2. Starting values and Cost function

Optimisation can produce good solutions which meet general design specifications in most cases. From the technical perspective, the optimisation can be categorised into two types, which are global optimisation and local optimisation. Both use specific algorithms to get the desired solution. Usually, the local optimisation is faster, but may only work well when good starting values are given; otherwise, the optimal solution may not be found. The global optimisation is more useful when good starting values are not known; but it may take longer time to find the solution.

Since the optimisation method used here is local optimisation, for the same optimisation algorithm, two different sets of starting value may lead to two completely different results. Therefore, a good set of starting value is critical to the optimisation. Here, the [M] and Q_e of the standard 4th order lowpass prototype Chebyshev filter are used as the starting value. They are sufficient for the optimisation algorithm to find the optimal solution. The 4th order lowpass prototype quasi-elliptic response given in Figure I.3 is an example that obtained from such starting values.

Cost function is introduced to quantify the error between the result in current iteration and the expected goal. Sampling points are the positions where the error is measured. In this case, there are in total 11 sampling points. They are marked in Figure I.3. The 5 red inverted triangles in the middle mark the 3 reflection poles (*RP*s) and the 2 band limits (*BL*s). The 4 red triangles at the bottom mark the 4 reflection zeros (*RZ*s). The 2 green squares at the bottom mark the 2 transmission zeros (*TZ*s).

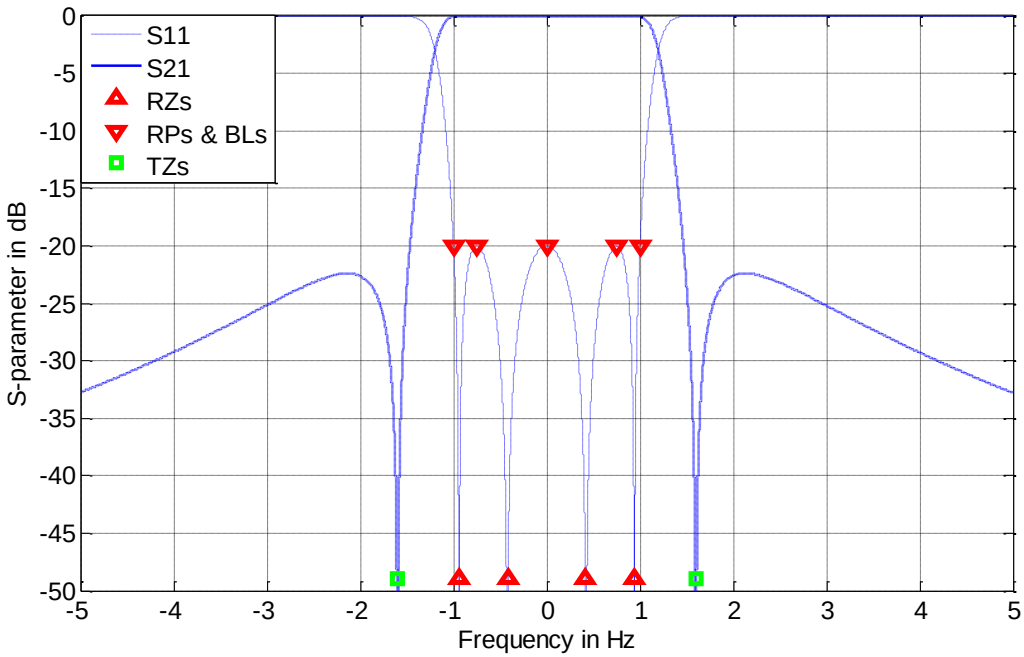

Figure I.3 A lowpass prototype quasi-elliptic response and sampling points for cost function

The cost function *CF* is given as,

$$CF = \sum_{i=1}^{n} RZw_i \left|S_{11}(\Omega_{RZi})\right| + \sum_{i=1}^{2} BLw_i \left|\left|S_{11}(\Omega_{BLi})\right| - RL\right| + \sum_{i=1}^{n-1} RPw_i \left|\left|S_{11}(\Omega_{RPi})\right| - RL\right| + \sum_{i=1}^{2} TZw_i \left|S_{21}(\Omega_{TZi})\right| \tag{I-1}$$

where the RZw_i, BLw_i, RPw_i and TZw_i are the weights of each term; Ω_{RZi}, Ω_{BLi}, Ω_{RPi} and Ω_{TZi} are the positions of the sampling points; *n* is the order of the filter; *RL* is the return loss level.

The optimisation is implemented in MATLAB, and for convenience, only the final results are given. The four *RZ*s are placed at ±0.9397, ±0.4226; the two *TZ*s are placed at ±1.6; the three *RP*s are at 0, ±0.7457; the two *BL*s are at ±1; the *n* is 4; the *RL* is 20dB. The optimised coupling matrix and external *Q*-factors for the 4th order lowpass prototype quasi-elliptic filter are given in (I-2),

$$[M] = \begin{pmatrix} 0 & 0.8306 & 0 & -0.2963 \\ 0.8306 & 0 & 0.8145 & 0 \\ 0 & 0.8145 & 0 & 0.8306 \\ -0.2963 & 0 & 0.8306 & 0 \end{pmatrix}, \tag{I-2}$$

$$Q_{eS} = Q_{eL} = 0.9670$$

Appendix II: Topology Selection for Tunable Notch Filter

It is not possible to investigate all multi-passband filters one by one; however, the filters with the same type of multi-passband resonator section share similar characteristics. Therefore, only selected examples are discussed here. In order to figure out what topologies are more suitable to be used in tunable notch filters design, some comparisons and discussions are given.

Two 6^{th} order triple-passband topologies are used here as the representatives. They represent two types of filters; one is with parallel coupled resonator sections, the other one is with non-parallel coupled resonator sections. The two filters have different characteristics, and their characteristics apply to the two types of filters they represent.

The tunable notch filters achieve flexibility in three aspects, which are notch positions tuning, centre frequency tuning and bandwidth tuning. The discussion on topology selection is based on a comparative approach. It figures out how much affection will be made to the design parameters (coupling matrix and external Q-factors) of each filter, if the filter specifications change. A reference example is given first in Section 1, together with the relevant filter specifications and design parameters, which will be used as are reference to compare with other examples. With different filter specifications, we can have different design parameters and responses which correspond to the specification. The comparisons show the changes in the corresponding design parameters. The synthesis method used here is the analytical synthesis method proposed in Chapter 3.

1. The Reference Example

Below are the topologies of the two 6^{th} order tunable notch filters; both produce triple-passband responses. All couplings and resonator frequencies are tunable.

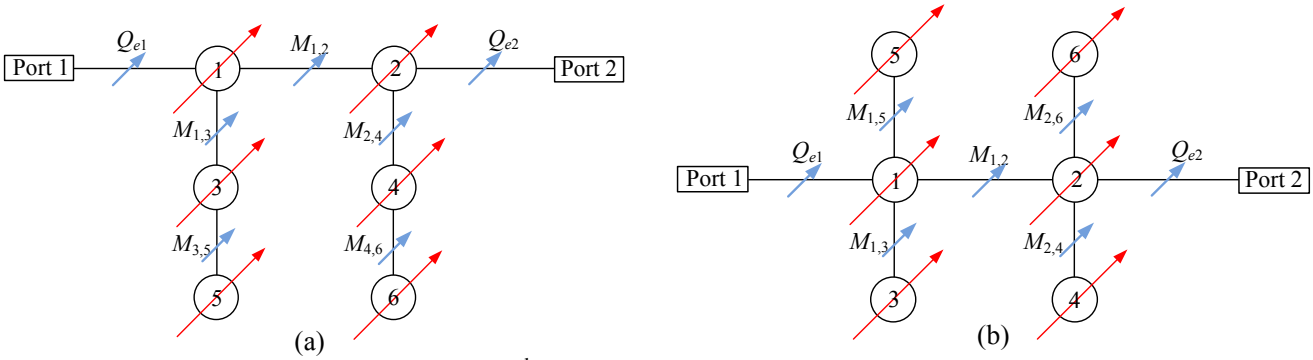

Figure II.1 The topologies of two 6th order tunable notch filters. (a) based on series coupled resonator section, (b) based on parallel coupled resonator section

The one shown in Figure II.1(a) is formed of series coupled resonator sections, while the right one is built up by parallel coupled resonator sections. The red arrows indicate the tuning abilities in resonator frequencies while the blue arrows mean the tuning abilities in couplings. The reference response is given in Figure II.2, which has two notches evenly placed on the passband. With the same filter specifications, both filters can generate this response, but the relevant design parameters are different.

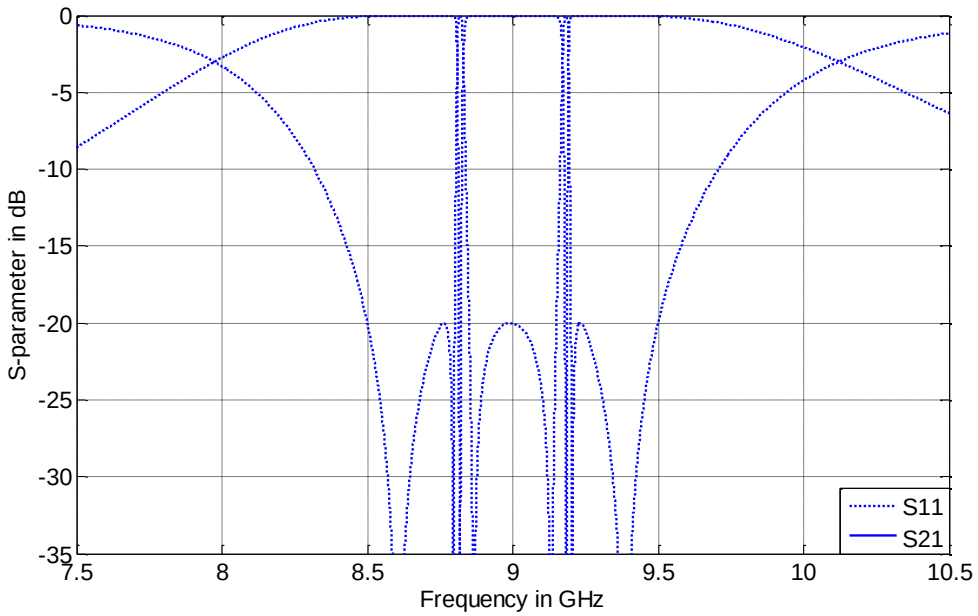

Figure II.2 The reference response

The filter specifications and corresponding design parameters are given in Table II.1. The two filters share the same specifications, but have different design parameters.

<table>
<tr><th colspan="8">Filter specifications</th></tr>
<tr><td colspan="6">Centre frequency</td><td>Notch positions</td><td>Passband width</td></tr>
<tr><td colspan="6">9.00GHz</td><td>8.83GHz, 9.17GHz</td><td>1GHz</td></tr>
<tr><th colspan="8">Design parameters (filter with series coupled sections)</th></tr>
<tr><td colspan="6">Coupling matrix</td><td>External Q-factor</td><td>Resonator frequency</td></tr>
<tr><td colspan="6">$\begin{pmatrix} -0.0033 & 0.1665 & 0.0327 & 0 & 0 & 0 \\ 0.1665 & -0.0033 & 0 & 0.0327 & 0 & 0 \\ 0.0327 & 0 & -0.0018 & 0 & 0.0405 & 0 \\ 0 & 0.0327 & 0 & -0.0018 & 0 & 0.0405 \\ 0 & 0 & 0.0405 & 0 & 0.0012 & 0 \\ 0 & 0 & 0 & 0.0405 & 0 & 0.0012 \end{pmatrix}$</td><td>6.637</td><td>1&2: 8.99GHz
3&4: 8.99GHz
5&6: 9.01GHz</td></tr>
<tr><th colspan="8">Design parameters (filter with parallel coupled sections)</th></tr>
<tr><td colspan="6">Coupling matrix</td><td>External Q-factor</td><td>Resonator frequency</td></tr>
<tr><td colspan="6">$\begin{pmatrix} -0.0033 & 0.1665 & 0.0236 & 0 & 0.0227 & 0 \\ 0.1665 & -0.0033 & 0 & 0.0236 & 0 & 0.0227 \\ 0.0236 & 0 & -0.0409 & 0 & 0 & 0 \\ 0 & 0.0236 & 0 & -0.0409 & 0 & 0 \\ 0.0227 & 0 & 0 & 0 & 0.0403 & 0 \\ 0 & 0.0227 & 0 & 0 & 0 & 0.0403 \end{pmatrix}$</td><td>6.637</td><td>1&2: 8.99GHz
3&4: 8.83GHz
5&6: 9.17GHz</td></tr>
</table>

Table II.1 The filter specifications and design parameters of the reference response shown in Figure II.2

From the table above, it can be found that for the filter with parallel coupled resonator sections, its notch positions are directly determined by the frequencies of the bandstop resonators (resonator 3&4, 5&6); but this feature does not apply to the filter with series coupled resonator sections.

2. Notch Position Tuning

The notch position tuning is discussed in this section. Only the notch positions are tuned, while all other filter specifications remain the same as the reference example shown in Section 1. Four examples are given; all of them are compared with the reference given in Section 1. The changes in design parameters are labelled in blue, if the change is smaller than 10%; it is labelled in red, if the change is more than 10%.

2.1 *Example 1: Only one notch tuned*

In this example, only one notch is tuned from its original position, the other one remains unchanged. Figure II.3 shows the response. The relevant filter specifications and design parameters are given in Table II.2.

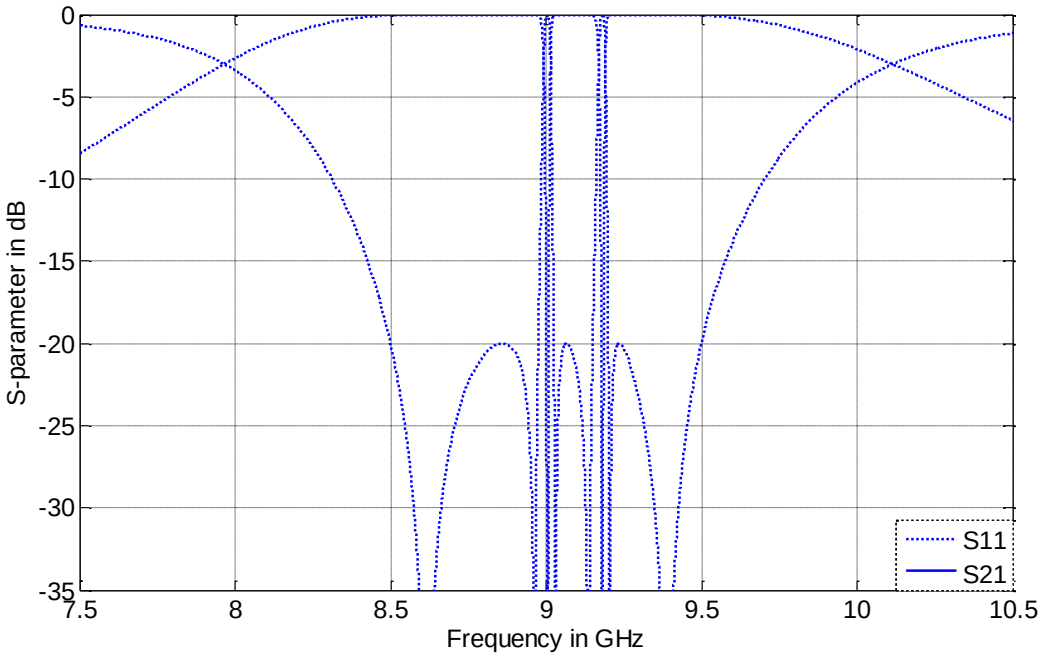

Figure II.3 The response of the 6th order tunable notch filter for example 1

Filter specifications		
Centre frequency	Notch positions	Passband width
9.00GHz	9.00GHz, 9.17GHz	1GHz

Design parameters (filter with series coupled sections)								
Coupling matrix							External Q-factor	Resonator frequency
$\begin{pmatrix} -0.0033 & 0.1665 & 0.0336 & 0 & 0 & 0 \\ 0.1665 & -0.0033 & 0 & 0.0336 & 0 & 0 \\ 0.0336 & 0 & 0.0199 & 0 & 0.0195 & 0 \\ 0 & 0.0336 & 0 & 0.0199 & 0 & 0.0195 \\ 0 & 0 & 0.0195 & 0 & 0.0210 & 0 \\ 0 & 0 & 0 & 0.0195 & 0 & 0.0210 \end{pmatrix}$							6.637	1&2: 8.99GHz 3&4: 9.09GHz 5&6: 9.10GHz
Design parameters (filter with parallel coupled sections)								
Coupling matrix							External Q-factor	Resonator frequency
$\begin{pmatrix} -0.0033 & 0.1665 & 0.0241 & 0 & 0.0234 & 0 \\ 0.1665 & -0.0033 & 0 & 0.0241 & 0 & 0.0234 \\ 0.0241 & 0 & 0.0010 & 0 & 0 & 0 \\ 0 & 0.0241 & 0 & 0.0010 & 0 & 0 \\ 0.0234 & 0 & 0 & 0 & 0.0403 & 0 \\ 0 & 0.0234 & 0 & 0 & 0 & 0.0403 \end{pmatrix}$							6.637	1&2: 8.99GHz 3&4: 9.00GHz 5&6: 9.17GHz

Table II.2 The filter specifications and design parameters of the response for example 1

2.2 *Example 2: Two notches close to passband centre*

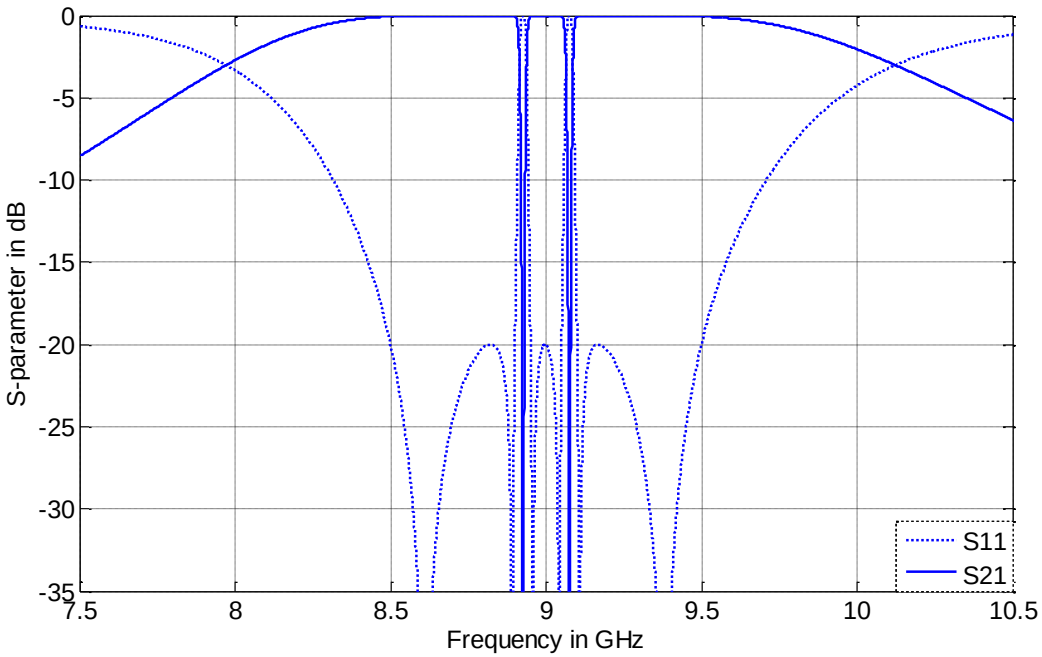

Figure II.4 The response of the 6th order tunable notch filter for example 2

Filter specifications		
Centre frequency	Notch positions	Passband width
9.00GHz	8.93GHz, 9.07GHz	1GHz
Design parameters (filter with series coupled sections)		
Coupling matrix	External Q-factor	Resonator frequency
$\begin{pmatrix} -0.0033 & 0.1665 & 0.0348 & 0 & 0 & 0 \\ 0.1665 & -0.0033 & 0 & 0.0348 & 0 & 0 \\ 0.0348 & 0 & 0.0000 & 0 & 0.0166 & 0 \\ 0 & 0.0348 & 0 & 0.0000 & 0 & 0.0166 \\ 0 & 0 & 0.0166 & 0 & 0.0002 & 0 \\ 0 & 0 & 0 & 0.0166 & 0 & 0.0002 \end{pmatrix}$	6.637	1&2: 8.99GHz 3&4: 9.00GHz 5&6: 9.00GHz
Design parameters (filter with parallel coupled sections)		
Coupling matrix	External Q-factor	Resonator frequency
$\begin{pmatrix} -0.0033 & 0.1665 & 0.0247 & 0 & 0.0245 & 0 \\ 0.1665 & -0.0033 & 0 & 0.0247 & 0 & 0.0245 \\ 0.0247 & 0 & -0.0165 & 0 & 0 & 0 \\ 0 & 0.0247 & 0 & -0.0165 & 0 & 0 \\ 0.0245 & 0 & 0 & 0 & 0.0166 & 0 \\ 0 & 0.0245 & 0 & 0 & 0 & 0.0166 \end{pmatrix}$	6.637	1&2: 8.99GHz 3&4: 8.93GHz 5&6: 9.07GHz

Table II.3 The filter specifications and design parameters of the response for example 2

2.3 *Example 3: Two notches close to passband edge*

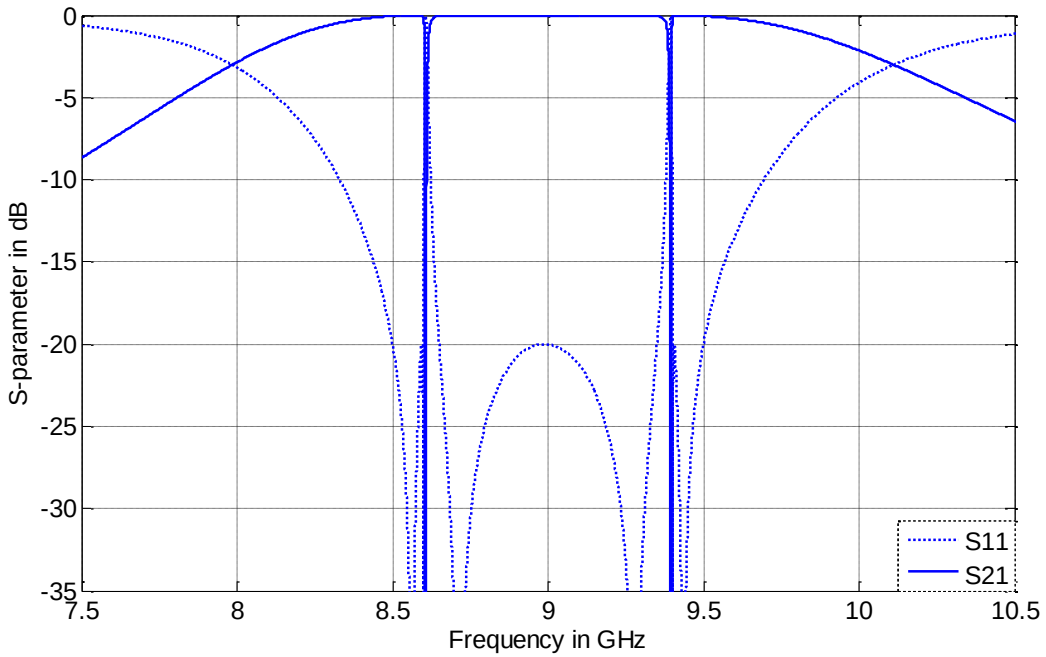

Figure II.5 The response of the 6th order tunable notch filter for example 3

Filter specifications								
Centre frequency							Notch positions	Passband width
9.00GHz							8.63GHz, 9.37GHz	1GHz
Design parameters (filter with series coupled sections)								
Coupling matrix							External Q-factor	Resonator frequency
–0.0033	0.1665	0.0217	0	0	0		6.637	1&2: 8.99GHz
0.1665	–0.0033	0	0.0217	0	0			
0.0217	0	–0.0095	0	0.0874	0			3&4: 8.96GHz
0	0.0217	0	–0.0095	0	0.0874			
0	0	0.0874	0	0.0057	0			5&6: 9.03GHz
0	0	0	0.0874	0	0.0057			
Design parameters (filter with parallel coupled sections)								
Coupling matrix							External Q-factor	Resonator frequency
–0.0033	0.1665	0.0216	0	0.0204	0		6.637	1&2: 8.99GHz
0.1665	–0.0033	0	0.0216	0	0.0204			
0.0216	0	–0.0896	0	0	0			3&4: 8.63GHz
0	0.0216	0	–0.0896	0	0			
0.0204	0	0	0	0.0859	0			5&6: 9.37GHz
0	0.0204	0	0	0	0.0859			

Table II.4 The filter specifications and design parameters of the response for example 3

2.4 *Example 4: Two notches close to passband edge at the same side*

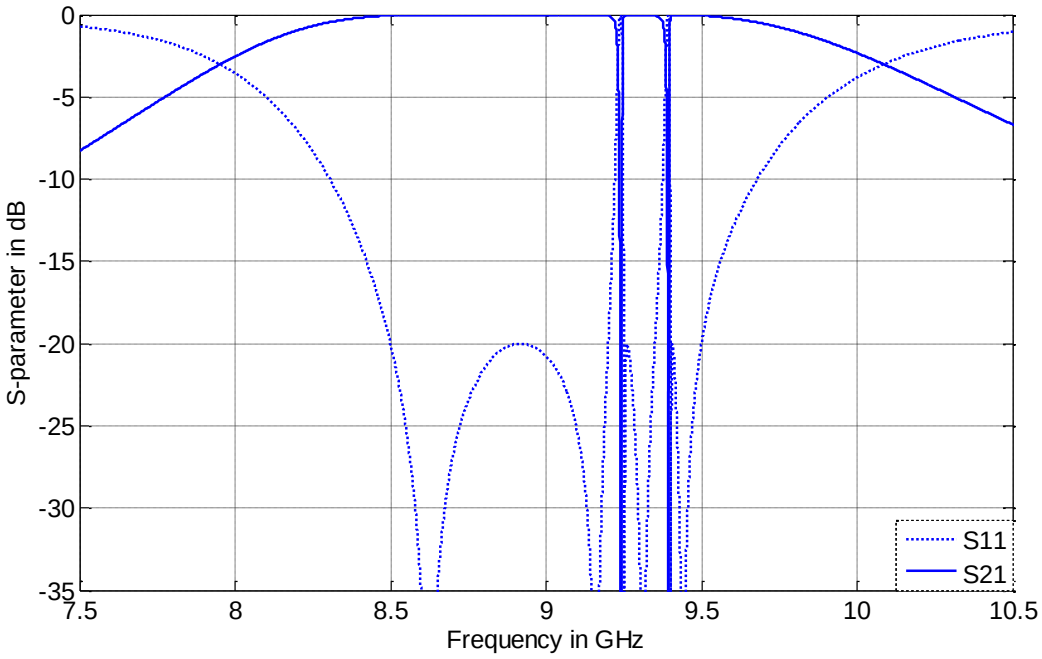

Figure II.6 The response of the 6th order tunable notch filter for example 4

Filter specifications		
Centre frequency	Notch positions	Passband width
9.00GHz	9.23GHz, 9.37GHz	1GHz
Design parameters (filter with series coupled sections)		
Coupling matrix	External *Q*-factor	Resonator frequency
$\begin{pmatrix} -0.0033 & 0.1665 & 0.0248 & 0 & 0 & 0 \\ 0.1665 & -0.0033 & 0 & 0.0248 & 0 & 0 \\ 0.0248 & 0 & 0.0669 & 0 & 0.0162 & 0 \\ 0 & 0.0248 & 0 & 0.0669 & 0 & 0.0162 \\ 0 & 0 & 0.0162 & 0 & 0.0715 & 0 \\ 0 & 0 & 0 & 0.0162 & 0 & 0.0715 \end{pmatrix}$	6.637	1&2: 8.99GHz 3&4: 9.30GHz 5&6: 9.33GHz
Design parameters (filter with parallel coupled sections)		
Coupling matrix	External *Q*-factor	Resonator frequency
$\begin{pmatrix} -0.0033 & 0.1665 & 0.0221 & 0 & 0.0209 & 0 \\ 0.1665 & -0.0033 & 0 & 0.0221 & 0 & 0.0209 \\ 0.0221 & 0 & 0.0528 & 0 & 0 & 0 \\ 0 & 0.0221 & 0 & 0.0528 & 0 & 0 \\ 0.0209 & 0 & 0 & 0 & 0.0856 & 0 \\ 0 & 0.0209 & 0 & 0 & 0 & 0.0856 \end{pmatrix}$	6.637	1&2: 8.99GHz 3&4: 9.23GHz 5&6: 9.37GHz

Table II.5 The filter specifications and couplings of the response for example 4

2.5 Discussion on Notch Position Tuning

For the filters with series coupled resonator sections, the characteristics are concluded as follow:

- The notch positions are not solely determined by the resonant frequencies of the bandstop resonators; but are controlled by both inter-resonator couplings and resonant frequencies of the bandstop resonators. Even if there is only one notch being tuned, all inter-resonator couplings and resonant frequencies of bandstop resonators will change.

- Inter-resonator couplings change significantly during the notch position tuning. The maximum changes for $M_{1,3}$ and $M_{2,4}$ are 34%; the maximum changes for $M_{3,5}$ and $M_{4,6}$ are 116% (example 3).
- The bandpass resonators and the couplings between not change during notch position tuning.

For the filters with parallel coupled resonator sections, the characteristics are:

- Although the inter-resonator couplings change along with the notch position tuning, the changes are less than 10% in these examples.
- The frequencies of bandstop resonators are exactly the positions of the notches.

3. Passband Centre Frequency Tuning

In this section, only the centre frequency is tuned. All other specifications remain the same as the reference example in Section 1. Two examples are given below.

3.1 *Example 5: Passband Tuned Down*

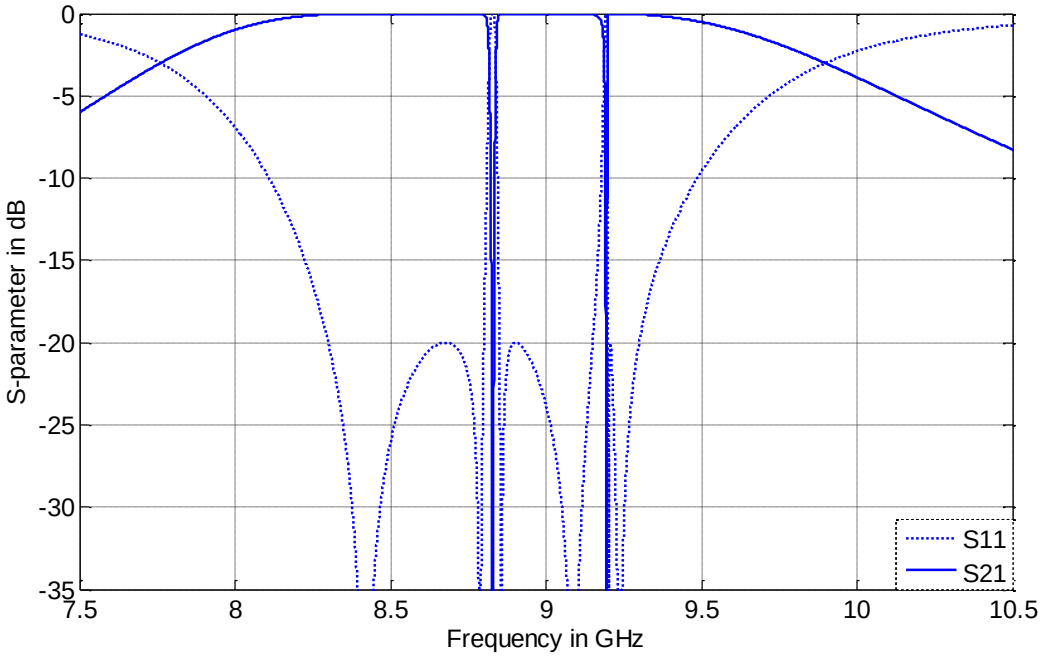

Figure II.7 The response of the 6th order tunable notch filter for example 5

Filter specifications		
Centre frequency	Notch positions	Passband width
8.80GHz	8.83GHz, 9.17GHz	1GHz
Design parameters (filter with series coupled sections)		
Coupling matrix	External Q-factor	Resonator frequency
$\begin{pmatrix} -0.0083 & 0.1707 & 0.0290 & 0 & 0 & 0 \\ 0.1707 & -0.0083 & 0 & 0.0290 & 0 & 0 \\ 0.0290 & 0 & 0.0297 & 0 & 0.0366 & 0 \\ 0 & 0.0290 & 0 & 0.0297 & 0 & 0.0366 \\ 0 & 0 & 0.0317 & 0 & 0.0646 & 0 \\ 0 & 0 & 0 & 0.0366 & 0 & 0.0646 \end{pmatrix}$	6.474	1&2: 8.76GHz 3&4: 8.93GHz 5&6: 9.09GHz
Design parameters (filter with parallel coupled sections)		
Coupling matrix	External Q-factor	Resonator frequency
$\begin{pmatrix} -0.0083 & 0.1707 & 0.0245 & 0 & 0.0207 & 0 \\ 0.1707 & -0.0083 & 0 & 0.0245 & 0 & 0.0207 \\ 0.0245 & 0 & 0.0065 & 0 & 0 & 0 \\ 0 & 0.0245 & 0 & 0.0065 & 0 & 0 \\ 0.0207 & 0 & 0 & 0 & 0.0877 & 0 \\ 0 & 0.0207 & 0 & 0 & 0 & 0.0877 \end{pmatrix}$	6.474	1&2: 8.76GHz 3&4: 8.83GHz 5&6: 9.17GHz

Table II.6 The filter specifications and couplings of the response for example 5

3.2 *Example 6: Passband Tuned Up*

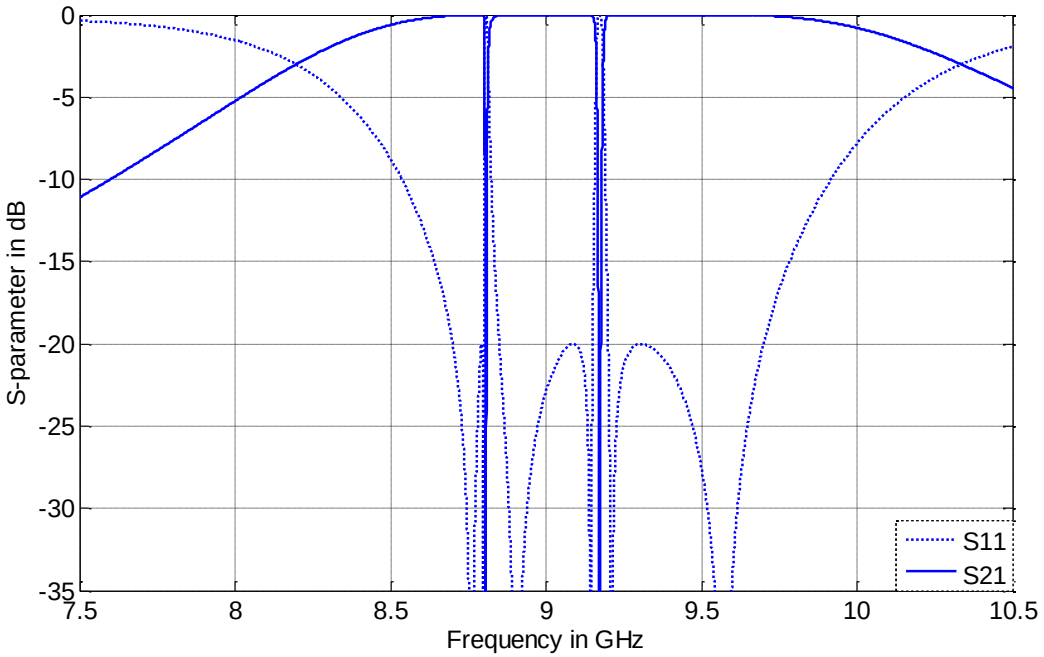

Figure II.8 The response of the 6th order tunable notch filter for example 6

Filter specifications		
Centre frequency	Notch positions	Passband width
9.20GHz	8.83GHz, 9.17GHz	1GHz
Design parameters (filter with series coupled sections)		
Coupling matrix	External *Q*-factor	Resonator frequency
$\begin{pmatrix} 0.0018 & 0.1624 & 0.0286 & 0 & 0 & 0 \\ 0.1624 & 0.0018 & 0 & 0.0286 & 0 & 0 \\ 0.0286 & 0 & -0.0318 & 0 & 0.0379 & 0 \\ 0 & 0.0286 & 0 & -0.0318 & 0 & 0.0379 \\ 0 & 0 & 0.0379 & 0 & -0.0617 & 0 \\ 0 & 0 & 0 & 0.0379 & 0 & -0.0617 \end{pmatrix}$	6.802	1&2: 9.21GHz 3&4: 9.06GHz 5&6: 8.92GHz
Design parameters (filter with parallel coupled sections)		
Coupling matrix	External *Q*-factor	Resonator frequency
$\begin{pmatrix} 0.0018 & 0.1624 & 0.0213 & 0 & 0.0236 & 0 \\ 0.1624 & 0.0018 & 0 & 0.0213 & 0 & 0.0236 \\ 0.0213 & 0 & -0.0875 & 0 & 0 & 0 \\ 0 & 0.0213 & 0 & -0.0875 & 0 & 0 \\ 0.0236 & 0 & 0 & 0 & -0.0060 & 0 \\ 0 & 0.0236 & 0 & 0 & 0 & -0.0060 \end{pmatrix}$	6.802	1&2: 9.21GHz 3&4: 8.83GHz 5&6: 9.17GHz

Table II.7 The filter specifications and couplings of the response for example 6

3.3 Discussion on Passband Centre Frequency Tuning

The characteristics of the filters with series coupled resonator sections can be concluded as follow:

- The passband frequencies are not solely determined by the resonant frequencies of the bandpass resonators; but are determined by both inter-resonator couplings and resonant frequencies of all resonators.
- Although the positions of the notches are fixed during centre frequency tuning, the resonant frequencies of the bandstop resonators change.

- The maximum change in coupling between bandpass resonator $M_{1,2}$ is 2.4%, the maximum change in external Q-factor is 2.6%. They are not sensitive to the centre frequency tuning.

For the filters with parallel coupled resonator sections, its characteristics are concluded as follow:

- As long as the notch positions are fixed, the frequencies of bandstop resonators not change during the centre frequency tuning.
- The inter-resonator couplings are not sensitive to centre frequency tuning.

4. Passband Bandwidth Tuning

In this section, only the passband bandwidth is tuned. All other specifications remain the same as the reference given in Section 1.

4.1 *Example 7: Passband Tuned Wider*

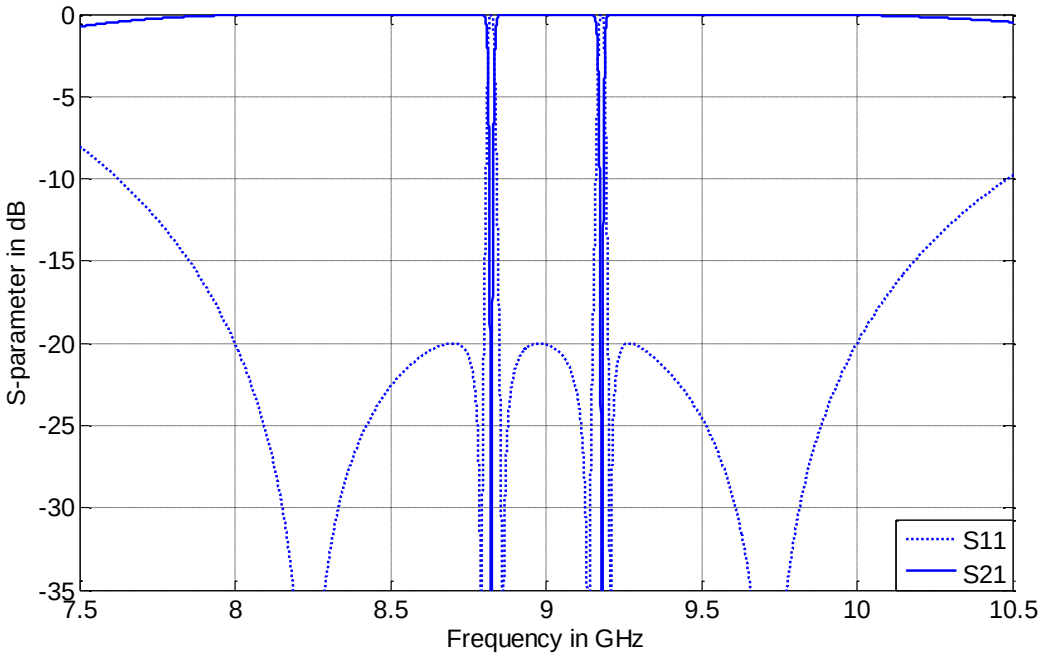

Figure II.9 The response of the 6th order tunable notch filter for example 7

Filter specifications		
Centre frequency	Notch positions	Passband width
9.00GHz	8.83GHz, 9.17GHz	2GHz
Design parameters (filter with series coupled sections)		
Coupling matrix	External Q-factor	Resonator frequency
$\begin{pmatrix} -0.0130 & 0.3532 & 0.0490 & 0 & 0 & 0 \\ 0.3532 & -0.0130 & 0 & 0.0490 & 0 & 0 \\ 0.0490 & 0 & -0.0013 & 0 & 0.0395 & 0 \\ 0 & 0.0490 & 0 & -0.0013 & 0 & 0.0395 \\ 0 & 0 & 0.0395 & 0 & 0.0012 & 0 \\ 0 & 0 & 0 & 0.0395 & 0 & 0.0012 \end{pmatrix}$	3.129	1&2: 8.94GHz 3&4: 8.99GHz 5&6: 9.01GHz
Design parameters (filter with parallel coupled sections)		
Coupling matrix	External Q-factor	Resonator frequency
$\begin{pmatrix} -0.0130 & 0.3535 & 0.0258 & 0 & 0.0249 & 0 \\ 0.3535 & -0.0130 & 0 & 0.0258 & 0 & 0.0249 \\ 0.0258 & 0 & -0.0396 & 0 & 0 & 0 \\ 0 & 0.0258 & 0 & -0.0396 & 0 & 0 \\ 0.0249 & 0 & 0 & 0 & 0.0394 & 0 \\ 0 & 0.0249 & 0 & 0 & 0 & 0.0394 \end{pmatrix}$	3.129	1&2: 8.94GHz 3&4: 8.83GHz 5&6: 9.17GHz

Table II.8 The filter specifications and couplings of the response for example 7

4.2 *Example 8: Passband Tuned Narrower*

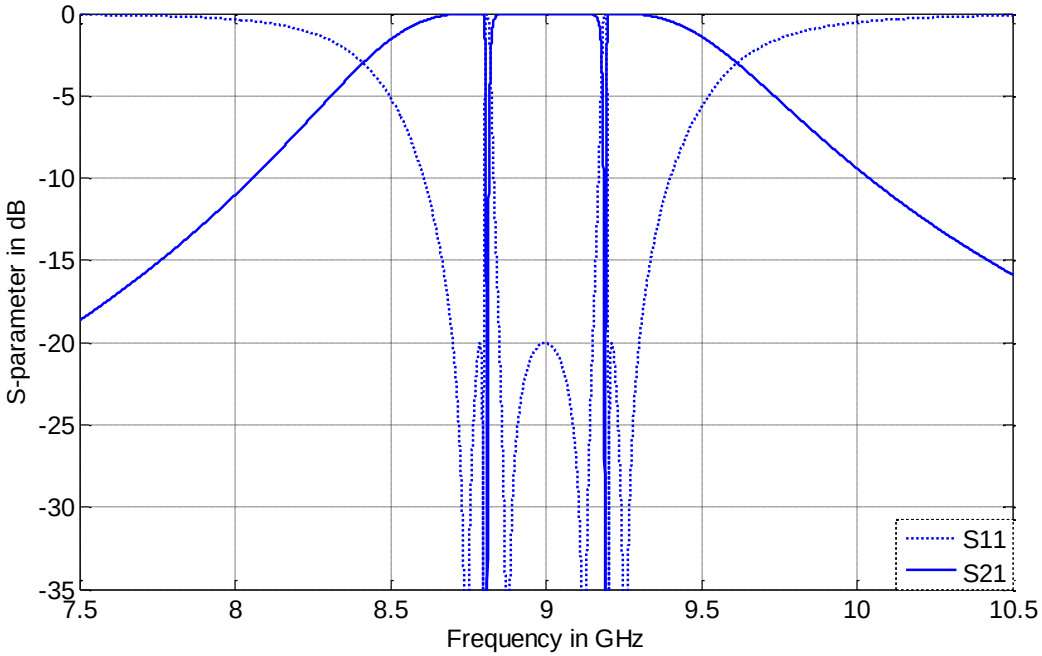

Figure II.10 The response of the 6th order tunable notch filter for example 8

Filter specifications		
Centre frequency	Notch positions	Passband width
9.00GHz	8.83GHz, 9.17GHz	0.6GHz
Design parameters (filter with series coupled sections)		
Coupling matrix	External Q-factor	Resonator frequency
$\begin{pmatrix} -0.0011 & 0.0924 & 0.0211 & 0 & 0 & 0 \\ 0.0924 & -0.0011 & 0 & 0.0211 & 0 & 0 \\ 0.0211 & 0 & -0.0021 & 0 & 0.0421 & 0 \\ 0 & 0.0211 & 0 & -0.0021 & 0 & 0.0421 \\ 0 & 0 & 0.0421 & 0 & 0.0013 & 0 \\ 0 & 0 & 0 & 0.0421 & 0 & 0.0013 \end{pmatrix}$	11.960	1&2: 9.00GHz 3&4: 8.99GHz 5&6: 9.01GHz
Design parameters (filter with parallel coupled sections)		
Coupling matrix	External Q-factor	Resonator frequency
$\begin{pmatrix} -0.0011 & 0.0924 & 0.0214 & 0 & 0.0207 & 0 \\ 0.0924 & -0.0011 & 0 & 0.0214 & 0 & 0.0207 \\ 0.0214 & 0 & -0.0412 & 0 & 0 & 0 \\ 0 & 0.0214 & 0 & -0.0412 & 0 & 0 \\ 0.0207 & 0 & 0 & 0 & 0.0399 & 0 \\ 0 & 0.0207 & 0 & 0 & 0 & 0.0399 \end{pmatrix}$	11.960	1&2: 9.00GHz 3&4: 8.83GHz 5&6: 9.17GHz

Table II.9 The filter specifications and couplings of the response for example 8

4.3 Discussion on Passband Bandwidth Tuning

The characteristics for the filter with series coupled resonator sections can be concluded as follow:

- The passband bandwidth are primarily determined by the coupling between bandpass resonators $M_{1,2}$, the external Q-factors and the couplings between bandpass resonators and bandstop resonators $M_{1,3}$, $M_{2,4}$.
- During the passband width tuning, the frequencies of resonators change as well.

- The couplings between bandstop resonators $M_{3,5}, M_{4,6}$ and the resonant frequencies of all resonators are not sensitive to the passband width tuning.

For the filter with parallel coupled resonator sections:

- The coupling between bandpass resonators $M_{1,2}$ and the external Q-factors are the dominant factors that determine the passband bandwidth; other parameters are not sensitive to the passband bandwidth tuning.
- The frequencies of resonators are not sensitive to the passband bandwidth tuning.
- The inter-resonator couplings between bandpass resonators and bandstop resonators $M_{1,3}, M_{2,4}, M_{1,5}$ and $M_{2,6}$ are not sensitive to passband bandwidth tuning.

5. Conclusion

Given the comparisons and discussions above, it is quite obvious that the topology with parallel coupled resonator sections is more practical for a tunable filter, because the tuning parameters have more independence. This feature allows each tuning parameter controls one kind of filter specification, which significantly simplifies the tuning procedure.

Appendix III: The Comparison on *S*-Parameters Plotted from Two Different Approaches

The analytical synthesis technique generates *S*-parameters and design parameters (coupling matrix, external *Q*-factor, etc.) through separate routines; the *S*-parameters are plotted from (2-32) using Cameron's characteristic polynomials [1], rather than directly plotted from (2-28) using the design parameters. Hence, for analytical synthesis technique, the *S*-parameters cannot be directly controlled by the design parameters. In order to control *S*-parameters by the design parameters, the *S*-parameters should be plotted using (2-28). However, the accuracy of *S*-parameters directly plotted from design parameters may depends on the *FBW* [2]. A comparison is carried out in the following sections to investigate the difference between the *S*-parameters plotted from the two different approaches.

The topology shown in Figure III.1 is used as an example in this section.

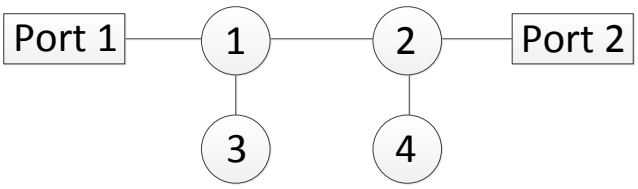

Figure III.1 A 4th order notch filter

1. Lowpass to Bandpass Frequency Transformation

The frequency transformation here is the conventional lowpass to bandpass frequency transformation discussed in Chapter 2. However, the lowpass response here refers to a lowpass notch response, rather than a prototype Chebyshev or Butterworth response which is synthesised from the transfer function. The frequency transformation is illustrated below,

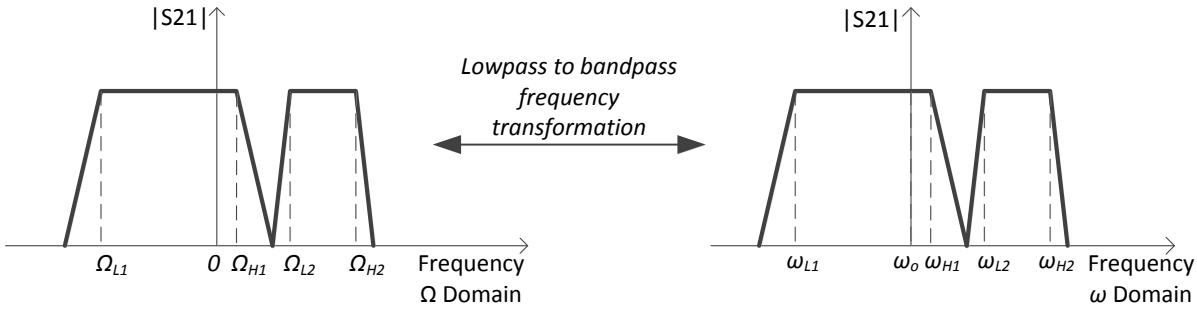

Figure III.2 A schematic of the proposed lowpass to bandpass frequency transformation

where Ω_{Li} and Ω_{Hi} (i=1,2) are the passband limits for the lowpass response in Ω domain. In the de-normalised ω domain, ω_{Li} and ω_{Hi} (i=1,2) are the de-normalised passband limits; ω_o is the passband centre frequency.

The corresponding lowpass to bandpass frequency transformation is,

$$\Omega = \frac{(\Omega_{H2} - \Omega_{L1})}{2} \cdot \frac{\omega_o}{BW}\left(\frac{\omega}{\omega_o} - \frac{\omega_o}{\omega}\right) \tag{III-1}$$

in which BW is calculated by

$$BW = \omega_{H2} - \omega_{L1} \tag{III-2}$$

In the case of $\Omega_{L1} = -1$ and $\Omega_{H2} = 1$, it will be a lowpass prototype response, which simplifies (III-1) as,

$$\Omega = \frac{\omega_o}{BW}\left(\frac{\omega}{\omega_o} - \frac{\omega_o}{\omega}\right) = \frac{1}{FBW}\left(\frac{\omega}{\omega_o} - \frac{\omega_o}{\omega}\right) \tag{III-3}$$

It should be noticed that only two parameters are required to fully define this frequency transformation, which are the centre frequency ω_o and fractional bandwidth FBW.

The lowpass prototype notch response and the corresponding normalised design parameters are obtained using the approach given below.

2. The Lowpass Prototype Notch Response and The Corresponding Normalised Design Parameters

The lowpass prototype notch response is plotted directly from corresponding normalised design parameters (normalised coupling matrix, external *Q*-factors). The normalised design parameters are produced from a set of de-normalised design parameters that are obtained by the analytical synthesis technique. Because the frequency transformation involves narrow-band approximation ($\omega/\omega_o \approx 1$), the responses and design parameters are more accurate in narrow-band cases. Therefore, the lowpass prototype notch response and the normalised design parameters are generated from a de-normalised with very narrow band (*FBW* = 0.01%).

2.1 A de-normalised narrow-band Notch Response and The Corresponding Design Parameters (ω Domain)

Figure III.3 shows a narrow-band notch response plotted from the analytical synthesis technique, the corresponding filter specifications and design parameters are presented in Table III.1.

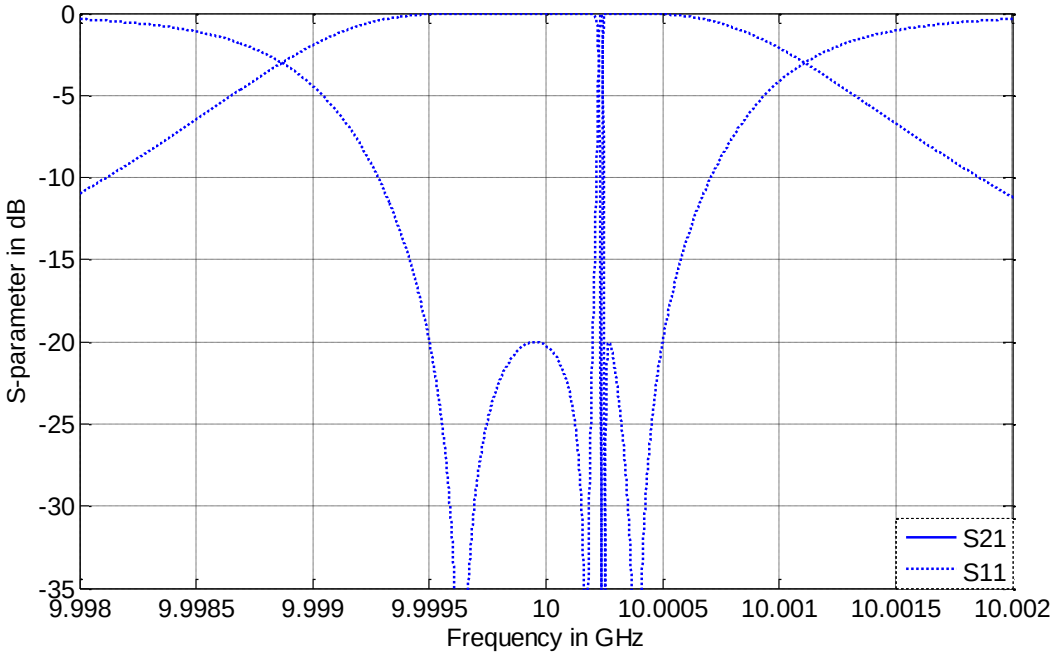

Figure III.3 The de-normalised notch response *(FBW*=0.01%)

The above response is in the de-normalised frequency domain (ω domain), with $\omega_{L1} = 9.9995$ GHz and $\omega_{H2} = 10.0005$ GHz. By applying (2-16), the centre frequency ω_o and fractional bandwidth *FBW* can be calculated as 10.00000GHz and an *FBW* of 0.010% (accurate up to five decimal places). The filter specifications and corresponding design parameters are listed below.

Filter specifications (ω domain)			
Centre frequency	Notch position	Passband width	Notch width
10.00000GHz	10.00023GHz	0.00100GHz	0.00005GHz
Design parameters (ω domain)			
Coupling matrix		External *Q*-factor	Resonator frequency
$\begin{pmatrix} -0.0237 & 1.5790 & 0.1969 & 0 \\ 1.5790 & -0.0237 & 0 & 0.1969 \\ 0.1969 & 0 & 0.4737 & 0 \\ 0 & 0.1969 & 0 & 0.4737 \end{pmatrix} \times 10^{-4}$		6.9982×10^{3}	1&2: 10.00000GHz 3&4: 10.00023GHz

Table III.1 The filter specifications and design parameters (*FBW*=0.01%)

2.2 The Lowpass Prototype Notch Response and The Corresponding Normalised Design Parameters (Ω domain)

The normalised design parameters are obtained from the de-normalised design parameters in Table III.1 by using (2-24); the results are shown below,

<table>
<tr><th colspan="4">Normalised Filter specifications (Ω domain)</th></tr>
<tr><td>Centre frequency</td><td>Notch position</td><td>Passband width</td><td>Notch width</td></tr>
<tr><td>0Hz</td><td>0.4737Hz</td><td>2.0000Hz</td><td>0.1000Hz</td></tr>
<tr><th colspan="4">Normalised Design parameters (Ω domain)</th></tr>
<tr><td colspan="2">Coupling matrix</td><td>External Q-factor</td><td>Resonator frequency</td></tr>
<tr><td colspan="2">$\begin{pmatrix} -0.0237 & 1.5790 & 0.1969 & 0 \\ 1.5790 & -0.0237 & 0 & 0.1969 \\ 0.1969 & 0 & 0.4737 & 0 \\ 0 & 0.1969 & 0 & 0.4737 \end{pmatrix}$</td><td>0.6998</td><td>1&2:
-0.0237Hz

3&4:
0.4737Hz</td></tr>
</table>

Table III.2 The normalised filter specifications and design

The lowpass notch response below is plotted directly from the above normalised design parameters using the lowpass to bandpass frequency transformation given in (III-1).

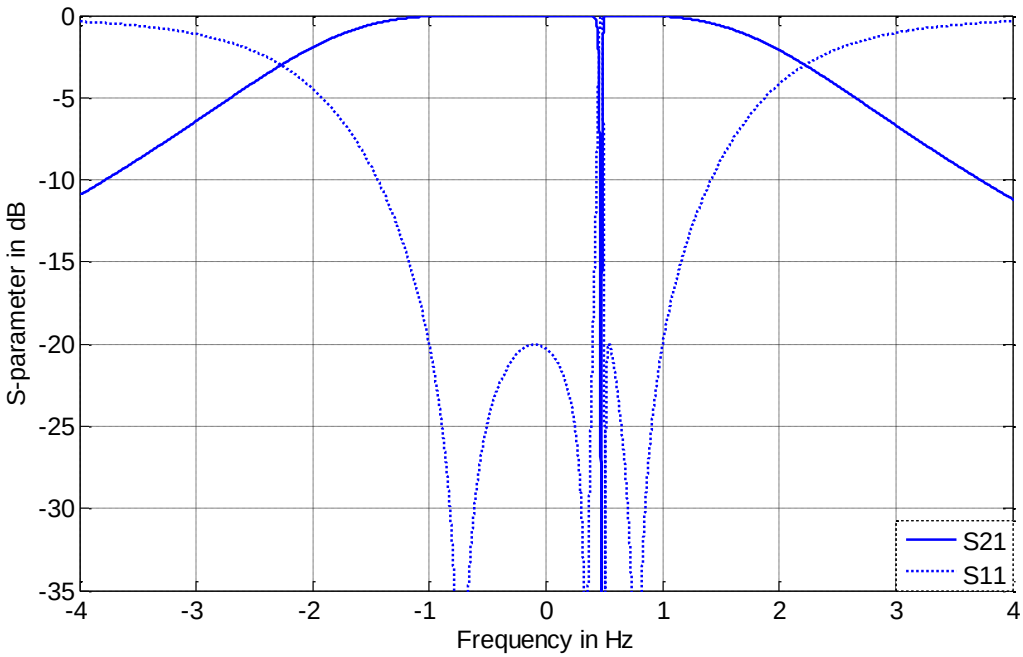

Figure III.4 The normalised notch response

It can be seen from Figure III.4 that Ω_{L1} is -1.0000, Ω_{H2} is 1.0000. The values are accurate up to four decimal places, which indicate that this can be considered as a standard lowpass prototype notch response.

3. Comparison 1 (ω_{L1}=9.500 GHz, ω_{H2}=10.500 GHz)

In this section, the de-normalised responses plotted from the two different approaches are presented and compared. The passband limits are set as 9.500 GHz and 10.500GHz. The ω_o and *FBW* can be calculated as 9.987 GHz and 10.0%, respectively.

3.1 The Responses Plotted from Analytical Synthesis

Below is the response plotted from the analytical synthesis technique; the corresponding filter specifications and design parameters are shown in Table III.3.

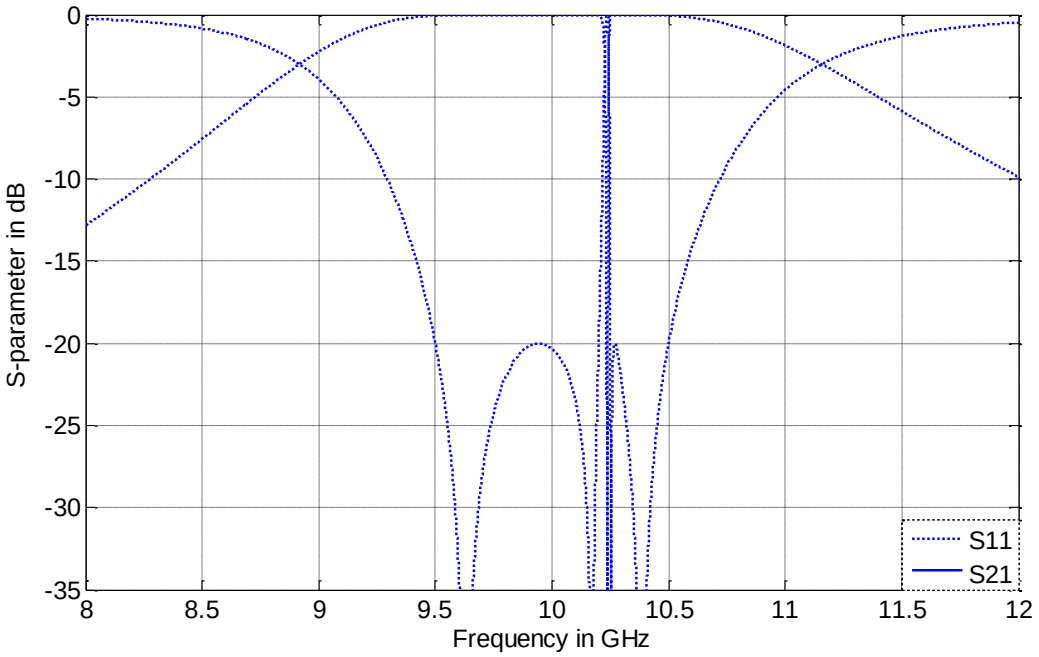

Figure III.5 The de-normalised notch response from analytical synthesis *(FBW*=10.0%)

Desired Filter specifications (ω domain)			
Centre frequency	Notch position	Passband width	Notch width
9.987GHz	10.234GHz	1.000GHz	0.050GHz
Actual Filter specifications (ω domain)			

Centre frequency	Notch position	Passband width	Notch width
9.987GHz	10.234GHz	1.000GHz	0.050GHz
Design parameters (ω domain)			
Coupling matrix		External Q-factor	Resonator frequency
$\begin{pmatrix} -0.0024 & 0.1583 & 0.0192 & 0 \\ 0.1583 & -0.0024 & 0 & 0.0192 \\ 0.0192 & 0 & 0.0494 & 0 \\ 0 & 0.0192 & 0 & 0.0494 \end{pmatrix}$		6.981	1&2: 9.975GHz 3&4: 10.234GHz

Table III.3 The corresponding filter specifications and design parameters of the response

There are two sets of filter specifications in the above table, which are desired filter specification and actual filter specification. The former one is the specification used to generate the response and the design parameters; while the latter one is the specification that read from the response. Because the analytical synthesis technique generates the S-parameters from the passband limits, these two sets of filter specifications are identical.

3.2 The Responses Plotted from Design Parameters

Figure III.6 and Table III.4 show the response and corresponding design parameters obtained from the lowpass prototype shown in Section 2.2.

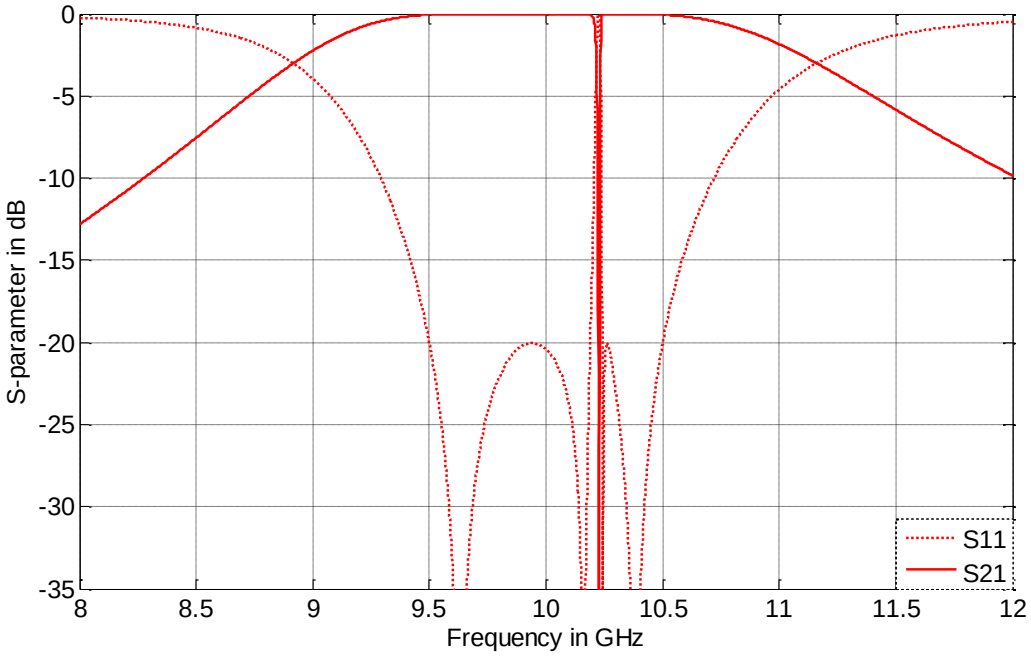

Figure III.6 The de-normalised notch response plotted from design parameters *(FBW*=10.0%)

<table>
<tr><th colspan="4">Desired Filter specifications (ω domain)</th></tr>
<tr><td>Centre frequency</td><td>Notch position</td><td>Passband width</td><td>Notch width</td></tr>
<tr><td>9.987GHz</td><td>10.234GHz</td><td>1.000GHz</td><td>0.050GHz</td></tr>
<tr><th colspan="4">Actual Filter specifications (ω domain)</th></tr>
<tr><td>Centre frequency</td><td>Notch position</td><td>Passband width</td><td>Notch width</td></tr>
<tr><td>9.987GHz</td><td>10.227GHz</td><td>1.000GHz</td><td>0.051GHz</td></tr>
<tr><th colspan="4">Design parameters (ω domain)</th></tr>
<tr><td colspan="3">Coupling matrix</td><td>External Q-factor</td><td>Resonator frequency</td></tr>
<tr><td colspan="3">$\begin{pmatrix} -0.0024 & 0.1581 & 0.0197 & 0 \\ 0.1581 & -0.0024 & 0 & 0.0197 \\ 0.0197 & 0 & 0.0474 & 0 \\ 0 & 0.0197 & 0 & 0.0474 \end{pmatrix}$</td><td>6.989</td><td>1&2:
9.975GHz

3&4:
10.227GHz</td></tr>
</table>

Table III.4 The corresponding filter specifications and design parameters

It can be read from Figure III.6 that the passband limits ω_{L1} and ω_{H2} are 9.500GHz and 10.500GHz, respectively, which satisfy the proposed passband limits. However, the notch position is 0.010GHz lower than the proposed frequency, while the notch width is 0.001GHz wider than the proposed notch width.

3.3 The Comparison

For easier comparison, Figure III.7 displays the notch responses plotted from the two different approaches on the same graph.

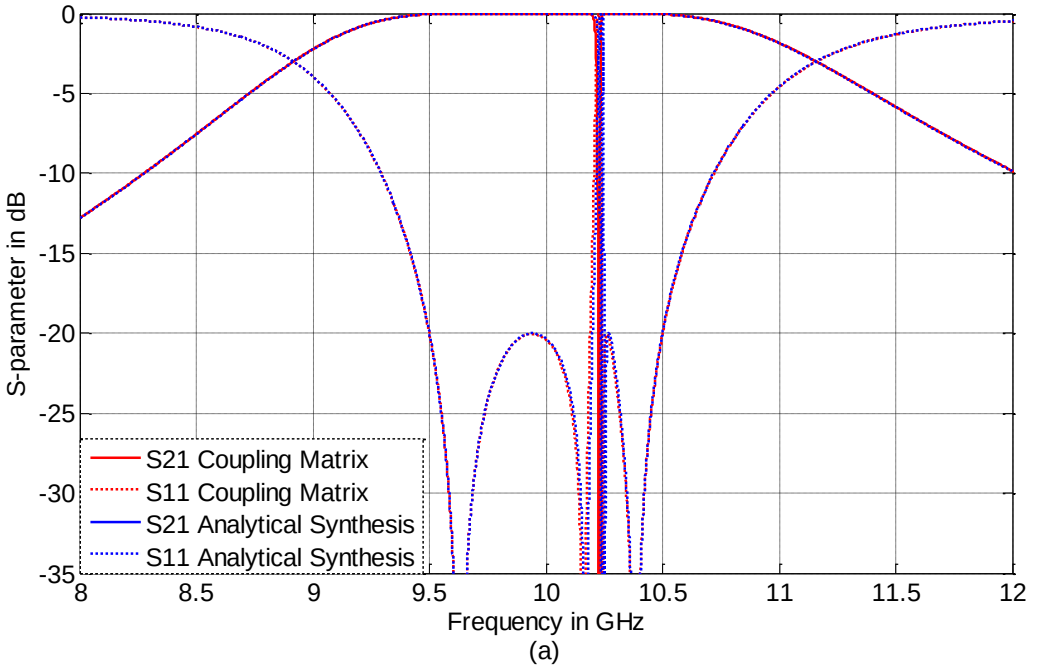

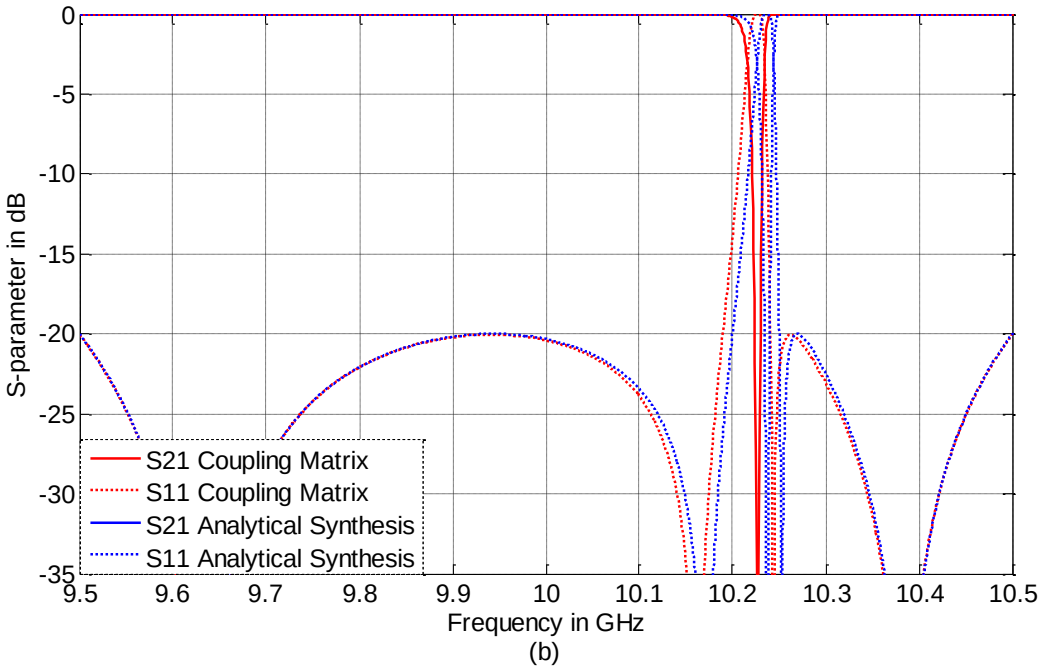

Figure III.7 The comparison of de-normalised notch responses from the two approaches *(FBW*=10.0%), (a) full-scale response, (b) extended partial response for passband

The *S*-parameters plotted from the analytical synthesis satisfy the desired passband specifications more accurately; while the *S*-parameters from the design parameters is slightly distorted. In general, the two set of design parameters are very close; the maximum error between them is only 2.5%.

4. Comparison 2 (ω_{L1}=7.500 GHz, ω_{H2}=12.500 GHz)

In this section, the comparison goes to the case of having a ω_o of 9.682GHz and an *FBW* of 51.6%. The analysis follows the same procedure as the previous section.

4.1 The Responses Plotted from Analytical Synthesis

Figure III.8 shows the response plotted from the analytical synthesis technique; the corresponding filter specifications and design parameters are shown in Table III.5.

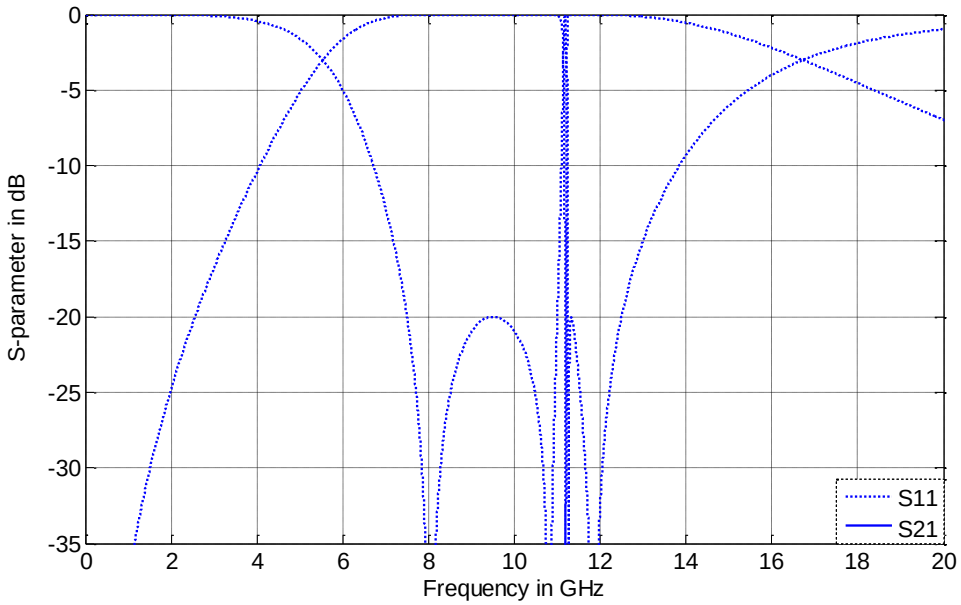

Figure III.8 The de-normalised notch response from analytical synthesis *(FBW*=51.6%)

Desired Filter specifications (ω domain)			
Centre frequency	Notch position	Passband width	Notch width
9.682GHz	11.195GHz	5.000GHz	0.250GHz
Actual Filter specifications (ω domain)			
Centre frequency	Notch position	Passband width	Notch width
9.682GHz	11.195GHz	5.000GHz	0.250GHz
Design parameters (ω domain)			
Coupling matrix		External *Q*-factor	Resonator frequency
$\begin{pmatrix} -0.0127 & 0.8206 & 0.0889 & 0 \\ 0.8206 & -0.0127 & 0 & 0.0889 \\ 0.0889 & 0 & 0.2913 & 0 \\ 0 & 0.0889 & 0 & 0.2913 \end{pmatrix}$		1.347	1&2: 9.621GHz 3&4: 11.195GHz

Table III.5 The corresponding filter specifications and design parameters (*FBW*=51.6%)

The *S*-parameters satisfy the desired passband specifications accurately.

4.2 The Response Plotted from Design Parameters

The responses and design parameters given in Figure III.9 and Table III.6 are obtained from the lowpass prototype shown in Section 2.2.

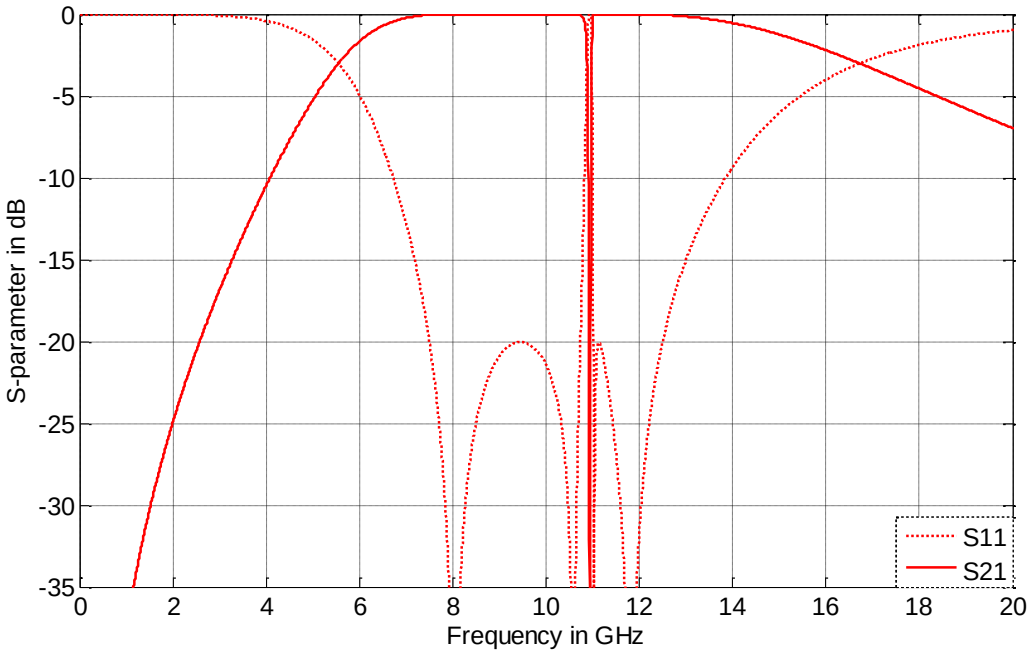

Figure III.9 The de-normalised notch response directly from design parameters *(FBW*=51.6%)

Desired Filter specifications (*ω* domain)			
Centre frequency	Notch position	Passband width	Notch width
9.682GHz	11.195GHz	5.000GHz	0.250GHz
Actual Filter specifications (*ω* domain)			
Centre frequency	Notch position	Passband width	Notch width
9.682GHz	10.938GHz	5.000GHz	0.278GHz
Design parameters (*ω* domain)			
Coupling matrix		External *Q*-factor	Resonator frequency
$\begin{pmatrix} -0.0122 & 0.8154 & 0.1017 & 0 \\ 0.8154 & -0.0122 & 0 & 0.1017 \\ 0.1017 & 0 & 0.2446 & 0 \\ 0 & 0.1017 & 0 & 0.2446 \end{pmatrix}$		1.355	1&2: 9.624GHz 3&4: 10.938GHz

Table III.6 The corresponding filter specifications and design parameters of the response (*FBW*=51.6%)

The *S*-parameters in Figure III.9 satisfies the proposed passband limits. However, the notch position is 0.257GHz lower, while the width is 0.028GHz wider than the proposed specifications.

4.3 The Comparison

The two responses plotted from the two approaches display together on Figure III.10; (a) is the full-scale response; (b) is the extended partial response on the passband area.

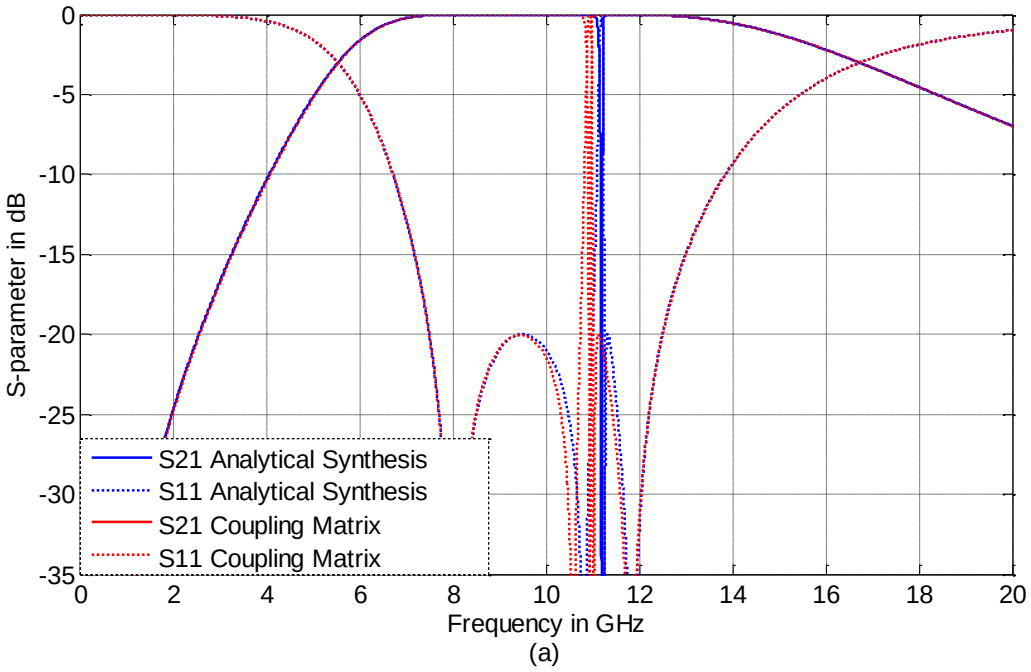

(a)

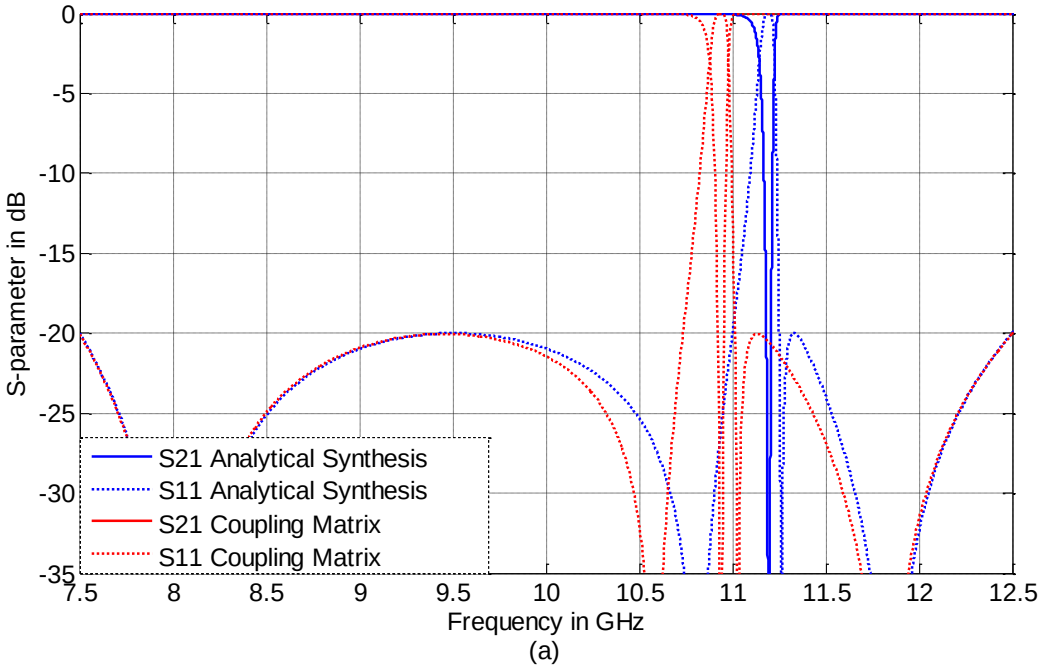

Figure III.10 The comparison of de-normalised notch responses from the two approaches *(FBW*=51.6%), (a) full-scale response, (b) partial response near centre frequency

It can be seen from Figure III.10 that, the S-parameters plotted from design parameters has a larger distortion compared to the previous case with an *FBW* of 10.0%; besides the distortion, the notch positions and notch width also has a larger mismatch against the proposed specifications, but the centre frequency and the *FBW* still match the proposed specifications accurately. The maximum error for the design parameters increases to 14.4 %, compared to 2.5% of the previous case.

5. Discussion

The *S*-parameters and design parameters obtained from analytical synthesis technique satisfies the desired passband specifications accurately regardless of the *FBW*. For the *S*-parameters plotted from design parameters, the distortion is an inevitable issue, as it involves narrow-band approximation, which satisfies the following condition,

$$\omega / \omega_o \approx 1 \qquad \text{(III-4)}$$

This indicates that the *S*-parameters are more accurate when they are closer to the centre frequency. This explains why the example with a larger *FBW* has a more serious distortion than the example with a smaller *FBW*.

The tunable notch filter discussed in this thesis is a narrow-band case. Therefore, the response and design parameters that obtained from lowpass prototype are still valid for the filter design.

Reference:

1. Cameron, R.J., R. Mansour, and C.M. Kudsia, *Microwave Filters for Communication Systems: Fundamentals, Design and Applications*2007: Wiley.
2. Hong, J.-S. and M.J. Lancaster, *Microstrip Filters for RF/Microwave Applications*2001: John Wiley and Sons Ltd, United Kingdom.

Appendix IV: Publication List

1. M. Guo, M. J. Lancaster and C. Constantinou, "A New Multi-Passband Filter Synthesis Technique". *31st ARMMS conference*, *UK*, Nov 2015 (Published)
2. M. Guo, M. J. Lancaster, " Design of Five-Passband Rectangular Waveguide Filter with Chebyshev Response", *IEEE Microwave and Wireless Components Letters,* 2016 (submitted)
3. M. Guo, M. J. Lancaster, "Design of a tunable BPF and a tunable notch filter with a novel coupling tuning structure", *IEEE Microwave and Wireless Components Letters*, 2016 (In plan to submit)

A NEW MULTI-PASSBAND FILTER SYNTHESIS TECHNIQUE

Mofei Guo[1]*, Michael J. Lancaster[2]*, Costas Constantinou[3]*

*School of Electronics, Electrical and System Engineering, the University of Birmingham, Birmingham, B15 2TT, U.K.

[1] mxg848@bham.ac.uk, [2] m.j.lancaster@bham.ac.uk, [3] c.constantinou@bham.ac.uk

Abstract:

This paper looks at a new design method for resonator-based multi-passband filters. The technique is able to design an arbitrary number of passbands. The design procedure is based on calculating the coupling matrix for a particular topology of coupled resonators. The physical design parameters, such as the centre frequency of each resonator, the coupling between resonators and the external Q-factors can all be analytically synthesised from the filter specifications. In the paper we will show designs for both Chebyshev and quasi-elliptic multi-passband filters. Theoretically, this method can produce any number of passbands where each band shares the same shape.

Two simulated and one measured example of filters designed through this method are given; the three examples are: (1) A 10th order uneven bandwidth five-passband filter with Chebyshev response; (2) A 20th order uneven bandwidth five-passband filter with quasi-elliptic response; (3) Measured results from a 4th order dual-passband waveguide resonator based filter.

I. INTRODUCTION

Conventionally, the low-pass prototype Chebyshev response can be mapped into a higher frequency band with the well-known frequency transformation technique. This can be done using [3].

$$\Omega = B(\omega) = \frac{\omega_0}{BW}\left(\frac{\omega}{\omega_0} - \frac{\omega_0}{\omega}\right) \qquad \text{Equation 1}$$

where ω is the frequency variable for de-normalised response; Ω is the normalised frequency variable for low-pass prototype response; ω_0 is the centre frequency of the de-normalised passband; BW is the bandwidth of the passband (equal ripple bandwidth for Chebyshev response). Figure 3.1 gives a illustrative view of the de-normalised procedure based on (2-1). In the figure, ω_L and ω_H are the lower and higher band limits for de-normalised passband, respectively.

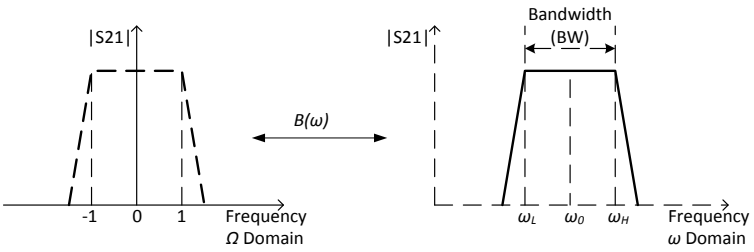

Figure 1. The conventional de-normalised procedure for bandpass filter

Now, let us consider a situation, by applying a new frequency transformation formula $M(\omega)$, the low-pass prototype response can be mapped into multiple higher frequency bands in the de-normalised procedure. Figure 3.2 gives an illustrative view of this procedure, showing ω_{Li} and ω_{Hi} (i=1,2,3,…,M) are the band limits for ith passband on the de-normalised response.

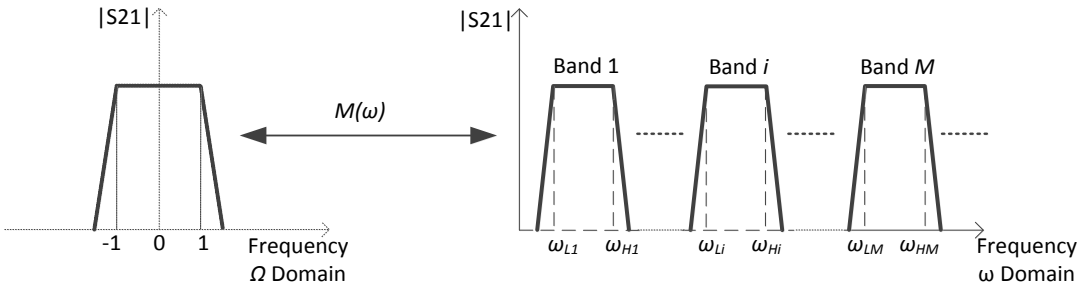

Figure 2. The de-normalised procedure for multi-passband filter

This paper aims to present the multi-passband filter synthesis technique step by step. A new generalised approach of multi-passband filter design is given. It allows the number of passband and the bandwidth of each individual passband to be set as an arbitrary value. With given band limits of each passband, and specifications of the low-pass prototype response, a multi-passband response can be generated with coupling matrix and external Q-factors synthesised at the same time. Some design examples of multi-passband filters with corresponding frequency transformation formulas which are based on this approach are presented.

II. GENERALISED MULTI-PASSBAND RESONATOR SECTIONS

The synthesis techniques for multi-passband filter will be discussed from the topology point of view. Before that, the concept of multi-passband resonator sections is introduced. They are called multi-passband resonator sections, since the resonators in each section are coupled by inverters. Basically, the multi-passband resonator section can be categorised into three types which are shown in Figure 3. For the first type, all bandstop resonators are directly connected to the bandpass resonator; it is named as parallel coupled resonator section. For the second type, the bandstop resonators have an inline layout and only one bandstop resonator is directly connected to the bandpass resonator; it is named as series coupled resonator section. The third one is the mixed coupled resonator section which contains both parallel and series couple resonator at the same time. The bigger circles represent bandpass resonators; the smaller circles represent bandstop resonators; the solid lines stand for couplings between resonators; the dashed lines mean some unshown re-occurring parts.

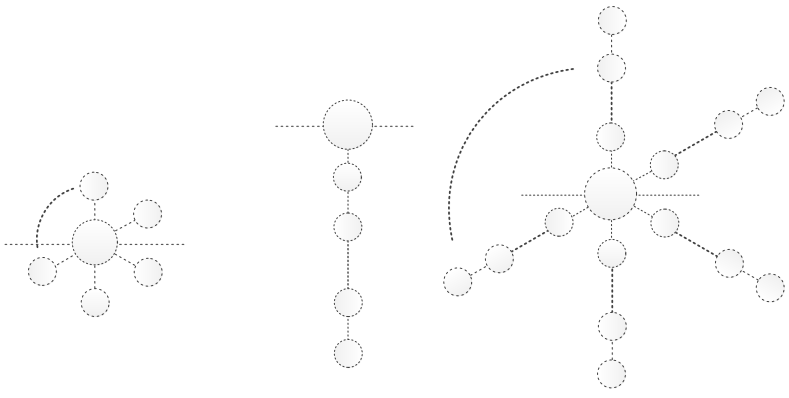

Figure 3. Different kind of multi-passband resonator sections: (a) parallel, (b) series, (c) mixed

The multi-passband filters we discussed here are built up with these sections. For each section, there is only one bandpass resonator, but the number of bandstop resonator is not limited. Within one particular multi-passband filter, all the sections share the same topology; the repeating sections are connected through the bandpass resonators. It is actually the multi-passband resonator section that ultimately determines the frequency transformation formula and the multi-passband response in this multi-passband synthesis technique [4].

A. PARALLEL COUPLED RESONATOR SECTION

Figure 4 shows a generalised multi-passband filter which is built up by parallel coupled resonator sections. Resonator 1 to *n* are the bandpass resonators. For example, if these *n* bandpass resonators generate an n^{th} order Chebyshev response, then each passband of this multi-passband filter will have the same n^{th} order Chebyshev response.

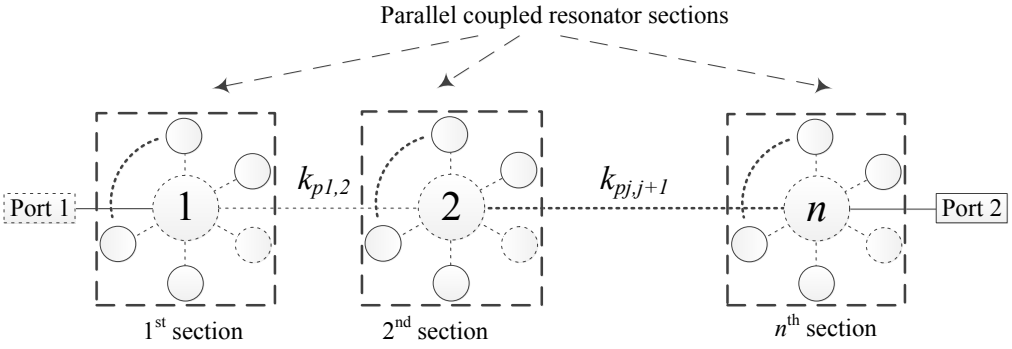

Figure 4. The topology of a generalised multi-passband filter which is built up by parallel coupled resonator sections. The bigger circles represent bandpass resonators; the smaller circles represent bandstop resonators.

The couplings in between bandpass resonators $k_{pj,j+1}$ (j=1,2,...,n-1) can be calculated by [4],

$$k_{pj,j+1} = \frac{J_{j,j+1}}{b_1}, \qquad J_{j,j+1} = \frac{1}{\sqrt{g_j \cdot g_{j,j+1}}} \ (j=1,2,...,n-1) \qquad \text{Equation 2}$$

in which $J_{j,j+1}$ (j=1,2,...,n-1) are the values of J-inverters of low-pass prototype filter. In the case of filter with Chebyshev response, they can be obtained from standard Chebyshev filter synthesis procedure that are calculated from g-values in Equation 2; b_1 is the susceptance slope parameter of the resonators whose centre frequency is ω_{o1} which can be calculated from [5], in which C_i and L_i are the equivalent capacitance and inductance of i^{th} resonator.

$$b_i = \omega_{oi} \cdot C_i, \qquad \omega_{oi} = \frac{1}{\sqrt{L_i \cdot C_i}} \qquad (i=1,2,3,...,M) \qquad \text{Equation 3}$$

Figure 5 presents a detailed picture of the 1st section of the multi-passband filter that is shown in Figure 4. The multi-passband filter is made up of *n* sections like this. It shows a generalised topology of a single parallel coupled resonator section. *M* is the number of resonators in one parallel coupled resonator section. *M* could be any positive integers. In each resonator section, the bandpass resonator is directly coupled to *M*-1 bandstop resonators. So there will be $M \times n$ resonators in total for the multi-passband filter. ω_{oi} and b_i (i=1,2,3,...,M) are the centre frequency and susceptance slope parameter for the i^{th} resonator, respectively. When i=1, the resonator is a bandpass resonator; when i=2,3,...,M, the resonator is a bandstop resonator. All the *n* sections which are shown in Figure 4 share the same layout and parameters.

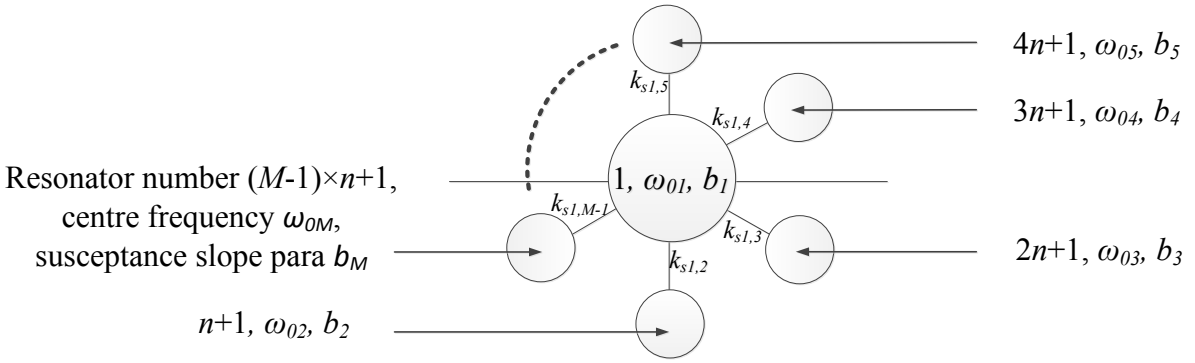

Figure 5. 1st parallel coupled resonator section (*n* is the order of the each passband, *M* is the total number of passbands

The couplings between the bandpass resonator and all bandstop resonators are calculated by

$$k_{s1,i} = \frac{1}{\sqrt{b_1 \cdot b_i}} \ (i=2,3,\ldots,M\text{-}1) \qquad \text{Equation 4}$$

The above equation together with the frequency transformation $M_P(\omega)$ for the multi-passband filter with such parallel coupled resonator sections is based on [4] but generalised,

$$\Omega = M_P(\omega) = b_1\left(\frac{\omega}{\omega_{o1}} - \frac{\omega_{o1}}{\omega}\right) - \frac{1}{b_2\left(\frac{\omega}{\omega_{o2}} - \frac{\omega_{o2}}{\omega}\right)} - \frac{1}{b_3\left(\frac{\omega}{\omega_{o3}} - \frac{\omega_{o3}}{\omega}\right)} - \frac{1}{b_4\left(\frac{\omega}{\omega_{o4}} - \frac{\omega_{o4}}{\omega}\right)} - \frac{1}{b_5\left(\frac{\omega}{\omega_{o5}} - \frac{\omega_{o5}}{\omega}\right)} \cdots\cdots - \frac{1}{b_M\left(\frac{\omega}{\omega_{oM}} - \frac{\omega_{oM}}{\omega}\right)}$$

Equation 5

By applying Equation 5, the prototype bandpass response can be mapped into *M* different frequency bands. Figure 6 gives an illustrative view of this procedure, in which ω_{Li} and ω_{Hi} (*i*=1,2,...,*M*) are the lower and higher passband limits for Band *i* (*i*=1,2,...,*M*), respectively. What should be noticed is that, for the multi-passband filter built up with this parallel coupled resonator sections, the centre frequencies of bandstop resonators ω_{oi} (*i*=2,3,...,*M*) are also the frequencies of transmission zeros between each band. There are *M* bands in total for this multi-passband filter.

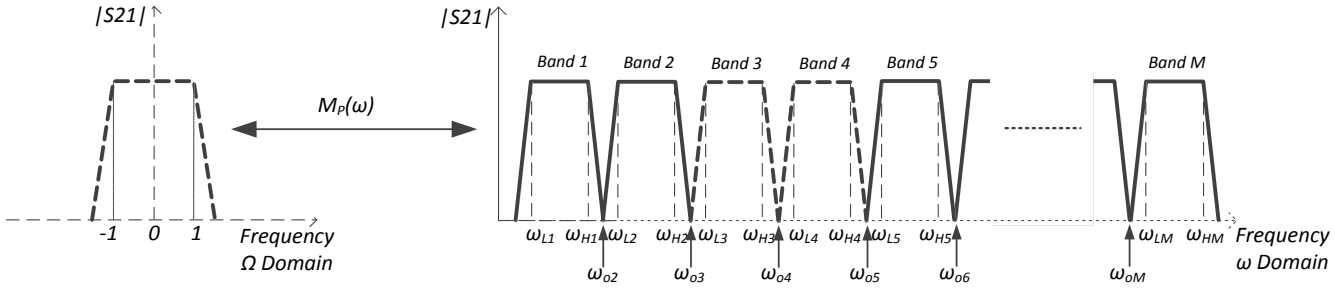

Figure 6. A schematic S21 for multi-passband synthesis technique with parallel coupled resonator section

It should be noted that filter with this topology could have a large number of couplings to each passband resonator, which may be difficult for practical implementation.

B. SERIES COUPLED RESOANTOR SECTION

The topology of a generalised multi-passband filter based on series coupled resonator sections is shown in Figure 3.26. Again, the resonators from 1 to *n* are the bandpass resonators. These bandpass resonators determine the shape of each passband for this multi-passband filter.

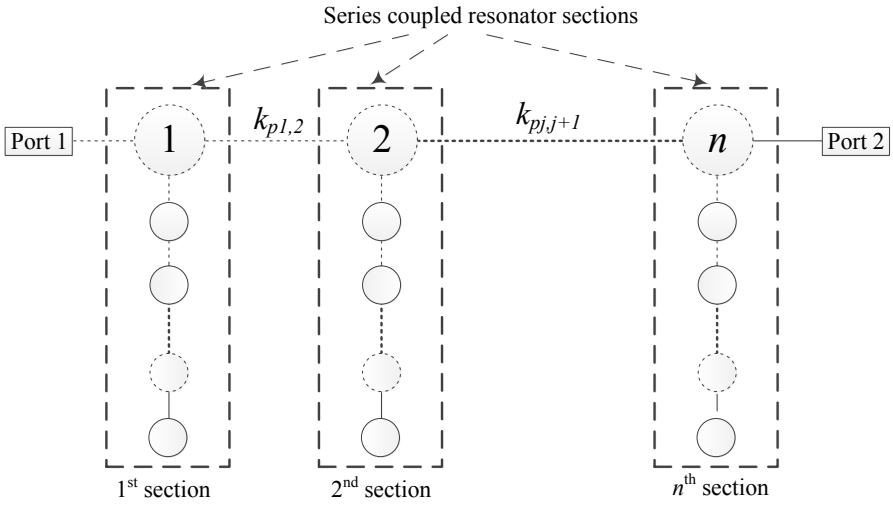

Figure 7. The topology of a generalised multi-passband filter which is built up by series coupled resonator sections. The bigger circles represent bandpass resonators; the smaller circles represent bandstop resonators.

Figure 3.27 shows the detailed layout of the 1st section in Figure 3.26. Similar to the previous parallel case, there are also *n* repeating sections in one multi-passband filter. Each section contains one bandpass resonator which resonates at ω_{o1} and *M*-1 bandstop resonators resonate at ω_{oi} (*i*=2,3,...,*M*). There are $M \times n$ resonators in this multi-passband filter, as well.

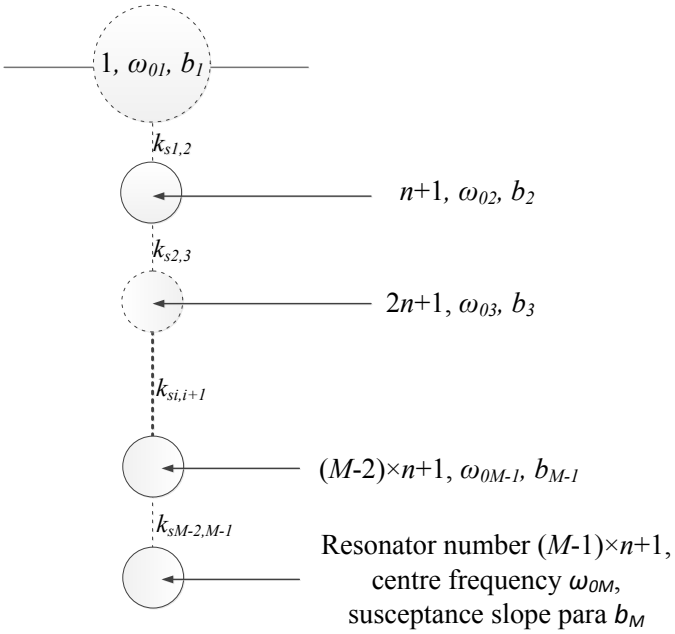

Figure 8. 1st series coupled resonator section (*n* is the order of the each passband, *M* is the total number of passbands)

The couplings between the resonators in one section are defined by,

$$k_{si,i+1} = \frac{1}{\sqrt{b_i \cdot b_{i+1}}} \quad (i=1,2,\ldots,M\text{-}2) \qquad \text{Equation 6}$$

The frequency transformation $M_S(\omega)$ for this series coupled resonator section based multi-passband filter is generalised from [6],

$$\Omega = M_S(\omega) = b_1\left(\frac{\omega}{\omega_{o1}} - \frac{\omega_{o1}}{\omega}\right) - \cfrac{1}{b_2\left(\frac{\omega}{\omega_{o2}} - \frac{\omega_{o2}}{\omega}\right) - \cfrac{1}{b_3\left(\frac{\omega}{\omega_{o3}} - \frac{\omega_{o3}}{\omega}\right) - \ddots - \cfrac{1}{b_{M-1}\left(\frac{\omega}{\omega_{oM-1}} - \frac{\omega_{oM-1}}{\omega}\right) - \cfrac{1}{b_M\left(\frac{\omega}{\omega_{oM}} - \frac{\omega_{oM}}{\omega}\right)}}}}$$

Equation 7

The illustrative procedure of this multi-passband de-normalising process carried out by Equation 7 is shown in Figure 3.28.

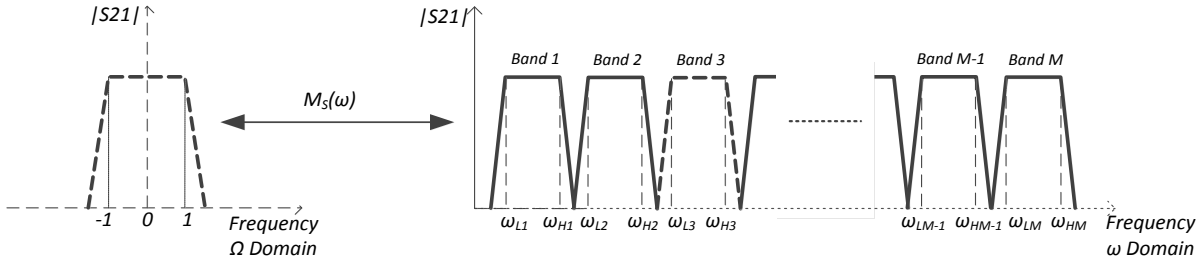

Figure 9. Schematic S21 for multi-passband synthesis technique with series coupled resonator section

There are *M* passbands in total for this multi-passband filter as well. But it should be noticed that, compared to the parallel coupled resonator section based topology, ω_{oi} (i=2,3,…,M) are not the transmission zeros between each band anymore; they only act as the centre frequencies of the i^{th} (i=2,3,…,M) resonator.

C. MIXED COUPLED RESONATOR SECTION — AN EXAMPLE FOR FIVE-PASSBAND RESPONSE

Figure 3.29 shows a generalised multi-passband filter made up of mixed coupled resonator sections which includes both parallel and series coupled resonator structures. Resonator 1 to resonator *n* are still bandpass resonators, which determine the passband shape in the de-normalised multi-passband response.

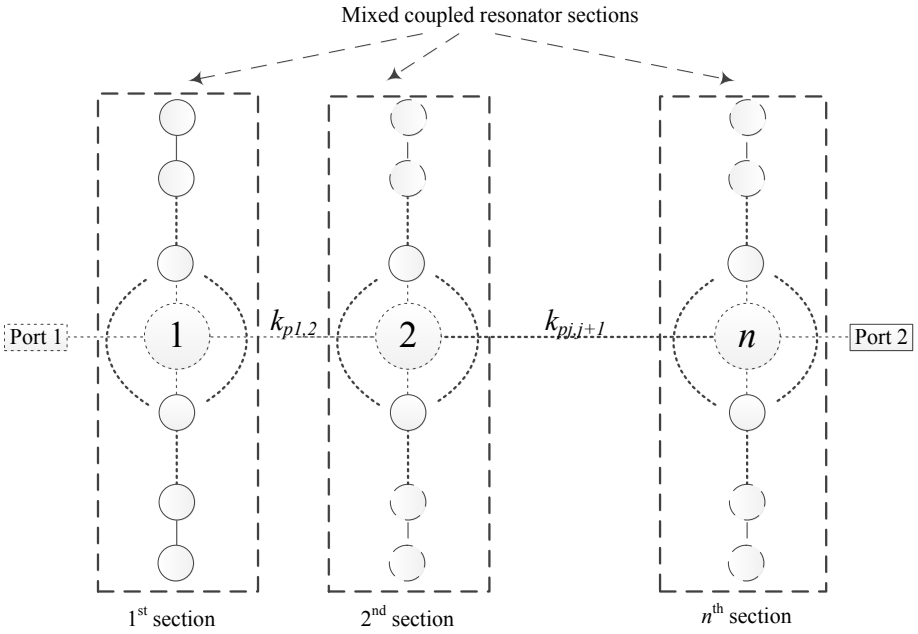

Figure 10. The topology of a generalised multi-passband filter which is built up by mixed coupled resonator sections. The bigger circles represent bandpass resonators; the smaller circles represent bandstop resonators.

Because of the complex in parameter naming, an intuitive example topology of a single mixed coupled resonator section is given in Figure 11, rather than a generalised topology. But it still gives a good indication of the structure.

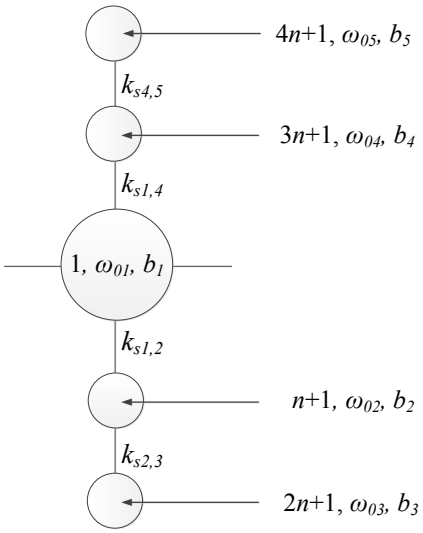

Figure 11. An example of mixed coupled resonator section (for five-passband response)

In Figure 11, resonator 1 is the bandpass resonator; all the other four resonators are bandstop resonators. Two bandstop resonators (resonator n+1 and resonator 3n+1) are directly connected to the bandpass resonator; while the other two bandstop resonators (resonator 2n+1 and resonator 4n+1) are connected to the adjacent bandstop resonators. The inter resonator coupling in this mixed coupled section can be calculated using Equation 4 and Equation 6. With this particular kind of mixed couple resonator section, a five-passband filter is given as an example. The frequency transformation for this five-passband filter is

$$\Omega = F(\omega) = b_1\left(\frac{\omega}{\omega_{o1}} - \frac{\omega_{o1}}{\omega}\right) - \frac{1}{b_2\left(\frac{\omega}{\omega_{o2}} - \frac{\omega_{o2}}{\omega}\right) - \frac{1}{b_3\left(\frac{\omega}{\omega_{o3}} - \frac{\omega_{o3}}{\omega}\right)}} - \frac{1}{b_4\left(\frac{\omega}{\omega_{o4}} - \frac{\omega_{o4}}{\omega}\right) - \frac{1}{b_5\left(\frac{\omega}{\omega_{o5}} - \frac{\omega_{o5}}{\omega}\right)}}$$

Equation 8

The corresponding frequency transformation procedure is presented in Figure 3.31.

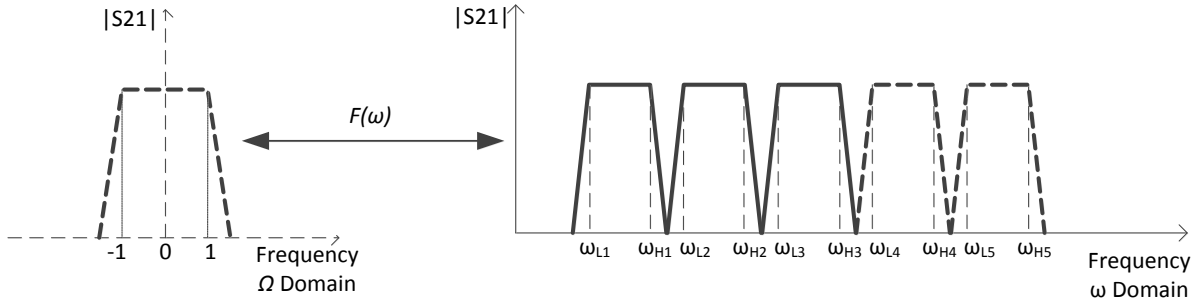

Figure 12. Schematic S21 for five-passband synthesis technique with mixed coupled resonator section

Specified examples are given in next section to validate the general theory of multi-passband filter synthesis technique which is proposed here.

III. SIMULATED AND MEASURED MULTI-PASSBAND FILTER EXAMPLES

To validate the synthesis technique, two examples of five-passband filters with simulated results are given. In addition, one example of dual-passband filters with measured result is given. The first is a 10th order uneven bandwidth five-passband filter with Chebyshev response (simulated). This is followed by another more complex example of a 20th order uneven bandwidth five-passband filter with quasi-elliptic response (simulated); this shows the flexibility of the synthesis technique. A fabricated 4th order dual-passband filter with Chebyshev response (measured) is given at the end of the paper.

A. EXAMPLE 1: A 10TH ORDER UNEVEN BANDWIDTH FIVE-PASSBAND FILTER WITH CHEBYSHEV RESPONSE (SIMULATED RESULT)

Figure 13 shows a 10th order five-passband filter which is built up with the mixed coupled resonator sections shown in Figure 11.

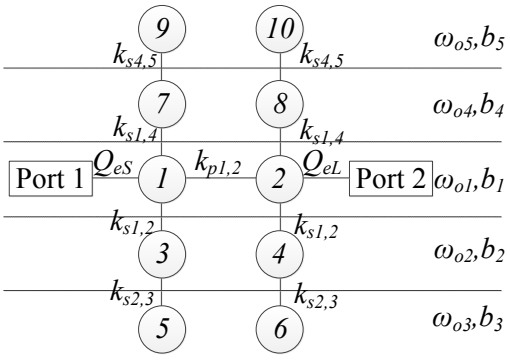

Figure 13. The topology of a 10th order five-passband filter (each passband has a 2nd order Chebyshev response)

The frequency transformation in (3-44) maps ω_{Li} and ω_{Hi} (i=1,2,3,4,5) on the de-normalised frequency domain to -1 and 1 on normalised frequency domain (see Figure 3.31), this process can be interpreted as,

$$\begin{aligned} &F(-\omega_{L1}) = F(-\omega_{L2}) = F(-\omega_{L3}) = F(-\omega_{L4}) = F(-\omega_{L5}) \\ &= F(\omega_{H1}) = F(\omega_{H2}) = F(\omega_{H3}) = F(\omega_{H4}) = F(\omega_{H5}) = 1 \end{aligned} \qquad \text{Equation 9}$$

let

$$VF(\omega) = F(\omega) - 1 \qquad \text{Equation 10}$$

Now, ω_{Li} and ω_{Hi} (i=1,2,3,4,5) are the zeros of $VF(\omega)$, while $VF(\omega)$ can also be expressed in terms of polynomial as,

$$VF(\omega) = \frac{ZF(\omega)}{PF(\omega)} = \frac{\omega^{10} + z_9\omega^9 + z_8\omega^8 + z_7\omega^7 + z_6\omega^6 + z_5\omega^5 + z_4\omega^4 + z_3\omega^3 + z_2\omega^2 + z_1\omega + z_0}{p_9\omega^9 + p_8\omega^8 + p_7\omega^7 + p_6\omega^6 + p_5\omega^5 + p_4\omega^4 + p_3\omega^3 + p_2\omega^2 + p_1\omega + p_0} \qquad \text{Equation 11}$$

$ZF(\omega)$ and $PF(\omega)$ are the numerator and denominator of the $VF(\omega)$, respectively. As shown in (3-48), they are expressed in terms of polynomials; z_i (i=0,1,...,9) are the normalised coefficients of $ZF(\omega)$; p_i (i=0,1,...,9) are the coefficients of $PF(\omega)$.

By using (3-44), (3-47) and (3-48), z_i (i=0,1,...,9) can be obtained in terms of ω_{oi} and b_i (i=1,2,3,4,5). Meanwhile, $-\omega_{Li}$ and ω_{Hi} (i=1,2,3,4,5) are the zeros of $VF(\omega)$. Therefore, z_i (i=0,1,...,9) can also be obtained in terms of ω_{Li} and ω_{Hi} (i=1,2,3,4,5) from the equation below,

$$\begin{aligned} &\omega^{10} + z_9\omega^9 + z_8\omega^8 + z_7\omega^7 + z_6\omega^6 + z_5\omega^5 + z_4\omega^4 + z_3\omega^3 + z_2\omega^2 + z_1\omega + z_0 = \\ &(\omega + \omega_{L1})\cdot(\omega + \omega_{L2})\cdot(\omega + \omega_{L3})\cdot(\omega + \omega_{L4})\cdot(\omega + \omega_{L5})\cdot(\omega - \omega_{H1})\cdot(\omega - \omega_{H2})\cdot(\omega - \omega_{H3})\cdot(\omega - \omega_{H4})\cdot(\omega - \omega_{H5}) = 0 \end{aligned}$$

Equation 12

A 10th order equation set which only contains ω_{oi}, b_i, ω_{Li} and ω_{Hi} (i=1,2,3,4,5) has been established. Therefore, ω_{oi} and b_i (i=1,2,3,4,5) can be derived with given ω_{Li} and ω_{Hi} (i=1,2,3,4,5). Hence, the five-passband frequency transformation in (3-44) is fully defined.

A numerical example is given below. This example is based on the topology shown in Figure 13. The passband limits and corresponding design parameters are given in Table 3.7. The design parameters are obtained from passband limits by using the theory proposed above.

Passband limits	**Design parameters**
ω_{L1}=9.20 GHz	ω_{o1}=9.94 GHz
ω_{H1}=9.29 GHz	ω_{o2}=9.59 GHz
ω_{L2}=9.41 GHz	ω_{o3}=9.43 GHz
ω_{H2}=9.67 GHz	ω_{o4}=10.35 GHz
ω_{L3}=9.80 GHz	ω_{o5}=10.43 GHz
ω_{H3}=10.17 GHz	b_1=9.22
ω_{L4}=10.25 GHz	b_2=51.88
ω_{H4}=10.48 GHz	b_3=12.16
ω_{L5}=10.57 GHz	b_4=78.94
ω_{H5}=10.70 GHz	b_5=13.30

Table 1. The passband limits and design parameters for five-passband filter

The corresponding coupling matrix is defined below,

$$[M]=\begin{pmatrix} k_{1,1} & k_{p1,2} & k_{s1,2} & 0 & 0 & 0 & k_{s1,4} & 0 & 0 & 0 \\ k_{p1,2} & k_{2,2} & 0 & k_{s1,2} & 0 & 0 & 0 & k_{s1,4} & 0 & 0 \\ k_{s1,2} & 0 & k_{3,3} & 0 & k_{s2,3} & 0 & 0 & 0 & 0 & 0 \\ 0 & k_{s1,2} & 0 & k_{4,4} & 0 & k_{s2,3} & 0 & 0 & 0 & 0 \\ 0 & 0 & k_{s2,3} & 0 & k_{5,5} & 0 & 0 & 0 & 0 & 0 \\ 0 & 0 & 0 & k_{s2,3} & 0 & k_{6,6} & 0 & 0 & 0 & 0 \\ k_{s1,4} & 0 & 0 & 0 & 0 & 0 & k_{7,7} & 0 & k_{s4,5} & 0 \\ 0 & k_{s1,4} & 0 & 0 & 0 & 0 & 0 & k_{8,8} & 0 & k_{s4,5} \\ 0 & 0 & 0 & 0 & 0 & 0 & k_{s4,5} & 0 & k_{9,9} & 0 \\ 0 & 0 & 0 & 0 & 0 & 0 & 0 & k_{s4,5} & 0 & k_{10,10} \end{pmatrix}$$

Equation 13

The non-diagonal elements in the matrix (inter-resonator couplings) can be calculated using Equation 2, Equation 3 and Equation 6; the diagonal elements (self-couplings) can be calculated with the following equation, in which f_{0i} is the resonant frequency of i^{th} resonator, f_0 is the centre frequency of the filter.

$$k_{i,i}=\left(\frac{f_{0i}}{f_0}-\frac{f_0}{f_{0i}}\right) \qquad \text{Equation 14}$$

The external Q-factors can be calculated from,

$$Q_{eS}=\frac{b_1}{J_{S1}^{\ 2}}=b_1\cdot g_0\cdot g_1,\quad Q_{eL}=\frac{b_1}{J_{nL}^{\ 2}}=b_1\cdot g_n\cdot g_{n+1} \qquad \text{Equation 15}$$

For this example, the coupling matrix and external Q-factors are calculated below,

$$[M]=\begin{pmatrix}
-0.0020 & 0.1803 & 0.0457 & 0 & 0 & 0 & 0.0371 & 0 & 0 & 0 \\
0.1803 & -0.0020 & 0 & 0.0457 & 0 & 0 & 0 & 0.0371 & 0 & 0 \\
0.0457 & 0 & -0.0737 & 0 & 0.0398 & 0 & 0 & 0 & 0 & 0 \\
0 & 0.0457 & 0 & -0.0737 & 0 & 0.0398 & 0 & 0 & 0 & 0 \\
0 & 0 & 0.0398 & 0 & -0.1074 & 0 & 0 & 0 & 0 & 0 \\
0 & 0 & 0 & 0.0398 & 0 & -0.1074 & 0 & 0 & 0 & 0 \\
0.0371 & 0 & 0 & 0 & 0 & 0 & 0.0788 & 0 & 0.0309 & 0 \\
0 & 0.0371 & 0 & 0 & 0 & 0 & 0 & 0.0788 & 0 & 0.0309 \\
0 & 0 & 0 & 0 & 0 & 0 & 0.0309 & 0 & 0.0943 & 0 \\
0 & 0 & 0 & 0 & 0 & 0 & 0 & 0.0309 & 0 & 0.0943
\end{pmatrix}$$

$$Q_{eS} = Q_{eL} = 6.13$$

The circuit below is a waveguide implementation of the discussed 10th order five-passband filter with Chebyshev response simulated in CST microwave studio [7]. More details of how to use coupling matrix to generate such a waveguide filter is given in [8].

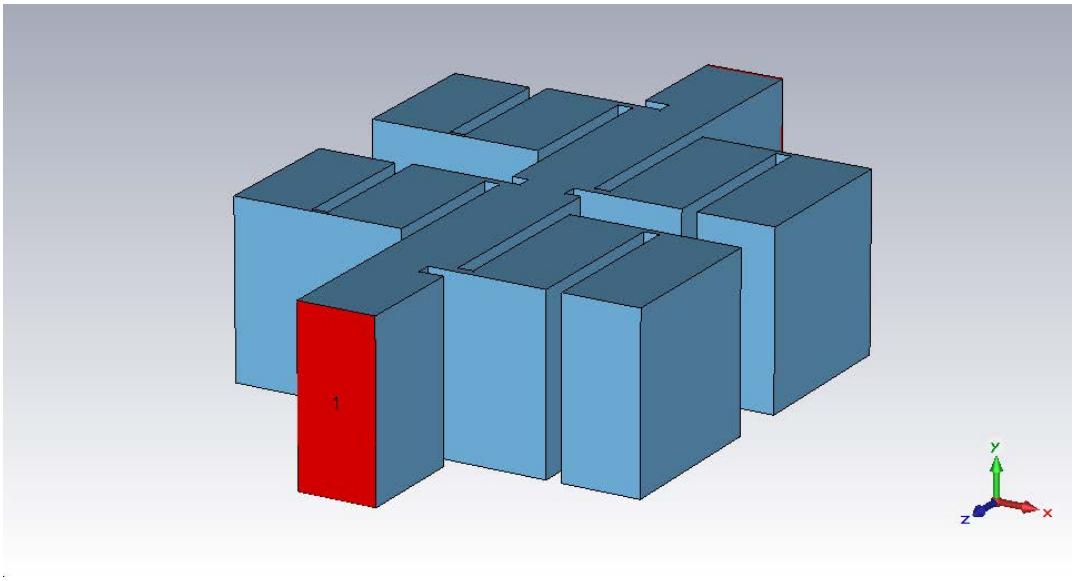

Figure 14. Waveguide implementation of 10th order five-passband filter (Chebyshev); the blue solid represents the air filling of the waveguide which is surrounded by perfect electric conductor. The red plane is the input port; the output port is placed at the other end.

The simulated S21 and S11 together with the calculated S11 are plotted in Figure 15. The simulated results show a good agreement with the calculated one.

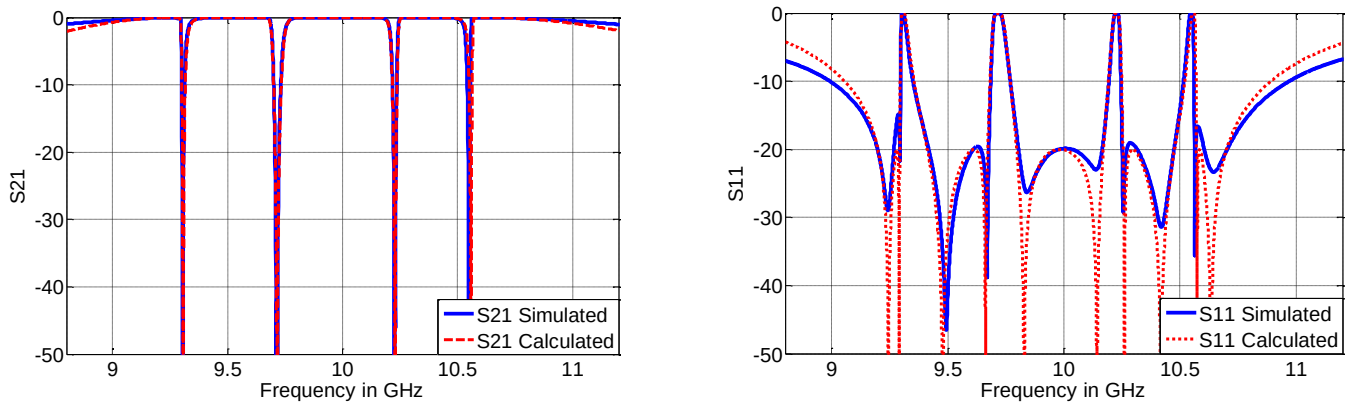

Figure 15. The S-parameter of a 10th order even bandwidth five-passband filter with Chebyshev response

(Passband 1: 9.20 ~ 9.29 GHz, Passband 2: 9.41 ~ 9.67 GHz, Passband 3: 9.80 ~ 10.17 GHz, Passband 4: 10.25 ~ 10.48 GHz, Passband 5: 10.57 ~ 10.70 GHz)

B. EXAMPLE 2: A 20TH ORDER UNEVEN BANDWIDTH FIVE-PASSBAND FILTER WITH QUASI-ELLIPTIC RESPONSE (SIMULATED RESULT)

This example is based on a 20th order five-passband filter topology shown in Figure 16. The five passbands are same as that in Example A, i.e. the design parameters are same as well (refer to Table 3.7). The difference is that in this example, each passband has a 4th order quasi-elliptic response with 20dB maximum return loss.

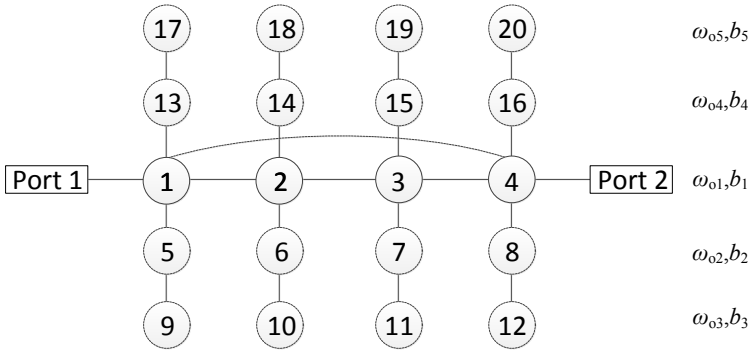

Figure 16. The topology of a 20th order five-passband filter (each passband has a 4th order quasi-elliptic response)

The corresponding coupling matrix can be calculated using Equation 2, Equation 3, Equation 6 and Equation 14. The external *Q*-factors can be obtained from Equation 15. The results are shown below,

$$[M]=\begin{pmatrix}
-0.0020 & 0.0901 & 0 & -0.0321 & 0.0457 & 0 & 0 & 0 & 0 & 0 & 0 & 0 & 0.0371 & 0 & 0 & 0 & 0 & 0 & 0 & 0 \\
0.0901 & -0.0020 & 0.0883 & 0 & 0 & 0.0457 & 0 & 0 & 0 & 0 & 0 & 0 & 0 & 0.0371 & 0 & 0 & 0 & 0 & 0 & 0 \\
0 & 0.0883 & -0.0020 & 0.0901 & 0 & 0 & 0.0457 & 0 & 0 & 0 & 0 & 0 & 0 & 0 & 0.0371 & 0 & 0 & 0 & 0 & 0 \\
-0.0321 & 0 & 0.0901 & -0.0020 & 0 & 0 & 0 & 0.0457 & 0 & 0 & 0 & 0 & 0 & 0 & 0 & 0.0371 & 0 & 0 & 0 & 0 \\
0.0457 & 0 & 0 & 0 & -0.0737 & 0 & 0 & 0 & 0.0398 & 0 & 0 & 0 & 0 & 0 & 0 & 0 & 0 & 0 & 0 & 0 \\
0 & 0.0457 & 0 & 0 & 0 & -0.0737 & 0 & 0 & 0 & 0.0398 & 0 & 0 & 0 & 0 & 0 & 0 & 0 & 0 & 0 & 0 \\
0 & 0 & 0.0457 & 0 & 0 & 0 & -0.0737 & 0 & 0 & 0 & 0.0398 & 0 & 0 & 0 & 0 & 0 & 0 & 0 & 0 & 0 \\
0 & 0 & 0 & 0.0457 & 0 & 0 & 0 & -0.0737 & 0 & 0 & 0 & 0.0398 & 0 & 0 & 0 & 0 & 0 & 0 & 0 & 0 \\
0 & 0 & 0 & 0 & 0.0398 & 0 & 0 & 0 & -0.1074 & 0 & 0 & 0 & 0 & 0 & 0 & 0 & 0 & 0 & 0 & 0 \\
0 & 0 & 0 & 0 & 0 & 0.0398 & 0 & 0 & 0 & -0.1074 & 0 & 0 & 0 & 0 & 0 & 0 & 0 & 0 & 0 & 0 \\
0 & 0 & 0 & 0 & 0 & 0 & 0.0398 & 0 & 0 & 0 & -0.1074 & 0 & 0 & 0 & 0 & 0 & 0 & 0 & 0 & 0 \\
0 & 0 & 0 & 0 & 0 & 0 & 0 & 0.0398 & 0 & 0 & 0 & -0.1074 & 0 & 0 & 0 & 0 & 0 & 0 & 0 & 0 \\
0.0371 & 0 & 0 & 0 & 0 & 0 & 0 & 0 & 0 & 0 & 0 & 0 & 0.0788 & 0 & 0 & 0 & 0.0309 & 0 & 0 & 0 \\
0 & 0.0371 & 0 & 0 & 0 & 0 & 0 & 0 & 0 & 0 & 0 & 0 & 0 & 0.0788 & 0 & 0 & 0 & 0.0309 & 0 & 0 \\
0 & 0 & 0.0371 & 0 & 0 & 0 & 0 & 0 & 0 & 0 & 0 & 0 & 0 & 0 & 0.0788 & 0 & 0 & 0 & 0.0309 & 0 \\
0 & 0 & 0 & 0.0371 & 0 & 0 & 0 & 0 & 0 & 0 & 0 & 0 & 0 & 0 & 0 & 0.0788 & 0 & 0 & 0 & 0.0309 \\
0 & 0 & 0 & 0 & 0 & 0 & 0 & 0 & 0 & 0 & 0 & 0 & 0.0309 & 0 & 0 & 0 & 0.0943 & 0 & 0 & 0 \\
0 & 0 & 0 & 0 & 0 & 0 & 0 & 0 & 0 & 0 & 0 & 0 & 0 & 0.0309 & 0 & 0 & 0 & 0.0943 & 0 & 0 \\
0 & 0 & 0 & 0 & 0 & 0 & 0 & 0 & 0 & 0 & 0 & 0 & 0 & 0 & 0.0309 & 0 & 0 & 0 & 0.0943 & 0 \\
0 & 0 & 0 & 0 & 0 & 0 & 0 & 0 & 0 & 0 & 0 & 0 & 0 & 0 & 0 & 0.0309 & 0 & 0 & 0 & 0.0943
\end{pmatrix}$$

$$Q_{eS}=Q_{eL}=8.92$$

The component shown in Figure 17 is a simulated waveguide implementation of the 20th order five-passband filter with quasi-elliptic response.

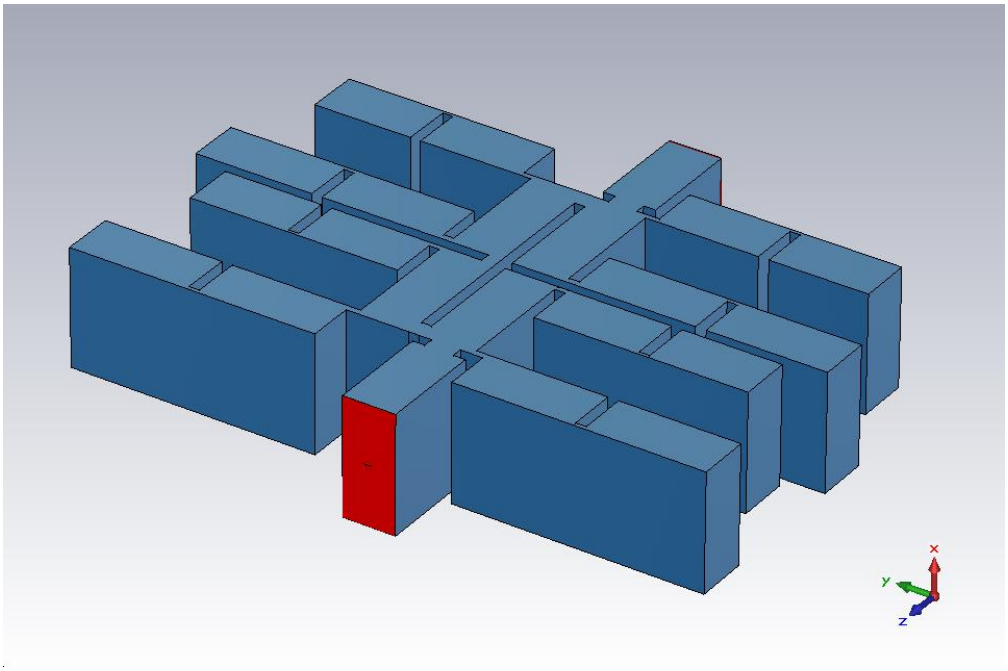

Figure 17. Waveguide implementation of 20th order five-passband filter (quasi-elliptic); the blue solid represents the air filling of the waveguide which is surrounded by perfect electric conductor. The red plane is the input port; the output port is placed at the other end.

The simulated S21 and S11 together with the calculated S11 are plotted in Figure 3.35,

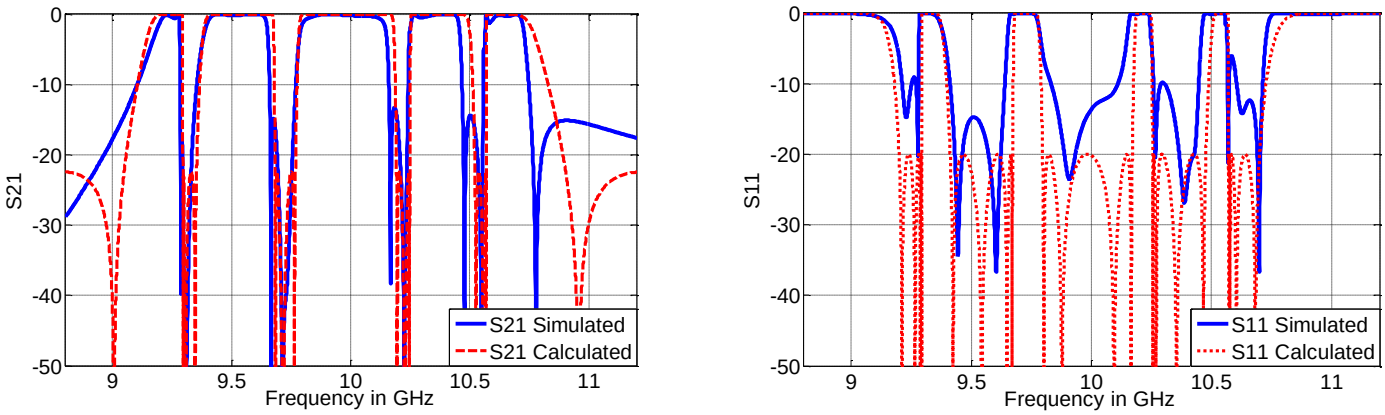

Figure 18. The S-parameter of a 20th order uneven bandwidth five-passband filter with quasi-elliptic response (Passband 1: 9.20 ~ 9.29 GHz, Passband 2: 9.41 ~ 9.67 GHz, Passband 3: 9.80 ~ 10.17 GHz, Passband 4: 10.25 ~ 10.48 GHz, Passband 5: 10.57 ~ 10.70 GHz)

The mismatch of S-parameter in the CST simulation is mainly due to the physical limitations of the waveguide circuit. As one resonator is coupled to up to 4 neighbour resonators at the same time, uncontrolled cross-couplings between non adjacent resonators may occur. Further works will improve the results. The uncontrolled cross-couplings might be further attenuated by re-arranging the circuit layout.

C. EXAMPLE 3: A 4TH ORDER UNEVEN BANDWIDTH DUAL-PASSBAND FILTER WITH CHEBYSHEV RESPONSE (MEASURED RESULT)

The 4th order dual-passband filter has a following topology; the corresponding frequency transformation is given in Equation 16. This example has two uneven passbands (refer to Table 2). Each passband has a 2nd order Chebyshev response with 20dB maximum return loss.

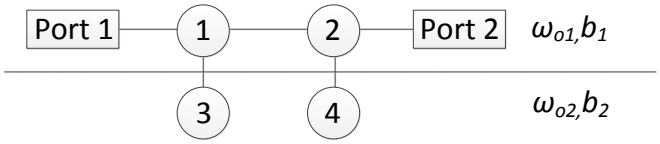

Figure 19. The topology of a 4th order dual-passband filter

$$\Omega = D(\omega) = b_1\left(\frac{\omega}{\omega_{o1}} - \frac{\omega_{o1}}{\omega}\right) - \frac{1}{b_2\left(\frac{\omega}{\omega_{o2}} - \frac{\omega_{o2}}{\omega}\right)} \quad \text{Equation 16}$$

The passband limits and corresponding design parameters are given in Table 2.

Passband limits	**Design parameters**
ω_{L1}=8.65 GHz	ω_{o1}=8.74 GHz
ω_{H1}=8.78 GHz	ω_{o2}=8.81 GHz
ω_{L2}=8.82 GHz	b_1=54.61
ω_{H2}=8.85 GHz	b_2=291.7

Table 2. The filter specifications and design parameters for dual-passband filter

The corresponding coupling matrix and external Q-factors can be calculated using Equation 2, Equation 3, Equation 14 and Equation 15; the results are given below,

$$[M] = \begin{pmatrix} -0.0023 & 0.0304 & 0.0079 & 0 \\ 0.0304 & -0.0023 & 0 & 0.0079 \\ 0.0079 & 0 & 0.0137 & 0 \\ 0 & 0.0079 & 0 & 0.0137 \end{pmatrix}$$

$$Q_{eS} = Q_{eL} = 36.30$$

Below is the structure of this 4th order filter which produces a dual-passband response; each passband has a 2nd order Chebyshev response.

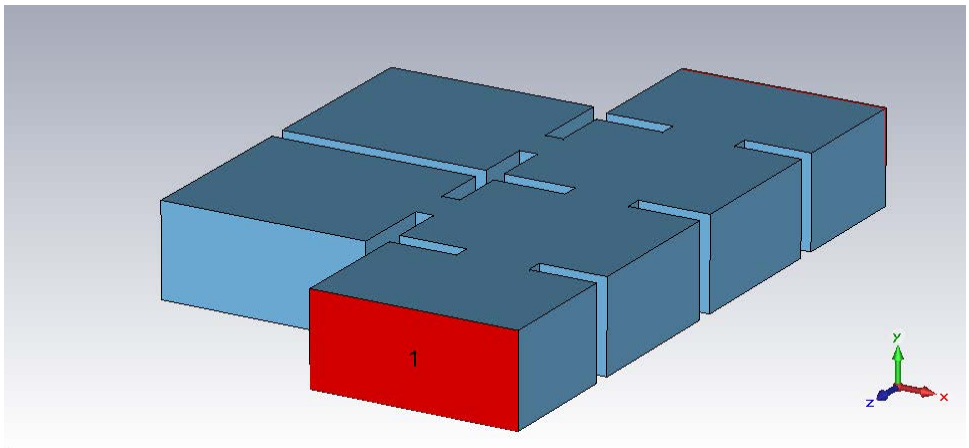

Figure 20. Waveguide implementation of 4th order five-passband filter (Chebyshev); the blue solid represents the air filling of the waveguide which is surrounded by perfect electric conductor. The red plane is the input port; the output port is placed at the other end.

The filter is designed based on the passbands specification shown in Table 2; the measured and calculated S-parameters are plotted below in Figure 21.

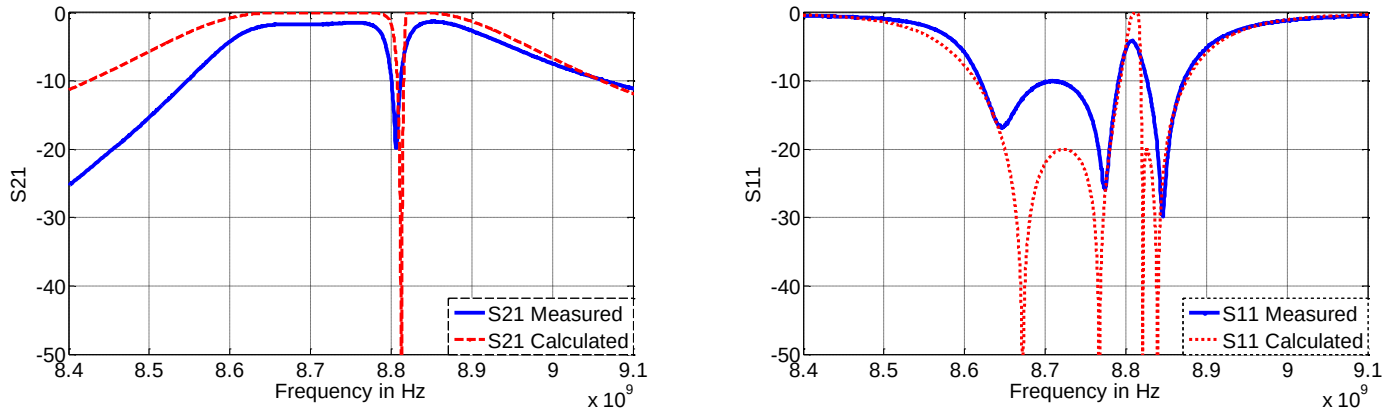

Figure 21. The S-parameter of a 4th order uneven bandwidth dual-passband filter with Chebyshev response (Passband 1: 8.65~ 8.78 GHz, Passband 2: 8.82 ~ 8.85 GHz)

The passband insertion loss is about 1.5dB. It is mainly due to the conductor loss by aluminium and non-perfect construction. Further works on fine tuning may improve the results.

IV. CONCLUSION

This paper has proposed a generalised analytical synthesis method for multi-passband filter design. The multi-passband resonator section is the key building block for the multi-passband filter discussed here; within one filter, there is only one kind of multi-passband resonator section. For one multi-passband resonator section, there is a unique frequency transformation corresponding to it. The multi-passband response is obtained by applying the frequency transformation to a low-pass prototype response. The number of the resonator in one multi-passband resonator section is the number of the passbands; the number of the re-occurring multi-passband resonator section determines the order of the response for each passband.

Two simulated five-passband filters and a measured dual-passband filter are given. They are all designed in X-band and designed in waveguide form. To illustrate the flexibility of this synthesis technique, the three examples all have arbitrary uneven bandwidths; two examples have Chebyshev response, while the other one has quasi-elliptic response. The simulated and measured results show good agreements with the theoretical calculated ones.

REFERENCES

1. Lancaster, M.J., *passive microwave device applications of high-temperature superconductors.* 1997.
2. Giuseppe Macchiarella, S.T., *Design Techniques for Dual-passband Filters.* IEEE TRANSACTION ON MICROWAVE THEORY AND TECHNIQUES , 2005. **53**(11): p. 7.
3. Xiao-Ping Chen, K.W., Zhao-Long Li, *Dual-Band and Triple-Band Substrate Integrated Waveguide Filters With Chebyshev and Quasi-Elliptic Responses.* IEEE TRANSACTION ON MICROWAVE THEORY AND TECHNIQUES , 2007. **55**(12): p. 10.
4. Hao Di, B.W., Xin Lai and Chang-Hong Liang, *Synthesis and Realization of Novel Triple-passband Filter Based on Frequency Transformation.* Microwave Conference, 2009, APMC 2009. Asia Pacific, 2009: p. 4.
5. *CST Microwave Studio 2013*, CST - Computer Simulation Technology AG.
6. Shang, X., W. Xia, and M.J. Lancaster, *The design of waveguide filters based on cross-coupled resonators.* Microwave and Optical Technology Letters, 2014. **56**(1): p. 3-8.

Design of A Five-Passband Rectangular Waveguide Filter with Chebyshev Response

Mofei Guo, Michael J. Lancaster, *Senior Member, IEEE*

***Abstract*— This paper reports a design method for a filter with five-passband. As an example, a rectangular waveguide filter with Chebyshev responses is given. The design technique is not limited to rectangular waveguide, but applies to all kinds of coupled resonator circuits. The filter has 10 resonators and works at X-band. The centre frequency and bandwidth of each passbands can be chosen arbitrarily, but every passband has a shape of a 2nd order Chebyshev response. The filter is manufactured and measured. The measured and simulated results show good agreement with the calculated ones, which verifies the proposed filter structure as well as the design procedure.**

***Index Terms*—Frequency transformation, multi-passband, waveguide.**

I. Introduction

The design of multi-passband filters has attracted attention recently, as they play increasingly important roles in modern wireless and satellite applications. Many of the design approaches for multi-passband filters that are found in the open literature use cross-coupled topologies to generate transmission zeros, in order to divide the single passband into two bands or more; the coupling matrices are derived using a variety of time consuming optimization methods [1-7]. Recently, as reported in [8-10], dual-passband and triple-passband filters can be synthesized using an analytical technique based on frequency transformations. It is well known that the low-pass prototype response can be mapped into frequency bands with the conventional lowpass to bandpass frequency transformation technique [11]. Similarly, a lowpass prototype response may be mapped into multiple frequency bands by applying a lowpass to multi-pass frequency transformation [12]. This process is achieved by the so-called inverter coupled resonator sections. A generalized synthesis technique has been discussed in [12], which can be used to design a filter with arbitrary number of passbands. What makes this technique distinct from the others is that it can produce an arbitrary number of asymmetrical passbands with control of the positions of the passband without the involvement of numerical optimisation [8]. In this paper, the design of a 10th order five-passband rectangular waveguide filter without cross-couplings is presented. It is the first demonstration of the generalized analytical synthesis technique discussed in [12]. The fabrication and measurement of the five-passband filter using such technique is given here for the first time. For the proposed filter, each passband has a shape of 2nd order Chebyshev response. All the coupling coefficients and external Q values can be directly synthesized from the 10 passband frequency limits of the 5 bands. All these frequency limits are chosen arbitrarily. The corresponding topology of the filter is given in Fig. 1(a). In this topology, there are 2 columns and 5 rows of resonators. Each column represents an inverter coupled resonator section, and both sections share the same topology. The topology of such section is determined by the frequency transformation which is discussed in the following paragraphs. Each section has 1 bandpass resonator and 4 bandstop resonators. There are two branches of bandstop resonators that are directly connected to the bandpass resonator. In each branch there are two bandstop resonators. The two sections are coupled through the bandpass resonators. Meanwhile, within each row, there are 2 resonators, and they all share the same resonant frequency ω_{oi} (i=1,2,3,4,5), and the susceptance slope parameter b_i (i=1,2,3,4,5). The physical waveguide configuration of the filter is given in Fig. 1(b). All the couplings in this rectangular waveguide filter are fulfilled by capacitive irises. The filter is symmetrical in the E-plane. Fig. 1(b) shows the lower half of the filter (E-plane cross sectional view). There are 10 cavities inside the filter acting as the 10 resonators. They are numbered in red together with the two ports which meet WR90 standard. The irises between the cavities provide the couplings between resonators. The cylindrical holes are for assembly screws.

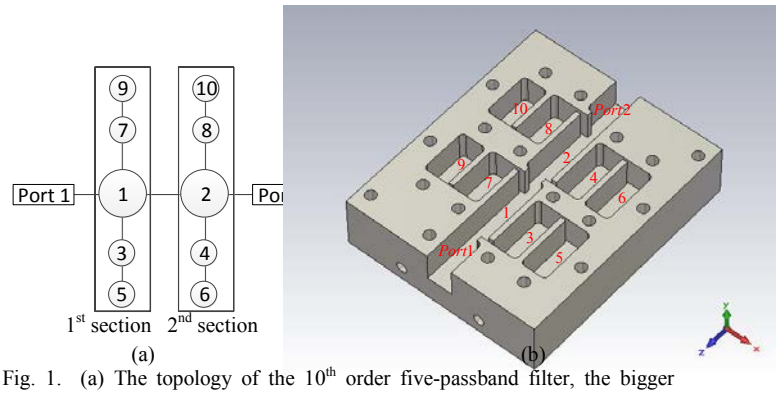

Fig. 1. (a) The topology of the 10th order five-passband filter, the bigger circles represent bandpass resonators, the smaller circles represent bandstop resonators, and the solid lines between circles are the direct couplings. (b) The physical configuration of the filter; it is the lower half from an E-plane cut.

M. Guo and M. J. Lancaster are with the School of Engineering, the University of Birmingham, Edgbaston, Birmingham, B15 2TT, U.K.

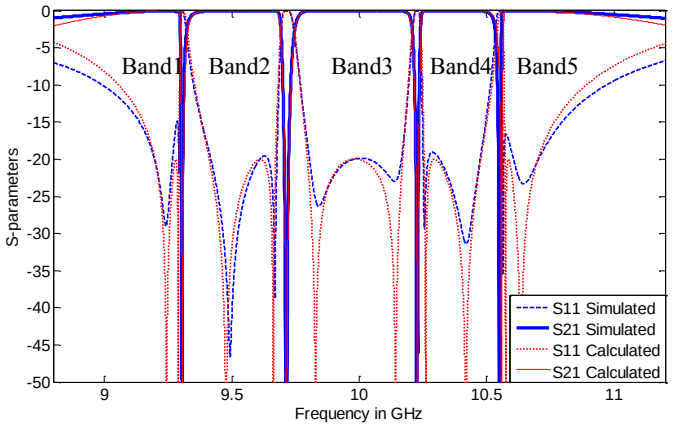

Fig. 2. The calculated and simulated responses of the 10th order five-passband filter, the passband numbers are labelled.

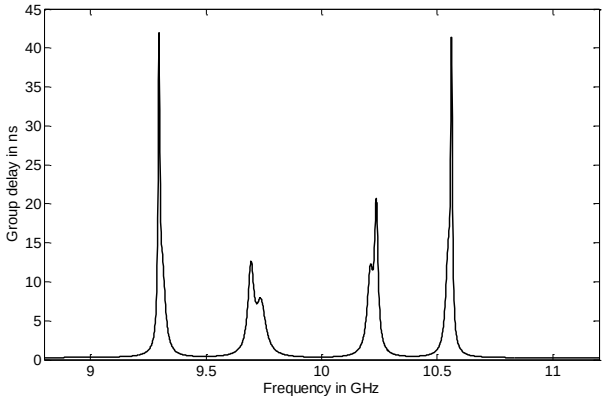

Fig. 3. The group delay of the calculated response for the 10th order five-passband filter.

II. Filter Design

The first step is to design a 2nd order lowpass prototype Chebyshev filter. The design theory for such filter is described in [1]. The specification of the lowpass prototype response is given as follows: the return loss (*RL*) is 20dB, the two passband limits are at ±1, the two reflection zeros (*RZ*s) are placed at ±0.7071 and the maximum return loss for passband is at 0. The *g*-values are calculated to be: g_0=1, g_1=0.6648, g_2=0.5445 and g_3=1.2210. Then by applying the following frequency transformation to the lowpass prototype response, it will be mapped into the five different frequency bands [12],

$$\Omega = b_1\left(\frac{\omega}{\omega_{o1}}-\frac{\omega_{o1}}{\omega}\right)-\cfrac{1}{b_2\left(\frac{\omega}{\omega_{o2}}-\frac{\omega_{o2}}{\omega}\right)-\cfrac{1}{b_3\left(\frac{\omega}{\omega_{o3}}-\frac{\omega_{o3}}{\omega}\right)}}-\cfrac{1}{b_4\left(\frac{\omega}{\omega_{o4}}-\frac{\omega_{o4}}{\omega}\right)-\cfrac{1}{b_5\left(\frac{\omega}{\omega_{o5}}-\frac{\omega_{o5}}{\omega}\right)}} \tag{1}$$

An example calculated response is plotted in red in Fig. 2. There are in total ten passband limits for this five-passband response. The corresponding group delay for the calculated response is given in Fig. 3. It can be seen that the delay near the edges of the passbands is large. This is inevitable due to the sharp slopes of the *S*21 between two consecutive passbands. It extends into the middle of the passbands [13]. In order to demonstrate the flexibility of the design technique, the five bands are placed arbitrarily, rather than having all the bands sharing the same bandwidth. From low to high, they are at 9.20, 9.29, 9.41, 9.67, 9.80, 10.17, 10.25, 10.48, 10.57 and 10.70 GHz. Once the passband limits are given, the resonant frequencies ω_{oi} (i=1,2,3,4,5), and the susceptance slope parameters b_i (i=1,2,3,4,5) are calculated from [12] to be: ω_{o1}=9.94GHz, ω_{o2}=9.59GHz, ω_{o3}=9.43GHz, ω_{o4}=10.35GHz, ω_{o5}=10.43GHz, b_1=9.22, b_2=51.88, b_3=12.16, b_4=78.94, b_5=13.30. Hence the frequency transformation (1) is fully defined [12]. From the equation below all the coupling coefficients and external *Q* values of this five-passband filter can be defined in terms of *g*-values (from the lowpass prototype), susceptance slope parameters b_i and the resonant frequencies ω_{oi} [12].

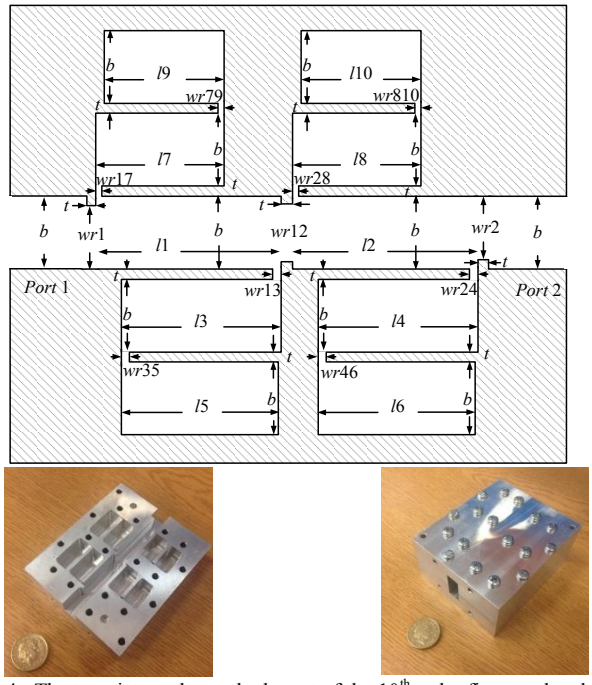

Fig. 4. The top picture shows the layout of the 10th order five-passband filter. The broad side dimension *a* of the cavity perpendicular to the E-plane cross section, therefore it is not shown in this layout. The bottom right picture is the assembled fabricated waveguide filter. Left is the disassembled lower half of the right fully assembled structure.

$$M_{12}=\frac{1}{b_1\sqrt{g_1\cdot g_2}},Q_{eS}=\frac{1}{b_1\sqrt{g_0\cdot g_1}},Q_{eL}=\frac{1}{b_1\sqrt{g_2\cdot g_3}}$$
$$M_{13}=M_{24}=\frac{1}{\sqrt{b_1\cdot b_2}},M_{17}=M_{28}=\frac{1}{\sqrt{b_1\cdot b_4}}, \tag{2}$$
$$M_{35}=M_{46}=\frac{1}{\sqrt{b_2\cdot b_3}},M_{79}=M_{810}=\frac{1}{\sqrt{b_4\cdot b_5}},$$
$$M_{2i-1\ \ 2i-1}=M_{2i\ \ 2i}=\left(\frac{\omega_{oi}}{\omega_o}-\frac{\omega_o}{\omega_{oi}}\right),i=1,2,3,4,5$$

The filter topology (shown in Fig. 1) is fully defined. The results are calculated to be: M_{12}=M_{21}=0.1803, M_{13}=M_{31}=M_{24}=M_{42}=0.0457, M_{35}=M_{53}=M_{46}=M_{64}=0.0398, M_{17}=M_{71}=M_{28}=M_{82}=0.0371, M_{79}=M_{97}=M_{810}=M_{108}=0.0309,M_{11}=M_{22}=0.0037, M33=

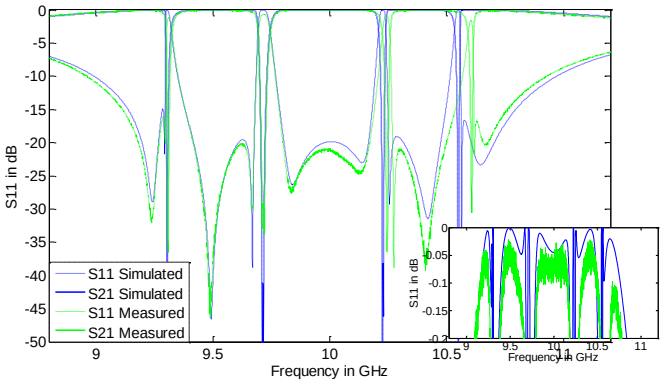

Fig. 5. The measured and simulated responses of the 10th order five-passband filter. The small extended picture shows the insertion loss of the filter.

III. TABLE I

IV. SUMMARY OF THE WAVEGUIDE DIMENSIONS

Label	*a*	*b*	*t*	*l*1	*l*2	*l*3
Dimension[1]	22.86	10.16	2.0	29.1	29.1	23.2
Label	*l*4	*l*5	*l*6	*l*7	*l*8	*l*9
Dimension[1]	23.2	23.1	23.1	19.7	19.7	18.9
Label	*l*10	*wr*1	*wr*2	*wr*12	*wr*13	*wr*35
Dimension[1]	18.9	8.0	8.0	7.0	1.2	0.8
Label	*wr*17	*wr*79	*wr*24	*wr*46	*wr*28	*wr*810
Dimension[1]	1.0	0.6	1.2	0.8	1.0	0.6

[1]all the dimensions are in mm

M44=-0.0680, M55=M66=-0.1017, M77=M88=0.0846, M99= M1010=0.1000, Q_e=6.13. Each of these coupling values is interpreted into physical dimension of a basic element within a rectangular waveguide filter, such as the resonator length *l* and the iris width *wr* [14]. All the dimensions are labelled in Fig. 4. After putting all the elements together, in order to accurately meet the required specification, further fine optimization on the structure can be done using CST [15]. The final optimized results simulated by CST are given in Table I. The corresponding simulated responses are plotted in blue in Fig. 2, together with the calculated ones. Excellent agreement is achieved between the two results. The mismatch near the edge of the passband region is due to the nature of the rectangular waveguide, as the neighboring modes are nearby.

V. FABRICATION AND MEASUREMENT

The filter is fabricated by a CNC milling machine using aluminum with an electrical conductivity of 3.56×10^7 S/m. In order to facilitate the milling by a CNC machine, the filter is cut through the E-plane, this means the filter will be assembled from the two parts. A photograph of the fully assembled filter and a photograph of the lower half alone are given in Fig. 4. The measured results are given in Fig. 5 together with the simulated results for the purpose of comparison. The measured *S*21 achieves an average mid-band insertion loss above 0.1dB for all five bands. It can be seen from Fig. 5 that the measured responses and the simulated ones show excellent agreements in general. The slight mismatch at band 4 and band 5 is due to the fabrication errors in iris79 and iris810, which affect the iris width *wr*79 and *wr*810. The errors are about 0.12mm wider than the calculated widths.

VI. CONCLUSION

A design method using an analytical synthesis technique for five-passband filter has been presented. It uses a frequency transformation to produce five-passband response from a single lowpass prototype. Since this does not involve any numerical optimisation, it offers a very fast solution once the filter specification is given. The frequency transformation is physically realised by inverter coupled resonator section, which is the key building block for the filter discussed here. A 10th order X-band five-passband filter is implemented in rectangular waveguide. The filter is specified to illustrate that the passband centre frequency and bandwidth are arbitrary chosen. The measured results show good agreement with the calculated and simulated ones. It should be noticed that this design method is not limited to waveguide circuits, but applies to all other kinds of coupled resonator circuits. It can be used to design not only Chebyshev filter, but also more complicated ones including quasi-elliptic filters.

REFERENCES

[1] Atia, W.A., Zaki, K.A., Atia, A.E., "Synthesis of general topology multiple coupled resonator filters by optimization," *IEEE MTTS Int. Microw. Symp*., Baltimore, USA, June 1998, pp. 821– 824

[2] Amari, S., "Synthesis of cross-coupled resonator filters using an analytical gradient-based optimisation technique," *IEEE TRANSACTIONS ON MICROWAVE THEORY AND TECHNIQUES*, 2000, **48**, (9), pp. 1559– 1564

[3] Jayyousi, A.B., Lancaster, M.J., "A gradient-based optimisation technique employing determinants for the synthesis of microwave coupled filters," *IEEE MTTS Int. Microw. Symp*., Fort Worth, USA, June 2004, pp. 1369–1372

[4] Nicholson, G.L., Lancaster, M.J., "Coupling matrix synthesis of crosscoupled microwave filters using a hybrid optimisation algorithm," *IEEE TRANSACTIONS ON MICROWAVE ATTENNAS AND PROPAGATION*, 2009, **3**, (6), pp. 950–958

[5] Cameron, R.J., "Advanced coupling matrix synthesis techniques for microwave filters," *IEEE TRANSACTIONS ON MICROWAVE THEORY AND TECHNIQUES*, 2003, **51**, (1), pp. 1 –10

[6] Lee, J., Sarabandi, K., "A synthesis method for dual-passband microwave filters," *IEEE TRANSACTIONS ON MICROWAVE THEORY AND TECHNIQUES*, 2007, **55**, (6), pp. 1163– 1170

[7] X. Shang, Y. Wang, G. L. Nicholson and M. J. Lancaster, "Design of multiple-passband filters using coupling matrix optimization," in *IET Microwaves, Antennas & Propagation*, vol. 6, no. 1, pp. 24-30, January 11 2012.

[8] Giuseppe Macchiarella, S.T., "Design Techniques for Dual-passband Filters," *IEEE TRANSACTIONS ON MICROWAVE THEORY AND TECHNIQUES*, 2005. **53**(11): p. 7.

[9] Xiao-Ping Chen, K.W., Zhao-Long Li, "Dual-Band and Triple-Band Substrate Integrated Waveguide Filters With Chebyshev and Quasi-Elliptic Responses," *IEEE TRANSACTIONS ON MICROWAVE THEORY AND TECHNIQUES*, 2007. **55**(12): p. 10.

[10] Hao Di, B.W., Xin Lai and Chang-Hong Liang, "Synthesis and Realization of Novel Triple-passband Filter Based on Frequency Transformation," Microwave Conference, 2009, APMC 2009. Asia Pacific, 2009: p. 4.

[11] Hong, J.-S. and M.J. Lancaster, *Microstrip Filters for RF/Microwave Applications*2001: John Wiley and Sons Ltd, United Kingdom.

[12] M. Guo, M. J. Lancaster and C. Constantinou, "A New Multi-Passband Filter Synthesis Technique," 31st ARMMS conference, UK, Nov 2015

[13] Huang, F., "Dual-Band Superconducting Spiral Filters Including Narrow Bandstop Notches," *IEEE TRANSACTIONS ON MICROWAVE THEORY AND TECHNIQUES*, 2009. **57**(5): p. 8.

[14] Pozar, D.M., *Microwave Engineering (Third Edition)*2005: John Wiley & Sons, Inc.

[15] CST Microwave Studio 2013, CST - Computer Simulation Technology AG